Structural and Biochemical Studies of ABC Transporters using DARPin Binders

Dissertation

Zur

Erlangung der naturwissenschaftlichen Doktorwürde
(Dr. sc. nat.)
vorgelegt der
Mathematisch-naturwissenschaftlichen Fakultät
der
Universität Zürich
von

Anshumali Mittal
aus
Indien

Promotionskomitee
Prof. Dr. Markus G. Grütter (Vorsitz)
Prof. Dr. Raimund Dutzler
Prof. Dr. Tilman Schirmer

Zürich, 2012

CONTENTS

SUMMARY

A cell cannot sustain without the cell membrane as the proteins embedded in the cell membrane are vital for different functions such as RNA, solute and protein transport and signal transduction across the membrane. About 60 % of approved drug targets are membrane proteins. Some members of the ABC transporter protein family are responsible for multidrug resistance to chemotherapeutic drugs. Like other membrane proteins, the understanding of ABC transporters function has been hampered by difficulties in membrane protein structure determination using x-ray crystallography. Therefore, new strategies to obtain crystals of membrane proteins suitable for structure determination are needed. In this thesis, *in vitro* selected designed ankyrin repeat proteins (DARPins) have been used as tools for structural and functional studies of four bacterial ABC transporters. In Chapter A of this thesis, membrane proteins, particularly ABC transporters and chaperone assisted co-crystallization are introduced.

Chapter B, C and D of this thesis describe the *in vitro* selection of DARPins using ribosome display against detergent solubilized bacterial ABC transporter MsbA and the cytosolic nucleotide binding domain of MsbA, respectively. About 2000 DARPins were screened to identify a high affinity (K_D of 80 nM) binder specific for MsbA, which was named DARPin_55. MsbA could be crystallized alone in its inward-facing state and its structure was partially solved at 7 Å using molecular replacement. Co-crystallization trials of MsbA with DARPin_55 did not result in crystals. Interestingly, DARPin_55 increased the ATPase activity of MsbA by a factor of two. Methanethiosulfonate mediated cross-links between two single cysteines on the DARPin and MsbA saturated at a stoichiometry of 1 DARPin binding to homodimeric MsbA. This provided the first experimental evidence suggesting asymmetry in homodimeric MsbA. The binding epitope of DARPin_55 could be determined using extensive electron paramagnetic resonance (EPR) and cysteine cross-linking measurements and was mapped to the transmembrane region of MsbA. For the first time, experimental evidence for asymmetry in the transmembrane domain of a homodimeric ABC transporter was provided.

It was tremendously challenging to identify a specific, monomeric and high affinity DARPin that binds to detergent solubilized MsbA. Most of the ELISA positive DARPins were either unspecific or found to form soluble aggregates as analyzed by size exclusion

chromatography. It was reasoned that this may be due to the accumulation of hydrophobic binders during the ribosome display selection cycles against membrane proteins. To avoid these problems, the cytosolic domain of MsbA (nucleotide binding domain or NBD) was also used for DARPin binder selection (Chapter D). About 1500 binders were screened to find a DARPin specific for the NBD, which was named DNBD_14. Interestingly, DNBD_14 did not bind to the full length protein, implying that the epitope is likely to be located in the region where the transmembrane domain interacts with the nucleotide binding domain in full length MsbA.

Chapter E of this thesis describes the *in vitro* selection of DARPins using ribosome display against detergent solubilized bacterial ABC transporter LmrCD. The identification of LmrCD specific binders was done by ELISA experiments (*in vitro*) and by the functional screening in *L. lactis* cells (*in vivo*). Three LmrCD specific DARPin activators were found in the *in vivo* screening. These binders stimulated the basal ATPase activity of reconstituted LmrCD in proteoliposomes and increased the daunomycin resistance in *L. lactis* cells. The cytosolic part of the transmembrane domain of LmrD chain was identified as the epitope for all DARPin activators.

Chapter F (in the appendix) summarizes initial efforts in identifying specific DARPins against two different ABC transporters, namely LmrA and YDDA. Selection and screening of DARPins against LmrA was performed using a N2C DARPin library. LmrA specific DARPin binders were used for co-crystallization trials, which unfortunately did not result in crystals. DARPin selections against YDDA were performed using a N3C DARPin library. The enriched library of DARPins was screened by ELISA to identify 9 YDDA specific binders. A thorough analysis of the YDDA-DARPin complex by SEC revealed that the DARPins failed to elute in complex with YDDA. Although, DARPin selections against LmrA & YDDA were only partially successful, the gained experience was important to establish a work flow for the selection and screening of DARPins against membrane proteins. In Chapter B, C, D and E, this methodology helped to find monomeric and specific DARPin binders for MsbA, the NBD of MsbA and LmrCD, respectively.

The work presented in this thesis illustrates the potential of *in vitro* selected binders to recognize novel conformational states of membrane transporters and thereby facilitating their structural and functional characterization.

ZUSAMMENFASSUNG

Eine Zelle kann ohne Zellmembran nicht überleben. Proteine in der Zellwand übernehmen lebensnotwendige Funktionen wie z.B. den Transport von RNA, gelösten Substanzen und Proteinen sowie der Weitergabe von Signalen über die Membran. Ungefähr 60% der Zielmoleküle von Medikamenten sind Membranproteine. Einige Vertreter aus der Proteinfamilie der ABC Transporter sind verantwortlich für die Resistenz gegen chemotherapeutische Medikamente. Schwierigkeiten bei der Bestimmung von Proteinstrukturen von ABC Transportern mittels Röntgenkristallisation sind der Grund für ein immer noch mangelhaftes Verständnis der Funktion dieser wichtigen Proteinfamilie. Darum sind neue Strategien gefragt, um Membranproteinkristalle zu züchten, welche sich zur Strukturbestimmung eignen. In dieser Dissertation wurden DARPins benutzt, um die Struktur und Funktion von vier bakteriellen ABC Transportern zu untersuchen. In Kapitel A werden Membranproteine, im speziellen ABC Transporter, und die Methode der sogenannten „chaperone-assisted crystallography“ beschrieben.

Die Kapitel B, C und D beschreiben die *in vitro* Selektion von DARPins gegen den in Detergenz gereinigten ABC Transporter MsbA sowie die zytosolische Nukleotid indungsdomäne von MsbA mittels Ribosome Display. Ungefähr 2000 DARPins wurden auf Bindung gegen MsbA getestet. Dabei wurde ein MsbA-spezifischer Binder mit einer geschätzten Affinität von K_D = 80 nM identifiziert, der DARPin_55 genannt wurde. Versuche MsbA zusammen mit DARPin_55 zu kristallisieren waren nicht von Erfolg gekrönt. In der Abwesenheit von DARPin_55 konnte MsbA in einem gegen innen geöffneten Zustand kristallisiert werden. Eine partielle Struktur konnte bei einer Auflösung von 7 Å gelöst werden. Interessanterweise erhöhte DARPin_55 die ATPase Aktivität von MsbA um das Zweifache. Mittels Methanethiolsulfonat wurden Vernetzungen und damit räumliche Nähe zwischen gewissen Cystein-Paaren auf dem DARPin und MsbA nachgewiesen. Diese Vernetzungsversuche zeigten, dass die Bindungsstoichiometrie von DARPin_55 und homodimerem MsbA 1:1 beträgt, was darauf hinwies, dass DARPin_55 einen asymmetrischen Zustand von MsbA erkennt. Die Bindungsstelle von DARPin_55 konnte mittels electron paramagnetic resonance (EPR) Messungen und einer Vielzahl von Vernetzungen zwischen Cysteinen genauer bestimmt werden und wurde auf dem transmembranen Bereich von MsbA lokalisiert. Damit wurde der ersten experimentellen

Hinweis für das Bestehen von Asymmetrie im transmembranen Bereich eines homodimeren ABC Tranporters erbracht.

Es war eine grosse Herausforderung, einen spezifischen, monomeren DARPin zu identifizieren, der mit hoher Affinität an in Detergenz gereinigtes MsbA bindet. Die meisten ELISA-positiven DARPins waren entweder unspezifisch oder bildeten lösliche Aggregate, was mittels Gelfiltrations-Chromatografie (size exclusion chromatography oder SEC) nachgewiesen werden konnte. Es wurde daraus geschlossen, dass dies wegen der Anreicherung von hydrophoben Bindern während der Selektion mittels Ribosome Display gegen das untersuchte Membranproteine geschah. Um solche Probleme zu vermeiden wurde die DARPin Selektion auch gegen den cytosolischen Teil von MsbA (genannt nucleotide binding domain oder NBD) durchgeführt (Kapitel D). Ungefähr 1500 Binder wurden analysiert. Dabei wurde ein für das NBD spezifischen DARPin gefunden, der DNBD_14 genannt wurde. Interessanterweise bindet DNBD_14 nicht an MsbA in seiner vollen Länge. Dies weist darauf hin, dass sich die Bindungsstelle von DNBD_14 wahrscheinlich in einer Region befindet, in welcher der Transmembranteil von MsbA mit dem NBD interagiert.

Kapitel E der Thesis beschreibt die *in vitro* Selektion von DARPins gegen Detergenz gereinigten, bakteriellen ABC Transporter LmrCD mittels Ribosome Display. Die Identifikation von LmrCD spezifischen Bindern wurde mit ELISA Experimenten (*in vitro*) und funktionalem Screening in *L. lactis* Zellen (*in vivo*) durchgeführt. *In vivo* Screening führte zur Identifikation von drei verschiedenen, aktivierenden DARPins. Die Binder stimulierten die basale ATPase Aktivität von rekonstituiertem LmrCD in Proteoliposomen und erhöhten die Daunomycin Resistenz in *L. lactis* Zellen. Der zytosolische Teil der Transmembran Domäne der LmrD Kette wurde als Bindungsepitop aller drei aktivierenden DARPins identifiziert.

Kapitel F (im Appendix) fasst erste Bemühungen zusammen, einen spezifischen DARPin gegen zwei verschiedene ABC Transporter zu identifizieren, nämlich LmrA und YDDA. Für die DARPin Selektion gegen LmrA wurde eine sogenannte N2C DARPin Bibliothek verwendet. LmrA-spezifische DARPin Binder wurden für Ko-Kristallisationsversuche verwendet, welche unglücklicherweise keine Kristalle hervorbrachten. DARPin Selektionen gegen YDDA wurden mit einer N3C DARPin Bibliothek durchgeführt. Dabei wurden 9 YDDA-spezifische Binder identifiziert. Eine gründliche Analyse der YDDA-DARPin Komplexe durch SEC zeigte, dass die DARPins nicht zusammen mit YDDA eluierten. Obwohl die DARPin

Selektionen gegen LmrA und YDDA nur teilweise erfolgreich waren, war die gewonnene Erfahrung wichtig, um einen Arbeitsablauf für die Selektion und Identifikation von DARPins gegen Membranproteine zu etablieren. Diese Methode half monomere und spezifische DARPins gegen MsbA und NBD_MsbA zu finden (wie in den Kapiteln B, C und D beschrieben).

Die in dieser Dissertation präsentierte Arbeit zeigt das Potential von *in vitro* selektionierten Bindern auf, um neue Konformationen von Membrantransportern zu erkennen und dadurch ihre strukturelle und funktionelle Charakterisierung zu ermöglichen.

CHAPTER A

A.1 Introduction

A cell is the basic unit of life and the plasma membrane defines its territory and controls what substances have to go in and out of the cell. The major components of plasma membranes are lipids, proteins and carbohydrates, held together by noncovalent interactions. The "Fluid Mosaic Model", described by Singer and Nicolson, explains the membrane as a fluid phospholipid bilayer, wherein proteins and lipids can freely diffuse within the plane of the membrane[1].

The basic structure of the plasma membrane is provided by the lipid bilayer, which is impermeable for ions and other solutes. The other component of the bilayer are membrane proteins, that perform various functions such as ion, RNA and protein transport across the membrane, signal transduction and attachment to neighboring cell[2]. In 1992, the structure of a bilayer of pure DOPC lipids was determined[3]. This study suggested that the hydrophobic core is 30 Å thick and interface region is 15 Å thick on either side[4] (Figure_A1).

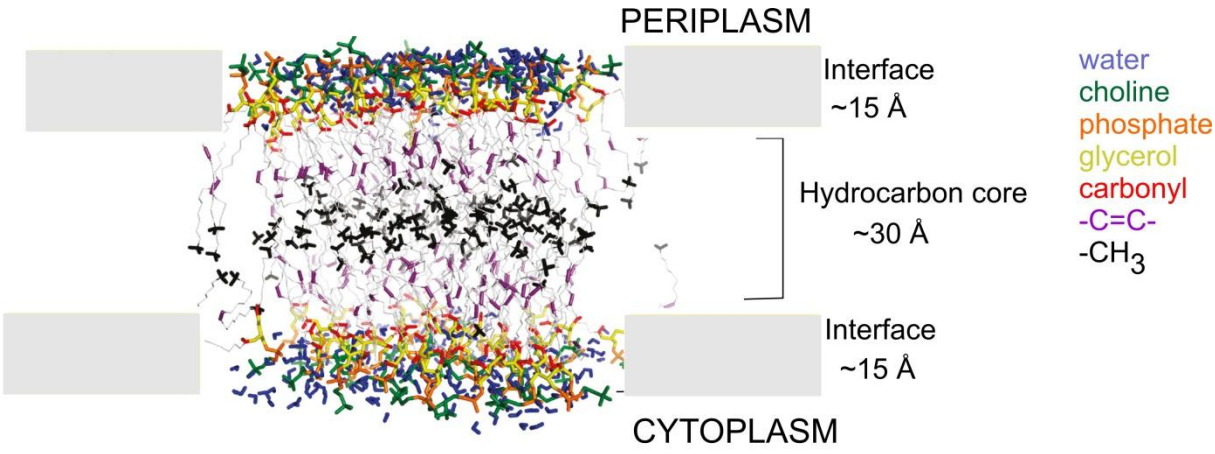

Figure_A1. Illustration of lipid bilayer. The figure is adapted from Linnea et al[4].

Membrane proteins can be classified as integral proteins, peripheral proteins, and lipid-bound proteins, based on their interactions with the lipid layer. The transmembrane region of the membrane proteins are either α-helices or β-sheets (Figure_A2). The inner membrane of bacteria is typically spanned by α-helices, while the outer membrane is abundant in proteins consisting of β-sheets, in form of closed barrels (therefore called β-barrels)[5]. Members of β-barrel protein are composed of a varied number of β-strands, such as OmpA

(8 β-strands), porins (16 β-strands) and FepA (22 β-strands). Some of them are pore forming proteins and allow selected hydrophilic solutes to cross the lipid bilayer of the outer membrane[6]. The α-helical transmembrane proteins vary from channels (K^+ or Cl^- channels etc)[7,8], receptors (bacteriorhodopsin, β-adrenergic receptor etc)[9,10] to transporters (AcrB, Sav1866 and MsbA etc)[11-13], and are associated with different functions. The focus of this thesis is on transport proteins, in particular ABC transporters.

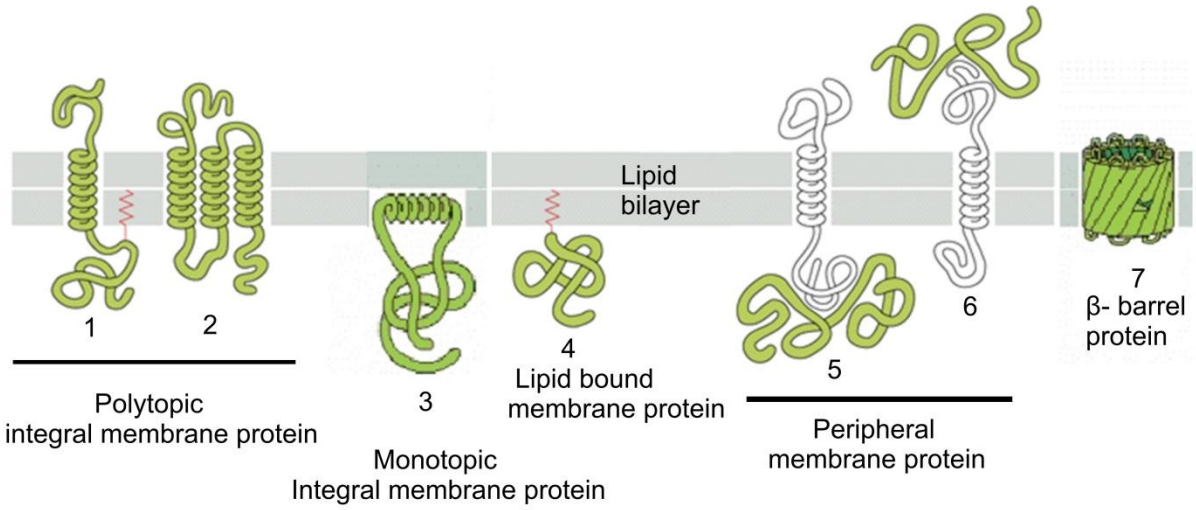

Figure_A2. Various ways in which membrane proteins associate with the lipid bilayer. (1) Single pass transmembrane protein. **(2)** multiple pass transmembrane protein. **(3)** In monotopic proteins, an amphipathic α–helix dips into the lipid bilayer and does not cross the membrane. **(4)** In lipid bound proteins, attachment to the bilayer is facilitated by a covalently attached lipid linker. **(5,6)** Some of the proteins are attached to the transmembrane proteins through noncovalent interactions. **(7)** β–sheet proteins. The figure is adapted from the textbook ´´Molecular Biology of the cell´´ and was further modified.

A.2 Classification of transport proteins

The lipid bilayer is the skin of a cell, which serves as a barrier to the passage of polar molecules. Cells have evolved ways to accomplish the transport of water soluble molecules in order to import nutrients, export toxins or waste products and maintain ion gradients. This suggests that transport is an essential function of every living cell and therefore, classification of transporters is required.

The international Union of Biochemistry and Molecular Biology has approved a classification system for membrane transport proteins including ion channels. This classification system is termed as “transporter classification database” (TCDB). TCDB is a freely accessible web resource (www.tcdb.org) and is based on structural, functional and evolutionary information about transport systems from different living organism[14]. The TCDB is an organized repository of published information from over 10000 references (Table 1).

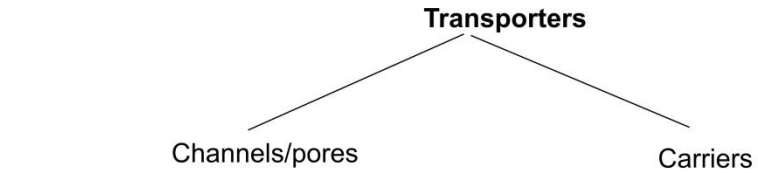

1.A. α-Type channels
1.B. β-Barrel porins
1.C Pore-forming toxins (proteins and peptides)
1.D. Non-ribosomally synthesized channels
1.E. Holins
1.F. Vesicle fusion pores
1.G. Paracellular channels

2. Electro chemical potential-driven transporters
   2.A. Porters (Uniporters, symporters, antiporters)
   2.B. Nonribosomally synthesized porters
   2.C. ino-gradient-driven energizers

3. Primary active transporters
   3.A. P-P-bond-hydrolysis-driven transporters
   3.A.1. The ABC superfamily
   3.A.2. The F-type ATPase superfamily
   3.A.3. The P-type ATPase superfamily
   3.B. Decarboxylation-driven transporters
   3.C. Methyltransfer-driven transportes
   3.D. Oxidoreduction-driven transporters
   3.E. Light absorption-driven transporters

4. Group translocators
   4.A. Phosphotransfer-driven group translocators
   4.B. Nicotinamide ribonucleoside uptake transporters
   4.C. Acyl CoA ligase-coupled transporters

5. Transport electron carriers
   5.A. Transmembrane 2-electron transfer carriers
   5.B. Transmembrane 1-electron transfer carriers

6. Accessory factors involved in transport
   6.A. Auxiliary transport proteins
   6.B. Ribosomally synthesized protein/peptide toxins that target channels and carriers
   6.C. Non-ribosomally synthesized toxins that target channels and carriers

7. Incompletely characterized transport systems
   7.A. Recognized transporters of unknown biochemical mechanism
   7.B. Putative transport proteins
   7.C. Functionally characterized transporters lacking identified sequences.

Table 1. Classification of transporters accrding to the TC system Saier (2000)[14]. The ABC transporter superfamily dicussed in this thesis is marked in red.

Transporter proteins in cell membrane may be divided into channels and carriers. Channels function as selective pores that regulate the flow of ions across the membrane and open in response to a chemical or electrical signal, temperature, or mechanical force, depending on the type of channel. All channel proteins mediate transportation across the cell membrane by passive transport or facilitated diffusion. Carrier proteins are also called permeases or transporters. These proteins bind to the substrate to be transported specifically and undergo a series of conformational changes in order to transfer the substrate across the cell

membrane. These carrier proteins mediate the transfer across the membrane by passive or active transport. Secondary active transporters use the energy from ion driven concentration gradient to drive the translocation of substrate across the membrane. Primary active transporter such as ATP-binding cassette (ABC) transporters couple ATP binding and hydrolysis to the transport of a variety of substrates against their electrochemical gradient[15] (Figure_A3).

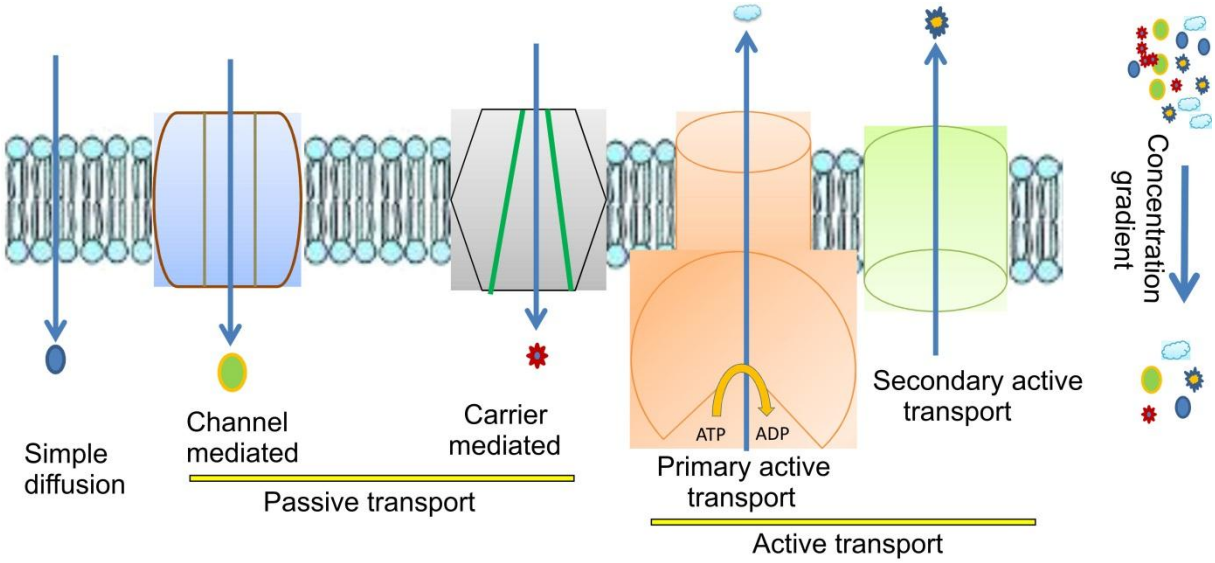

Figure_A3. Solutes cross cell membranes by passive or active transport.

A.2.1 ABC transporters

A.2.1.1 Introduction

ABC transporters are one of the largest superfamily of membrane proteins and are found in all kingdoms of life. They are primary active transporters, which act as exporters, importers, receptors and channels. ABC exporters are found in both eukaryotes and prokaryotes while importers are identified exclusively in prokaryotes[16]. These transmembrane proteins mediate a plethora of physiological phenomena, including transport of metabolic products, nutrients, proteins, peptides, lipids, polysaccharides, ions and drugs[17,18]. Genetic disorders in ABC transporters can lead to several human malfunctions including cystic fibrosis, neurological disease, retinal degeneration, cholesterol and bile transport defects, anemia, and drug resistance. Many ABC genes play a role in the maintenance of the lipid bilayer and in the transport of fatty acids and sterols within the body[17]. Based on phylogenetic analysis, human ABC transporters are divided into seven subfamilies (subfamily ABCA to subfamily ABCG). This particular study focuses on bacterial homologs of the ABCB subfamily. The ABCB

subfamily is unique in that it contains both full and half transporters and some of the members are characterized to be involved in multidrug resistance (MDR)[19]. At the molecular level, ABC transporters consist of four domains, two transmembrane domains (TMDs) and two nucleotide-binding domains (NBDs). The TMDs are composed of multiple α-helices, which form the pathway to transport the substrate and provide specificity. The NBDs also known as ATP-binding cassettes, power the transporter by binding and hydrolyzing ATP that is coupled to conformational changes in the TMDs to mediate unidirectional transport across the membrane[18].

A.2.1.1.1 Nucleotide binding domains

Structure determination of ABC transporter proteins initially started with the crystallization of hydrophilic ATP-binding subunits in isolation from the full transporters. The first structure of an NBD in complex with ATP was determined for histidine permease HisP at 1.5 Å resolution. This structure provided the details of interaction between the conserved NBD motifs and ATP but did not reveal the dimer interface of the domain[20]. Later, the crystal structures of a symmetrical NBD dimer formed by the E171Q mutant of the ABC transporter MJ0796 in complex with two ATP molecules, the NBD of the maltose transporter (MalK) with and without ATP and the NBD of the haemolysin transporter (HlyB) revealed a head-to-tail arrangement of the NBD-NBD dimer interface sandwiching two molecules of nucleotide at the interface[21-23]. The structure of the NBD monomer can be divided into two subdomains: a larger RecA-like core-subdomain and a helical subdomain[24]. The RecA-like core-subdomain comprises of 6 conserved motifs, which are the Walker A motif (yellow), the Walker B motif (green), the Q loop (purple), the A loop (red), the D loop (orange) and the H loop (dark blue). The helical subdomain contains ABC signature motif (cyan) (Figure_A4A). A nucleotide binding site (NBS) is comprised of the D loop and ABC signature motif (LSGGQ) of one NBD and the Walker A and B motifs and the H loop as well as the Q loop from the second NBD (Figure_A4B). This head-to-tail arrangement of the NBD dimer interface was first predicted by Jones and George[25] and later has also been verified in full length transporter structures[12,13]. In the inward facing state of ABC transporter, the TMDs are replenished with substrates and the NBDs are partially or fully disengaged. The binding of 2 ATP molecules leads to formation of the closed NBD dimer and TMDs adopt an outward facing state. The transition from the inward facing to the outward facing state has been associated with a switch from high to low affinity for the substrate[26]. The hydrolysis of ATP in the NBDs revert

the transporter back to the inward facing state. Switching between the inward and the outward facing state therefore facilitates vectorial transport of substrate across the membrane. This transport mechanism has been termed as ATP-switch model[26].

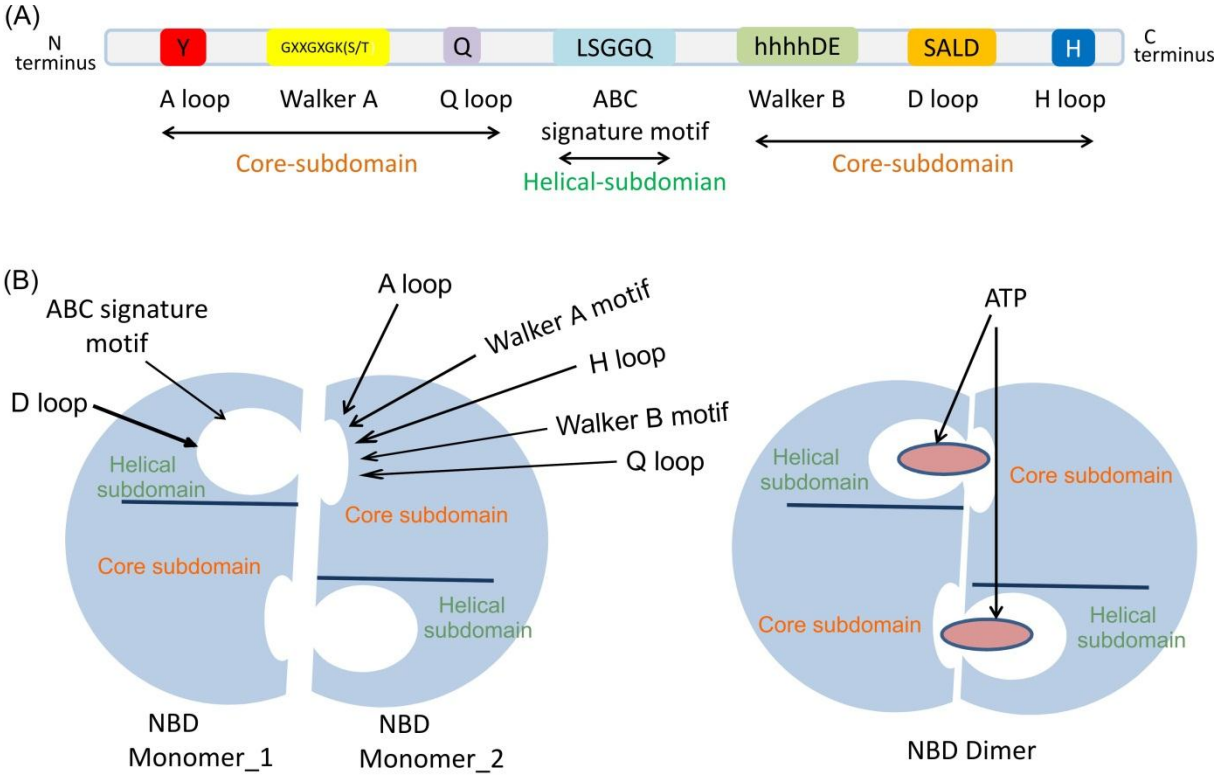

Figure_A4. (A). Schematic representation of conserved regions in the NBD of ABC transporters. From N to C terminus, the conserved regions of the core and the helical subdomains are shown. Each conserved region is denoted by the single amino acids code, where X stands for any amino acid and h represents the hydrophobic amino acid. **(B)** The NBD monomer can be divided into two subdomains: a larger RecA-like core-subdomain and a helical subdomain. All conserved regions of these two subdomains involved in the formation of a nucleotide binding site are illustrated. A closed NBD dimer is formed, when an ATP molecule is bound to each of the two nucleotide binding sites formed by the helical-subdomain of one NBD monomer and the core-subdomain of the second NBD.

A.2.1.1.2 Transmembrane domains

The membrane spanning domains of ABC transporters are structurally heterogeneous and three distinct folds are currently recognized based on structural studies of full length ABC transporters[27]. These folds are named type I ABC importer (or small ABC importers), type II ABC importer (or large ABC importers) and ABC exporter folds[27,28] (Figure_A5).

The type I ABC importer fold was originally observed in the transmembrane subunit of molybdate/tungstate transporter ModBC from *Archaeoglobus fulgidus* [29] and was later found in the transmembrane subunit of $MalFGK_2$[30] and Met transporter MetI[31]. The type I fold is composed of minimally 5 TM helices in each transmembrane domain subunit. A total

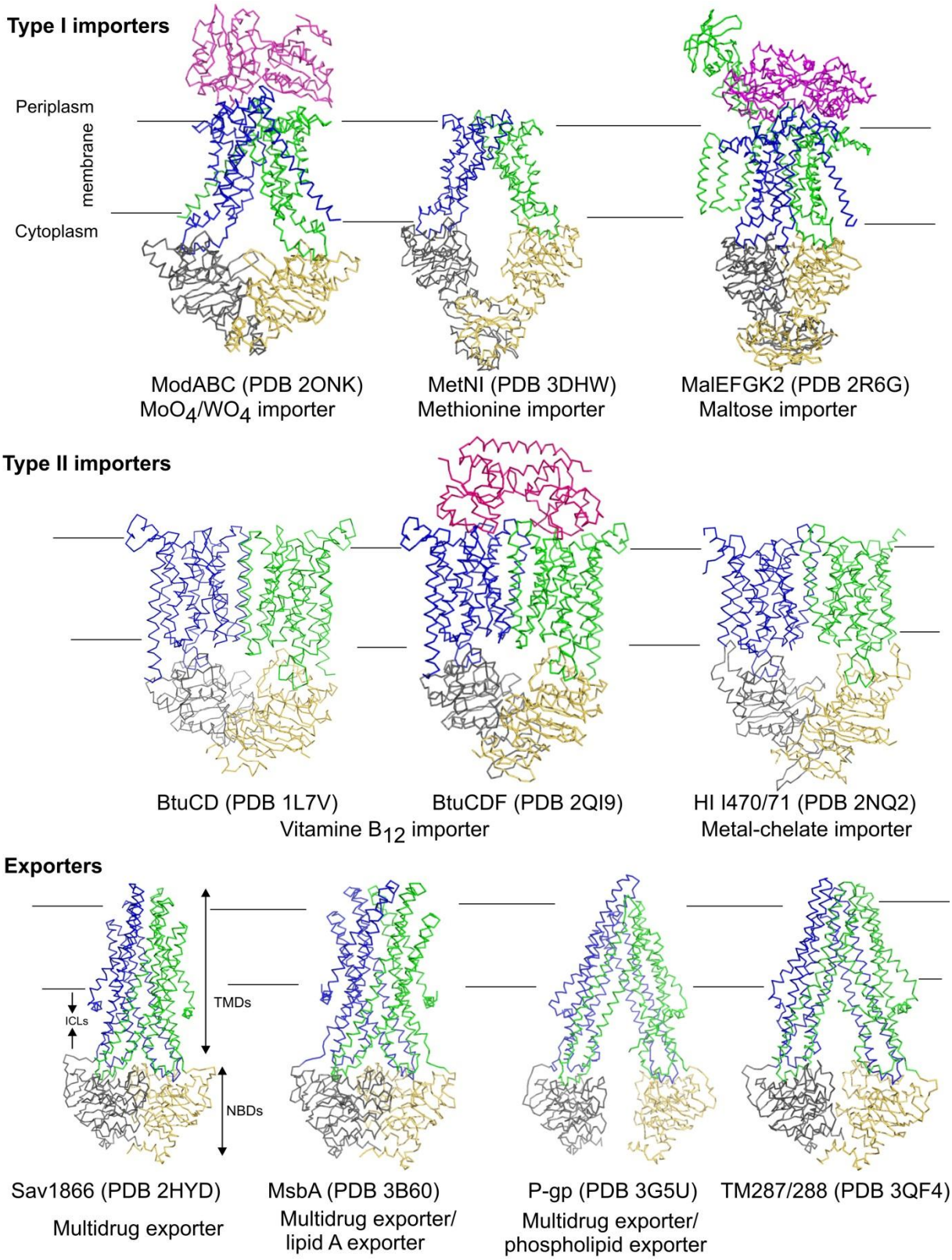

Figure_A5. Structures of type I, type II ABC importers and ABC exporters.

of 10, 12 and 14 transmembrane helices are found in the methionine, molybdate and maltose transporters, respectively[16]. The conformational changes generated by ATP binding and hydrolysis are transmitted from the NBD to the TMD by ''coupling helices''[32]. Coupling helices are located at the tips of the cytoplasmic loops of TM-helices and interact with the α-helical subdomain of NBDs. In the type I importers, coupling helices are formed between TM3 and TM4. The type II ABC importer fold is found in BtuCD and in Hi1471, and contains 10 TM helices in each subunit (20 helices in a full transporter). In this fold, coupling helices are formed between TM6 and TM7. The ABC exporter fold was first observed in Sav1866[32], MsbA[12] and subsequently in TM287/288[33]. In Sav1866, MsbA and TM287/288 each TMD is composed of 6 TM helices (12 in a full transporter). In the outward facing conformation, the TM-spanning region is organized into two wings and each wing is composed of TM3, TM4, TM5, and TM6 of one subunit and TM1, TM2 of the other due to domain swapping. The unique feature of ABC exporters is that the transmembrane domains extend into the cytoplasm by 25 Å. These extended parts of the TMDs are called intracellular loops (ICLs).

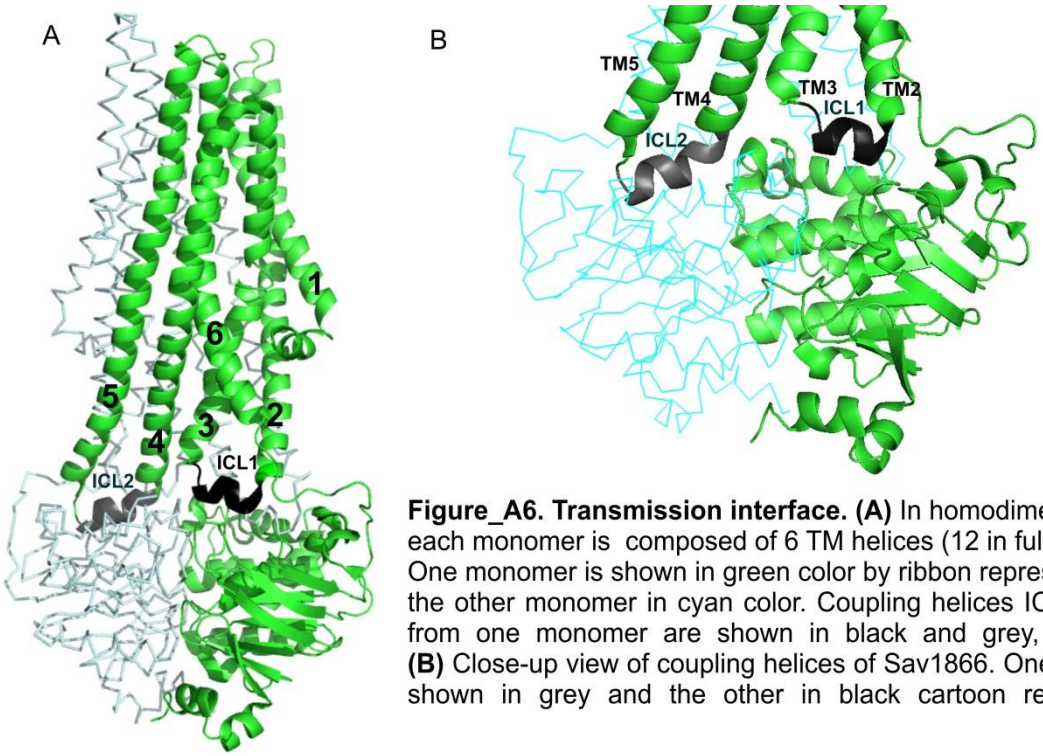

Figure_A6. Transmission interface. (A) In homodimeric Sav1866, each monomer is composed of 6 TM helices (12 in full transporter). One monomer is shown in green color by ribbon representation and the other monomer in cyan color. Coupling helices ICL1 and ICL2 from one monomer are shown in black and grey, respectively. **(B)** Close-up view of coupling helices of Sav1866. One monomer is shown in grey and the other in black cartoon representation.

The transmission interface between the TMDs and NBDs of ABC exporters is established by intracellular loops ICL1 (loop between TM2 and TM3) and ICL2 (loop between TM4 and TM5). These ICLs contain short helices oriented roughly parallel to the membrane plane. The coupling helix 1 (ICL-1) contacts the NBDs of both subunits, while coupling helix 2 (ICL-2) interacts with that of the opposite subunit exclusively[32] (domain swapping) (Figure_A6).

A.3 Membrane protein crystallization

Membrane proteins are difficult to handle due to their amphipathic surface. The hydrophilic surface is exposed to the aqueous environment on both sides of the membrane while the hydrophobic surface is embedded within the lipid bilayer. Non-ionic detergents are used to extract membrane proteins from the lipid bilayers. The detergent mimics the lipid bilayer by covering the hydrophobic surface of the protein generating a protein-detergent micelle. Structure determination of proteins at the atomic level is important for providing insight into the mechanisms of protein function. Crystallization is currently the optimal method for obtaining three-dimensional structural models at atomic resolution for large proteins and membrane proteins.

Membrane proteins are notoriously difficult to crystallize. Even if crystals are obtained their diffraction is often found to be limited, which poses a major barrier to solve a structure. A variety of techniques exist to produce suitable three dimensional crystals; these are based on detergent (in surfo)[7,32], lipid systems (in cubo)[34,35] or on the use of lipid bicelles[34]. The basis of the in surfo method is the incorporation of protein into detergent micelles. The in surfo method has been the most successful and widely used method for membrane protein crystallization.

Conformational heterogeneity, surface chemistry and polydisperse character of membrane proteins are common obstacles in determining the crystal structure of these proteins. A successful alternative approach to overcome these problems is to use auxiliary binding protein, commonly termed as ‘’crystallization chaperones’’. Crystallization chaperones bind to a specific conformation of a target protein, thereby minimizing the conformational heterogeneity and increasing the hydrophilic surface area for crystal lattice formation[36]. These chaperones are divided into two categories; antibody based and non-antibody based scaffolds.

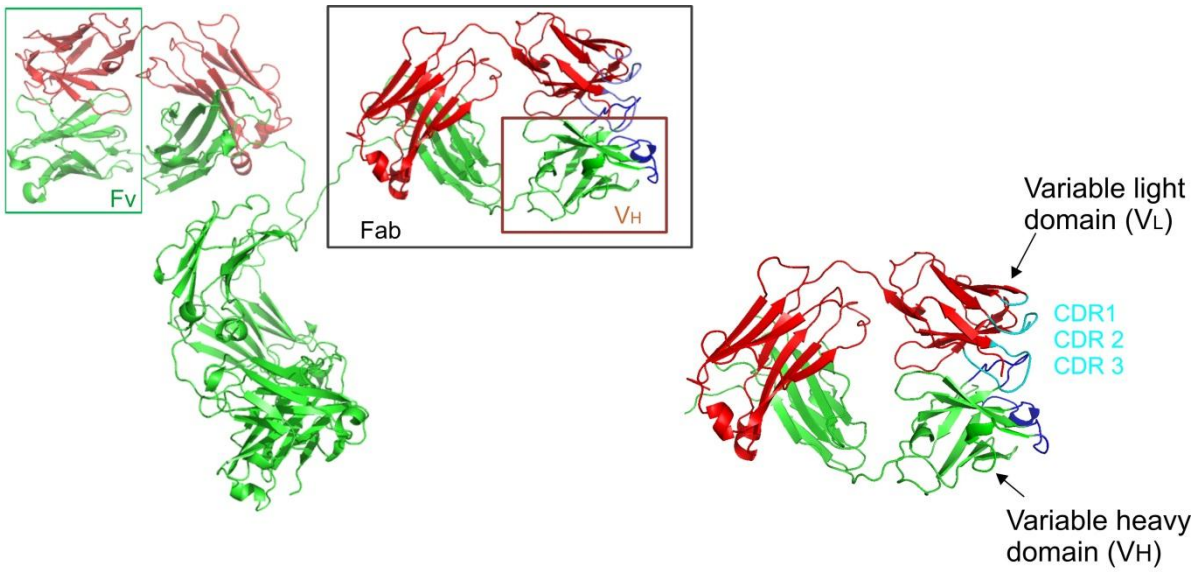

Figure_A7. An antibody molecule. The figure is made using pymol (PDB 1IGT).

A.3.1 Complexing with antibody based scaffolds

The crystal structure of a full length monoclonal antibody IgG2a (PDB 1IGT)[36] is shown in Figure_A7. It is a heterotetramer of 2 heavy chains (green) and 2 light chains (red). The antigen binding site (blue) is formed by 3 loops from each domain, which are highly diverse in sequence and length (3 from light chains (cyan) and 3 from heavy chains (dark blue)). The fragment antigen-binding (Fab fragment) is part of an antibody that binds to an antigen and it is composed of one constant and one variable domain from each heavy and light chain of the antibody. The antigen-binding unit can be further reduced to the Fv consisting of the variable light and heavy chains (V_L and V_H). A single chain variable fragment (scFv) is generated by fusing the V_L and V_H through a polypeptide linker[37-41]. In 1993, Hamers-Casterman *et al* discovered a novel antibody format devoid of light chains in the camelid species, termed as heavy chain antibodies[42] or nanobodies (VHHs). The simplest antigen-binding unit, VHHs is similar in size to the heavy chain variable region domain of Fv fragments from conventional antibodies. The first use of antibody based chaperones can be traced back to co-crystallization of N9 neuraminidase in complex with a Fab fragments originating from monoclonal antibodies[43]. Since then, antibody based chaperones have been successfully used in structure determination of several soluble[44] and membrane proteins[45,46] that are difficult to crystallize. Antibody based scaffolds, Fabs[45] and Fvs[47] in particular, are the dominant chaperones used for the co-crystallization of membrane proteins. In addition to the well-established Fab or Fv fragments, single chain antibody domain such as scFvs or

nanobodies are also used to crystallize challenging proteins such as MazE[48] and β2-adrenergic receptor[49].

A.3.2 Complexing with alternative scaffolds

Non-antibody scaffold based binders such as affibodies, monobodies, and repeat proteins have been developed by protein engineering techniques. These alternative scaffolds retain antibody like properties such as specificity and affinity. They have been developed to improve some of the undesirable properties of antibody based scaffolds. Many of the novel scaffolds are free of disulfide bonds and exhibit high expression yields in bacteria. This thesis focuses on *in vitro* selected **d**esigned **a**nkyrin **r**epeat **p**rote**in** (DARPin) binders. Ankyrin repeat proteins occur in all phyla and mediate important protein–protein interactions in cell compartments[50]. Binz *et al* have used the ankyrin repeat fold to design a consensus based library[51]. Their modular structure is built from stacked, 33-amino acid repeats, each consisting of a β-turn, followed by a pair of antiparallel α helices and a loop that connect to the next repeat[52]. Varying numbers of repeats are stabilized by adding the N and C-terminal capping-repeats, which seal the hydrophobic core from the solvent. Target specific DARPins are selected using ribosome display[51] or phage display[53], and the enriched selected library is further screened by ELISA[54]. A DARPin molecule is often abbreviated as NXC, where X indicates number of internal repeats (Figure_A8).

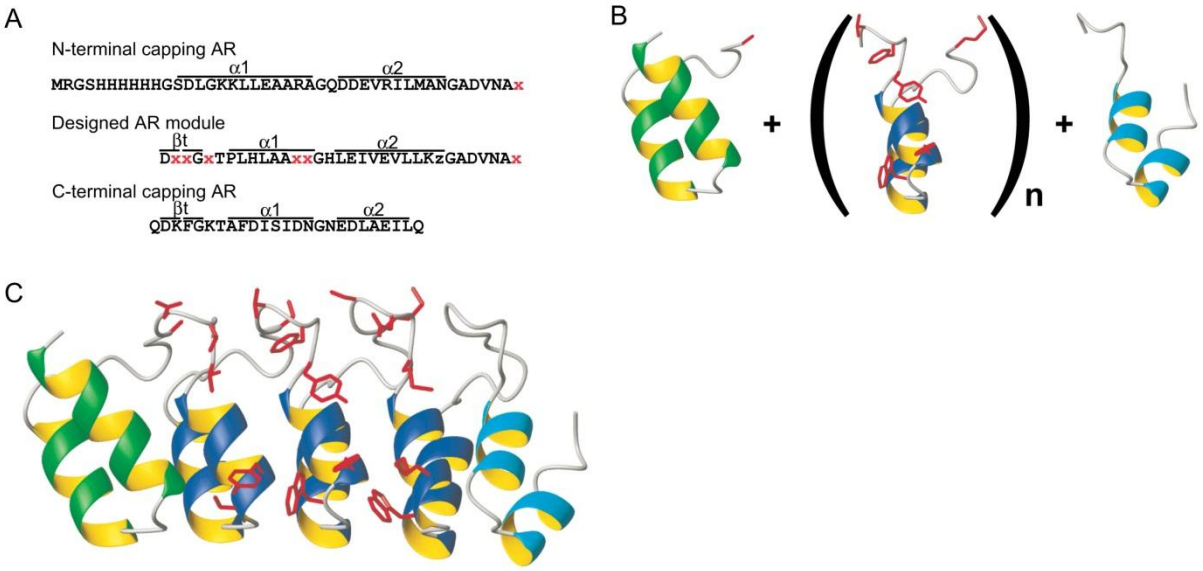

Figure_A8. **(A)** Sequences of the N-terminal cap, the designed internal repeat and the C-terminal cap. The internal repeat module consists of 33 residues, 26 of them are framework residues and 6 are randomized for potential interaction (red x, any of the 20 natural amino acids except cysteine, glycine or proline; z, any of the amino acids asparagine, histidine or tyrosine). **(B)** A DARPin molecule consists of an N-terminal cap (green), varying numbers internal repeat (blue) and a C-terminal cap. **(C)** A N3C DARPin binder with 3 internal repeats is shown. The figure is adapted from Binz et al[52].

Target specific DARPins have been used successfully for the crystallization of several soluble proteins[55-57]. The first structure of a membrane protein in complex with a DARPin was reported for the multidrug transporter AcrB, which was crystallized in an asymmetric conformation[58] (Figure_A9). This work demonstrated the effectiveness of DARPins as a tool for structural and functional studies of challenging proteins.

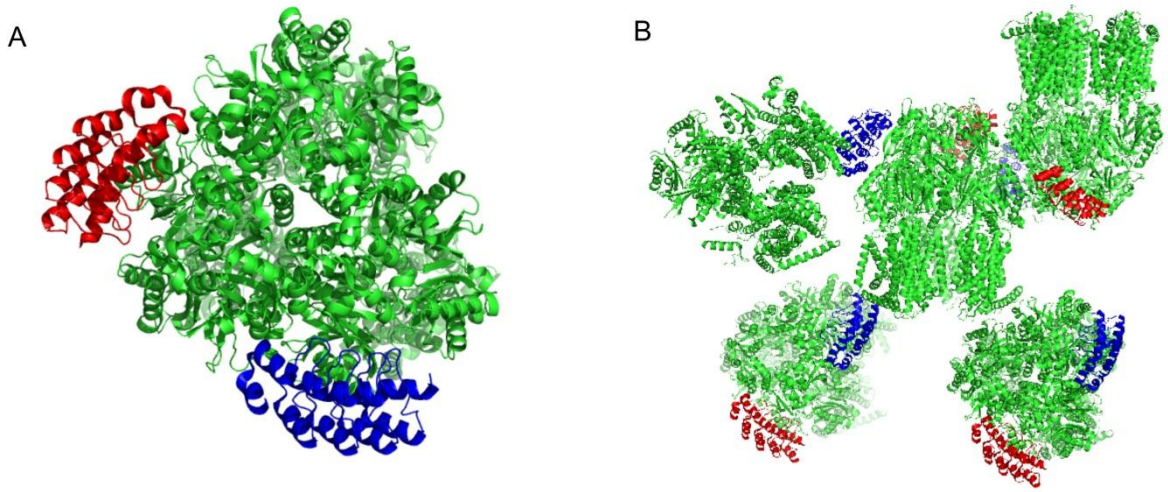

Figure_A9. AcrB-DARPin complex. (A) Two DARPin molecules (red and blue) bind to homotrimeric AcrB (green), and thereby recognize an asymmetric conformation adopted by the transporter. **(B)** Crystal contacts between AcrB molecules are mediated by DARPin. The figure is made using pymol (PDB 2J8S).

A.4 References

1. Singer, S.J. & Nicolson, G.L. The fluid mosaic model of the structure of cell membranes. *Science* **175**, 720-31 (1972).
2. von Heijne, G. The membrane protein universe: what's out there and why bother? *J Intern Med* **261**, 543-57 (2007).
3. Wiener, M.C. & White, S.H. Structure of a fluid dioleoylphosphatidylcholine bilayer determined by joint refinement of X-ray and neutron diffraction data. III. Complete structure. *Biophys J* **61**, 434-47 (1992).
4. Hedin, L.E., Illergard, K. & Elofsson, A. An introduction to membrane proteins. *J Proteome Res* **10**, 3324-31 (2011).
5. Bos, M.P., Robert, V. & Tommassen, J. Biogenesis of the gram-negative bacterial outer membrane. *Annu Rev Microbiol* **61**, 191-214 (2007).
6. Bos, M.P. & Tommassen, J. Biogenesis of the Gram-negative bacterial outer membrane. *Curr Opin Microbiol* **7**, 610-6 (2004).
7. Doyle, D.A. et al. The structure of the potassium channel: molecular basis of K^+ conduction and selectivity. *Science* **280**, 69-77 (1998).
8. Dutzler, R., Campbell, E.B., Cadene, M., Chait, B.T. & MacKinnon, R. X-ray structure of a ClC chloride channel at 3.0 Å reveals the molecular basis of anion selectivity. *Nature* **415**, 287-94 (2002).
9. Luecke, H., Schobert, B., Richter, H.T., Cartailler, J.P. & Lanyi, J.K. Structure of bacteriorhodopsin at 1.55 Å resolution. *J Mol Biol* **291**, 899-911 (1999).
10. Rasmussen, S.G. et al. Crystal structure of the β-2 adrenergic receptor-Gs protein complex. *Nature* **477**, 549-55 (2011).
11. Murakami, S., Nakashima, R., Yamashita, E. & Yamaguchi, A. Crystal structure of bacterial multidrug efflux transporter AcrB. *Nature* **419**, 587-93 (2002).
12. Ward, A., Reyes, C.L., Yu, J., Roth, C.B. & Chang, G. Flexibility in the ABC transporter MsbA: Alternating access with a twist. *Proc Natl Acad Sci U S A* **104**, 19005-10 (2007).
13. Dawson, R.J. & Locher, K.P. Structure of the multidrug ABC transporter Sav1866 from Staphylococcus aureus in complex with AMP-PNP. *FEBS Lett* **581**, 935-8 (2007).
14. Saier, M.H., Jr., Yen, M.R., Noto, K., Tamang, D.G. & Elkan, C. The Transporter Classification Database: recent advances. *Nucleic Acids Res* **37**, D274-8 (2009).
15. Dahl, S.G., Sylte, I. & Ravna, A.W. Structures and models of transporter proteins. *J Pharmacol Exp Ther* **309**, 853-60 (2004).
16. Rees, D.C., Johnson, E. & Lewinson, O. ABC transporters: the power to change. *Nat Rev Mol Cell Biol* **10**, 218-27 (2009).
17. Dean, M., Hamon, Y. & Chimini, G. The human ATP-binding cassette (ABC) transporter superfamily. *J Lipid Res* **42**, 1007-17 (2001).
18. Higgins, C.F. ABC transporters: from microorganisms to man. *Annu Rev Cell Biol* **8**, 67-113 (1992).
19. Dean, M., Rzhetsky, A. & Allikmets, R. The human ATP-binding cassette (ABC) transporter superfamily. *Genome Res* **11**, 1156-66 (2001).
20. Hung, L.W. et al. Crystal structure of the ATP-binding subunit of an ABC transporter. *Nature* **396**, 703-7 (1998).
21. Smith, P.C. et al. ATP binding to the motor domain from an ABC transporter drives formation of a nucleotide sandwich dimer. *Mol Cell* **10**, 139-49 (2002).
22. Schmitt, L., Benabdelhak, H., Blight, M.A., Holland, I.B. & Stubbs, M.T. Crystal structure of the nucleotide-binding domain of the ABC-transporter haemolysin B:

identification of a variable region within ABC helical domains. *J Mol Biol* **330**, 333-42 (2003).
23. Zaitseva, J. et al. A structural analysis of asymmetry required for catalytic activity of an ABC-ATPase domain dimer. *EMBO J* **25**, 3432-43 (2006).
24. Davidson, A.L. & Chen, J. ATP-binding cassette transporters in bacteria. *Annu Rev Biochem* **73**, 241-68 (2004).
25. Jones, P.M. & George, A.M. Subunit interactions in ABC transporters: towards a functional architecture. *FEMS Microbiol Lett* **179**, 187-202 (1999).
26. Higgins, C.F. & Linton, K.J. The ATP switch model for ABC transporters. *Nat Struct Mol Biol* **11**, 918-26 (2004).
27. Locher, K.P. Review. Structure and mechanism of ATP-binding cassette transporters. *Philos Trans R Soc Lond B Biol Sci* **364**, 239-45 (2009).
28. Oldham, M.L., Davidson, A.L. & Chen, J. Structural insights into ABC transporter mechanism. *Curr Opin Struct Biol* **18**, 726-33 (2008).
29. Hollenstein, K., Frei, D.C. & Locher, K.P. Structure of an ABC transporter in complex with its binding protein. *Nature* **446**, 213-6 (2007).
30. Oldham, M.L., Khare, D., Quiocho, F.A., Davidson, A.L. & Chen, J. Crystal structure of a catalytic intermediate of the maltose transporter. *Nature* **450**, 515-21 (2007).
31. Kadaba, N.S., Kaiser, J.T., Johnson, E., Lee, A. & Rees, D.C. The high-affinity *E. coli* methionine ABC transporter: structure and allosteric regulation. *Science* **321**, 250-3 (2008).
32. Dawson, R.J. & Locher, K.P. Structure of a bacterial multidrug ABC transporter. *Nature* **443**, 180-5 (2006).
33. Hohl, M., Briand, C., Grutter, M.G. & Seeger, M.A. Crystal structure of a heterodimeric ABC transporter in its inward-facing conformation. *Nat Struct Mol Biol* **19**, 395-402 (2012).
34. Caffrey, M. Membrane protein crystallization. *J Struct Biol* **142**, 108-32 (2003).
35. Nollert, P., Navarro, J. & Landau, E.M. Crystallization of membrane proteins in cubo. *Methods Enzymol* **343**, 183-99 (2002).
36. Harris, L.J., Larson, S.B., Hasel, K.W. & McPherson, A. Refined structure of an intact IgG2a monoclonal antibody. *Biochemistry* **36**, 1581-97 (1997).
37. Liu, Y.S. & Putnam, F.W. Primary structure of a human IgA1 immunoglobulin. I. Isolation, composition, and amino acid sequence of the chymotryptic peptides. *J Biol Chem* **254**, 2839-49 (1979).
38. Low, T.L., Liu, Y.S. & Putnam, F.W. Primary structure of a human IgA1 immunoglobulin. II. Isolation, composition, and amino acid sequence of the tryptic peptides of the whole alpha1 chain and its cyanogen bromide fragments. *J Biol Chem* **254**, 2850-8 (1979).
39. Liu, Y.S., Low, T.L. & Putnam, F.W. Primary structure of a human IgA1 immunoglobulin. III. Isolation, composition, and amino acid sequence of the thermolysin peptides. *J Biol Chem* **254**, 2859-64 (1979).
40. Putnam, F.W., Liu, Y.S. & Low, T.L. Primary structure of a human IgA1 immunoglobulin. IV. Streptococcal IgA1 protease, digestion, Fab and Fc fragments, and the complete amino acid sequence of the alpha 1 heavy chain. *J Biol Chem* **254**, 2865-74 (1979).
41. Infante, A.J. & Putnam, F.W. Primary structure of a human IgA1 immunoglobulin. V. Amino acid sequence of a human IgA lambda light chain (Bur). *J Biol Chem* **254**, 9006-16 (1979).

42. Hamers-Casterman, C. et al. Naturally occurring antibodies devoid of light chains. *Nature* **363**, 446-8 (1993).
43. Air, G.M., Webster, R.G., Colman, P.M. & Laver, W.G. Distribution of sequence differences in influenza N9 neuraminidase of tern and whale viruses and crystallization of the whale neuraminidase complexed with antibodies. *Virology* **160**, 346-54 (1987).
44. Prongay, A.J. et al. Preparation and crystallization of a human immunodeficiency virus p24-Fab complex. *Proc Natl Acad Sci U S A* **87**, 9980-4 (1990).
45. Zhou, Y., Morais-Cabral, J.H., Kaufman, A. & MacKinnon, R. Chemistry of ion coordination and hydration revealed by a K^+ channel-Fab complex at 2.0 Å resolution. *Nature* **414**, 43-8 (2001).
46. Dutzler, R., Campbell, E.B. & MacKinnon, R. Gating the selectivity filter in ClC chloride channels. *Science* **300**, 108-12 (2003).
47. Iwata, S., Ostermeier, C., Ludwig, B. & Michel, H. Structure at 2.8 Å resolution of cytochrome c oxidase from Paracoccus denitrificans. *Nature* **376**, 660-9 (1995).
48. Loris, R. et al. Crystal structure of the intrinsically flexible addiction antidote MazE. *J Biol Chem* **278**, 28252-7 (2003).
49. Rasmussen, S.G. et al. Structure of a nanobody-stabilized active state of the β-2 adrenoceptor. *Nature* **469**, 175-80 (2011).
50. Bork, P. Hundreds of ankyrin-like repeats in functionally diverse proteins: mobile modules that cross phyla horizontally? *Proteins* **17**, 363-74 (1993).
51. Binz, H.K. et al. High-affinity binders selected from designed ankyrin repeat protein libraries. *Nature Biotechnology* **22**, 575-582 (2004).
52. Kohl, A. et al. Designed to be stable: crystal structure of a consensus ankyrin repeat protein. *Proc Natl Acad Sci U S A* **100**, 1700-5 (2003).
53. Steiner, D., Forrer, P. & Pluckthun, A. Efficient selection of DARPins with sub-nanomolar affinities using SRP phage display. *J Mol Biol* **382**, 1211-27 (2008).
54. Huber, T., Steiner, D., Rothlisberger, D. & Pluckthun, A. *In vitro* selection and characterization of DARPins and Fab fragments for the co-crystallization of membrane proteins: The $Na^{(+)}$-citrate symporter CitS as an example. *J Struct Biol* **159**, 206-21 (2007).
55. Bandeiras, T.M. et al. Structure of wild-type Plk-1 kinase domain in complex with a selective DARPin. *Acta Crystallogr D Biol Crystallogr* **64**, 339-53 (2008).
56. Lo, Y.C. et al. Structural basis for recognition of diubiquitins by NEMO. *Mol Cell* **33**, 602-15 (2009).
57. Schweizer, A. et al. Inhibition of caspase-2 by a designed ankyrin repeat protein: specificity, structure, and inhibition mechanism. *Structure* **15**, 625-36 (2007).
58. Sennhauser, G., Amstutz, P., Briand, C., Storchenegger, O. & Grütter, M.G. Drug Export Pathway of Multidrug Exporter AcrB Revealed by DARPin Inhibitors. *PLoS Biology* **5**, e7 (2007).

CHAPTER B

Asymmetry in the homodimeric ABC transporter MsbA recognized by a DARPin

Anshumali Mittal, Simon Böhm, Markus G. Grütter, Enrica Bordignon, Markus A. Seeger

B.1 Abstract

B.2 Introduction

B.3 Experimental procedure

B.4 Results

B.5 Discussion

B.6 References

B.7 Supplementary information

"This research was originally published in the ***Journal of Biological Chemistry*** Vol. 287, No. 24, pp. 20395-20406, June 8, 2012, © the American Society for Biochemistry and Molecular Biology."

THE JOURNAL OF BIOLOGICAL CHEMISTRY VOL. 287, NO. 24, pp. 20395–20406, June 8, 2012

Asymmetry in the Homodimeric ABC Transporter MsbA Recognized by a DARPin*[S]

Received for publication, March 7, 2012, and in revised form, April 2, 2012 Published, JBC Papers in Press, April 20, 2012, DOI 10.1074/jbc.M112.359794

Anshumali Mittal[‡1], **Simon Böhm**[§], **Markus G. Grütter**[‡], **Enrica Bordignon**[§2], **and Markus A. Seeger**[‡3]

From the [‡]*Department of Biochemistry, University of Zurich, 8057 Zurich, Switzerland and the* [§]*Laboratory of Physical Chemistry, ETH Zurich, 8093 Zurich, Switzerland*

Background: ABC exporters are suggested to hydrolyze ATP sequentially implying the existence of asymmetries.
Results: An *in vitro* selected binder (DARPin) was identified that binds to homodimeric MsbA at a stoichiometric ratio of 1:1.
Conclusion: The DARPin recognizes asymmetries in MsbA.
Significance: Selected binding proteins are useful tools to recognize membrane transporters in novel conformational states.

ABC transporters harness the energy from ATP binding and hydrolysis to translocate substrates across the membrane. Binding of two ATP molecules at the nucleotide binding domains (NBDs) leads to the formation of an outward-facing state. The conformational changes required to reset the transporter to the inward-facing state are initiated by sequential hydrolysis of the bound nucleotides. In a homodimeric ABC exporter such as MsbA responsible for lipid A transport in *Escherichia coli*, sequential ATP hydrolysis implies the existence of an asymmetric conformation. Here we report the *in vitro* selection of a designed ankyrin repeat protein (DARPin) specifically binding to detergent-solubilized MsbA. Only one DARPin binds to the homodimeric transporter in the absence as well as in the presence of nucleotides, suggesting that it recognizes asymmetries in MsbA. DARPin binding increases the rate of ATP hydrolysis by a factor of two independent of the substrate-induced ATPase stimulation. Electron paramagnetic resonance (EPR) measurements are found to be in good agreement with the available crystal structures and reveal that DARPin binding does not affect the large nucleotide-driven conformational changes of MsbA. The binding epitope was mapped by cross-linking and EPR to the membrane-spanning part of the transmembrane domain (TMD). Using cross-linked DARPin-MsbA complexes, 8-azido-ATP was found to preferentially photolabel one chain of the homodimer, suggesting that the asymmetries captured by DARPin binding at the TMDs are propagated to the NBDs. This work demonstrates that *in vitro* selected binders are useful tools to study the mechanism of membrane proteins.

ATP-binding cassette (ABC)[4] transporters are primary active transporters, which act as exporters, importers, receptors, and channels. These transmembrane proteins mediate a plethora of physiological phenomena, including transport of metabolic products, nutrients, proteins, peptides, lipids, polysaccharides, ions, and drugs (1). In humans, malfunction of ABC transporters leads to several genetic disorders including cystic fibrosis, neurological diseases, retinal degeneration, cholesterol, and bile transport defects, anemia, and insufficient drug response.

MsbA is a homodimeric ABC exporter involved in the transport of lipid A and lipopolysaccharides to the outer leaflet of the inner membrane of several Gram-negative bacteria (2), and the *msbA* gene is essential in *Escherichia coli* (3). MsbA is homologous to the multidrug transporter LmrA of Gram-positive *Lactococcus lactis* (4) and mammalian multidrug resistance transporters such as P-glycoprotein (5) and shows overlapping substrate specificity with them (6, 7). At a molecular level, ABC transporters consist of four domains, two transmembrane domains (TMDs) and two nucleotide-binding domains (NBDs). In ABC exporters, the TMDs are composed of at least six transmembrane helices, which form the substrate transport pathway and provide specificity. The NBDs are also known as ATP-binding cassettes and drive the transport cycle by binding and hydrolyzing ATP. The motional energy of the NBDs are coupled to conformational changes in the TMDs which alternate between an inward- and an outward-facing state and thereby form a pathway to mediate unidirectional transport across the membrane (8).

Current molecular understanding of ABC exporters is based on crystal structures of Sav1866 (8) solved at 3 Å in its outward-facing state, P-glycoprotein solved at 3.8 Å in its inward-facing state (5), and the structures of three homologues of MsbA solved in three different conformations at resolutions ranging

* This work was funded by the Swiss NCCR Structural Biology program, an Ambizione Grant from the Swiss National Science Foundation (to M. A. S.) and a Forschungskredit of the University of Zurich (to M. A. S.).
[S] This article contains supplemental Figs. S1–S10 and Table S1.
[1] Affiliated with the Ph.D. Program in Molecular Life Sciences of the Life Science Zurich Graduate School.
[2] To whom correspondence may be addressed: Laboratory of Physical Chemistry, ETH Zurich, Switzerland; E-mail: enrica.bordignon@phys.chem.ethz.ch.
[3] To whom correspondence may be addressed: Department of Biochemistry, University of Zurich, Switzerland; E-mail: m.seeger@bioc.uzh.ch.

[4] The abbreviations used are: ABC, ATP-binding cassette; DARPins, designed ankyrin repeat proteins; EPR, electron paramagnetic resonance; ISOVs, inside-out vesicles; RSOVs, right-side-out vesicles; SEC, size exclusion chromatography; DEER, Double Electron Electron Resonance; AMP-PNP, adenosine 5′-(β,γ-imino)triphosphate; TMD, transmembrane domain; NBD, nucleotide binding domain, M5M, 1,5-pentanediyl bismethanethiosulfonate; M11M, 3,6,9-trioxaundecane-1,11-diyl-bismethanethiosulfonate; DTT, dithiothreitol; MTSSL, 1-oxyl-2,2,5,5-tetramethyl-Δ3-pyrroline-3-methyl) methanethiosulfonate.

from 3.7 Å to 5.5 Å (9). Based on these crystal structures, large conformational changes are expected to occur in ABC exporters upon nucleotide binding and hydrolysis, which could be confirmed by cross-linking experiments and EPR measurements (10–14).

The mechanistic details of how the binding and hydrolysis of ATP at the NBDs is coupled to the transport process at the TMDs are still a matter of controversy. In many heterodimeric ABC transporters, one of the two ATPase sites deviates from the consensus sequence and is therefore called the degenerate site (15). Such heterodimeric ABC exporters mainly hydrolyze ATP at the consensus site and thus operate in an asymmetric fashion. In homodimeric ABC exporters such as BmrA as well as in P-glycoprotein which is a fused heterodimer but exhibits two consensus ATPase sites, biochemical experiments demonstrated that only one ATP molecule is trapped by vanadate in the post-hydrolytic state per ABC transporter dimer (16, 17). It was concluded that ABC exporters hydrolyze the two ATP molecules sequentially instead of simultaneously, possibly involving a mechanism of alternating catalytic sites (18). This mechanism implies that the NBD homodimer must switch to an asymmetric conformation before ATP is hydrolyzed at one of the two catalytic sites. In support of this notion, asymmetric homodimers have been observed in crystal structures of the ATP-bound NBDs of the ABC transporter HlyB (19). On the other hand, current crystal structures of outward-facing MsbA and Sav1866 feature two bound AMP-PNP at the NBDs (thus representing a pre-hydrolytic state) and display only minor structural differences between the two chains, that are related by 2-fold non-crystallographic symmetry (9, 20). Molecular dynamics simulation using the symmetric Sav1866 and MsbA structures as starting points revealed that the NBDs readily switch to an asymmetric state in which only one molecule of ATP enters the hydrolysis reaction at a time (21, 22). Further work addressing the question of asymmetry in ABC exporters is clearly needed to resolve the apparent discrepancies between asymmetries found based on biochemical experiments and the symmetric crystal structures of the homodimers Sav1866 and MsbA.

Designed Ankyrin Repeat Proteins (DARPins) represent a well-established randomized scaffold used as an alternative to antibody fragments (Fabs and scFvs) and have been selected against a variety of target proteins (23–25). A growing number of DARPin co-crystal structures demonstrate the successful application of such designed binding proteins as crystallization aids (24). Besides possible improvements of crystal diffraction, DARPins have the potential to trap the targeted protein in alternate conformations. DARPins selected against the multidrug transporter AcrB for example trap this protein in an asymmetric state with two DARPins bound to the homotrimer (25, 26). In the absence of DARPins, AcrB was initially crystallized in its symmetric and later in its asymmetric state (27, 28).

Here, we describe the selection of DARPins against detergent-purified MsbA using ribosome display. We identified a DARPin which binds to the homodimeric transporter in a 1:1 stoichiometric ratio. The DARPin binding epitope was mapped to the TMDs and was found to be located away from the 2-fold symmetry axis of MsbA, suggesting that the DARPin recognizes asymmetries in MsbA. DEER measurements revealed that addition of the DARPin to MsbA does not influence the large ATP-induced conformational changes during transporter cycling. Nevertheless, DARPin binding enhances the basal ATPase activity of the transporter without impairing the substrate-induced stimulation suggesting that the catalytic cycle is accelerated when asymmetric MsbA conformations are populated.

EXPERIMENTAL PROCEDURES

Purification, Biotinylation, and Spin Labeling of MsbA and DARPin—A detailed description of the cloning, expression, and purification of MsbA is given in the supplemental Experimental Procedures. MsbA was expressed in *E. coli* C43 (DE3) cells from a pBAD vector and purified using β-UDM as detergent. DARPin expression and purification has been described previously (29). Enzymatic biotinylation was facilitated by fusing an Avi-tag sequence to the of MsbA. Single cysteine mutants at positions A25C, R103C, N191C, S206C, and S246C of MsbA were introduced by site-directed mutagenesis taking Cys-less *msbA* (C88S/C315S) as template. Likewise, single cysteine mutants were also introduced into the N- and C-terminal caps of DARPin_55 (which is Cys-less by design) at the positions S12C, K16C, E29C, D151C, and D160C. For methanethiosulfonate cross-linking and spin labeling, single cysteine mutants of MsbA and DARPin were purified by supplementing 5 mM dithiothreitol (DTT), which was removed (PD-10 column, GE Healthcare) prior to labeling with 10 times molar excess of MTSSL ((1-oxyl-2,2,5,5-tetramethyl-Δ3-pyrroline-3-methyl) methanethiosulfonate; Toronto Research Chemicals). Excess spin label was removed by size exclusion chromatography. For the EPR measurements, DARPin-MsbA complexes were made by spin labeling the freshly purified proteins individually, followed by gel-filtration of the protein complex.

Selection and Screening of DARPin Specific to MsbA—The N3C DARPin library (23) was used for binder selection by ribosome display as described (25, 30). Four rounds of selections were carried out following the solution panning strategy (29). 0.05% of β-UDM were used to maintain MsbA in active form. Single clones of the enriched pool of DARPins from the 4th selection round were expressed from the vector $pQE30_{myc5}$ (29)in *E. coli* XL-1 Blue yielding DARPins carrying an N-terminal RGS-His_6 tag (MRGSHHHHHH) and a C-terminal Myc_5 tag (5 times amino acid sequence MEQKLISEEDLNE). Single DARPin clones were analyzed for binding to $bMsbA_{AviC}$ by crude cell extract ELISAs as described previously (29).

SEC of Isolated DARPins and the MsbA-DARPin Complexes—ELISA-positive MsbA-specific DARPins were subcloned into pQE30 (Qiagen) devoid of the C-terminal Myc_5 tag for further biochemical analysis. A molar excess (2 to 3 times) of freshly gel-filtrated monomeric DARPins were mixed with MsbA and incubated in 20 mM Tris/HCl (pH 7.5), 150 mM NaCl, and 0.05% β-UDM for at least 30 min at 4 °C for complex formation. The protein complex was separated on a Superdex 200 10/300 GL column (GE Healthcare) (supplemental Fig. S4). The fractions corresponding to the MsbA-DARPin complex were analyzed by on-chip protein analysis according to the manufacturer's protocol (Protein 80 Kit, Agilent Technologies) (supplemental Fig. S8).

Cysteine Cross-linking of MsbA and DARPin_55 Mutants—For cross-linking studies, two thiol-specific homobifunctional cross-linkers namely M5M (1,5-pentanediyl bismethanethiosulfonate, Toronto Research Chemicals) and M11M (3,6,9-trioxaundecane-1,11-diyl-bismethanethiosulfonate, Toronto Research Chemicals) with spacer arms of 9.1 Å and 16.9 Å were used (32). The MsbA and DARPin_55 mutant proteins were mixed at ratios of 1:3 and incubated with 0.5 mM of cross-linker for 15 min at 4 °C (if not stated otherwise). The reactions were stopped by addition of SDS sample buffer and separated by non-reducing SDS-PAGE. The ability of DARPin_55_29C to cross-link to MsbA_191C was also tested using inside-out membrane vesicles (ISOVs) containing overexpressed MsbA_191C (with detergent purified MsbA_191C, this cross-link is readily formed). To this end, MsbA_191C containing ISOVs (6 mg in 3 ml) were mixed with DARPin_55_29C (35 mg in 7 ml) and M11M (1 mM) was added. After incubation for 30 min, *N*-ethylmaleimide (NEM, 10 mM) was added to react with the remaining free cysteines for another 30 min. Subsequently, MsbA was purified according to the standard protocol and subjected to non-reducing SDS-PAGE (supplemental Fig. S8).

ATPase Assay—The ATPase activity of purified protein was measured from the release of P_i from ATP in a colorimetric malachite green assay as described (33). Briefly, purified protein (200 nM) in 50 mM K-HEPES buffer pH 7.4 containing 0.05% β-UMD, 2.5 mM $MgCl_2$ and 2 mM ATP was incubated at 30 °C in a total reaction volume of 50 μl for 10–15 min. MsbA was inactivated by heating at 80 °C for 2 min and free P_i was measured using malachite green solution. The A_{600} of the samples was measured in a Microplate reader Infinite M100 (TECAN) and compared with the A_{600} of standards containing 0.5–4 nmol P_i. Readings were corrected for P_i contamination originating from the ATP and buffer. DARPin_55-stimulated ATPase activity of MsbA was performed by adding DARPin_55 at concentrations as indicated to MsbA (200 nM) 15 min prior to the assay start. All cysteine mutants used in this study showed ATPase activity comparable to the wild-type. Spin labeling did not affect the activity of MsbA (supplemental Table S1).

Reconstitution of MsbA into Liposomes—Detergent-purified MsbA was reconstituted into lipid membrane vesicles made of polar *E. coli* lipids and egg phosphatidylcholine mixed at a ratio of 3:1 (34). For EPR and DARPin binding experiments, the reconstitution buffer was 20 mM Tris/HCl pH 7.4, 150 mM NaCl, for ATPase activity measurements it was 50 mM K-HEPES pH 7.0. $MgCl_2$ was added only where indicated shortly before performing ATPase activity or EPR experiments to avoid aggregation of the liposomes. The amount of reconstituted MsbA was determined by the Bio-Rad D_C Protein Assay according to manufacturer's protocol and compared BSA protein concentration standards. Binding of DARPin_55 to the reconstituted MsbA was tested by incubating the DARPin_55 with reconstituted MsbA (3:1 ratios) or empty liposomes for 15 min at 4 °C. Unbound DARPin_55 was removed by three buffer washes after centrifugation at 20,000 × *g* for 20 min at 4 °C. The pelleted liposomes were dissolved in SDS buffer and were separated by SDS-PAGE (15% acrylamide gel) followed by SYPRO ruby staining (supplemental Fig. S6*B*).

Distance Measurements by Pulse EPR Experiments—Dipolar time evolution data were acquired using the four-pulse DEER (Double Electron Electron Resonance) experiment (35). DEER traces were measured in a home-made high power Q band spectrometer equipped with a home-made oversized resonator (36). All pulse lengths were set to 12 ns and deuterium modulation artifacts were averaged (8 times d1 time increment of 16 ns). The pump frequency was placed at the maximum intensity of the nitroxide spectrum, and the observer frequency 80 MHz lower. All samples were prepared independently from different batches and the DEER traces were found to be reproducible. Samples contained 10% (*v*/*v*) d8-glycerol and were shock-frozen in liquid nitrogen before measurement. Data analysis was performed with the software DeerAnalysis 2010 (37). The simulation of the possible spin label rotamers attached at selected positions in MsbA was performed using the Matlab program package MMM based on a rotamer library approach (38).

8-N_3-[α-^{32}P]ATP Photolabeling—MsbA191C (1.5 μM) and DARPin_55_29C (6 μM) were cross-linked with M11M (1.5 mM) in 20 mM Tris, pH 7.5, 150 mM NaCl, 0.05% β-UDM containing 3 mM $MgCl_2$. 8-N_3-[α-^{32}P]ATP (1 μM, 0.6 Ci/mmol) was added to 10 μl protein sample (quadruplicates), and the reaction mixtures were incubated at 25 °C for 5 min followed by UV irradiation (100 millijoules, UV cross-linker, Hoefer) on ice. Labeled cross-linked MsbA-DARPin complex was analyzed by SDS-PAGE and photolabeling was quantified using a phosphor imager (Molecular Dynamics, Storm 840). To analyze the amount of cross-linking, four aliquots were supplemented with cold 8-N_3-ATP followed by UV radiation, SDS-PAGE and staining with SYPRO Ruby (Invitrogen). The fluorescent signal was read with the LAS-3000 imaging system, and the bands were quantified using the Aida software (Raytest).

RESULTS

In Vitro Selection and Identification of DARPins Specific for MsbA—DARPin selection against biotinylated avi-tagged MsbA ($bMsbA_{AviC}$) was performed using ribosome display with a DARPin library containing three randomized modules (23, 31, 39) (supplemental Fig. S1). From 2000 DARPin clones analyzed for binding to $bMsbA_{AviC}$ by an initial ELISA (supplemental Fig. S2), 42 DARPins were further analyzed using a specificity ELISA in which besides $bMsbA_{AviC}$ the ABC transporter LmrCD and the secondary-active multidrug transporter AcrB (both prepared as biotinylated Avi-tagged proteins) were used (supplemental Fig. S3). This assay revealed 37 MsbA-specific DARPins that were further analyzed by size-exclusion chromatography. 27 of these DARPins displayed various degrees of oligomerization (soluble aggregates) and 6 of them showed monomer/dimer equilibrium and were therefore excluded. The remaining 4 MsbA-specific DARPins were monomeric but only one DARPin (named DARPin_55) formed a stable complex with MsbA that could be isolated by size exclusion chromatography (supplemental Fig. S4). The affinity of DARPin_55 for MsbA was estimated by competition ELISA (23), in which the binding of $bMsbA_{AviC}$ to immobilized $DARPin\_55_{myc5}$ was competed by pre-incubation with increasing amounts of free DARPin_55. The dissociation constant K_D derived from these experiments was 80 nM (supplemental Fig. S5). Hence, from

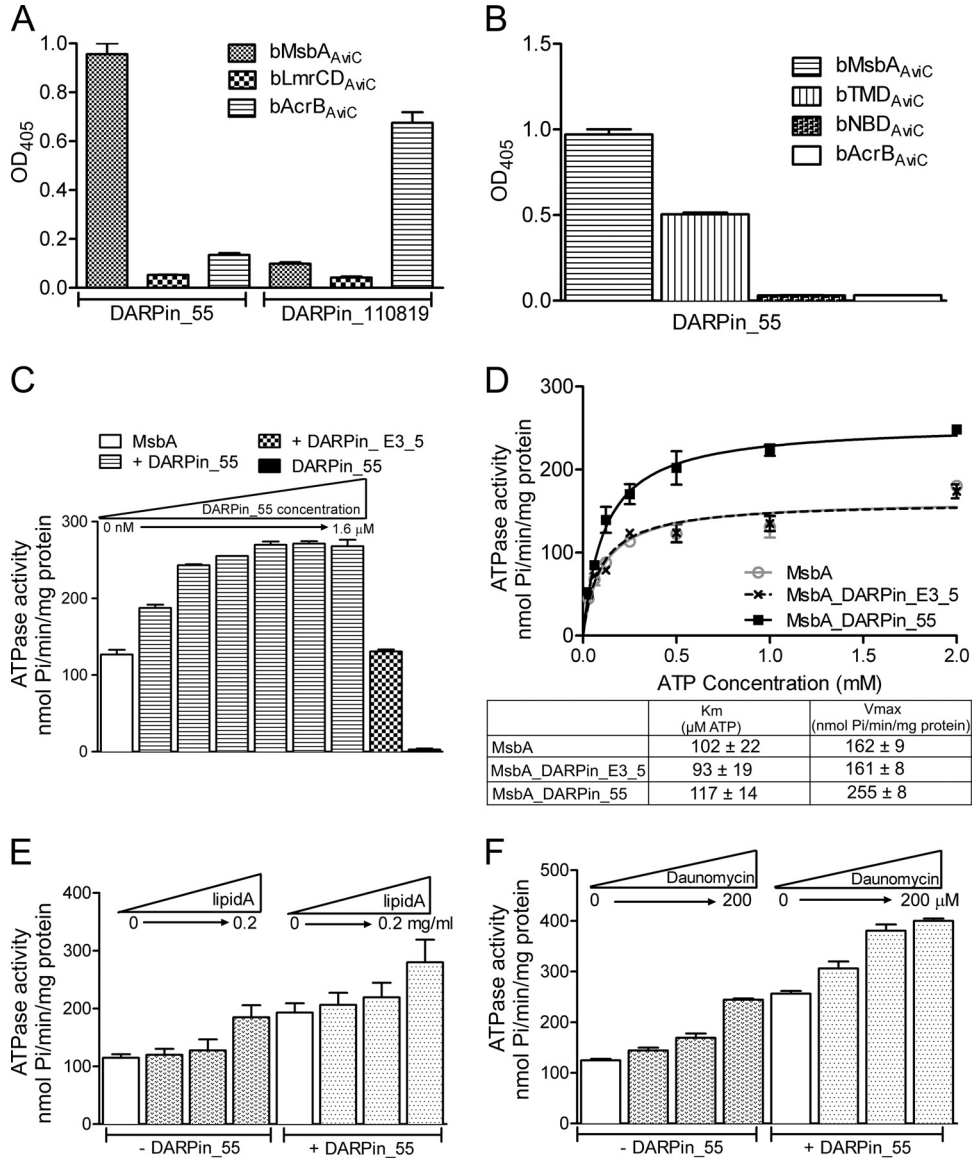

	Km (μM ATP)	Vmax (nmol Pi/min/mg protein)
MsbA	102 ± 22	162 ± 9
MsbA_DARPin_E3_5	93 ± 19	161 ± 8
MsbA_DARPin_55	117 ± 14	255 ± 8

FIGURE 1. **Characterization of DARPin_55: Specificity, epitope mapping and modulation of ATPase activity of MsbA.** *A*, ELISA to determine binding specificity of DARPin_55. DARPin_55 specifically binds to its target protein bMsbA$_{AviC}$ but not to the control proteins bLmrCD$_{AviC}$ and bAcrB$_{AviC}$. DARPin_110819 specifically recognizing bAcrB$_{AviC}$ was used as a control. *B*, ELISA assay to delineate DARPin_55 binding to subdomains of MsbA. DARPin_55 binds to the transmembrane domain (bTMD$_{AviC}$) but not to the nucleotide binding domain (bNBD$_{AviC}$) of MsbA. bAcrB$_{AviC}$ is used as a negative control. *C*, modulation of basal ATPase activity of detergent-solubilized MsbA in complex with DARPin_55. DARPin_55 was added to MsbA (200 nM) in a 2-fold serial dilution series ranging from 50 nM to 1.6 μM leading to a stimulation of the ATPase activity of MsbA by up to 2.1-fold. Addition of the unselected DARPin E3_5 (1 μM) to MsbA does not increase its ATPase activity. DARPin_55 (1 μM) alone does not hydrolyze ATP. *D*, ATPase activity of MsbA was determined in the presence of DARPin_55 (1 μM) or E3_5 (1 μM) as well as in absence of DARPins at varying ATP concentrations. Addition of DARPin_55 results in a higher maximal rate of ATP hydrolysis (V_{max}), while the apparent affinity for ATP (K_m) is not affected. *E* and *F*, stimulations of the ATPase activity of MsbA by substrates and DARPin_55 are additive. Lipid A was added to detergent-purified MsbA at concentrations of 0, 0.05, 0.1, and 0.2 mg/ml *E*, daunomycin was added at concentrations of 0, 50, 100, and 200 μM *F* and ATPase was measured in the absence and presence of DARPin_55 (1 μM). Error bars represent standard deviations.

2000 potential DARPin binders analyzed, we could identify one specific high-affinity binder (Fig. 1*A*).

The ATPase Activity of MsbA Is Stimulated upon Complex Formation with DARPin_55—The effect of DARPin binding to MsbA was studied with respect to the ATPase activity of the transporter. The basal ATPase activity of detergent-purified MsbA (200 nM) was stimulated up to 2.1-fold upon complex formation with DARPin_55 (serial dilution from 50 nM to 1.6 μM) in a dose-dependent manner reaching its maximum at a concentration of 400 nM DARPin_55 (Fig. 1*C*). Addition of the control DARPin E3_5 (39, 40) did not alter the ATPase activity of MsbA and DARPin_55 alone did not hydrolyze ATP. By determining the Michaelis-Menten kinetics of ATP hydrolysis it was found that DARPin_55 binding increases the maximal velocity V_{max} (increase from 162 ± 9 to 255 ± 8 nmol P_i/min/mg MsbA) while the apparent K_m of the ATPase activity remains unchanged (102 ± 22 and 117 ± 14 μM ATP for MsbA and the MsbA/DARPin_55 complex, respectively) (Fig. 1*D*). Lipid A and daunomycin are known substrates of MsbA and were found to stimulate the ATPase activity of the detergent-purified transporter about 2-fold in the absence (41) and 3–4 fold in complex with DARPin_55. This implies that drug-in-

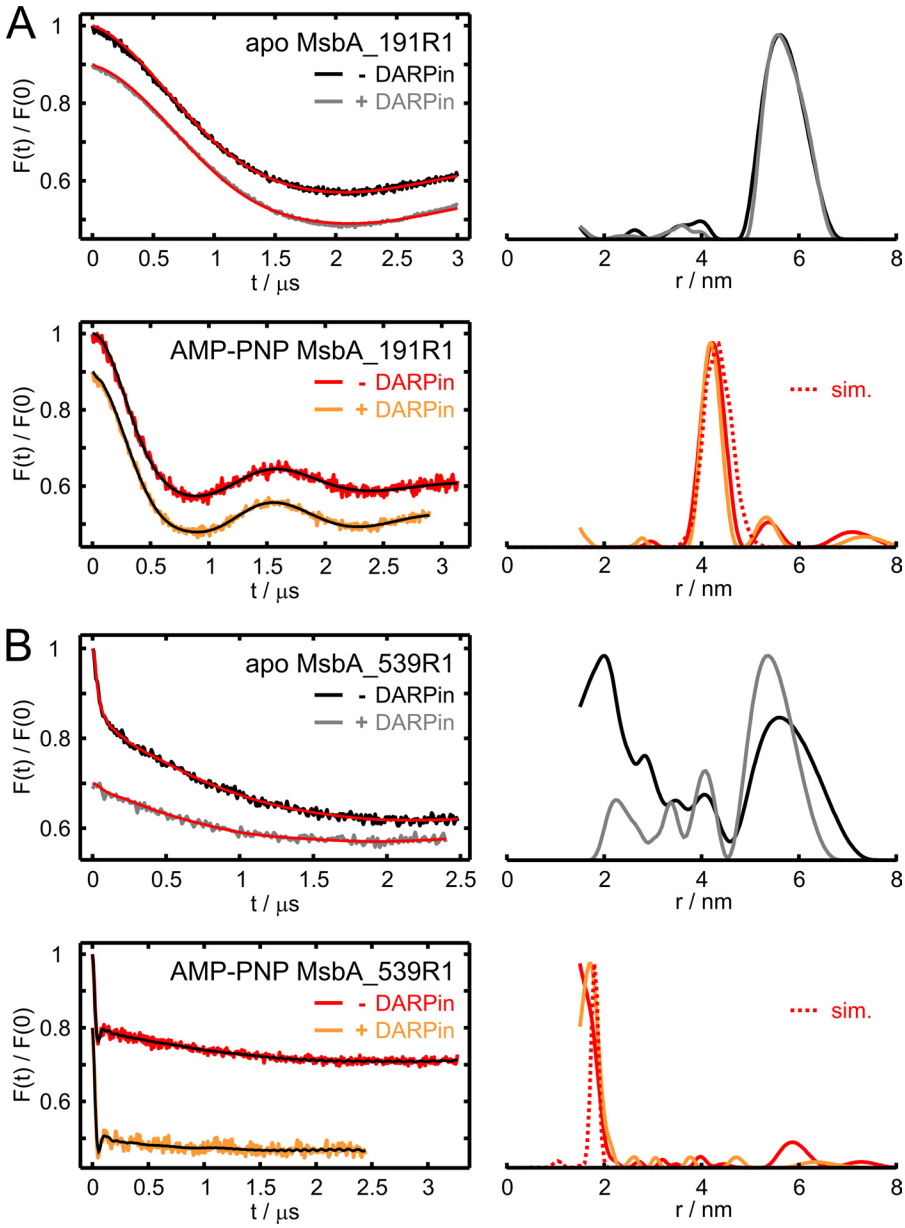

FIGURE 2. **Intra-MsbA distance measurements by DEER reveal no major conformational changes of the transporter upon binding of wild-type DARPin.** *A*, *left*, normalized DEER form factors F(t) and fits obtained with DeerAnalysis2010 on detergent-purified MsbA_191R1 alone and in complex with wild-type DARPin_55. Traces were detected in the apo-state and in the AMP-PNP-state (5 mM AMP-PNP and 5 mM $MgCl_2$) in the absence and in the presence of DARPin_55, as indicated. *Right*, distance distributions obtained with Tikhonov regularization parameters 100 or 1000. The intra-MsbA distances simulated based on the AMP-PNP x-ray structure (PDB 3B60) are superimposed (*red dotted*). *B*, DEER analysis on MsbA_539R1 alone and in complex with DARPin_55 analogous to *A*.

duced and DARPin_55-mediated stimulations of the basal ATPase activity of MsbA are additive (Fig. 1, *E* and *F*). Therefore, DARPin binding does not appear to interfere with MsbA's capability to bind its cargo substrates. MsbA and the MsbA_E506Q (42) mutant (whose ATPase activity is abolished) were reconstituted in proteoliposomes (34). The addition of lipid A and daunomycin stimulate the ATPase activity of reconstituted MsbA about 2-fold as described previously (supplemental Fig. S6) (41). In contrast to detergent-purified MsbA the basal ATPase activity of reconstituted MsbA was not stimulated by the addition of DARPin_55, because DARPin_55 does not bind to membrane-embedded MsbA as discussed below (supplemental Fig. S7).

Binding of DARPin Does Not Impair MsbA Ability to Undergo Conformational Changes—To study the possible structural effects induced by DARPin binding to the transporter, single cysteine mutants of MsbA were labeled with MTSSL and interspin distances between the two labeled sites were measured by DEER in the apo- and AMP- PNP- stsates. The DEER analysis on two representative spin-labeled sites (position 191 in the TMDs and position 539 in the NBDs) is presented in Fig. 2. The 191–191 distance in the apo-state centered at 5.8 nm was found to be in line with the apo crystal structure (9), showing a C_α-C_α distance of 4.7 nm. The distance decreased to 4.1 nm upon addition of AMP-PNP and $MgCl_2$ (Fig. 2*A*), which fully agrees with the interspin distance simulated with the program MMM

(38) based on the AMP-PNP structure of MsbA. Upon complex formation with DARPin_55, MsbA showed the same distance distributions, indicating that the detergent-solubilized MsbA retained the ability to accomplish the conformational changes induced by nucleotide binding (Fig. 2*A*).

The AMP-PNP-state exhibited a sharp 1.8 nm distance between the two 539 labels located in the NBDs, both in the absence and presence of DARPin_55 (Fig. 2*B*). The obtained distance is again in perfect agreement with the crystallographic data, strongly indicating that DARPin binding does not lead to major structural changes in MsbA. The apo-state of the 539 mutant of MsbA showed a peak at about 6 nm in line with the inverted V-shaped apo crystal structure, which is characterized by a C_α-C_α distance of 6.4 nm. A second broad peak between 2 and 4 nm was present which might represent intermediate conformations adopted during NBD closure or disengagement. However, these intermediate states were only observed in this particular mutant and they were strongly suppressed after reconstitution into liposomes (supplemental Fig. S6). Interestingly, adding DARPin_55 to the apo-state of the 539 mutant of MsbA diminished the short distances but did not affect the 6 nm peak suggesting a stabilization of the open-apo structure by DARPin_55 in analogy to the reconstitution into liposomes (Fig. 2*B*, supplemental Fig. S6). Taking into consideration all tested mutants, the inverted V-shaped crystal structure and the outward-facing AMP-PNP bound structure (9) appear to describe the conformational changes of detergent-solubilized MsbA appropriately.

DARPin_55 Binds to the Transmembrane Domain of Detergent-purified MsbA—To delineate the binding epitope of DARPin_55 on full-length MsbA we used purified sub-domains of MsbA, namely the TMD and the NBD. For this purpose, the domains were purified as Avi-tagged biotinylated proteins ($bTMD_{AviC}$ and $bNBD_{AviC}$) and binding to DARPin_55 was assessed by the same ELISA setup as used to identify MsbA-specific DARPins described above (Fig. 1*B*, supplemental Fig. S2). This ELISA experiment revealed that DARPin_55 binds to the transmembrane domain ($bTMD_{AviC}$) but not to the nucleotide binding domain ($bNBD_{AviC}$) of MsbA. Binding of DARPin_55 to $bTMD_{AviC}$ resulted in a comparatively smaller ELISA signal than binding to full length $bMsbA_{AviC}$. This could be due to partially unstructured regions on the TMDs in the absence of the NBDs. Binding of DARPin_55 was further tested using membrane vesicles containing overexpressed MsbA and MsbA reconstituted in proteoliposomes (supplemental Fig. S7). In contrast to detergent-purified MsbA, DARPin_55 did not bind to the membrane-embedded transporter indicating that the binding epitope on MsbA cannot be accessed by DARPin_55 because it is (at least partially) masked by the lipid bilayer.

Cysteine Cross-linking of DARPin and MsbA Mutants—To further specify the binding epitope of DARPin_55 on MsbA, single cysteines were introduced into MsbA and DARPin_55 and proximities between these cysteines were detected using the thiol-specific homobifunctional cross-linkers M5M and M11M. A total of nine single cysteine mutants were made at different positions in the cytoplasmic part of the TMD of MsbA and in DARPin_55 (four in MsbA at positions 103, 191, 206, and 246 and five in DARPin_55 at positions 12, 16, 29, 151, and 160). Using ELISA, each mutated DARPin was confirmed to bind to every single cysteine MsbA mutant (data not shown). All possible combinations of MsbA and DARPin_55 cysteines mutants were then cross-linked as described in the experimental procedures. The single cysteine mutants of MsbA alone did not form any cross-linked products in the presence of M11M and M5M (Fig. 3*A*) nor could any of the DARPin mutants be cross-linked to Cys-less MsbA (supplemental Fig. S8). Cysteines introduced at the N terminus of DARPin_55 (at positions 12, 16, and 29) were efficiently cross-linked to MsbA_191C and to a lesser extent to MsbA_206C and MsbA_246C with both cross-linkers (supplemental Fig. S8). MsbA_103C formed only faint cross-linking products with all DARPin mutants tested. Likewise, the cysteines at the C terminus of DARPin_55 (at positions 151 and 160) were only poorly cross-linked with the four MsbA single cysteine mutants with either cross-linker. These faint cross-linking products seemed promiscuous and were therefore considered as background. In summary, the N terminus of DARPin_55 is in close proximity to the MsbA_191C position whereas the orientation of the C-terminal part of DARPin_55 could not be resolved by only this analysis.

One Molecule of DARPin_55 Binds to the MsbA Homodimer—The maximal degree of DARPin cross-linking to MsbA never seemed to exceed 50% of the MsbA chains (supplemental Fig. S8). To further investigate this phenomenon, cross-linking between DARPin_55_29C and MsbA_191C was carried out in the absence of nucleotides as well as in the presence of AMP-PNP or ATP-vanadate using increasing amounts of DARPin (Fig. 3). Interestingly, cross-linking was saturated at a stoichiometry of approximately one DARPin binding to homodimeric MsbA in its apo-state (Fig. 3*A*). The exact stoichiometry was quantified by SYPRO Ruby staining to 0.73 $\pm$ 0.01 DARPins cross-linked to MsbA (Fig. 4*A*). The presence of AMP-PNP or ATP-vanadate appears to diminish the cross-linking reaction (Fig. 3, *B* and *C*), which might be caused by a longer distance between the thiol groups in this state (see EPR data below) and/or a decreased binding affinity of the DARPin for the nucleotide-bound state(s) of MsbA. Despite multiple attempts, we were not able to perform surface plasmon resonance (SPR) measurements which would have allowed for the determination of binding constants of DARPin_55 recognizing different conformational states of MsbA. The ATPase activity of the DARPin_55_29C/MsbA_191C complex is stimulated by a factor of two compared with MsbA_191C alone and remains unchanged upon cross-linking using M11M (Fig. 3*D*). This indicates that the DARPin_55 remains bound to MsbA during its entire catalytic cycle. Binding stoichiometries were further studied by gel filtration experiments. The MsbA/DARPin_55 complex was separated from excess DARPin_55 by size-exclusion chromatography (supplemental Fig. S4) followed by a quantitative analysis of DARPin_55 and MsbA using the protein chip technology (Agilent Technologies) (supplemental Fig. S9). In agreement with the cross-linking results, the ratio between DARPin_55 and MsbA dimer was quantified to 0.8. The binding stoichiometries in the gel filtration assay as well as in the cross-linking experiment were slightly less than one DARPin bound per MsbA dimer. For the gel filtration assay, this is likely due to partial dissociation of DARPin_55 from

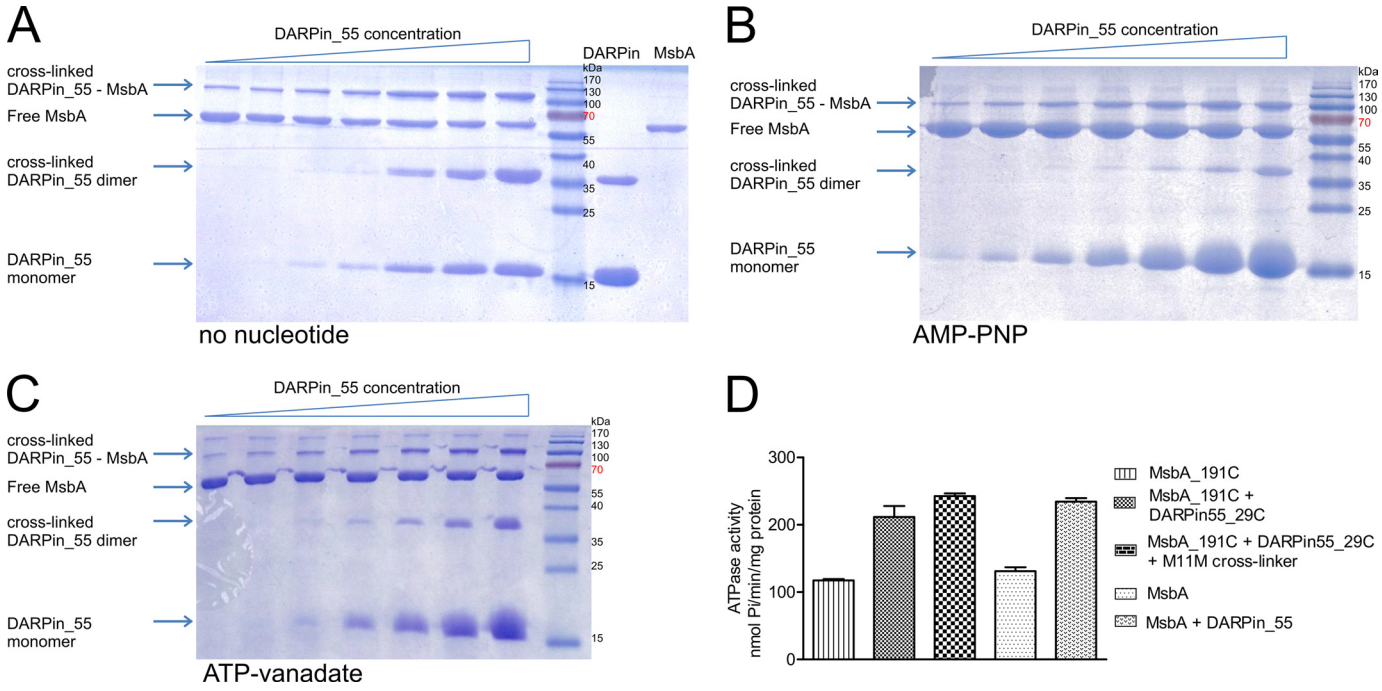

FIGURE 3. **Methanethiosulfonate-mediated cross-linking of one DARPin to homodimeric MsbA.** *A–C*, MsbA_191C (1 μM) was incubated with increasing amounts of DARPin_55_29C (from 500 nM to 16 μM) in the absence of nucleotides *A*, in the presence of $MgCl_2$ (3.5 mM) and AMP-PNP (3 mM) *B*, or ATP-vanadate (2.5 mM, each). *C*, protein complexes were cross-linked using the homobifunctional M11M cross-linker (2 mM) for 15 min at 4 °C and separated by non-reducing SDS-PAGE. *D*, ATPase activities of cross-linked MsbA191C-DARPin_55_29C complexes are equal to those of non-treated MsbA-DARPin complexes and are consistently increased by a factor of two compared with MsbA alone.

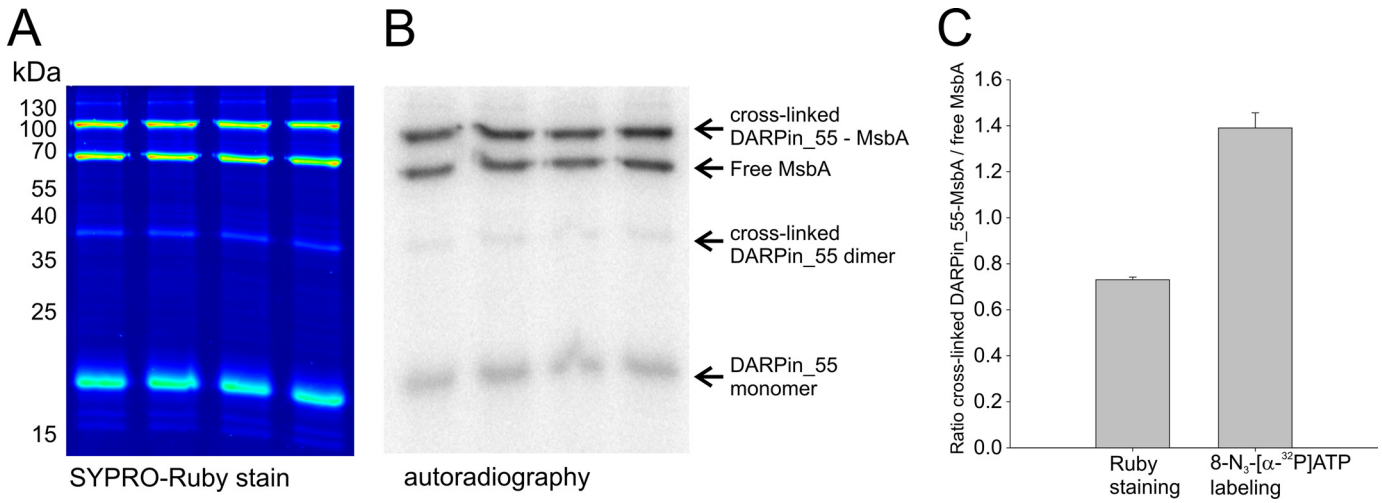

FIGURE 4. **Preferential nucleotide binding to one chain of asymmetrically stabilized MsbA as determined by 8-N_3-[α-^{32}P]ATP photolabeling.** *A* and *B*, DARPin_55_29C was cross-linked to MsbA_191C using M11M, followed by addition of 8-N_3-[α-^{32}P]ATP (1 μM) and UV-cross-linking (performed as quadruplicates). The samples were separated by non-reducing SDS-PAGE and analyzed by SYPRO Ruby staining *A* and autoradiography *B*. *C*, band intensities corresponding to cross-linked DARPin-MsbA complex and free MsbA monomer obtained in *A* and *B* were quantified.

MsbA during the size-exclusion run whereas in the cross-linking experiment, some of the thiol moieties of the cysteines might have undergone oxidation during the purification and as a consequence would not react with the methanethiosulfonate cross-linker. At this point, two scenarios can explain the binding stoichiometry of one DARPin bound per homodimeric MsbA: (i) Binding of the first DARPin molecule to MsbA sterically prevents binding of the second or (ii) the DARPin recognizes asymmetries in MsbA.

EPR Distances between DARPin_55 and MsbA—To rule out possible steric clashes between the two DARPins in the complex, the binding epitope of DARPin_55 on MsbA was mapped by EPR. Various combinations of five spin-labeled single cysteine mutants spanning the MsbA structure (positions 25, 65, 103, 191, 482) and two spin-labeled DARPin_55 (positions 29 or 160) were measured to extract interspin distances by DEER.

Because of the 1:1 stoichiometric ratio between DARPin_55 and MsbA, binding of one spin-labeled DARPin to the homodimeric spin-labeled transporter gives rise to a three-spin complex. This was confirmed by measuring the spin concentration in the MsbA-DARPin complexes using continuous wave EPR (data not shown). To disentangle the intra-MsbA from the

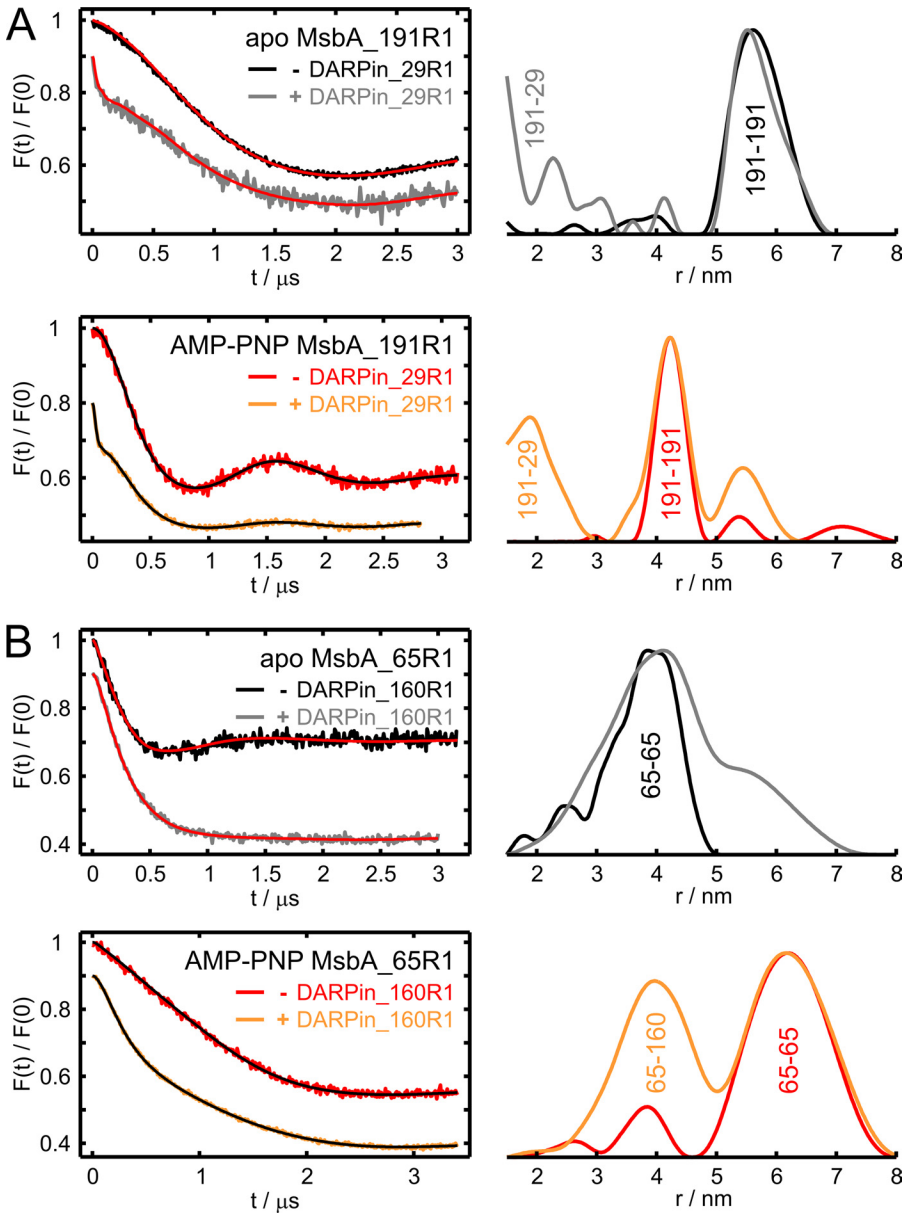

FIGURE 5. **Determination of the binding epitope of DARPin_55 by DEER.** *A*, *left*, normalized DEER form factors F(t) and fits obtained with DeerAnalysis2010 on detergent-purified MsbA_191R1 alone and in complex with DARPin_55 spin labeled at position 29 (N-cap). Traces were detected in the apo-state and in the AMP-PNP-state (5 mM AMP-PNP and 5 mM $MgCl_2$) in the absence and in the presence of DARPin_55_29R, as indicated. *Right*, distance distributions obtained with Tikhonov regularization parameters 100 or 1000. Assigned MsbA-DARPin distances are marked in the distance distribution. *B*, DEER analysis on MsbA_65R1 alone and in complex with DARPin_55 spin labeled at position 160 (C-cap) analogous to *A*. The vicinity of the intra-MsbA and DARPin-MsbA distances in the apo-state prevented a clear assignment of the DEER constraint.

MsbA-DARPin distances, we measured the MsbA alone and in the presence of the DARPin. To reduce the known effects of three-spin artifacts in the distance distributions (44), the intra-MsbA and the MsbA-DARPin distances should be as distinct as possible.

Among all combinations tested, only two (MsbA_191R1-DARPin_55_29R1 and MsbA_65R1-DARPin_55_160R1, with R1 denoting the MTSSL spin-labeled side chain) resulted in extractable MsbA-DARPin distances (Fig. 5) (all DEER distances are presented in Fig. 6). The intra-MsbA_191R1 distances in the apo- and AMP-PNP- states are shown in Fig. 5*A*. Addition of DARPin_55_29R1 resulted in the appearance of a short distance peak at 1.5–2 nm confirming the close proximity of the N-terminal region (N-cap) of DARPin_55 to position 191 in the TMDs already observed by cross-linking (supplemental Fig. S8). Interestingly, the distance between these two positions becomes slightly longer (~2 nm) in the presence of AMP-PNP. In agreement with the DEER results obtained with unlabeled DARPin_55 (Fig. 2*A*), the intra-MsbA_191R1 distance remains unchanged upon addition of DARPin_55_29R1 in the apo-state and in the presence of AMP-PNP (Fig. 5*A*). The longer distance observed between the two nitroxide labels in MsbA and DARPin_55 might explain the reduced degree of M11M mediated cross-linking observed upon addition of nucleotides (Fig. 3, *B* and *C*).

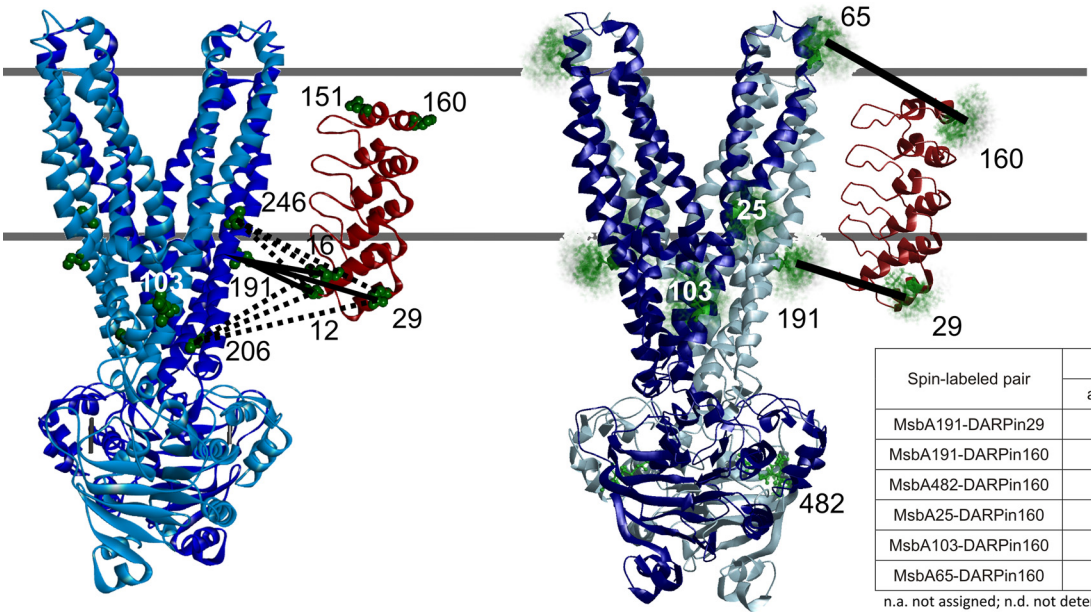

Spin-labeled pair	MsbA-DARPin distance	
	apo state	AMP-PNP
MsbA191-DARPin29	~ 2 nm	~ 2 nm
MsbA191-DARPin160	> 5 nm	n.d.
MsbA482-DARPin160	> 7 nm	n.d.
MsbA25-DARPin160	> 6 nm	n.d.
MsbA103-DARPin160	> 6 nm	n.d.
MsbA65-DARPin160	n.a.	3.9 nm

n.a. not assigned; n.d. not determined.

FIGURE 6. **The MsbA-DARPin complex based on cross-linking and DEER data.** *A*, overview of the cross-linking data (supplemental Fig. S8) using the x-ray structure of MsbA (PDB 3B60) and a homology model of DARPin_55 as templates. The *black straight lines* indicate thiol pairs showing strong cross-links, the *black dotted lines* denote pairs showing weak cross-links. *B*, overview of interspin distances between MsbA and DARPin_55. The possible spin label rotamers attached at selected positions in MsbA were simulated using the Matlab program package MMM and are indicated as *green clouds*. The *black straight lines* highlight the pairs for which DEER constraints were obtained. All DEER data including the restraints are presented in the table.

Whereas the position of the N-cap of DARPin_55 with respect to the TMD could be readily mapped by cross-linking and EPR, the orientation of the DARPin's C-cap was challenging to find, also because no cross-link could be established between the 151 and 160 positions of DARPin_55 and any of the MsbA mutants used (supplemental Fig. S8). After screening by DEER a number of complexes with DARPin_55 labeled at the C-cap (position 160), we found a clear distance constraint between the C-cap and the extracellular region of the transporter (position 65). In aggrement with the structural changes expected from the x-ray data, addition of AMP-PNP to isolated MsbA resulted in an increase of the 65–65 distance from 4 to 6 nm (Fig. 4*B*). When DARPin_55_160R1 was analyzed in complex with MsbA_65R1, we found a distinct MsbA-DARPin_55 distance centered at 3.9 nm in the AMP-PNP-state, while the overlap with the intra-MsbA distance prevented a clear MsbA-DARPin_55 distance assignment in the apo-state. In contrast, we could exclude distances < 5 nm between the C-cap of DARPin_55 and other spin labels in the NBDs (position 482) and in the cytoplasmic-facing region of the TMDs (positions 25, 103, 191) (Fig. 6). Based on these observations we could rule out that the C-cap is oriented toward the NBDs, thus the transmembrane domain of MsbA seems to be covered at least partially by DARPin_55. Importantly, the DARPin binding epitope was found to be far away from the 2-fold symmetry axis of MsbA, thus ruling out the possibility of steric clashes between two DARPins as the cause for the stoichiometric ratio observed.

The ATPase Sites of Asymmetrically Stabilized MsbA Display Different Nucleotide Binding Properties—Cross-linking DARPin_55_29C to asymmetric MsbA_191C provides the unprecedented advantage that the conformationally unequal chains of homodimeric MsbA can be separated by SDS-PAGE. Thus questions as whether the two ATPase sites of asymmetric MsbA display differences with respect to nucleotide binding can be for the first time addressed. The cross-linked DARPin-MsbA complex was incubated with 8-N_3-[α-^{32}P]ATP followed by UV cross-linking of the nucleotide to the two chains of MsbA. Subsequently, the proteins were separated by SDS-PAGE and the amount of cross-linking was determined by autoradiography (Fig. 4). The ratio between the bands of DARPin_55 cross-linked to MsbA and MsbA alone was quantified to be 0.73 $\pm$ 0.01 by SYPRO Ruby staining. Interestingly, the MsbA chain cross-linked to DARPin_55 showed a stronger photolabeling with 8-N_3-[α-^{32}P]ATP than the MsbA chain alone (ratio between MsbA-DARPin_55 to MsbA of 1.39 $\pm$ 0.07). This indicates that the MsbA monomer to which the DARPin was cross-linked to was photolabeled 1.9 times stronger than the free MsbA chain.

DISCUSSION

Asymmetries in the NBDs of ABC exporters arising from trapping of nucleotides by vanadate have been discussed since the mid-nineties when Urbatsch and Senior first described the catalytic cycle of P-glycoprotein and later were also found in the homodimeric transporter BmrA (16, 17). Using an *in vitro* selected DARPin binder, we provide here novel evidence supporting considerable asymmetries to be found in a well-studied ABC exporter.

Our biochemical analysis shows that DARPin_55 binds to the TMDs of MsbA in a stoichiometry of one DARPin per homodimeric transporter. The binding epitope was mapped to the TMDs of MsbA and therefore, the possibility that binding of the first DARPin sterically hinders binding of a second DARPin to the symmetry-related epitope on MsbA could be excluded. In further support of this notion, DARPin binding does not affect the closure of the NBDs and the transition to the

outward-facing state of MsbA upon addition of AMP-PNP. The DARPin therefore recognizes asymmetries in MsbA.

Asymmetric homodimers are not unusual. The epidermal growth factor receptor from *Drosophila* has been recently crystallized in an asymmetric state in complex with two growth factor ligands binding in a low- and a high-affinity mode (45). Caspase-9 is activated by dimerization and was crystallized as asymmetric homodimer exhibiting one active and one inactive catalytic site (46). However, despite serious efforts we did not succeed to solve the co-crystal structure of the MsbA-DARPin_55 complex and therefore the molecular details of the asymmetries in MsbA remain elusive.

Epitope mapping revealed that the DARPin binding site includes membrane-spanning portions of the TMD (Fig. 6). There are two observations which further support this unexpected finding. First, DARPin_55 only binds to MsbA in its detergent-purified but not in its membrane-bound form (supplemental Fig. S7). In a detergent-purified MsbA sample, free detergent monomers, protein-free detergent micelles and detergent bound to the membrane protein are in equilibrium (47). There is constant rapid exchange of detergents molecules between these pools. Lipid bilayers in contrast are more rigid (48). It is therefore likely that DARPin_55 partly displaces the detergent micelle, but not the relatively stiffer lipid membrane to bind to its epitope. Second, in agreement with the positioning of DARPin_55 with respect to the membrane boundary, the randomized positions in the β-turns of the second and the third DARPin repeat exclusively harbor hydrophobic amino acids (supplemental Fig. S10). These residues could mediate hydrophobic contacts with the transmembrane helices of MsbA, whereas in the first repeat, there are two glutamates which could interact with the cytoplasmic portion of the TMD. Importantly, DARPin_55 only recognizes MsbA, but not its homologue LmrCD or the multidrug transporter AcrB. Therefore, unspecific hydrophobic interactions of DARPin_55 with membrane proteins in general can be excluded. Interestingly, the presence of DARPin_55 increased the ATPase activity of the β-UDM-solubilized transporter by influencing the V_{max} term, independent of the substrate-induced stimulations. This finding is reminiscent of a recent biochemical characterization of the P-glycoprotein-specific antibody MRC16 the addition of which was found to increase the ATPase activity of the transporter in the absence as well as in the presence of the substrate nicardipine (49).

It has often been argued that *in vitro* selected binding proteins may distort the target protein thereby trapping it in an unnatural and non-physiological state. However, numerous examples of crystal structures solved alone and in complex with a binding partner in very similar conformations speak against this argument (as reviewed in Refs. 24, 50, 51). One prominent example reminiscent to the study presented here is the homotrimeric multidrug transporter AcrB, that has been crystallized alone and in complex with DARPins in an asymmetric conformation in which each conformer represents a consecutive step of the transport cycle (25, 27, 28). Only two DARPins were found to bind to the trimer, and at the third expected DARPin binding site, a steric clash between a conformationally altered subdomain of AcrB with the back side of the DARPin prevented binding (25, 26). The DARPins did not induce the asymmetric state, but rather recognized the intrinsic asymmetry of the targeted protein. It is therefore plausible that the asymmetric conformational states of MsbA to which DARPin_55 binds to belong to the intrinsic ensemble of possible conformations of the transporter.

DEER and cross-linking experiments show that DARPin_55 binds to homodimeric MsbA in the apo-state as well as in the presence of AMP-PNP and ATP-vanadate and therefore the recognized asymmetries in MsbA do not appear to be state-specific. In support of this notion, cross-linked MsbA-DARPin complexes retain their increased ATPase activity suggesting that the DARPin remains bound during the entire catalytic cycle. Importantly, DARPin binding does not trap MsbA in an asymmetric state, which would lead to an inhibition of the ATPase activity, but rather enables the transporter to interconvert between conformations necessary for function at a higher rate. Our findings stand in partial contrast to a recent study on P-glycoprotein antibodies MRK16 and UIC2, which were shown to bind to the transporter in the apo-state as well as in the presence of AMP-PNP (pre-hydrolytic state), but not if the transporter is trapped with ADP-vanadate (post-hydrolytic state) (49). In addition to earlier studies dealing with the asymmetric nature of the catalytic cycle at the NBDs (16, 17), our results indicate that distinct asymmetries also inhere to the TMDs of MsbA where the DARPin_55 epitope is located. Lipid A, the natural substrate of MsbA, is rather big (molecular weight of around 1.8 kDa) and asymmetric. Therefore, it is plausible to assume that only one molecule of lipid A can be accommodated by the substrate binding cavity of MsbA which might require asymmetries in the TMDs. We found that the ATPase activity of detergent-purified MsbA was stimulated by lipid A and daunomycin. Our observations with lipid A agree with a previous study (41), although the stimulation observed by us is not as pronounced as reported, whereas in the same study stimulation of the ATPase by daunomycin was not apparent. These differences might arise from the different detergents used for purification of MsbA (β-UDM in our case and β-DM in the mentioned study (41)). Interestingly, the stimulation of MsbA's ATPase activity by lipid A or daunomycin and DARPin_55 are additive (Fig. 1, *D* and *E*). DARPin binding therefore does not seem to interfere with substrate interactions at the binding cavity. 8-N_3-[α-^{32}P]ATP was shown to preferentially photolabel one of the chains of asymmetric homodimeric MsbA, hence supporting the notion that the asymmetries recognized by the DARPin at the TMDs are conformationally linked to the nucleotide binding sites at the NBDs and *vice versa*. Since photocross-linking using 8-N_3-[α-^{32}P]ATP is a non-equilibrium binding method, further biochemical analyses are difficult. Nevertheless, in symmetric MsbA both nucleotide binding sites are identical and expected to be labeled by equal amounts of 8-N_3-[α-^{32}P]ATP. This is not the case and therefore, the two nucleotide binding sites are different from each other. As previously proposed based on biochemical experiments and molecular dynamics simulations, the asymmetric switching at the NBDs might be a prerequisite for ATP hydrolysis (16, 17, 19, 21). Our data suggest that DARPin binding to MsbA populates asymmetric states of the transporter from an

ensemble of structurally similar conformations which exhibits increased basal ATPase activities and is fully compatible with its function to bind lipid A and drugs.

Acknowledgment—We thank Michael Hohl for valuable discussions.

REFERENCES

1. Holland, I. B. (2011) ABC transporters, mechanisms and biology: an overview. *Essays Biochem.* **50,** 1–17
2. Zhou, Z., White, K. A., Polissi, A., Georgopoulos, C., and Raetz, C. R. (1998) Function of *Escherichia coli* MsbA, an essential ABC family transporter, in lipid A and phospholipid biosynthesis. *J. Biol. Chem.* **273,** 12466–12475
3. Polissi, A., and Georgopoulos, C. (1996) Mutational analysis and properties of the msbA gene of *Escherichia coli*, coding for an essential ABC family transporter. *Mol. Microbiol.* **20,** 1221–1233
4. van Veen, H. W., Venema, K., Bolhuis, H., Oussenko, I., Kok, J., Poolman, B., Driessen, A. J., and Konings, W. N. (1996) Multidrug resistance mediated by a bacterial homolog of the human multidrug transporter MDR1. *Proc. Natl. Acad. Sci. U.S.A.* **93,** 10668–10672
5. Aller, S. G., Yu, J., Ward, A., Weng, Y., Chittaboina, S., Zhuo, R., Harrell, P. M., Trinh, Y. T., Zhang, Q., Urbatsch, I. L., and Chang, G. (2009) Structure of P-glycoprotein reveals a molecular basis for poly-specific drug binding. *Science* **323,** 1718–1722
6. Reuter, G., Janvilisri, T., Venter, H., Shahi, S., Balakrishnan, L., and van Veen, H. W. (2003) The ATP-binding cassette multidrug transporter LmrA and lipid transporter MsbA have overlapping substrate specificities. *J. Biol. Chem.* **278,** 35193–35198
7. Woebking, B., Reuter, G., Shilling, R. A., Velamakanni, S., Shahi, S., Venter, H., Balakrishnan, L., and van Veen, H. W. (2005) Drug-lipid A interactions on the *Escherichia coli* ABC transporter MsbA. *J. Bacteriol.* **187,** 6363–6369
8. Dawson, R. J., and Locher, K. P. (2006) Structure of a bacterial multidrug ABC transporter. *Nature* **443,** 180–185
9. Ward, A., Reyes, C. L., Yu, J., Roth, C. B., and Chang, G. (2007) Flexibility in the ABC transporter MsbA: Alternating access with a twist. *Proc. Natl. Acad. Sci. U.S.A.* **104,** 19005–19010
10. Zou, P., Bortolus, M., and McHaourab, H. S. (2009) Conformational cycle of the ABC transporter MsbA in liposomes: detailed analysis using double electron-electron resonance spectroscopy. *J. Mol. Biol.* **393,** 586–597
11. Smriti, Zou, P., and McHaourab, H. S. (2009) Mapping daunorubicin-binding sites in the ATP-binding cassette transporter MsbA using site-specific quenching by spin labels. *J. Biol. Chem.* **284,** 13904–13913
12. Borbat, P. P., Surendhran, K., Bortolus, M., Zou, P., Freed, J. H., and McHaourab, H. S. (2007) Conformational motion of the ABC transporter MsbA induced by ATP hydrolysis. *PLoS Biol.* **5,** e271
13. Zou, P., and McHaourab, H. S. (2009) Alternating access of the putative substrate-binding chamber in the ABC transporter MsbA. *J. Mol. Biol.* **393,** 574–585
14. Doshi, R., Woebking, B., and van Veen, H. W. (2010) Dissection of the conformational cycle of the multidrug/lipidA ABC exporter MsbA. *Proteins* **78,** 2867–2872
15. Procko, E., O'Mara, M. L., Bennett, W. F., Tieleman, D. P., and Gaudet, R. (2009) The mechanism of ABC transporters: general lessons from structural and functional studies of an antigenic peptide transporter. *FASEB J.* **23,** 1287–1302
16. Urbatsch, I. L., Sankaran, B., Weber, J., and Senior, A. E. (1995) P-glycoprotein is stably inhibited by vanadate-induced trapping of nucleotide at a single catalytic site. *J. Biol. Chem.* **270,** 19383–19390
17. Orelle, C., Dalmas, O., Gros, P., Di Pietro, A., and Jault, J. M. (2003) The conserved glutamate residue adjacent to the Walker-B motif is the catalytic base for ATP hydrolysis in the ATP-binding cassette transporter BmrA. *J. Biol. Chem.* **278,** 47002–47008
18. Senior, A. E., al-Shawi, M. K., and Urbatsch, I. L. (1995) The catalytic cycle of P-glycoprotein. *FEBS Lett.* **377,** 285–289
19. Zaitseva, J., Oswald, C., Jumpertz, T., Jenewein, S., Wiedenmann, A., Holland, I. B., and Schmitt, L. (2006) A structural analysis of asymmetry required for catalytic activity of an ABC-ATPase domain dimer. *EMBO J.* **25,** 3432–3443
20. Dawson, R. J., and Locher, K. P. (2007) Structure of the multidrug ABC transporter Sav1866 from *Staphylococcus aureus* in complex with AMP-PNP. *FEBS Lett.* **581,** 935–938
21. Aittoniemi, J., de Wet, H., Ashcroft, F. M., and Sansom, M. S. (2010) Asymmetric switching in a homodimeric ABC transporter: a stimulation study. *PLoS Comput. Biol.* 6, e1000762
22. Gyimesi, G., Ramachandran, S., Kota, P., Dokholyan, N. V., Sarkadi, B., and Hegedus, T. (2011) ATP hydrolysis at one of the two sites in ABC transporters initiates transport related conformational transitions. *Biochim. Biophys. Acta* **1808,** 2954–2964
23. Binz, H. K., Amstutz, P., Kohl, A., Stumpp, M. T., Briand, C., Forrer, P., Grütter, M. G., and Plückthun, A. (2004) High-affinity binders selected from designed ankyrin repeat protein libraries. *Nat. Biotechnol.* **22,** 575–582
24. Sennhauser, G., and Grütter, M. G. (2008) Chaperone-assisted crystallography with DARPins. *Structure* **16,** 1443–1453
25. Sennhauser, G., Amstutz, P., Briand, C., Storchenegger, O., and Grütter, M. G. (2007) Drug export pathway of multidrug exporter AcrB revealed by DARPin inhibitors. *Biol.* **5,** e7
26. Monroe, N., Sennhauser, G., Seeger, M. A., Briand, C., and Grütter, M. G. (2011) Designed ankyrin repeat protein binders for the crystallization of AcrB: plasticity of the dominant interface. *J. Struct. Biol.* **174,** 269–281
27. Murakami, S., Nakashima, R., Yamashita, E., Matsumoto, T., and Yamaguchi, A. (2006) Crystal structures of a multidrug transporter reveal a functionally rotating mechanism. *Nature* **443,** 173–179
28. Seeger, M. A., Schiefner, A., Eicher, T., Verrey, F., Diederichs, K., and Pos, K. M. (2006) Structural asymmetry of AcrB trimer suggests a peristaltic pump mechanism. *Science* **313,** 1295–1298
29. Huber, T., Steiner, D., Röthlisberger, D., and Plückthun, A. (2007) *In vitro* selection and characterization of DARPins and Fab fragments for the co-crystallization of membrane proteins: The Na(+)-citrate symporter CitS as an example. *J. Struct. Biol.* **159,** 206–221
30. Zahnd, C., Amstutz, P., and Plückthun, A. (2007) Ribosome display: selecting and evolving proteins *in vitro* that specifically bind to a target. *Nat. Methods* **4,** 269–279
31. Deleted in proof
32. Loo, T. W. (2001) Determining the dimensions of the drug-binding domain of human P-glycoprotein using thiol cross-linking compounds as molecular rulers. *J. Biol. Chem.* **276,** 36877–36880
33. Venter, H., Velamakanni, S., Balakrishnan, L., and van Veen, H. W. (2008) On the energy-dependence of Hoechst 33342 transport by the ABC transporter LmrA. *Biochem. Pharmacol.* **75,** 866–874
34. Geertsma, E. R., Nik Mahmood, N. A., Schuurman-Wolters, G. K., and Poolman, B. (2008) Membrane reconstitution of ABC transporters and assays of translocator function. *Nat. Protoc.* **3,** 256–266
35. Pannier, M., Veit, S., Godt, A., Jeschke, G., and Spiess, H. W. (2000) Dead-time free measurement of dipole-dipole interactions between electron spins. *J. Magn Reson* **142,** 331–340
36. Forrer, J., García-Rubio, I., Schuhmam, R., Tschaggelar, R., and Harmer, J. (2008) Cryogenic Q-band (35GHz) probehead featuring large excitation microwave fields for pulse and continuous wave electron paramagnetic resonance spectroscopy: performance and applications. *J. Magn Reson* **190,** 280–291
37. Jeschke, G., Chechik, V., Ionita, P., Godt, A., Zimmermann, H., Banham, J., Timmel, C. R., Hilger, D., and Jung, H. (2006) DeerAnalysis2006 - a comprehensive software package for analyzing pulsed ELDOR data. *Appl. Magn. Res.* **30,** 473–498
38. Polyhach, Y., Bordignon, E., and Jeschke, G. (2011) Rotamer libraries of spin labelled cysteines for protein studies. *Phys. Chem. Chem. Phys.* **13,** 2356–2366
39. Binz, H. K., Stumpp, M. T., Forrer, P., Amstutz, P., and Plückthun, A. (2003) Designing repeat proteins: well-expressed, soluble and stable proteins from combinatorial libraries of consensus ankyrin repeat proteins. *J. Mol. Biol.* **332,** 489–503
40. Kohl, A., Binz, H. K., Forrer, P., Stumpp, M. T., Plückthun, A., and

Grütter, M. G. (2003) Designed to be stable: crystal structure of a consensus ankyrin repeat protein. *Proc. Natl. Acad. Sci. U.S.A.* **100,** 1700–1705
41. Eckford, P. D., and Sharom, F. J. (2008) Functional characterization of *Escherichia coli* MsbA: interaction with nucleotides and substrates. *J. Biol. Chem.* **283,** 12840–12850
42. Schultz, K. M., Merten, J. A., and Klug, C. S. (2011) Characterization of the E506Q and H537A dysfunctional mutants in the *E. coli* ABC transporter MsbA. *Biochemistry* **50,** 3599–3608
43. Deleted in proof
44. Jeschke, G., Sajid, M., Schulte, M., and Godt, A. (2009) Three-spin correlations in double electron-electron resonance. *Phys. Chem. Chem. Phys.* **11,** 6580–6591
45. Alvarado, D., Klein, D. E., and Lemmon, M. A. (2010) Structural basis for negative cooperativity in growth factor binding to an EGF receptor. *Cell* **142,** 568–579
46. Renatus, M., Stennicke, H. R., Scott, F. L., Liddington, R. C., and Salvesen, G. S. (2001) Dimer formation drives the activation of the cell death protease caspase 9. *Proc. Natl. Acad. Sci. U.S.A.* **98,** 14250–14255
47. Wiener, M. C. (2004) A pedestrian guide to membrane protein crystallization. *Methods* **34,** 364–372
48. Booth, P. J. (2005) Sane in the membrane: designing systems to modulate membrane proteins. *Curr. Opin. Struct. Biol.* **15,** 435–440
49. Ritchie, T. K., Kwon, H., and Atkins, W. M. (2011) Conformational analysis of human ATP-binding cassette transporter ABCB1 in lipid nanodiscs and inhibition by the antibodies MRK16 and UIC2. *J. Biol. Chem.* **286,** 39489–39496
50. Koide, S. (2009) Engineering of recombinant crystallization chaperones. *Curr. Opin. Struct. Biol.* **19,** 449–457
51. Lee, S. Y., Lee, A., Chen, J., and MacKinnon, R. (2005) Structure of the KvAP voltage-dependent K+ channel and its dependence on the lipid membrane. *Proc. Natl. Acad. Sci. U.S.A.* **102,** 15441–15446

SUPPLEMENTARY INFORMATION

Asymmetry in the homodimeric ABC transporter MsbA recognized by a DARPin

Anshumali Mittal[1], Simon Böhm[2], Markus G. Grütter[1], Enrica Bordignon[2*], Markus A. Seeger[1*]

[1]*Department of Biochemistry, University of Zurich, Switzerland*
[2]*Laboratory of Physical Chemistry, ETH Zürich, Switzerland*

Running title: Asymmetry in MsbA recognized by a DARPin

*Correspondence to: Markus A. Seeger (m.seeger@bioc.uzh.ch) and Enrica Bordignon (enrica.bordignon@phys.chem.ethz.ch)

SUPPLEMENTARY EXPERIMENTAL PROCEDURES

Generation of genetic constructs

The *E.coli msbA* gene was cloned into the pBAD24 (1) for the protein production in *E. coli*. The 5' end of *msbA gene* was extended with sequences encoding a His-10 sequence, a C3 protease site (L-E-V-L-F-Q-G-P) and a linker (D-E-A-E-K-L-F-N-Q). The 3' end of *msbA* gene was amplified using a reverse primer priming on the *msbA* gene. The PCR amplified product flanked by NcoI and XbaI restriction sites was ligated into the *E. coli* expression vector pBAD24 (1) yielding the expression vector pBADMsbA (expressed protein termed $MsbA_{His}$). The Avi-tag (G-L-N-D-I-F-E-A-Q-K-I-E-W-H-E) coding sequence was added to the 3' end of *msbA*, which facilitated site specific biotinylation of the target protein as will be described in another manuscript (Seeger and van Veen, submitted). The wild type *E.coli msbA* gene was mutated to cys-less *msbA* (C88S/C315S) and single cysteine mutants at the positions A25C, R103C, N191C, S206C and S246C of *msbA* were introduced by site directed mutagenesis. Likewise, single cysteine mutants were also introduced into the N- and C- terminal caps of DARPin_55 (which is cys-less by design) at the positions S12C, K16C, E29C, D151C and D160C. ATPase-inactive MsbA mutant was generated by mutating the conserved glutamate of the Walker B motif to glutamine (referred to as MsbA_E506Q mutant). The transmembrane domain (amino acid number 1 to 348) and nucleotide binding domain (starting from amino acid number 337 to 582) were cloned to contain an N-terminal His_{10}-tag and a C-terminal Avi-tag sequence (the expressed protein

termed as TMD_{AviC} and NBD_{AviC} respectively) into pBAD24 (1). All constructs were confirmed by DNA sequencing (Microsynth).

Protein expression, purification and spin labeling

MsbA expression was performed in *E.coli* C43(DE3) (2) cells, grown in 2YT media. Protein production was induced at OD_{600} of 0.8 with 0.02% L-arabinose (Sigma) for 12-14 hours at 25°C. Harvested cell pellets were resuspended in 20 mM Tris/HCl (pH 7.4), 150 mM NaCl, 25 μg/ml DNaseI and protease inhibitor cocktail (Sigma) and cells were lysed using EmulsiFlex-C3 (Avestin). Unbroken cells and cell debris were removed by centrifugation at 8000 rpm (SS34 rotor) for 10 min at 4°C and membrane vesicles were then harvested by centrifugation at 45,000 rpm (Ti70 rotor) for 60 min at 4°C. MsbA was solubilized from membrane vesicles using 1% β-DDM in 50 mM Tris/HCl (pH 7.4), 150 mM NaCl (TBS) at 4°C for 90 minutes. The insolubilized membrane fraction was removed by centrifugation at 45,000 rpm (Ti70 rotor) for 60 min at 4°C and cleared lysate was loaded onto a Ni^{2+}-NTA gravity flow column containing 1.5 ml resin (Qiagen). The resin was washed with 35 mM imidazole pH 7.5, TBS and 0.05 % β-UDM (50 ml) and MsbA was eluted from the column in the same buffer containing 250 mM imidazole pH 7.5 (7 ml). Avi-tagged MsbA was enzymatically biotinylated *in vitro* using purified BirA yielding $bMsbA_{AviC}$ (3). Every MsbA preparation used in this work was separated from aggregated material by gel filtration (Superdex 200, 10/300, GE Healthcare) in 20 mM Tris/HCl (pH 7.5), 150 mM NaCl and 0.05% β-UDM and the fractions of the homogenous main peak corresponding to dimeric MsbA were pooled. Purified MsbA was supplemented with 10% glycerol and was snap-frozen in liquid nitrogen and stored at -80°C. Freezing of MsbA did not decrease its ATPase activity even after prolonged storage and did not lead to aggregation of the protein (not shown). Single cysteine mutants of MsbA for methanthiosulfonate cross-linking and spin labeling were purified by supplementing 5 mM dithiothreitol (DTT) to the Ni^{2+}-NTA washing and elution buffers. In order to spin label MsbA, DTT was removed on a PD-10 column (GE Healthcare) in TBS containing 0.05% β-UDM buffer according to the manufacturer's protocol. Single cysteine MsbA was spin labeled at 4°C overnight using a 10 times molar excess of MTSSL ((1-Oxyl-2,2,5,5-tetramethyl-Δ3-pyrroline-3-methyl) methanethiosulfonate; Toronto Research Chemicals). Excess spin label was removed by size exclusion chromatography. DARPin expression and purification has been described previously (4). In case of the single cysteine mutants of DARPin_55, 5 mM DTT was added during the Ni^{+2}-NTA purification. DTT was removed by the size-exclusion chromatography (Superdex 200, 10/300, GE Healthcare) in 20 mM Tris/HCl pH 7.5, 150 mM NaCl. Monomeric DARPin_55 was snap-frozen in the presence of 10% of glycerol in liquid nitrogen and stored at -80 °C. For the EPR measurements, DARPin-MsbA complexes were made by spin labeling the proteins individually, followed by gel-filtration of the protein complex.

SUPPLEMENTARY REFERENCES

1. Guzman, L. M., Belin, D., Carson, M. J., and Beckwith, J. (1995) *J Bacteriol* **177**, 4121-4130
2. Miroux, B., and Walker, J. E. (1996) *J Mol Biol* **260**, 289-298
3. Cull, M. G., and Schatz, P. J. (2000) *Methods Enzymol* **326**, 430-440
4. Huber, T., Steiner, D., Röthlisberger, D., and Plückthun, A. (2007) *J Struct Biol* **159**, 206-221

SUPPLEMETARY TABLE

Supplementary Table S1

MsbA mutant	ATPase activity nmol/min/mg protein
MsbA*	136.7 ± 8.3
MsbA_cysless	130.8 ± 9.2
MsbA_V65C	230.1 ± 16.9
MsbA_V65C_R1	234 ± 22.2
MsbA_R103C	121.1 ± 0.7
MsbA_R103C_R1	115.7 ± 5.9
MsbA_N191C	111.3 ± 17.8
MsbA_N191C_R1	126.86 ± 20.6
MsbA_S482C	28.1 ± 6.5
MsbA_S482C_R1	29.0 ± 0.7
MsbA_L539C	133.9 ± 11.4
MsbA_L539C_R1	136.54 ± 9.1

*Wild-type;
R1, methanothiosulfonate spin label

SUPPLEMENTARY FIGURE LEGENDS

Figure S1. Schematic representation of the binder selection cycle using ribosome display

An mRNA library is *in vitro* translated and a ternary complex composed of mRNA, nascent polypeptide and ribosome (linkage of genotype to phenotype) is used for the binding selection against the immobilized target protein. Unbound ternary complexes are removed by washing whereas the mRNA encoding for bound DARPins is eluted by dissociating the ribosomal complex using EDTA. The released mRNA is reverse transcribed to DNA and is either used for another round of selection or is analyzed by expressing single clones of the enriched library followed by ELISA (picture adopted from Huber et al. (29))

Figure S2. Schematic drawing of the ELISA set up

First, an anti-myc antibody is immobilized on an ELISA plate coated with Protein A. DARPins are then captured by the anti-myc antibody via their C-terminal Myc5-tag. Biotinylated target protein (LmrCD, AcrB or MsbA in our study) are then allowed to bind to the DARPin of interest and target protein binding is detected using a streptavidin-alkaline phosphatase. Its activity is detected colourimetrically at OD_{405} using p-nitrophenyl phosphate as a substrate.

Figure S3. Exclusion of unspecific DARPin binders

42 DARPin clones were selected from the initial ELISA hits and were further analyzed in this specificity ELISA. Besides $bMsbA_{AviC}$, ABC transporter $bLmrCD_{AviC}$ and secondary-active multidrug transporter $bAcrB_{AviC}$ were used to identify unspecific binders. Out of 42 primary hits, 37 hits were exclusively binding to $bMsbA_{AviC,}$ while 5 clones were promiscuously binding to other target proteins in the ELISA.

Figure S4. Size-exclusion chromatography profile of the MsbA-DARPin_55 complex

MsbA and DARPin_55 were mixed at a molar ratio of 1:3 and incubated at 4 °C for 15 minutes. The MsbA-DARPin_55 complex and excess DARPin_55 were separated by size-exclusion chromatography (Superdex 200 10/300 GL column, GE Healthcare). The fractions containing the MsbA-DARPin_55 complex were quantified by on-chip protein analysis according to the

manufacturer's protocol (Protein 80 Kit, Agilent Technologies; Fig. S8). The ratio between DARPin55 and MsbA was determined to 0.8 suggesting that one DARPin binds to homodimeric MsbA.

Figure S5. Estimation of DARPin_55 binding affinity to MsbA by a competition ELISA

MsbA (50 nM) was pre-incubated with varying concentrations of free DARPin_55 (10 nM to 1000 nM) and the mixtures were allowed to bind to immobilized DARPin_55myc$_5$. At a free DARPin_55 concentration of 80 nM, half-maximal ELISA signal was observed, suggesting that the binding affinity of DARPin_55 is around 80 nM (as described by Binz et al (23)). Addition of the unselected DARPin E3_5 (1 μM) did not compete with MsbA binding to immobilized DARPin_55 myc$_5$. Error bars represent standard deviations.

Figure S6. Biochemical characterization of MsbA reconstituted into proteoliposomes

A and ***B*** The ATPase activity of reconstituted was measured in the absence and the presence of DARPin_55 using a concentration range of the MsbA substrates lipid A ***A*** and daunomycin ***B***. Error bars represent standard deviations. ***C*** and ***D*** DEER analysis of detergent-solubilized and reconstituted MsbA. MsbA spin-labeled at position 539 was used. *Left*, normalized DEER form factors F(t) and fits obtained with DeerAnalysis2010. *Right*, distance distributions obtained with Tikhonov regularization parameters 100 or 1000. ***C*** Interspin distances in the apo-state in β-UDM (black), β-DDM (green) and reconstituted in proteoliposomes (blue) are shown. This particular mutation was found to destabilize the apo-state conformation in β-UDM leading to the appearance of a main peak at about 6 nm and of additional short distances. Both β-DDM and liposomes stabilize the inward-facing conformation. ***D*** Analogous DEER analysis as in ***C*** but recorded in the presence of AMP-PNP and $MgCl_2$.

Figure S7. DARPin_55 does not bind to membrane-embedded MsbA

A Comparison of cross-linking of DARPin_55_29C to MsbA_191C in inside-out membrane vesicles (lane 2), reconstituted in proteoliposomes (lane 3) and in its detergent-solubilized form (lane 4). Cross-linking was not observed for membrane-embedded MsbA_191C. ***B*** DARPin_55 (3.5 μM) was allowed to bind to reconstituted wild-type MsbA (1 μM) in proteoliposomes and empty liposomes at 4°C for 30 minutes. Unbound DARPin_55 was removed by three washes and the protein was analyzed by SDS-PAGE followed by Ruby staining. DARPin_55 does not bind to reconstituted MsbA confirming the results described in ***A***.

Figure S8. SDS-PAGE analysis of M11M and M5M-mediated cross-links between single cysteine mutants of MsbA and DARPin_55

Cross-links were performed as described in the materials and methods. The analysis concludes that the N-terminus of DARPin_55 (positions 12, 16 and 29) is in close proximity to positions 191, 206 and 246 of MsbA while the C-terminus of DARPin_55 (positions 151 and 160) is far apart from any of the cysteines introduced into MsbA (see also Fig. 6).

Figure S9. Stoichiometry analysis of a DARPin_55-MsbA complex

A Calibration of protein concentration determination by on-chip protein analysis (Agilent Technologies). DARPin_55 at concentrations of 4 μM, 2 μM and 1 μM was analyzed on a protein chip, and the areas of the resulting peaks were plotted against the known protein concentration (determined at A_{280}). The error bars of duplicate measurements were very small and the data could be fitted by linear regression. Note that the curve does not intercept at the origin, which likely reflects the detection threshold of this method. For the quantification of the MsbA-DARPin_55 complex, the protein concentrations were chosen to be in the linear range of detection. ***B*** Raw data of on-chip analysis of the MsbA-DARPin_55 complex eluted after gel-filtration. Peaks 9 and 10 correspond to DARPin_55 and MsbA respectively and the peak area is quantified taking the internal standard peak 11 as reference using the manufacturer's software. Using calibrations curves as determined in ***A***, the stoichiometry between DARPin_55 and MsbA was determined.

Figure S10. Surface properties of DARPin_55

A A homology model of DARPin_55 was generated based on the coordinates of DARPin E3_5 (PDB entry 1MJ0) using SWISS-MODEL (51). The protein surface is colored according to its hydrophobicity (intensity of red color indicates increasing hydrophobicity) using the Eisenberg hydrophobicity scale (52). The DARPin scaffold is shown as cartoon and randomized residues are shown as sticks. ***B*** The sequence of DARPin_55 is depicted and randomized positions of the DARPin library are indicated in the Template_N3C sequence.

Figure S1

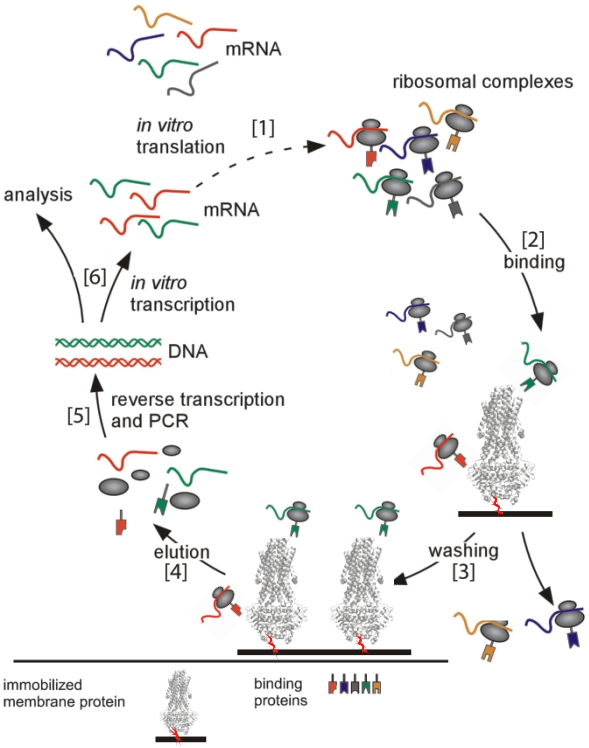

Figure S2

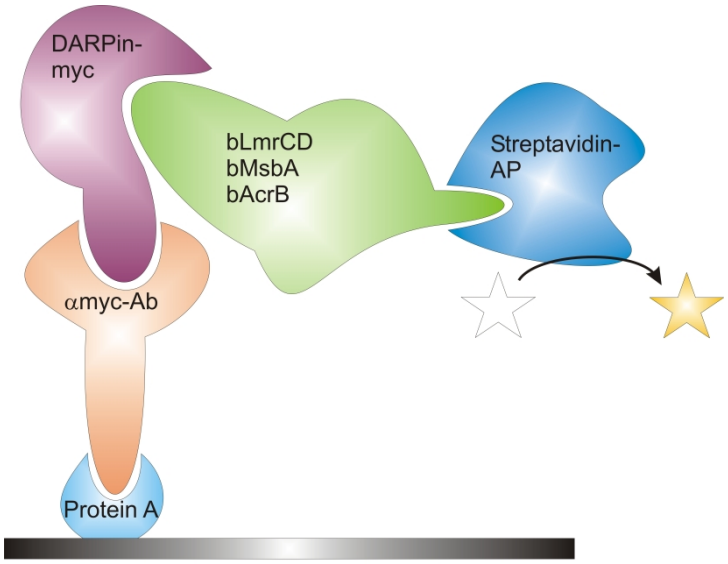

Figure S3

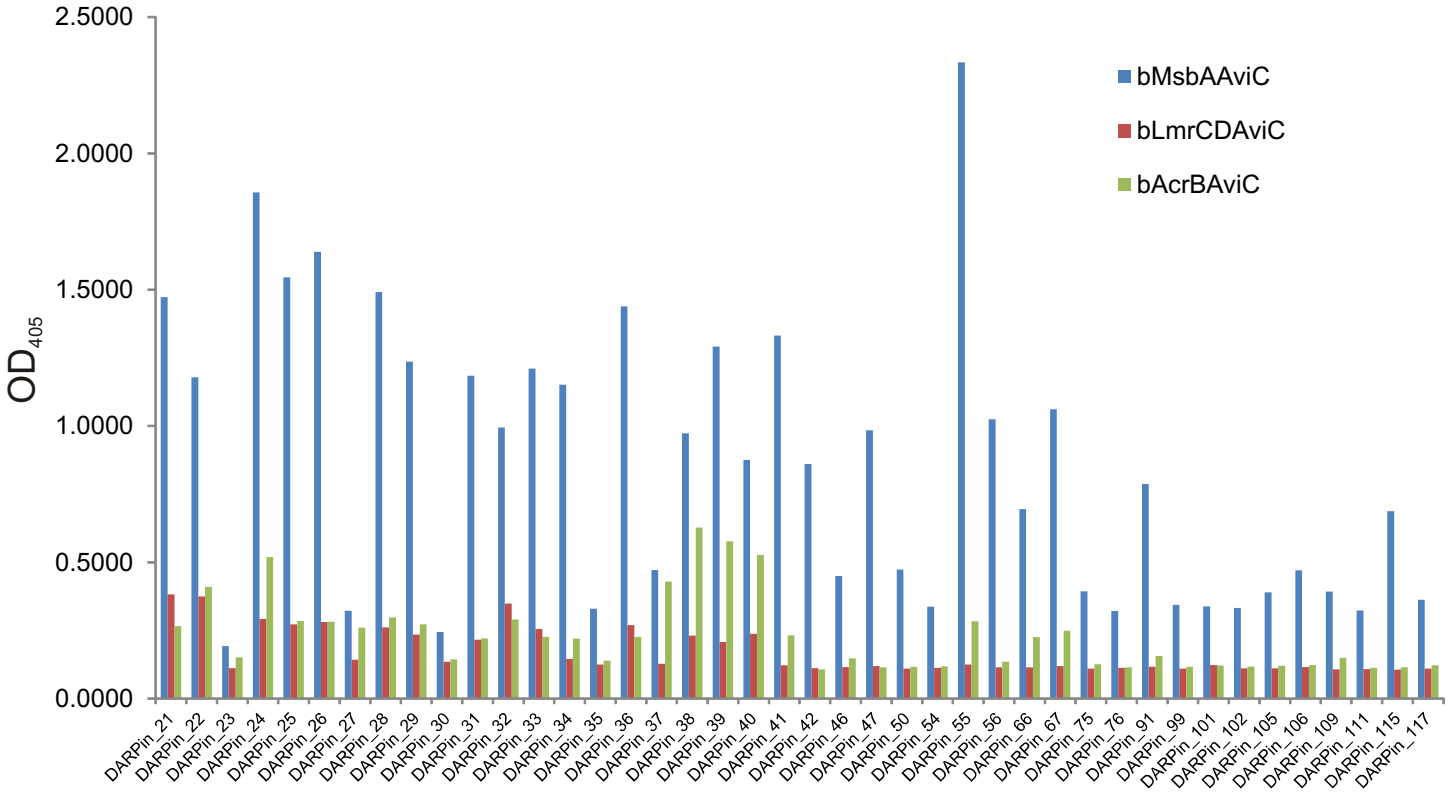

Figure S4

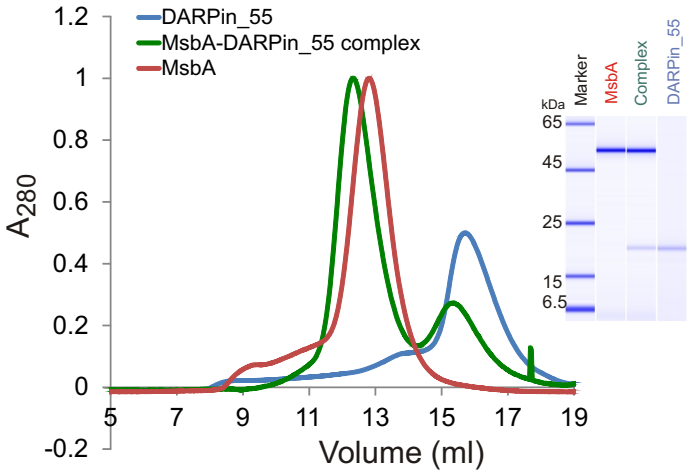

Figure S5

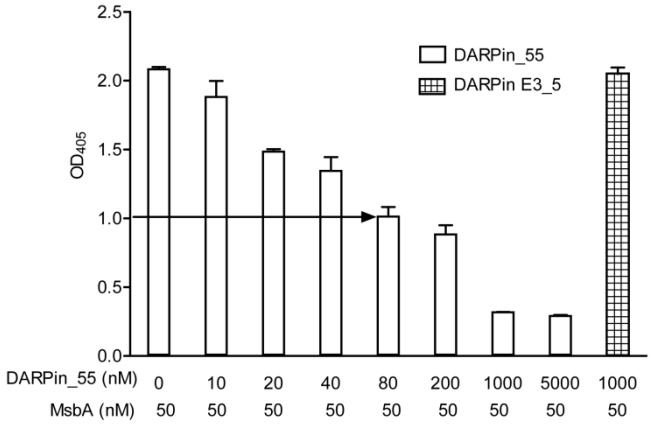

Figure S6

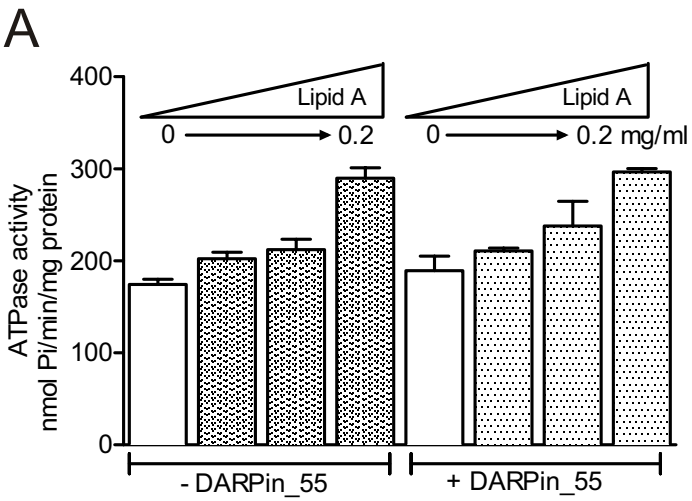

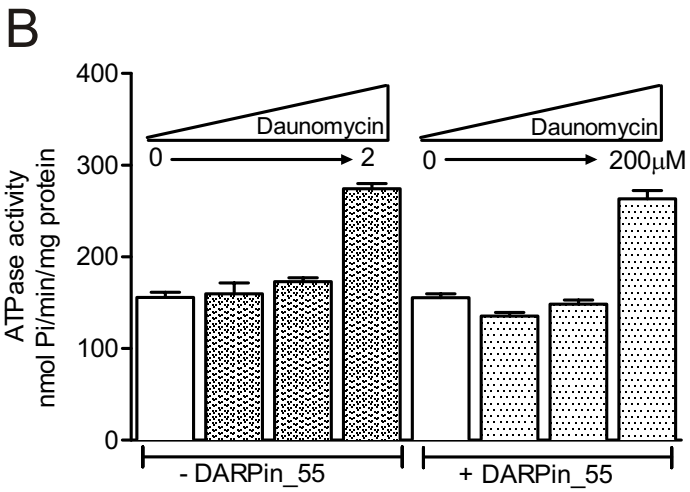

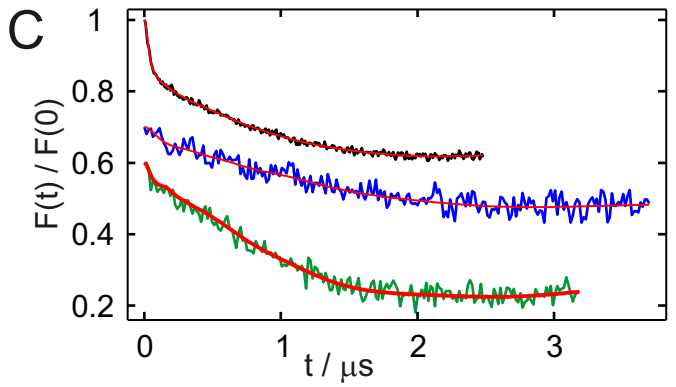

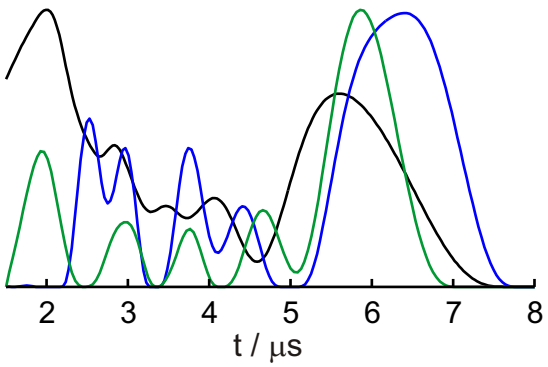

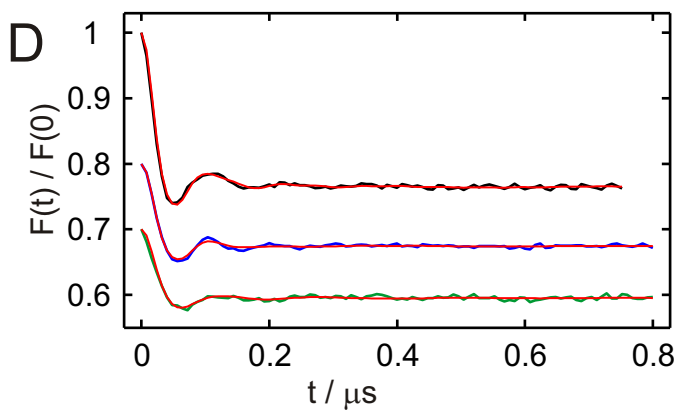

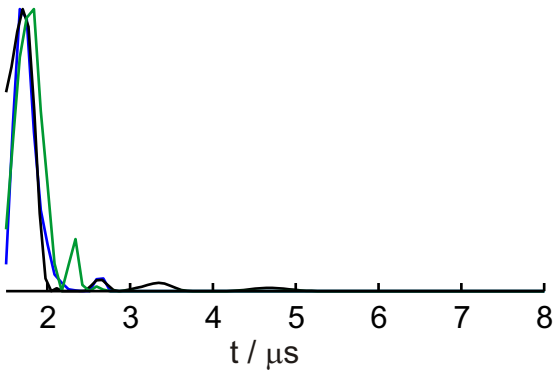

Figure S7

A

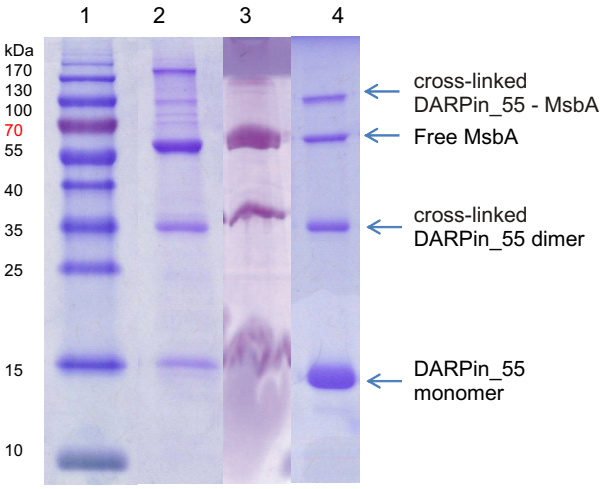
1
2
3
4
kDa
170
130
100
70
55
40
35
25
15
10
cross-linked DARPin_55 - MsbA
Free MsbA
cross-linked DARPin_55 dimer
DARPin_55 monomer

B

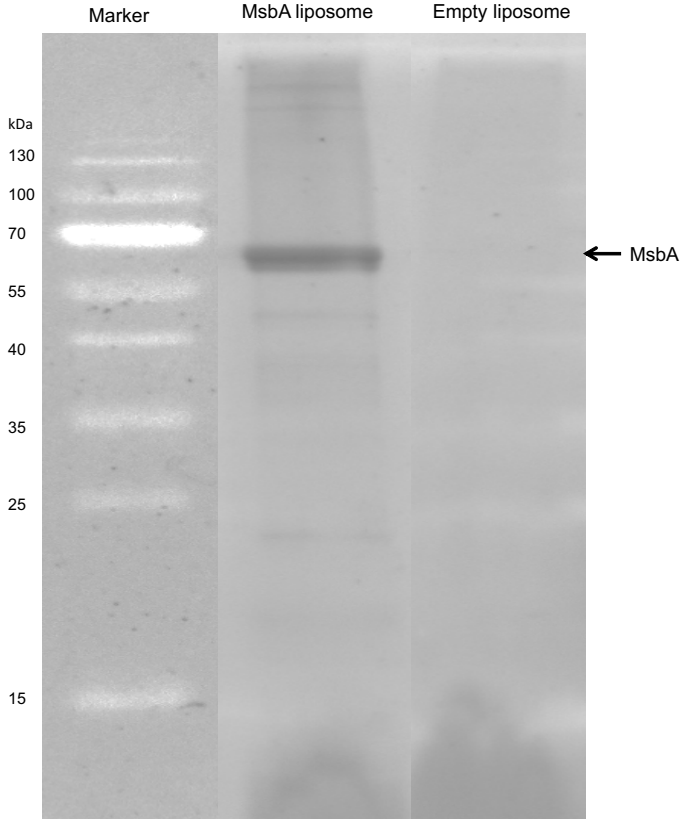
Marker
MsbA liposome
Empty liposome
kDa
130
100
70
55
40
35
25
15
MsbA

Figure S8

DARPin55_29C cross-linking with MsbA mutants (M11M and M5M cross-linkers)

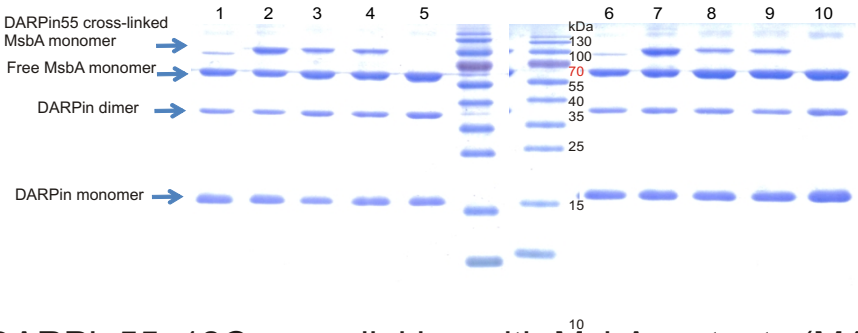

1. DARPin_29C_MsbA_103C_M11M
2. DARPin_29C_MsbA_191C_M11M
3. DARPin_29C_MsbA_206C_M11M
4. DARPin_29C_MsbA_246C_M11M
5. DARPin_29C_MsbA_cysless_M11M

6. DARPin_29C_MsbA_103C_M5M
7. DARPin_29C_MsbA_191C_M5M
8. DARPin_29C_MsbA_206C_M5M
9. DARPin_29C_MsbA_246C_M5M
10. DARPin_29C_MsbA_cysless_M5M

DARPin55_12C cross-linking with MsbA mutants (M11M and M5M cross-linkers)

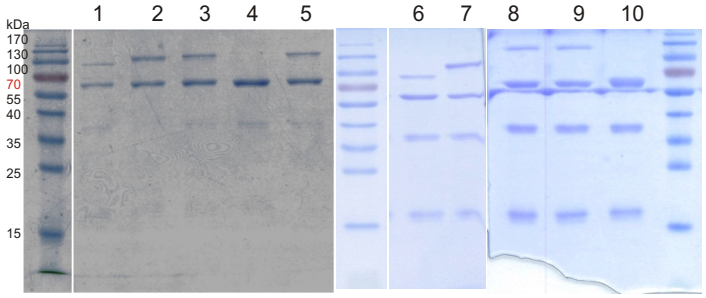

1. DARPin_12C_MsbA_103C_M11M
2. DARPin_12C_MsbA_191C_M11M
3. DARPin_12C_MsbA_206C_M11M
4. DARPin_12C_MsbA_cysless_M11M
5. DARPin_12C_MsbA_246C_M11M

6. DARPin_12C_MsbA_103C_M5M
7. DARPin_12C_MsbA_191C_M5M
8. DARPin_12C_MsbA_206C_M5M
9. DARPin_12C_MsbA_246C_M5M
10. DARPin_12C_MsbA_cysless_M5M

DARPin55_16C cross-linking with MsbA mutants (M11M and M5M cross-linkers)

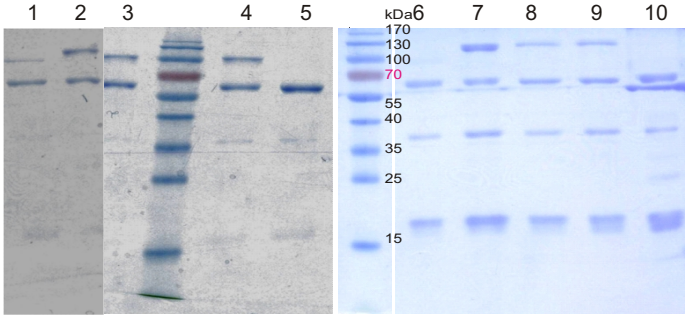

1. DARPin_16C_MsbA_103C_M11M
2. DARPin_16C_MsbA_191C_M11M
3. DARPin_16C_MsbA_206C_M11M
4. DARPin_16C_MsbA_246C_M11M
5. DARPin_16C_MsbA_cysless_M11M

6. DARPin_16C_MsbA_103C_M5M
7. DARPin_16C_MsbA_191C_M5M
8. DARPin_16C_MsbA_206C_M5M
9. DARPin_16C_MsbA_246C_M5M
10. DARPin_16C_MsbA_cysless_M5M

DARPin55_151C cross-linking with MsbA mutants (M11M and M5M cross-linkers)

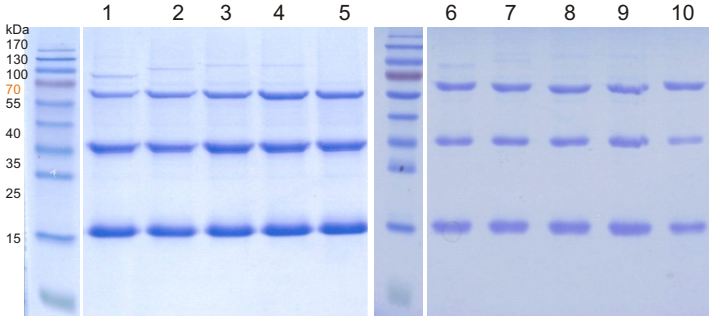

1. DARPin_151C_MsbA_103C_M11M
2. DARPin_151C_MsbA_191C_M11M
3. DARPin_151C_MsbA_206C_M11M
4. DARPin_151C_MsbA_246C_M11M
5. DARPin_151C_MsbA_cysless_M11M

6. DARPin_151C_MsbA_103C_M5M
7. DARPin_151C_MsbA_191C_M5M
8. DARPin_151C_MsbA_206C_M5M
9. DARPin_151C_MsbA_246C_M5M
10. DARPin_151C_MsbA_cysless_M5M

DARPin55_160C cross-linking with MsbA mutants (M11M and M5M cross-linkers)

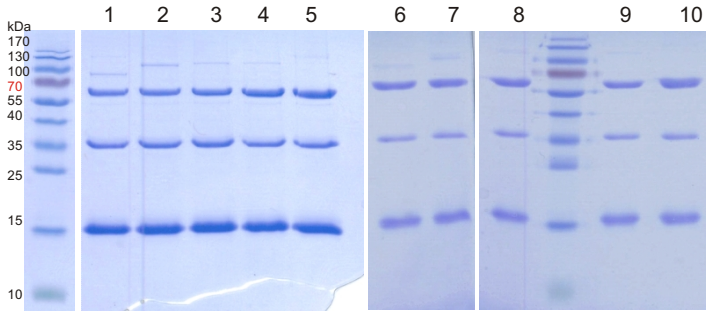

1. DARPin_160C_MsbA_103C_M11M
2. DARPin_160C_MsbA_191C_M11M
3. DARPin_160C_MsbA_206C_M11M
4. DARPin_160C_MsbA_246C_M11M
5. DARPin_160C_MsbA_cysless_M11M

6. DARPin_160C_MsbA_103C_M5M
7. DARPin_160C_MsbA_191C_M5M
8. DARPin_160C_MsbA_206C_M5M
9. DARPin_160C_MsbA_246C_M5M
10. DARPin_160C_MsbA_cysless_M5M

Figure S9

A

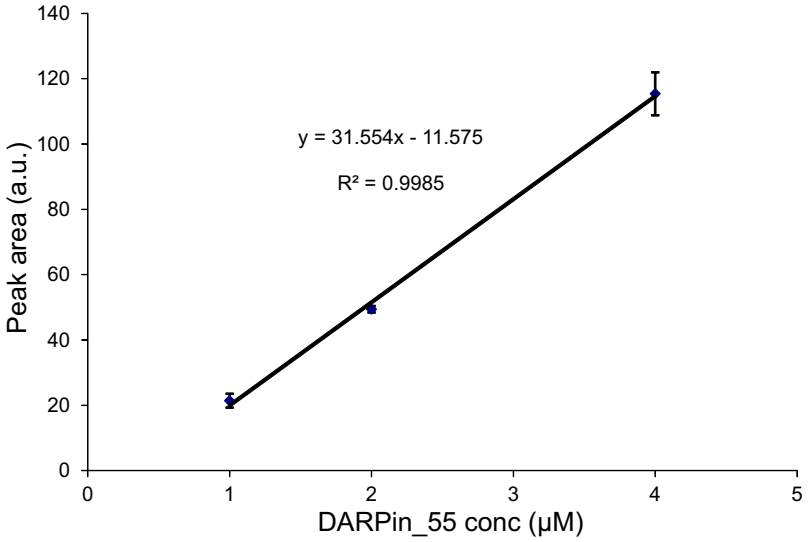
y = 31.554x - 11.575
R² = 0.9985
Peak area (a.u.)
DARPin_55 conc (µM)
0
20
40
60
80
100
120
140
0
1
2
3
4
5

B

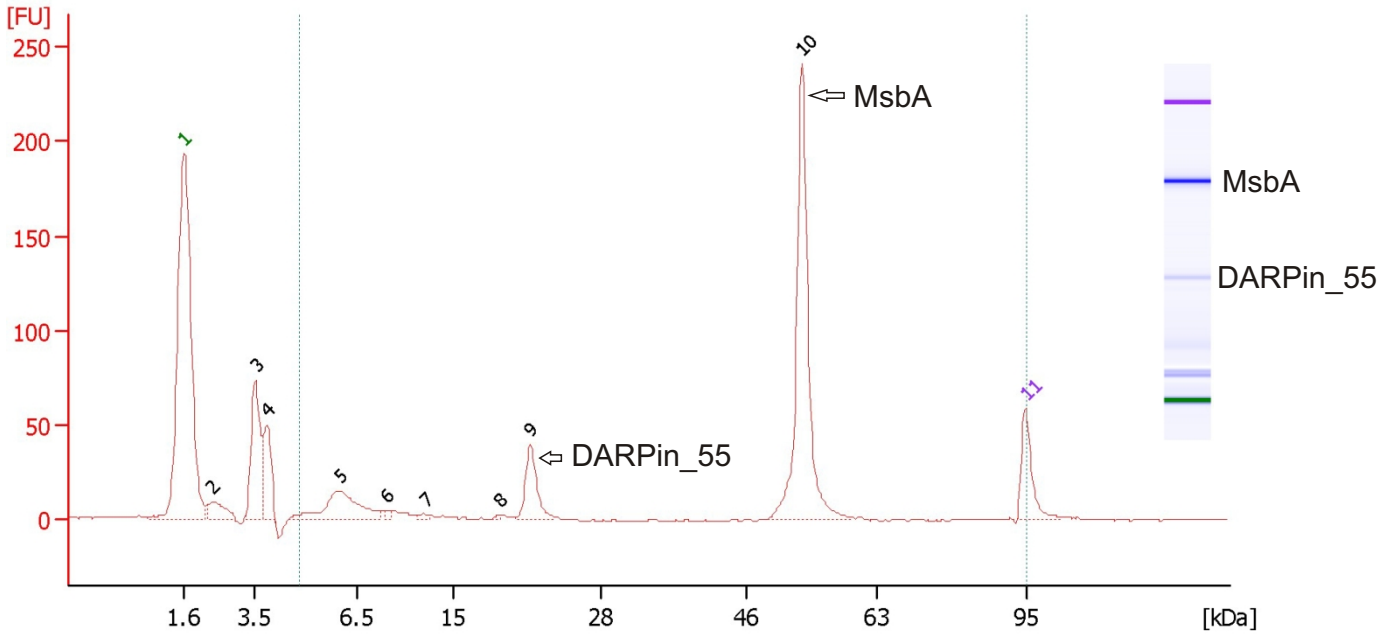
[FU]
250
200
150
100
50
0
1
2
3
4
5
6
7
8
9
10
11
⇦ MsbA
⇦ DARPin_55
MsbA
DARPin_55
1.6
3.5
6.5
15
28
46
63
95
[kDa]

Figure S10

A

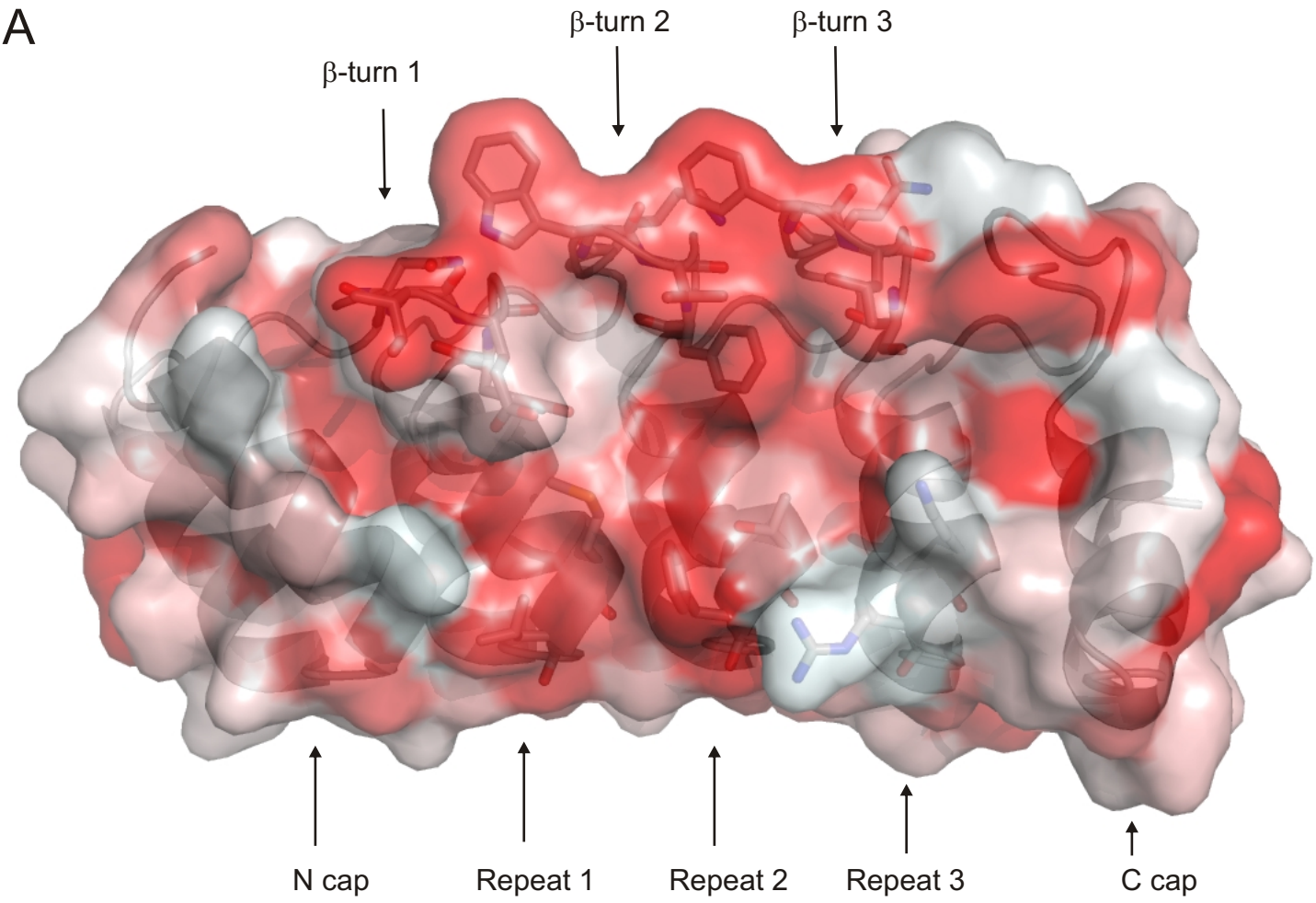

B

N-cap Repeat 1

```
Template_N3C    MRGSHHHHHHGSDLGKKLLEAARAGQDDEVRILMANGADVNAXDXXGXTPLHLSAXXGHL
DARPin_55       MRGSHHHHHHGSDLGKELLEAARADQDDEVRILMANGADVNANDIEGETPLRLAAMLGHL
```

Repeat 2

```
Template_N3C    EIVEVLLKXGADVNAXDXXGXTPLHLAAXXGHLEIIEVLVKXGADVNAXDXXGXSPLHLA
DARPin_55       EIVEVLLKNGADVNAKDWVGFTPLHLAATFGHLEIVEVLLKHGADVNAQDFLGSTPLHLA
```

Repeat 3 C-cap

```
Template_N3C    AXXGHLEIVEVLLKXGADVSAQDEFGKTAFDISIDNGNEDLAEILQKLN
DARPin_55       AKRGHLEIVEVLLKHGADVNAQDKFGKTAFDISIDNGNEDLAEILQKLN
```

CHAPTER C

Structural and functional studies of homodimeric ABC transporter MsbA using an *in vitro* selected DARPin binder

C.1 Introduction

The envelope of Gram-negative bacteria is composed of two distinct lipid membranes, an inner membrane, consisting of glycerophospholipids, and an outer membrane, which is an asymmetric bilayer. The outer leaflet of the outer membrane consists of lipopolysaccharides (LPS). A molecule of LPS consists of two parts - a covalently bound lipid component, termed lipid A, and a hydrophilic hetero-polysaccharide (Figure _C1). The lipid A moiety is unique to Gram-negative bacteria. It is a potent activator of the innate immune system in animals via the TLR-4 receptor[1,2]. First insights into MsbA function came from studies performed on an *E.coli htrB*-deficient mutant. HtrB is a lauroyl transferase involved in lipid A biosynthesis. Lack of HtrB results in the accumulation of LPS in the inner membrane of *E.coli* and is toxic at elevated temperatures. The overexpression of MsbA in the *htrB* mutant was found to restore the translocation of LPS to the outer membrane at 42°C. Further evidence came from an *E.coli* mutant called WD2, which carries a A270T substitution in MsbA[1]. WD2 is a temperature-sensitive mutant, in which the function of MsbA (A270T) is inhibited if cells are shifted from 30°C to 44°C. Using ^{32}P and ^{14}C- acetate labeling, it was shown that the export of newly made LPS and phospholipids to the outer membrane is hampered. These experiments demonstrated that MsbA is an essential component of the lipid A transport system in *E.coli*[1].

The first molecular structure of MsbA[3] (*E.coli* homologues of eukaryotic MDR ABC transporter) was reported by Chang and colleagues in 2001. However, the crystal structure of Sav1866[4] (53 % sequence similarity with MsbA) reported by the Locher group in 2006 indicated that the MsbA structures were incorrect in both, the hand and the topology. This lead to the retraction of all structures of MsbA published by the Chang group[3,5,6]. Chang and colleagues reported that the initial error in the structure determinations was the accidental inversion of the sign of the anomalous difference in a data-conversion step that converted

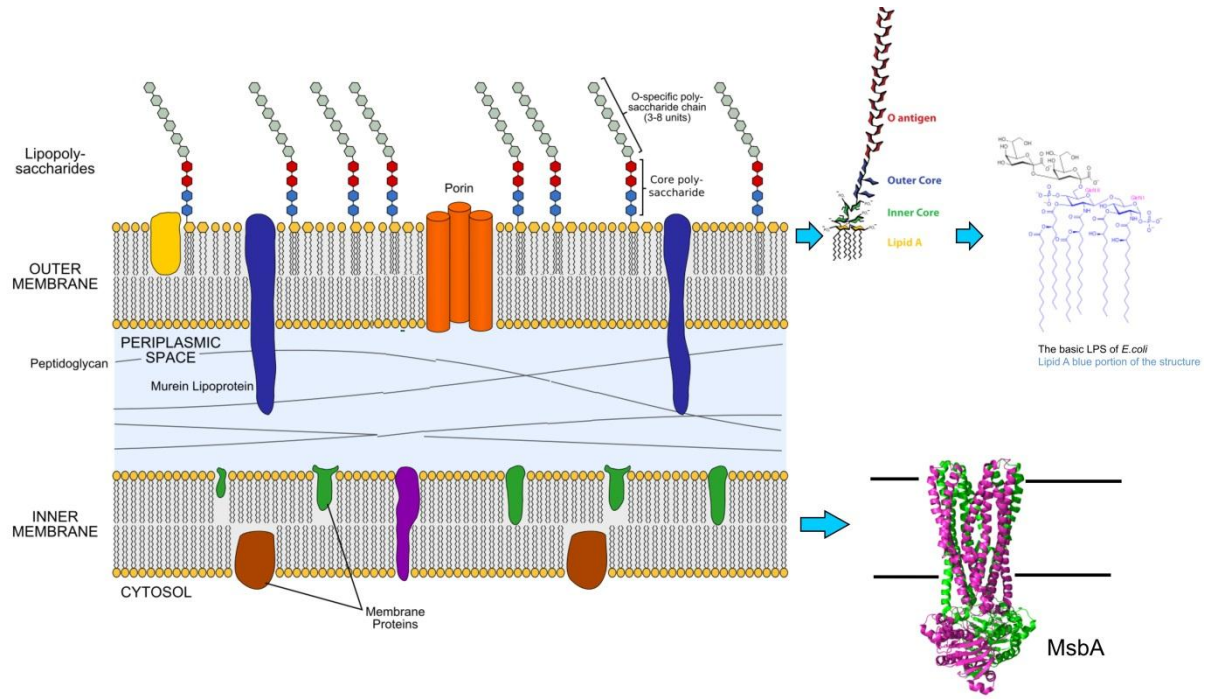

Figure_C1: Envelope of Gram-negative bacteria. MsbA is an inner membrane ABC transporter, with its nucleotide binding domains (NBDs) located in the cytoplasm. The NBDs energize the vectorial transporter by binding and hydrolysing ATP. MsbA accomplishes the transport of lipid A across the inner membrane by a primary active transport process. The figure has been taken from Wikipedia (http://en.wikipedia.org/wiki/Bacterial_outer_membrane) and the MsbA structure (PDB 3B60) has been added using the program Pymol.

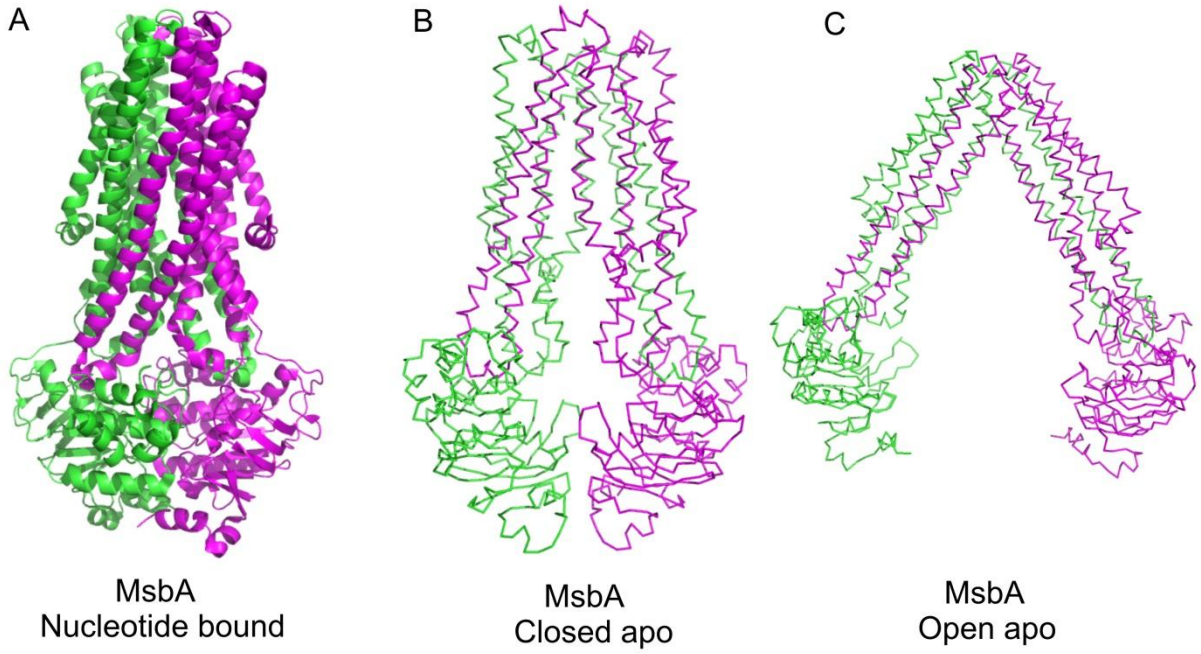

Figure_C2: Structures of different conformations of MsbA. (A) Nucleotide bound, outward-facing conformation at 3.7 Å (PDB 3B60), **(B)** Closed apo, inward-facing conformation at 5.5 Å (PDB 3B5X) and, **(C)** Open apo, inward-facing conformation at 5.3 Å (PDB 3B5W).

experimental intensity (I) values to structure factor moduli (F). Specifically, I(h, k, l) and I(-h, -k, -l) were converted to |F(-h, -k, -l)| and |F(h, k, l)|, respectively[7,8]. The corrected

structures of three homologues of MsbA[9] in three different conformations at resolutions ranging from 3.7 Å to 5.5 Å were published later (Figure_C2). These structures describe two inward-facing states obtained in the absence of nucleotides and one outward-facing state obtained in the presence of the nucleotide analog AMP-PNP. One nucleotide-free state is called open-apo state, in which NBDs are far apart. The second nucleotide-free state is named closed apo-state displaying the NBDs in partial molecular contact. In the nucleotide bound state, the MsbA structure is virtually identical to the Sav1866 structure, in which the NBDs dimerize and sandwich the two nucleotides at the binding interface.

Despite the availability of MsbA structures, many mechanistic details remain unclear due to the low-resolution data (between 3.7 Å and 5.5 Å). By using the **D**esigned **A**nkyrin **R**epeat **P**roteins (DARPins) technology, we hoped to trap ABC-transporters in novel conformational states. The DARPins represent a well-established randomized scaffold used as an alternative to antibody fragments (Fab and scFv) and have been selected against a variety of target proteins[10-15]. DARPins have the potential to trap the targeted protein in alternative conformations and have been previously shown to mediate crystal contacts[12,15,16]. A DARPin selected against the multidrug transporter AcrB for example, traps this protein in an asymmetric state with two DARPins bound to the homotrimer. The third subunit is in a different conformation in which the DARPin binding site is altered[15,16]. In the absence of the DARPins, AcrB was initially crystallized in a symmetric[17] and later in an asymmetric state[18,19]. In analogy to the work on AcrB, MsbA-specific DARPins can be used as crystallization chaperones that might lead to well diffracting crystals. This chapter describes the selection of DARPins against MsbA and summarizes our attempts to crystallize MsbA with the help of DARPins.

C.2 Results

C.2.1 Target protein (MsbA) biotinylation

Adequate biotinylation of the target protein is a prerequisite for ribosome display (RD) selections and ELISA screening. In RD selection using solution panning, the fraction of unbiotinylated target protein contributes to the loss of specific binders due to a lower degree of immobilization than estimated; while in our ELISA format, it competes with the biotinylated protein undesirably (Chapter B-Figure_S2 and section C.4.4.2). To overcome such methodological problems, we used the Avi-tag technology. The Avi tag is a fusion tag of

15 amino acids comprising a lysine residue that becomes specifically biotinylated by the biotin ligase enzyme (BirA). In the presence of biotin and ATP, BirA catalyzes amide linkage between the biotin and the lysine. The Avi tag is fused by genetic engineering to the target protein[20] either at the N or C terminus. The recombinant Avi-tagged protein is purified in the same manner as the target protein, and *in vitro* enzymatic biotinylation is carried out using purified BirA[21] (Figure_C3). Here in this thesis, we used *in vitro* enzymatic biotinylation facilitated by the Avi-tag methodology to achieve maximally biotinylated target protein for ribosome display selection procedure and binders screening by ELISA.

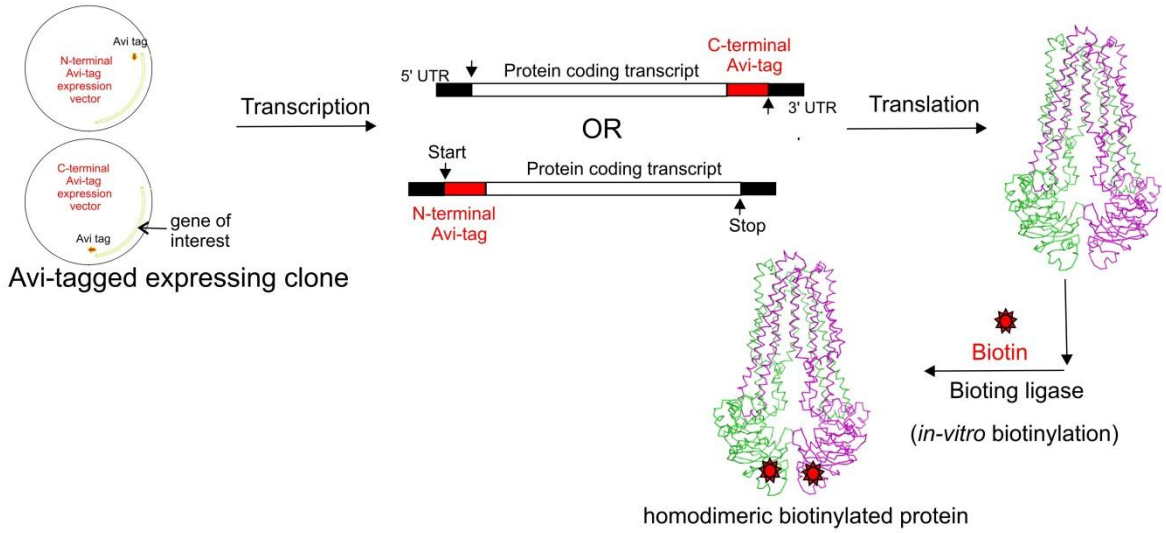

Figure_C3: Schematic representation of *in vitro* biotinylation. The Avi tag is fused by genetic engineering to either the 5' or 3' end of the gene of interest. The overexpressed protein with the Avi-tag at the N or C-terminus is purified by the same procedure as the wild type protein and *in vitro* biotinylation is carried out using the biotin ligase enzyme, ATP and biotin.

C.2.2 Selection and screening of MsbA specific DARPins

A ribosome display selection procedure is illustrated in Chapter B-Figure_S1. Briefly, biotinylated MsbA ($bMsbA_{AviC}$) was mixed with *in vitro* translated DARPin library and followed by capturing of the $bMsbA_{AviC}$-DARPin complexes with streptavidin-coated paramagnetic beads. The enriched DARPin pool of the fourth round of ribosome display was subcloned into the expression vector $pQE30_{myc5}$. Single clones (about 2000) of the fourth round were further analyzed by crude extract ELISA. In this ELISA set up, the selected DARPins were immobilized on the plate via myc-tag and the binding of membrane protein was detected (Chapter B-Figure_S2). The detergent solubilized membrane protein was added to the ELISA experiment at the latest possible stage in order to reduce the washing and incubation to a minimum. From the initial ELISA hits (not shown), about 42 of the DARPin clones (2.1 % of all examined) showed binding to $bMsbA_{AviC}$. To test whether the

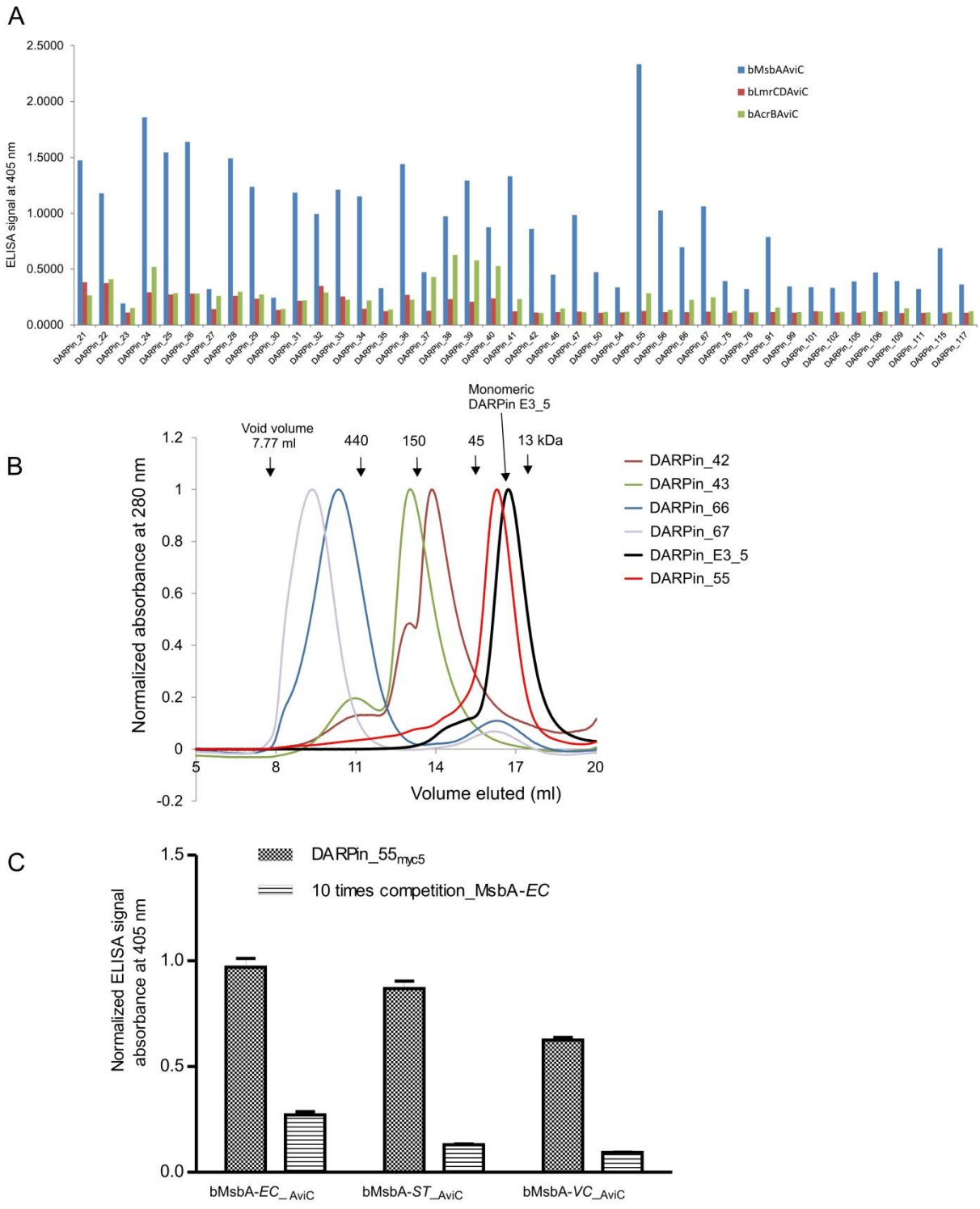

Figure_C4: (A) Cross specificity ELISA, DARPins that were identified to bind to MsbA in an ELISA screen (not shown) were tested for binding against three membrane proteins, namely $bMsbA_{AviC}$, $bLmrCD_{AviC}$ and $bAcrB_{AviC}$. Except for DARPin_38-40, the binders were found to be specific for MsbA. **(B) Gel-filtration analysis of the DARPins** using a Superdex 200 10/300 chromatography column. The previously characterized monomeric DARPin_E3_5 was used as a control. Out of 37 specific binders analzyed by SEC, one binder DARPin_55 was found to be monomeric. Other binders forming higher oligomers were not further analyzed. Elution volumes of proteins with known molecular weight are indicated. **(C)** DARPin_55 was probed for binding to $bMsbA\text{-}EC_{AviC}$ (of *E.coli*), and its close homologs from *Salmonella typhimurium* ($bMsbA\text{-}ST_{AviC}$) & *Vibrio cholerae* ($bMsbA\text{-}VC_{AviC}$) by ELISA. Binding specificity was verified by competing for binding to the biotinylated target protein using a 10 fold excess of non-biotinylated MsbA-EC.

binding is specific for MsbA, other biotinylated membrane proteins like $bLmrCD_{AviC}$ and $bAcrB_{AviC}$ were also included in the ELISA assay. About 37 of the DARPin clones (1.85% of all examined) were exclusively binding to $bMsbA_{AviC}$, while 5 clones were unspecifically binding to other target proteins in the ELISA (Figure_C4A). The 37 MsbA-specific DARPins were analyzed by SEC. About 27 clones displayed various degrees of oligomerization (soluble aggregates) and 6 clones displayed monomer/dimer equilibria and were therefore excluded (Figure_C4B). The remaining 4 MsbA-specific DARPins were monomeric but only one DARPin (0.05% of all examined) eluted in complex with purified MsbA in SEC (Figure_C5). The affinity of DARPin_55 for MsbA was determined by competition ELISA[10], where the binding of $bMsbA_{AviC}$ to immobilized $DARPin\_55_{myc5}$ was competed by pre-incubation with increasing amounts of free DARPin_55. The dissociation constant K_D estimated from these experiments was 80 nM. Hence, from 2000 potential DARPin binders analyzed, we could identify one specific and high affinity binder termed DARPin_55.

Binding of DARPin_55 was also analyzed with closely related homologues of *E.coli* MsbA, namely *Vibrio cholera* (MsbA-*VC*), and *Salmonella typhimurium* (MsbA-*ST*). DARPin_55 was found to bind to all three homologues. A competition ELISA was performed to test specific binding of DARPin_55, where *E.coli* MsbA was used as a competitor. DARPin_55 binding to bMsbA-ST_{AviC} and bMsbA-VC_{AviC} was competed by non-biotinylated MsbA-*E*C (Figure_C4C). The binding signal was decreased to the background level upon addition of excess competitor MsbA-*EC*, confirming specific binding of DARPin_55. The ELISA signal is reduced for bMsbA-ST_{AviC} and bMsbA-VC_{AviC}, which suggests lower binding affinity of DARPin_55 for these close homologues.

C.2.3 Crystallization of MsbA alone and the MsbA-DARPin_55 complex

The structures of MsbA from three closely related bacterial homologues, namely *Escherichia coli* (MsbA-*EC*), *Vibrio cholera* (MsbA-*VC*), and *Salmonella typhimurium* (MsbA-*ST*) were determined in three different conformations at resolution ranging from 3.7 Å to 5.5 Å. Nucleotide bound and open apo structures of MsbA were determined at 3.7 Å and 5.3 Å using MsbA-*ST* and MsbA-*EC,* respectively[9] (Figure_C2). We used MsbA-*EC* with and without DARPin_55 in the apo and the nucleotide bound state to set up crystallization plates.

C.2.3.1 Crystallization

The MsbA-DARPin_55 complex was concentrated to 15-16 mg/ml and used for crystallization while MsbA alone at 13-14 mg/ml served as a control (Figure_C5). Despite extensive efforts, the MsbA-DARPin_55 complex did not crystallize while MsbA alone crystallized in different conditions (Figure_C6). The initial conditions identified were further refined. The crystals appeared in 50 mM Tris-Cl pH 8.4, 15% PEG 400 and 1 M Ammonium formate at 20 °C and diffracted to 11 Å. To further improve the crystal quality, an additive screen including salts, small organic molecule, sugars, amino acids, dyes, cryo-preservatives, was performed. The condition was further refined using different PEG solutions (PEG 300, PEG 350 MME, PEG 4000, PEG 6000) and different buffers (HEPES and Glycine). Lipid A (the natural substrate of MsbA) as well as ATP or ADP with and without EDTA or $MgCl_2$ were also used to optimize the crystallization conditions. The optimized condition, which included jeffamine M600 50 % (v/v) as an additive to the original condition improved the diffraction quality of the crystals from 11 to 7 Å resolution (Figure_C6, A, B, C, D, E, F).

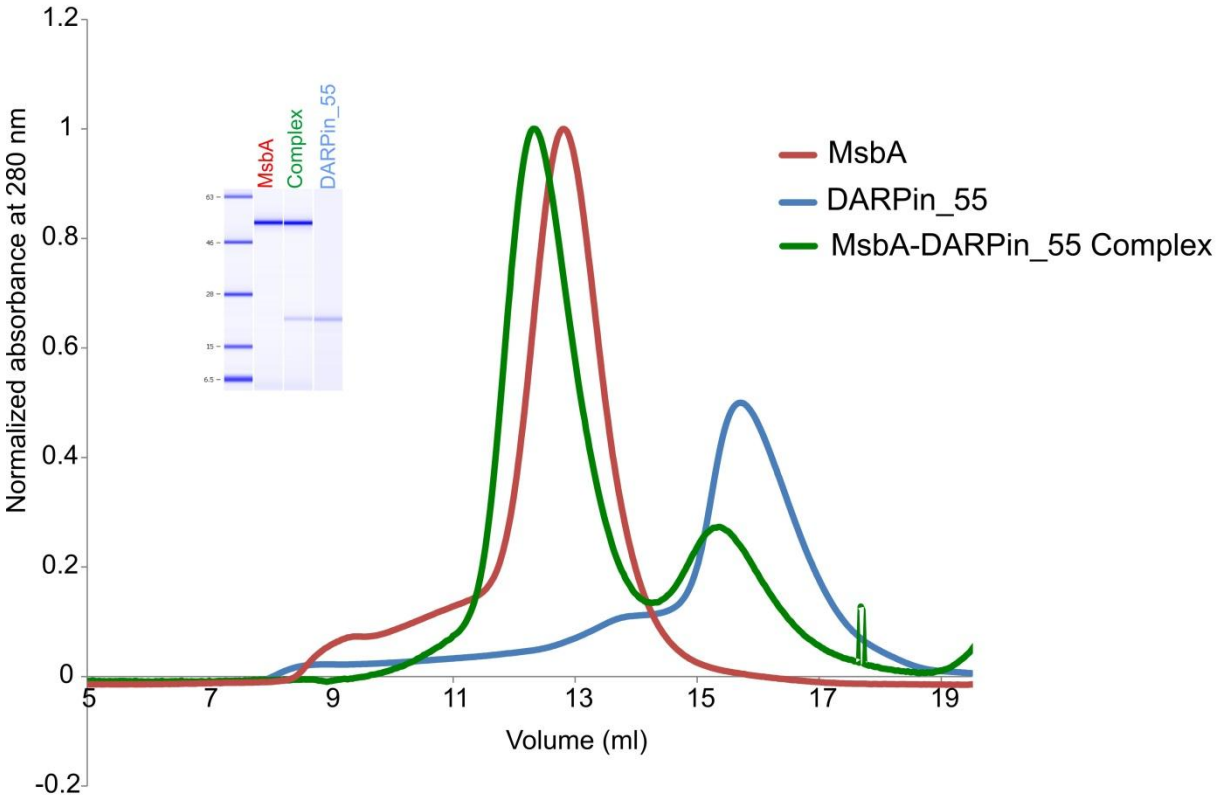

Figure_C5: Size-exclusion chromatography elution profile. MsbA and DARPin_55 were mixed at a 1:3 ratio and the complex was seperated by Superdex 200 10/300 gel-filtration column. The SDS–PAGE of the corresponding peak fractions are shown on the inset.

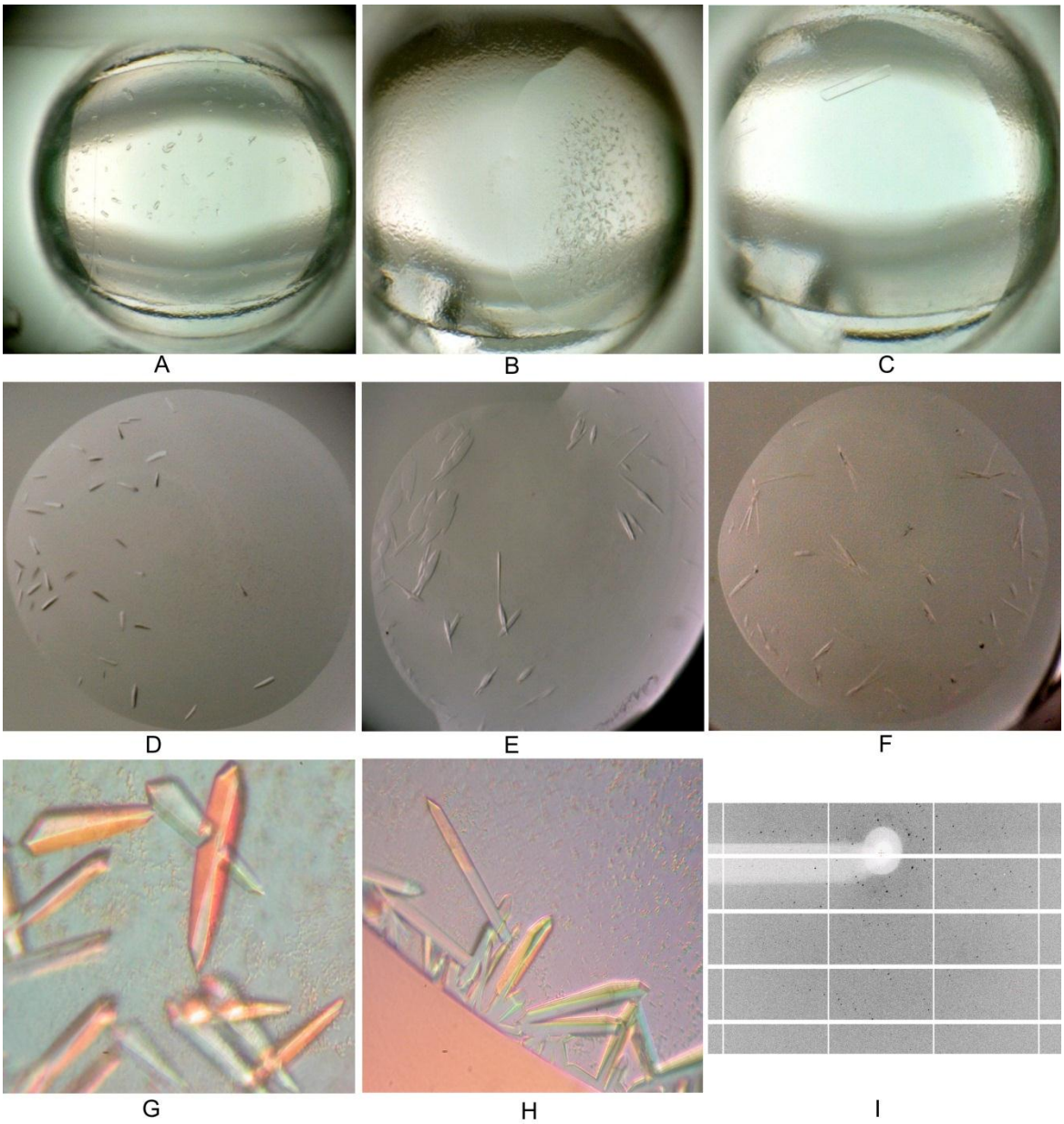

Figure_C6: Photographs of MsbA crystals in different conditions. (A, B) Crystals obtained from initial crystallization conditions (50 mM Tris pH 8.4,100 mM Potassium-Sodium tartarate and 25 % PEG 400). **(C)** Initial condition was refined and crystals diffracted to 10-16 Å resolution. **(D,E,F)** Crystals obtained from initial screens in 3 different conditions (first condition_figure D - 50 mM Tris pH 8.4, 1M Ammonium formate and 15 % PEG, second condition_figure E - 50 mM Tris pH 8.4, 100 mM KI and 15 % PEG 400 and third condition_figure F - 50 mM Sodium-cacodyl pH 5.5, 150 mM Potassium phosphate and 25 % PEG 400). **(G,H)** First condition was refined and crytals diffracted to > 7 Å resolution. **(I)** Diffraction pattern of Crystals from photograph G or H.

Homodimers in the asymmetric unit	Matthews coefficient V_M (Å^3/Dalton)	Solvent content (%)
1	18.78	93.45
2	9.39	86.90
3	6.26	80.35
4	4.69	73.80
5	3.76	67.25
6	3.13	60.70

Table 1. Cell content analysis of MsbA in $P2_1$ space group

	MsbA-*EC* (present study)	MsbA-*EC* (Chang's group) (PDB ID 3B60)
Detergent used in purification and crystallization	β-UDM	α-DDM
Crystal growth	3 days - 1 week	3 weeks - 2 months
Resolution range	48.79-7.20 Å	Native – 6.2 Å $OsCl_3$ Derivative – 5.3 Å
Space group	$P2_1$	P1
Unit cell	a= 119.01, b= 251.2, c= 179.5Å α= 90°, β= 109.16°, γ= 90°	a= 107.8, b= 126.1, c= 206.6 Å α= 83.5°, β= 76.3°, γ= 84.1°
(I)/σ(I)	11.9 (2)	-
Total no. of observations	49045 (7453)	-
Total no. of unique observations	14425 (2089)	-
Completeness	99.3 (99.8)	Native – 93 $OsCl_3$ derivative – 97
Redundancy	3.4 (3.6)	Native – 4.2 $OsCl_3$ derivative – 4.5
Distance between 567 (Glu) in two monomer chains	69 Å	74 Å
Refinement statistics		
Rwork and Rfree	50 / 56.8 *	28 / 31

Table 2. Comparison of statistics of MsbA-*EC* of present study and published MsbA structure in the apo state (PDB 3B60). * R factors are high because only part of the protein in the unit cell could be used in phasing.

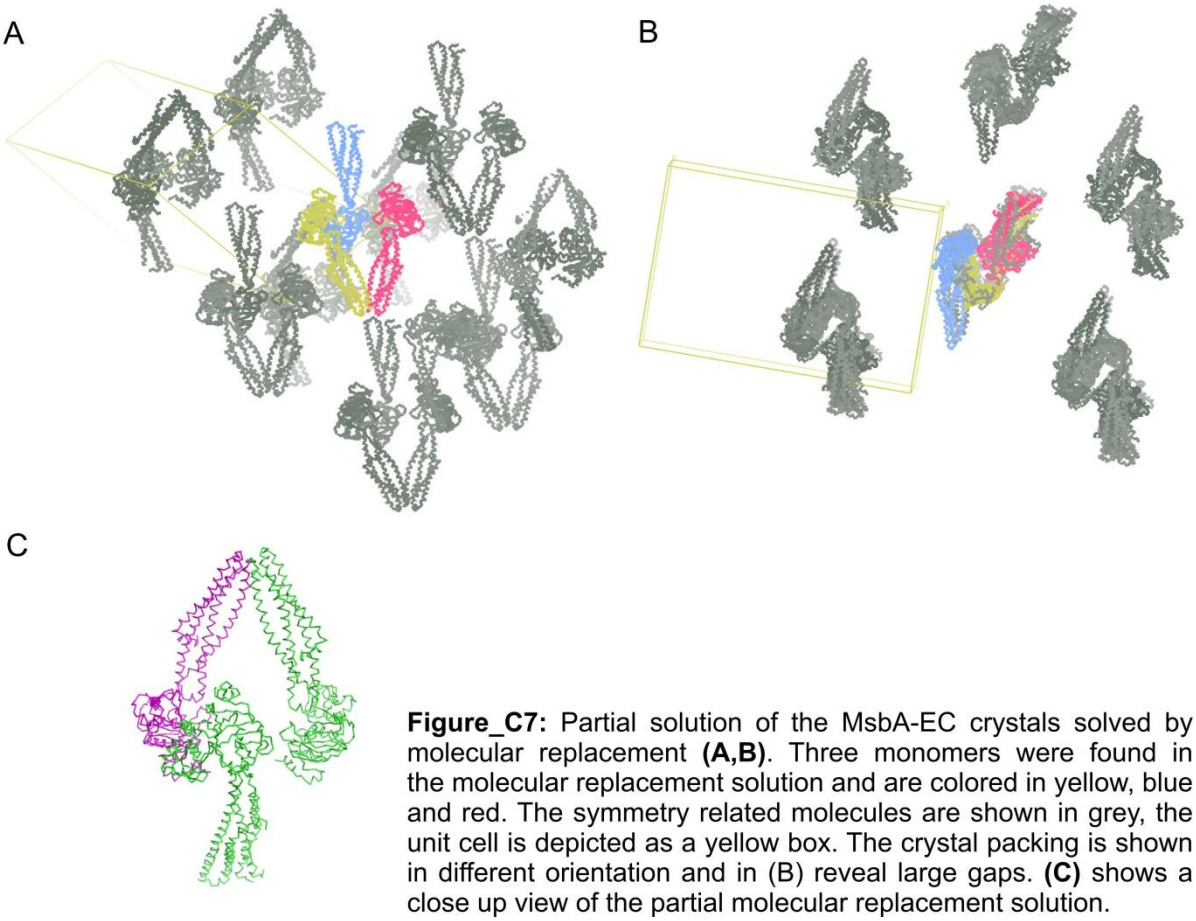

Figure_C7: Partial solution of the MsbA-EC crystals solved by molecular replacement **(A,B)**. Three monomers were found in the molecular replacement solution and are colored in yellow, blue and red. The symmetry related molecules are shown in grey, the unit cell is depicted as a yellow box. The crystal packing is shown in different orientation and in (B) reveal large gaps. **(C)** shows a close up view of the partial molecular replacement solution.

C.2.3.2 Crystallographic analysis

Data were collected on a Pilatus 6M detector at the Swiss Light Source (beamline X06SA), Villigen, and Switzerland. The MsbA crystals diffracted to a resolution of around 7 Å using the synchrotron light source. A complete data set of 180° was obtained with an oscillation range of 0.5°. The data were processed using the program XDS[22]. The space group was determined to be $P2_1$. The probable number of homodimers in the asymmetric unit is 4, 5 or 6, with solvent contents of 73.80, 67.25 or 60.70, respectively (Table 1). The Matthew's coefficient was calculated as V_m = 4.69, 3.76 or 3.13 $Å^3$/Dalton for 4, 5 or 6 molecule in the asymmetric unit, respectively (calculations were based on the molecular weight of dimeric MsbA as 135 kDa). The reported MsbA structure in the apo state (PDB ID 3B60) was determined in space group P1 with solvent content of 75.4 % and 4 molecules in the asymmetric unit. In general, membrane protein crystals contain solvent contents of around 70 %. We therefore considered 4 molecules in the asymmetric unit with the solvent content of 73.8 % for the molecular replacement (Table 1).

To determine the MsbA structure from the native data set, we tried molecular replacement using MsbA coordinates[9] (PDB ID: 3B5W) as a search model. We attempted molecular replacement in PHASER[23] using one monomeric chain of MsbA with and without TM4 and TM5 (the trans-membranes involved in domain swapping, which is deviating most between different MsbA structures (Figure_A6)) as search model. Phaser found only 3 MsbA monomers as molecular replacement solution. The log-likelihood-gain (LLG) and translation function (TFZ) were 42 and 13.5, respectively, when TM4 & TM5 were included in the MsbA search model. However, LLG was increased to 91 with a TFZ value of 13.5, if the truncated monomeric chain of MsbA devoid of TM4 & TM5 was used to calculate phases. The maximum likelihood asserts the best model probability based on the data provided[23]. A positive value of LLG and TFZ value greater than 10 indicate that the partial molecular replacement solution is likely to be correct. Therefore, we used the partial structure solution with the higher value for LLG for further analysis. The partial structure solution includes one MsbA dimer and one MsbA monomer, which is much less than the expected 8 MsbA monomers in the asymmetric unit. The 3 detected truncated monomer MsbA contain a relatively low fraction of the total scattering mass, which makes the detection of the remaining MsbA molecules very difficult due to the large signal to background at poor resolution (>7 Å). The partial structure solution was then optimized by rigid body refinement

using PHENIX. The Rfree and Rwork values obtained were very high. This is primarily due to the fact that only a partial structure could be used for phasing and structure factor calculation. The structure could not be further refined using Refmac5 (CCP4i) or PHENIX. A comparison of the structure determination of the present study and the published structure[9] has been included in Table 2. Crystals that diffract to higher resolution are needed to determine the full structure of MsbA in this crystal form.

C.3 Discussion

Despite the advances in macromolecular crystallography, structural studies of interesting macromolecules and membrane proteins are frequently hampered at several steps including high throughput screening of expression and purification, robotics crystallization (vapor diffusion, lipid cubic phase) and synchrotron radiation. Conformational heterogeneity, flexible structure and surface chemistry are reasons why a particular protein is difficult to crystallize. Such hurdles have been successfully overcome by co-crystallization of these proteins together with natural ligands[9,24] or by genetic engineering[25,26]. Chaperone assisted crystallography is a promising approach, which dates back to the co-crystallization of hen egg-white lysozyme and the Fab of a monoclonal anti-lysozyme antibody[27]. The concept behind chaperone assisted crystallography is to increase the probability of obtaining well-ordered crystals by minimizing the conformational heterogeneity of the target protein or by increasing the hydrophilic surface for potential crystal contacts. Antibody based chaperones have successfully been used to crystallize membrane proteins[28,29]. Non-antibody based scaffolds such as **D**esigned **A**nkyrin **R**epeat **P**rote**ins** (DARPins) have been developed by protein engineering with improved properties (Cysteine less scaffold, higher expression in bacteria)[10,30,31]. The continuously increasing numbers of co-crystal structures in complex with DARPins have validated the importance of this scaffold in macromolecular crystallography[32].

In the present study, MsbA has been successfully expressed and purified with a deca-his-tag at the N-terminus. Detergent (β-UDM) solubilized MsbA shows basal ATPase activity, indicating that the purified protein is suitable for functional characterization and crystallographic studies. MsbA can be expressed and purified in reasonable quantities, which makes it an attractive target for crystallization studies. MsbA was considered as a promising target to apply the chaperone assisted crystallography approach, because it provides crystals that diffract only to low resolution (5.3 Å and 5.5 Å)[9]. The resulting MsbA structures in two

different apo-states are currently of very poor quality. With MsbA-specific DARPins, it was hoped that: (i) the MsbA-DARPin complexes would give rise to better diffracting crystals, and (ii) DARPins potentially could trap the intrinsically flexible transporter in a different conformational state.

Here, the use of *in vitro* selection method is demonstrated to identify a specific binder for MsbA, named DARPin_55. DARPin_55 showed a homogenous monomeric gel-filtration profile, which is a critical requirement to separate the ''target protein-DARPin'' complex from excess DARPin by gel-filtration chromatography. The stoichiometry of MsbA and DARPin_55 was determined as 1 DARPin binding to homodimeric MsbA (Chapter B). Also, the possibility of using DARPin_55 in complex with other homologues of MsbA, namely MsbA-*VC*, and MsbA-*ST* for co-crystallization studies was investigated. DARPin_55 binds to MsbA-*ST* with a similar affinity as MsbA-*EC*, while binding affinity to MsbA-*VC* is about 60 % of the affinity to MsbA-*EC,* judged from ELISA signals (Figure_C4C). The epitope for DARPin_55 is located in the membrane spanning part of the transmembrane domain (TMDs) of MsbA (Chapter B). The TMD sequence identity between MsbA-*EC* and MsbA-*ST* and MsbA-*VC* is 97 and 64 %, respectively. It is therefore not surprising that DARPin_55 binds to MsbA-*ST* equally well as to MsbA-*EC*. Although the sequences of MsbA-*EC* and MsbA-*VC* are quite different, DARPin_55 specifically binds to MsbA-*VC* reasonably well (Figure_C4C) (as seen by ELISA), which would suggest that the binding epitope is rather conserved. This provided the opportunity to co-crystallize DARPin_55 in complex with MsbA_*EC* and MsbA_*ST*. However, the co-crystallization of DARPin_55 with either homologue did not lead to any crystal. Interestingly, several crystallization conditions for MsbA-EC and MsbA-ST alone were found. This indicates that in this particular case, addition of DARPin_55 was rather inhibiting than promoting crystal growth. Therefore, the chaperone assisted crystallography approach is not a generic method for obtaining better crystals, but remains one of many methods that can be used. The identification of only one MsbA-specific DARPin restricted our efforts to improve the current MsbA structures. In a previous study on AcrB, it was found that only a subset of DARPins could successfully be used as crystallization chaperones, whereas many DARPins were recalcitrant to co-crystallize in complex with AcrB[33].

One of the MsbA-EC crystallization conditions was refined and datasets to 7 Å were collected. A partial structure could be solved by molecular replacement. The partial structure

solution shows the inverted V shaped structure as reported previously[9]. Compared to the previous structure the distance between the NBDs are about 5 Å shorter. The distance differences between the two NBDs of MsbA can be attributed to the different detergent used in the purification and crystallization or to the intrinsic flexibility of the apo-state of MsbA.

Binders of other scaffolds such as Fabs, nanobodies etc. can be selected against MsbA. The identification of a number of binders of various scaffolds would increase the likelihood to find better diffracting co-crystals. The MsbA-DARPin_55 complex did not crystallize using the vapor diffusion method. In the future, lipid cubic phase could be an alternative to crystallize the MsbA-DARPin_55 complex.

C.4 Experimental procedure

C.4.1 Generation of genetic constructs

All the constructs of *E.coli* MsbA used in this study are described in Chapter B. *Salmonella typhimurium and Vibrio cholerae msbA* genes were amplified using forward primers (MsbA_ST_PstI_F and MsbA_VC_PstI_F) and reverse primers (MsbA_ST_XbaI_R and MsbA_VC_XbaI_R). The PCR amplified product flanked by PstI and XbaI restriction sites was ligated into the *E. coli* expression vector pBAD24[34] . These expression vectors were named as pBADMsbA_ST and pBADMsbA_VC (expressed protein were termed $MsbA\_ST_{His}$ and $MsbA\_VC_{His}$ respectively).

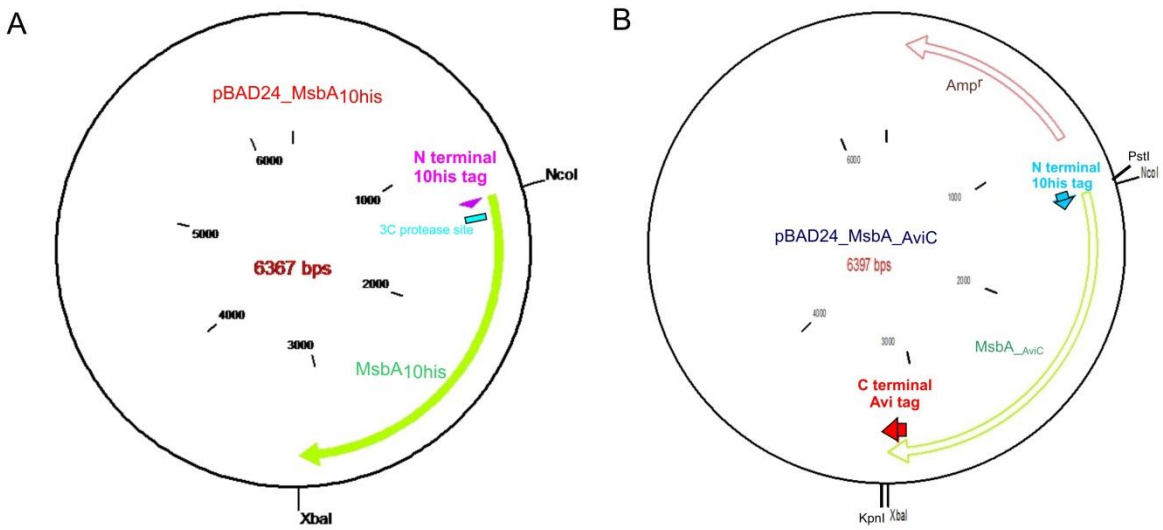

Figure_C8: Plasmid map of MsbA. (A) MsbA construct used in crystallization studies. **(B)** C-terminally Avi-tagged MsbA construct used in ribosome display and ELISA screening.

The generation of C-terminally Avi-tagged MsbA constructs of 3 different homologues is described here. A DNA fragment encoding the Avi-tag sequence flanked by the restriction sites NheI and BamHI was formed by annealing the two oligonucleotides avitag_for and avitag_rev, and was ligated into the *E.coli* cloning vector pGEM using the NcoI and XbaI restriction sites. This vector was named as pGEM_Avi. The *E.coli msbA* gene was cloned into pGEM_Avi vector between the NcoI and NheI restriction site, amplified with the primers msbA_DecaHisN_for and msba_AviC_rev from the clone pNZMsbA[35]. Then the 3' Avi-tagged *E.coli msbA* gene was sub-cloned into pBAD24 using the restriction sites NcoI and XbaI resulting in pBADMsbA_EC$_{_AviC}$ (the expressed protein was termed as MsbA_EC$_{_AviC}$). The pBAD$_{AviC}$ vector backbone flanking PstI/KpnI restriction site was generated from the pBADMsbA_EC$_{_AviC}$ using the primers pBAD_10his_PstI_F and pBAD_N10his3C_KpnI. The *Salmonella typhimurium and Vibrio cholerae msbA* genes were amplified using forward primers (MsbA_ST_PstI_F, MsbA_VC_PstI_F) and reverse primers (MsbA_ST_XbaI_R, MsbA_VC_KpnI_R). The amplified product flanked by PstI and KpnI restriction sites was ligated into the *E. coli* expression vector pBAD$_{AviC}$ (expressed proteins were termed as MsbA_ST$_{_AviC}$ and MsbA_VC$_{_AviC}$, respectively) (Figure_C8).

C.4.2 Protein expression and purification

C.4.2.1 Expression and purification of MsbA

MsbA expression and purification has been described in Chapter B (see supplementary experimental procedure). For crystallization studies, the N-terminal deca-his-tag of MsbA was cleaved by overnight incubation of the IMAC purified protein with 3C protease at a 1:2 molar ratio. For MsbA-DARPin_55 complex formation, first concentrated DARPin_55 was gel filtrated in TBS$_{150}$-UDM buffer and monomeric fractions were mixed with freshly IMAC purified MsbA at a 3:1 ratio and further incubated for 15 minutes at 4 °C. The MsbA-DARPin_55 complex was separated by SEC from the excess DARPin_55. MsbA alone and the MsbA-DARPin_55 complex were concentrated on a 100 kDa cutoff (Millipore) filter to 13-14 and 15-16 mg/ml for crystallization experiments.

C.4.2.2 Expression and purification of DARPins

DARPin expression was performed in *E. coli* XL1-Blue in 2YT medium. Protein expression was induced with 0.5 mM IPTG at OD_{600} of 0.7 to 0.9 for 3–4 h at 37 °C. Harvested cell pellets were resuspended in 20 mM Tris/HCl (pH 7.4) buffers containing 150 mM NaCl, 25 µg/ml

DNaseI and protease inhibitor cocktail (Sigma). Cells were lysed using an EmulsiFlex-C3 (Avestin) cell disrupter. Unbroken cells and cell debris were removed by centrifugation at 20,000 rpm (SS34 rotor) for 30 minutes at 4 °C and the cleared lysate was applied to an IMAC column (Ni^{+2}–NTA, Qiagen). The resin was washed with 20 mM imidazole pH 7.5, TBS and 10% glycerol (30 ml) and DARPins were eluted from the column using 250 mM imidazole pH 7.5 and 10% glycerol (10 ml) in the same buffer. IMAC purified DARPins were analyzed by SEC using a Superdex 200, 10/300 (GE Healthcare) column.

C.4.3 Procedure of enzymatic biotinylation using BirA

The purified protein (for example $MsbA_{AviC}$ 5 µM) was enzymatically *in vitro* biotinylated by incubation with ATP (10 mM), Biotin (5 µM), magnesium acetate (10 mM), 10 % glycerol, TBS_{150}-UDM buffer and BirA ligase (3 µl from 8 mg/ml stock) with a total volume of 2.5 ml at 4°C overnight. We termed biotinylated Avi-tagged $MsbA_{AviC}$ as $bMsbA_{AviC.}$

C.4.4 Selection and screening of DARPin binders against MsbA

C.4.4.1 Selection of DARPin binders (Ribosome display)

The N3C DARPin library was used for DARPin selection against MsbA using ribosome display[10]. Ribosome display is a cell-free system for *in vitro* binder selection. The principle of binder selection strategy is the coupling of genotype (RNA, DNA) and phenotype (protein). In ribosome display, this coupling is achieved during *in vitro* translation by the ternary complex, consisting of mRNA (genotype), the ribosome and the nascent polypeptide (phenotype)[36]. Ribosome display has several advantages over other selection methods, as follows:

i). the diversity of the working library is not limited by transformation steps involved in contrast to Phage display,

ii). in contrast to immunization of animals, such as mice and llama, *in vitro* selection conditions can be monitored (for example, a suitable detergent or ligand can be included to avoid protein precipitation while in *in vivo* selection process conformational integrity of the protein cannot be controlled after injection into the animal).

A detailed process of DARPin binders selection by ribosome display has been described by Zahnd et al[31]. Briefly, a DNA library encoding open reading frames lacking stop codons is transcribed *in vitro*. The mRNA is *in vitro* translated; the encoded protein is not released and folds correctly on the ribosome. The mRNA-ribosome-protein complexes are used for affinity selection on an immobilized target protein. After washing, the bound

ribosomal complexes are dissociated using EDTA. The mRNA is purified and used for reverse transcription followed by PCR amplification. The PCR product can be used directly for the next ribosome display selection cycle[36] (Chapter B-Figure_S1). The selection of DARPin binders against MsbA was done using ribosome display following the standard protocol[31] with some modifications. Briefly, in all 4 selection rounds, 0.05 % of β-UDM detergent was used to maintain the MsbA in soluble state during the selection procedure. For membrane proteins solution panning has been shown to have advantages over surface panning[30]. In solution panning, biotinylated MsbA is immobilized on the surface of magnetic beads by virtue of the streptavidin-biotin interactions. Therefore, all 4 selection rounds were done using solution panning instead of surface panning. Streptavidin coated magnetic beads (Roche 11641778001 or Dynabeads MyoneTMStreptavidinT1 or Invitrogen 800.955.6288) were blocked in TBS-BSA (100 µl per 10 µl initial suspension) overnight at 4 °C or 2 hours at room temperature (RT) and washed once with WBT-BSA_0.05% β-UDM prior to use. A pre-panning step was included to remove the DARPins which unspecifically stick to the beads. In the pre-panning step, *in vitro* translated DARPin library (the translation mix, containing the ternary mRNA–ribosome–DARPin complexes) was incubated with streptavidin coated beads for 1 hour at 4°C. Unbound ternary complexes were mixed with $bMsbA_{AviC}$ (120 nM for first and second round, 60 nM for third and fourth round) for 1 hour (first and second round) or 45 minutes (third and fourth round). The panning solution was transferred to the fresh streptavidin magnetic beads and incubated for 15 minutes at 4°C. The immobilized $bMsbA_{AviC}$ binding to the streptavidin beads was washed 4 times with WBT-BSA-0.05% β-UDM. The washing time was increased from round to round (15 minutes total washing time in the first round to 120 minutes total washing time in the fourth round). After washing, the mRNA was eluted with 200 µl elution buffer, which disintegrates the ternary complex. Four rounds of ribosome display were performed. The number of PCR cycles after reverse transcription were reduced from round to round from 45 (first round) to 30 (fourth round). To avoid the capture of unspecific binders, we used hydrophilic (Roche 11641778001) and hydrophobic (Dynabeads® MyOne™ Streptavidin T1) streptavidin beads alternatively in the RD rounds.

C.4.4.2 Screening of specific DARPin binders (Crude cell extract ELISA)

The DARPin pool of the 4th selection round was cloned into $pQE30_{myc5}$ containing an N-terminal M-R-G-S-(H)6 tag and C-terminal Myc_5-tag (5 times amino acid sequence M-E-Q-K-L-

I-S-E-E-D-L-N-E) (the expressed protein is termed $DARPin_{myc5}$). Preparation of crude cell lysate and ELISA screening of the specific binders were done as described earlier[30]. Briefly, 96-well ELISA plates (Nunc MaxiSorp) were coated with Protein A (Sigma, 100 µl, 5 µg/ml in PBS) overnight at 4 °C and blocked with TBS-BSA (300 µl) for 2 hours at room temperature. Then, anti-myc antibody (Sigma, clone 9E10, 1:2000 diluted) was immobilized via a specific interaction between the coated Protein A and its constant Fc region for 3-4 hours at 4°C. After washing with TBS, the plate was incubated with the diluted $DARPin_{myc5}$ containing crude cell extracts for 1 hour, followed by another washing step and the incubation with 50 nM biotinylated target protein (100 µl). The wells were washed 3 times with TBS-BSA-0.05% β-UDM and incubated with Streptavidin-alkaline phosphatase conjugate for 30 minutes (Roche, 1:1000 diluted) at room temperature. Final extensive washes (TBS-BSA-0.05% β-UDM) for 4 times were made before the ELISA signal was developed using the p-nitrophenyl phosphate (pNPP) substrate and the OD_{405} was measured. Competition ELISA with purified DARPin proteins was performed to demonstrate the specificity of the selected DARPins for MsbA. For competition experiments, 500 nM of MsbA (competitor) were pre-incubated with 50 nM of $bMsbA_{AviC}$ before adding to the immobilized $DARPin_{myc5}$.

C.5 References

1. Doerrler, W.T., Reedy, M.C. & Raetz, C.R. An *Escherichia coli* mutant defective in lipid export. *J Biol Chem* **276**, 11461-4 (2001).
2. Poltorak, A. et al. Defective LPS signaling in C3H/HeJ and C57BL/10ScCr mice: mutations in Tlr4 gene. *Science* **282**, 2085-8 (1998).
3. Chang, G. & Roth, C.B. Structure of MsbA from *E. coli*: a homolog of the multidrug resistance ATP binding cassette (ABC) transporters. *Science* **293**, 1793-800 (2001).
4. Dawson, R.J. & Locher, K.P. Structure of the multidrug ABC transporter Sav1866 from Staphylococcus aureus in complex with AMP-PNP. *FEBS Lett* **581**, 935-8 (2007).
5. Chang, G. Structure of MsbA from *Vibrio cholera*: a multidrug resistance ABC transporter homolog in a closed conformation. *J Mol Biol* **330**, 419-30 (2003).
6. Reyes, C.L. & Chang, G. Structure of the ABC transporter MsbA in complex with ADP.vanadate and lipopolysaccharide. *Science* **308**, 1028-31 (2005).
7. Jeffrey, P.D. Analysis of errors in the structure determination of MsbA. *Acta Crystallogr D Biol Crystallogr* **65**, 193-9 (2009).
8. Geoffery Chang, C.B.R., Christopher L. Reyes, Owen Pornillos,Yen-Ju Chen, Andy P. Chen. Retraction. *Science* **VOL 314** 1875 (2006).
9. Ward, A., Reyes, C.L., Yu, J., Roth, C.B. & Chang, G. Flexibility in the ABC transporter MsbA: Alternating access with a twist. *Proc Natl Acad Sci U S A* **104**, 19005-10 (2007).
10. Binz, H.K. et al. High-affinity binders selected from designed ankyrin repeat protein libraries. *Nature Biotechnology* **22**, 575-582 (2004).
11. Koide, S. Engineering of recombinant crystallization chaperones. *Current Opinion in Structural Biology* **19**, 449-457 (2009).
12. Sennhauser, G. & Grütter, M.G. Chaperone-Assisted Crystallography with DARPins. *Structure* **16**, 1443-1453 (2008).
13. Stumpp MT & P., A. DARPins: a true alternative to antibodies. *Curr Opin Drug Discov Devel.* **10**, 153-159 (2007).
14. Bandeiras, T.M. et al. Structure of wild-type Plk-1 kinase domain in complex with a selective DARPin. *Acta Crystallographica Section D Biological Crystallography* **64**, 339-353 (2008).
15. Sennhauser, G., Amstutz, P., Briand, C., Storchenegger, O. & Grütter, M.G. Drug Export Pathway of Multidrug Exporter AcrB Revealed by DARPin Inhibitors. *PLoS Biology* **5**, e7 (2007).
16. Monroe, N., Sennhauser, G., Seeger, M.A., Briand, C. & Grütter, M.G. Designed ankyrin repeat protein binders for the crystallization of AcrB: Plasticity of the dominant interface. *Journal of Structural Biology* **174**, 269-281 (2011).
17. Murakami, S., Nakashima, R., Yamashita, E. & Yamaguchi, A. Crystal structure of bacterial multidrug efflux transporter AcrB. *Nature* **419**, 587-93 (2002).
18. Markus A. Seeger et al. Structural asymmetry of AcrB trimer suggests a peristaltic pump mechanism. *Science* **313**, 1295-1298 (2006).
19. Murakami, S., Nakashima, R., Yamashita, E., Matsumoto, T. & Yamaguchi, A. Crystal structures of a multidrug transporter reveal a functionally rotating mechanism. *Nature* **443**, 173-179 (2006).
20. Cull, M.G. & Schatz, P.J. Biotinylation of proteins *in vivo* and *in vitro* using small peptide tags. *Methods Enzymol* **326**, 430-40 (2000).
21. Driegen, S. et al. A generic tool for biotinylation of tagged proteins in transgenic mice. *Transgenic Res* **14**, 477-82 (2005).

22. Kabsch, W. Automatic processing of rotation diffraction data from crystals of initially unknown symmetry and cell constants. *J Appl Cryst* **26**, 795-800 (1993).
23. McCoy, A.J. et al. Phasercrystallographic software. *Journal of Applied Crystallography* **40**, 658-674 (2007).
24. Anderson, J., Ptashne, M. & Harrison, S.C. Cocrystals of the DNA-binding domain of phage 434 repressor and a synthetic phage 434 operator. *Proc Natl Acad Sci U S A* **81**, 1307-11 (1984).
25. Abramson, J. et al. Structure and mechanism of the lactose permease of *Escherichia coli*. *Science* **301**, 610-5 (2003).
26. Prive, G.G. & Kaback, H.R. Engineering the lac permease for purification and crystallization. *J Bioenerg Biomembr* **28**, 29-34 (1996).
27. Amit, A.G., Mariuzza, R.A., Phillips, S.E. & Poljak, R.J. Three-dimensional structure of an antigen-antibody complex at 6 Å resolution. *Nature* **313**, 156-8 (1985).
28. Iwata, S., Ostermeier, C., Ludwig, B. & Michel, H. Structure at 2.8 Å resolution of cytochrome c oxidase from *Paracoccus denitrificans*. *Nature* **376**, 660-9 (1995).
29. Dutzler, R., Campbell, E.B., Cadene, M., Chait, B.T. & MacKinnon, R. X-ray structure of a ClC chloride channel at 3.0 Å reveals the molecular basis of anion selectivity. *Nature* **415**, 287-94 (2002).
30. Huber, T., Steiner, D., Rothlisberger, D. & Pluckthun, A. *In vitro* selection and characterization of DARPins and Fab fragments for the co-crystallization of membrane proteins: The $Na^{(+)}$-citrate symporter CitS as an example. *J Struct Biol* **159**, 206-21 (2007).
31. Zahnd, C., Amstutz, P. & Pluckthun, A. Ribosome display: selecting and evolving proteins *in vitro* that specifically bind to a target. *Nat Methods* **4**, 269-79 (2007).
32. Sennhauser, G. & Grutter, M.G. Chaperone-assisted crystallography with DARPins. *Structure* **16**, 1443-53 (2008).
33. Monroe, N., Sennhauser, G., Seeger, M.A., Briand, C. & Grutter, M.G. Designed ankyrin repeat protein binders for the crystallization of AcrB: plasticity of the dominant interface. *J Struct Biol* **174**, 269-81 (2011).
34. Guzman, L.M., Belin, D., Carson, M.J. & Beckwith, J. Tight regulation, modulation, and high-level expression by vectors containing the arabinose P_{BAD} promoter. *J Bacteriol* **177**, 4121-30 (1995).
35. Woebking, B. et al. Drug-lipid A interactions on the *Escherichia coli* ABC transporter MsbA. *J Bacteriol* **187**, 6363-9 (2005).
36. Hanes, J. & Pluckthun, A. *In vitro* selection and evolution of functional proteins by using ribosome display. *Proc Natl Acad Sci U S A* **94**, 4937-42 (1997).

CHAPTER D

DARPin selection against the Nucleotide binding domain of homodimeric ABC transporter MsbA for structural and functional studies

D.1 Introduction

ABC (ATP-binding cassette) transporters are primary active transporters that translocate allocrites across the lipid bilayer. The term 'allocrite' was coined by Blight and Holland to describe the 'transport substrate', the compound that is translocated, but not changed chemically[1]. A prototypical ABC transporter consists of four domains, namely two cytosolic nucleotide binding domains (NBDs) and two transmembrane domains (TMDs). The amino acid sequence is highly conserved in the NBDs throughout the ABC transporter superfamily. The NBDs energize the transport cycle by binding and hydrolyzing ATP (Figure_D1). The TMDs are quite disparate in amino acid sequence and structural fold[2] (thereby, they are classified as Type I, II ABC importers and ABC exporters) and form a translocation pathway across the lipid membrane which determines the substrate specificity.

Multidrug resistance (MDR) in eukaryotes (example in cancer cells) has been implicated due to the overexpression of multidrug transporters. To understand the molecular mechanism of transport of chemically distinct molecules across the lipid membrane[3], structural information of these proteins is required. The expression and purification of full length ABC transporter proteins has always been more difficult than of isolated nucleotide binding domains. The first high-resolution structure of a bacterial ABC transporter's domain was determined for the isolated NBD of histidine permease[4]. Thereafter, about 50 crystal structures of NBDs ranging from bacteria to humans have been determined[5]. The structural fold of the NBD is conserved throughout the most distantly related members of ABC transporter superfamily. The structure of the NBD monomer can be divided into two subdomains: a larger RecA-like core-subdomain and a helical subdomain[6] (Figure_D2). The core-subdomain consists of 6 conserved motifs.

1). Walker A motif (yellow, consensus sequence GXXGXGKS[S/T], where X denotes any amino acid) (Figure_D2A). In a closed NBD dimer, the Walker A motif of the cis-NBD monomer and

Signature motif (light blue, LSGGQ) of the trans-NBD monomer sandwich the γ-phosphate of the bound ATP molecule that leads to the formation of a composite nucleotide binding site.

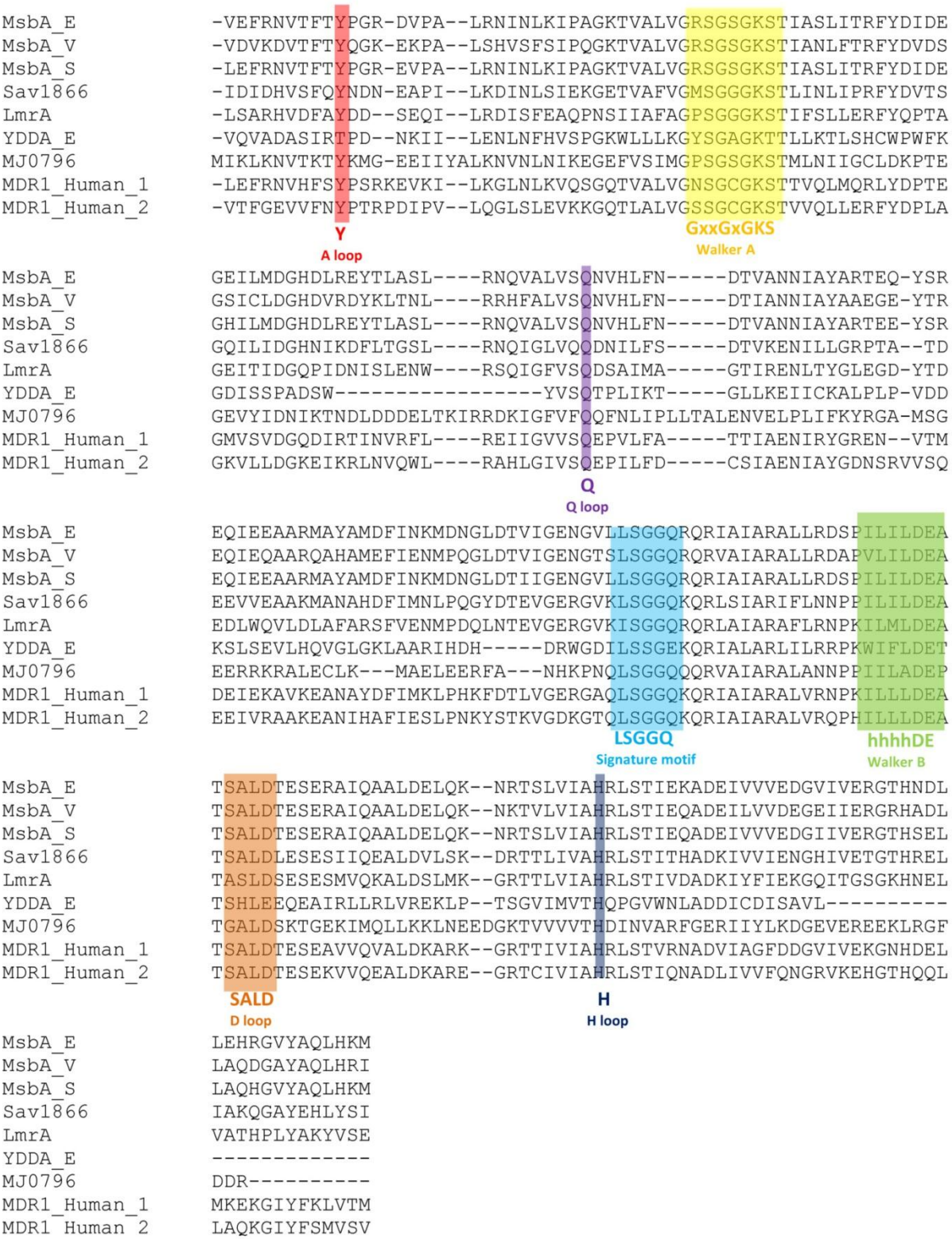

Figure_D1. Multiple sequence alignment of NBD´s from different ABC transporters. Conserved motifs are highlighted by different colors as described in the text. The alignment was created with ClustalW2.

2). Walker B motif (green, consensus sequence hhhhDE, where h is a hydrophobic amino acid). A conserved glutamate (hhhhD**E**) in the Walker B motif is important for the proper positioning of the γ-phosphate of the ATP and proposed to play a central role in the ATP hydrolysis by acting as a general base.[7]

3). The A loop (red) forms π-π interactions with the adenine ring of the bound ATP.

4). In the Q loop (purple), a conserved glutamine interacts with the γ-phosphate of ATP via a water molecule.

5). Residues of the D-loop (orange) in the cis-NBD make contact with residues of the trans-NBD and thereby play a role in the communication between the two catalytic sites.

6). In the H-loop (dark blue), a conserved histidine interacts with the Walker B glutamate and thereby plays a role in ATP hydrolysis.

The helical subdomain is unique to ABC transporters and is not seen in other ATPases. It contains the ABC signature motif (light blue, consensus sequence LSGGQ) which interacts with the γ-phosphate of ATP in the closed NBD dimer. The presence of this motif is diagnostic for members of ABC superfamily[6,8,9].

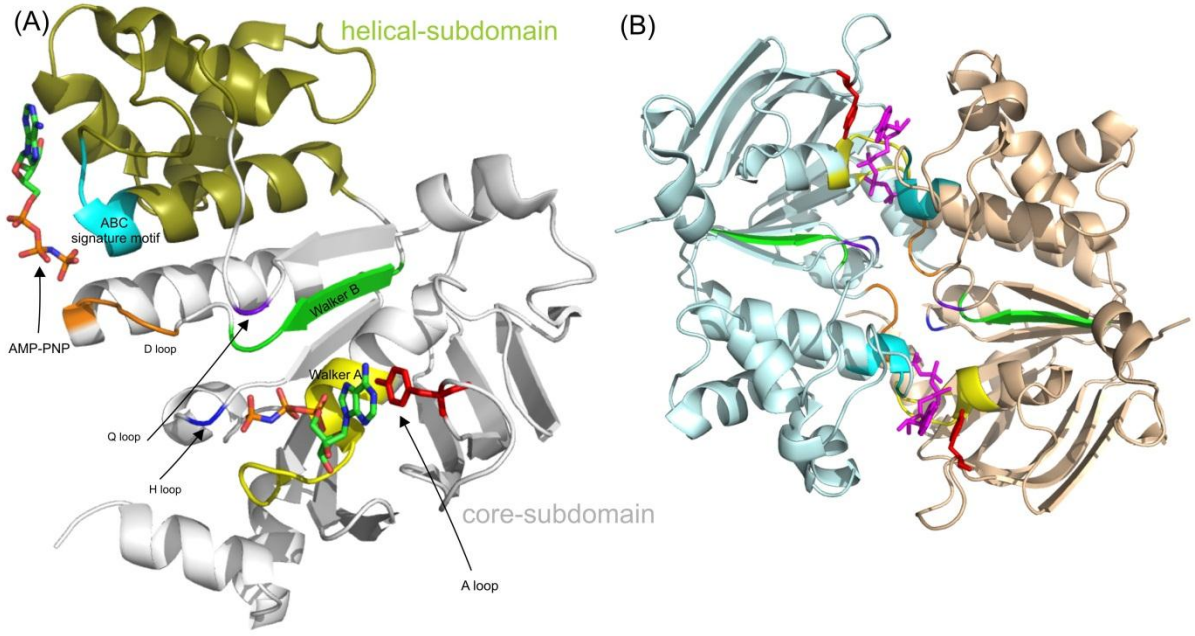

Figure_D2: Cartoon representation of the nucleotide binding domain monomer (A) and dimer (B) of MsbA. **(A)** The helical-subdomain is shown in olive green and the core-subdomain in grey color. The conserved motifs of the core-subdomain are the Walker A motif (yellow), the Walker B motif (green), the Q loop (purple), the A loop (red), the D loop (orange), the H loop (dark blue). The Signature motif (cyan) is part of the helical subdomain. **(B)** NBD dimer of MsbA, complexed with AMP-PNP. All conserved motif are shown with the same colors used for the NBD monomer and AMP-PNP is shown in magenta (Figures were made using pymol, PDB ID 3B60). In a closed NBD dimer, the Signature motif is in close contact with AMP-PNP.

DARPin selection against the full length ABC transporters resulted either into the binders those binding to the TMDs of the full length protein (MsbA-Chapter B, C and LmrCD-Chapter E) or the hydrophobic "sticky" binders forming various degrees of oligomers and were unsuitable for further studies (MsbA-Chapter B, C and YDDA-Chapter F). We tried to circumvent these problems by using the cytoplasmic nucleotide binding domain of MsbA as a target protein. These NBD specific binders increase the probability of co-crystallization of the MsbA-DARPin complex because cytosolic domains are not surrounded by the detergent micelles and therefore DARPin bound to the NBDs can increase the hydrophilic surface area for crystal lattice formation. At the functional level, any allosteric effect on the functionality of MsbA after DARPin binding will be analyzed by established ATPase assay. In this chapter, we used ribosome display to select specific binders against the isolated NBD of MsbA. We aimed to find specific and monomeric binders for the functional and structural characterization of MsbA.

D.2 Results

D.2.1 Selection and screening of DARPins against the NBD of MsbA

Selection against the NBD of MsbA was performed by Dr. Thilo Schroeder using the RD. The RD procedure is summarized in Chapter C.4.4.1. Briefly, the N3C DARPin DNA-library[10] was used and four rounds of RD selections were carried out following the surface panning strategy as described[10]. The enriched pool of binders from the fourth round of RD was sub-cloned into the expression vector pQE30. About 1500 clones were analyzed for binding to NBD-MsbA by crude extract ELISA. 19 binders (DNBD_1-19) were found in the initial ELISA screen and were further analyzed by ELISA using chemically biotinylated maltose binding protein (bMBP) as a control besides biotinylated nucleotide binding domain ($bNBD_{AviC}$). 10 of these clones were found exclusively binding to $bNBD_{AviC}$ (Figure_D3) and about half of the clones (9 of 19 clones) did bind to both $bNBD_{AviC}$-MsbA and bMBP and were therefore false positives (not shown).

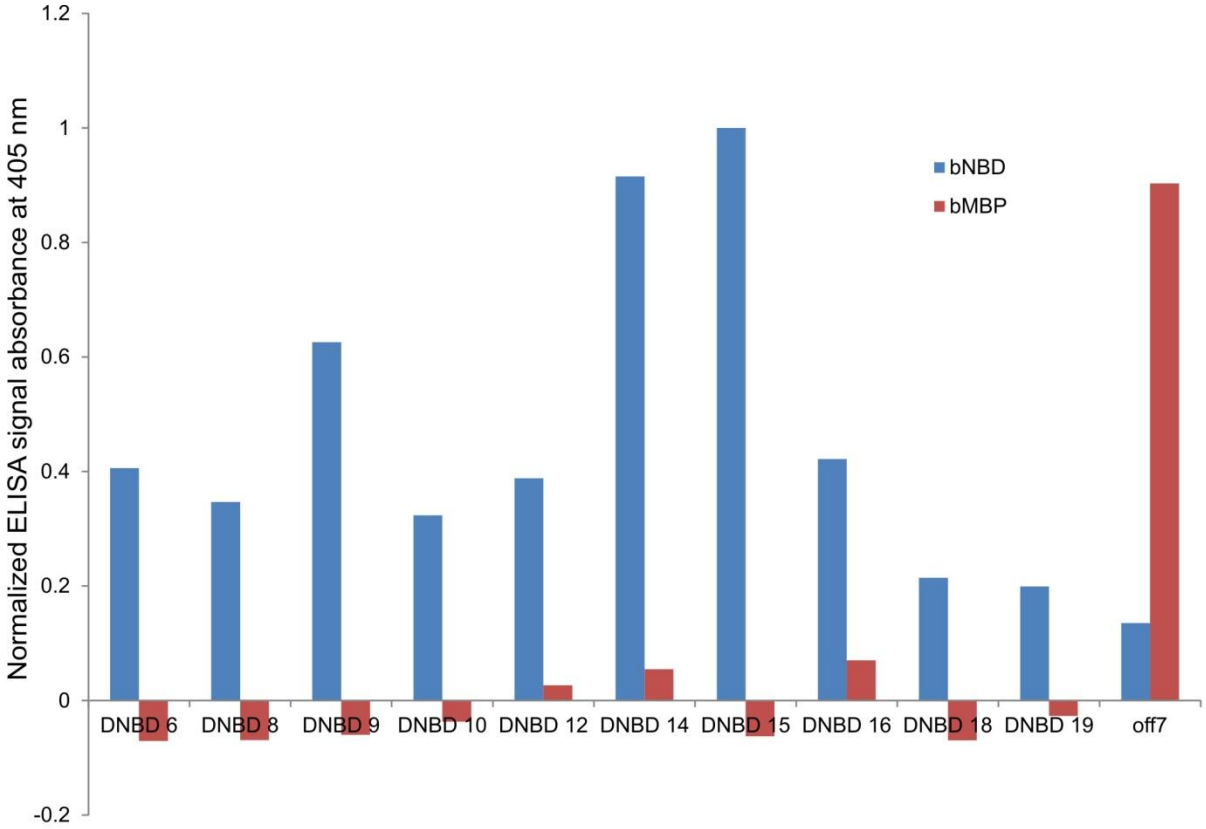

Figure_D3: Screening of NBD specific DARPin binders. off 7 is used as a positive control and is a specific binder for MBP.

D.2.2 Analysis of the NBD-DARPin complex formation

The plasmids of NBD-specific DARPin clones were sequenced to analyze the diversity of the selected binders. The multiple sequence alignment confirmed that all 10 specific binders were unique (Figure_D4). 6 out of 10 binders could be overexpressed and purified by IMAC and were further analyzed for homogeneity by size-exclusion chromatography (Figure_D5A). One DARPin named DNBD_14 (DARPin for the NBD) displayed a monomer/dimer equilibrium and eluted in complex with the NBD as analyzed by SEC (Figure_D5A, C). The other 5 DARPins displayed various degree of oligomerization (soluble aggregates) and were therefore excluded. Further, DNBD_14 binding to full length MsbA was analyzed by ELISA. It was found that DNBD_14 does not bind to full length MsbA (Figure_D6). DARPin_55 served as a control; the epitope for DARPin_55 has been shown to be located at the trans-membrane domain of MsbA (Chapter B), which could be confirmed in this ELISA. This result suggested that DNBD_14 binds to a region of the isolated NBD which interacts with the transmembrane domain in full length MsbA. Alternatively, the conformation of the isolated NBD might be different from the NBD conformation in the context of the full-length MsbA. In any case the epitope is accessible in

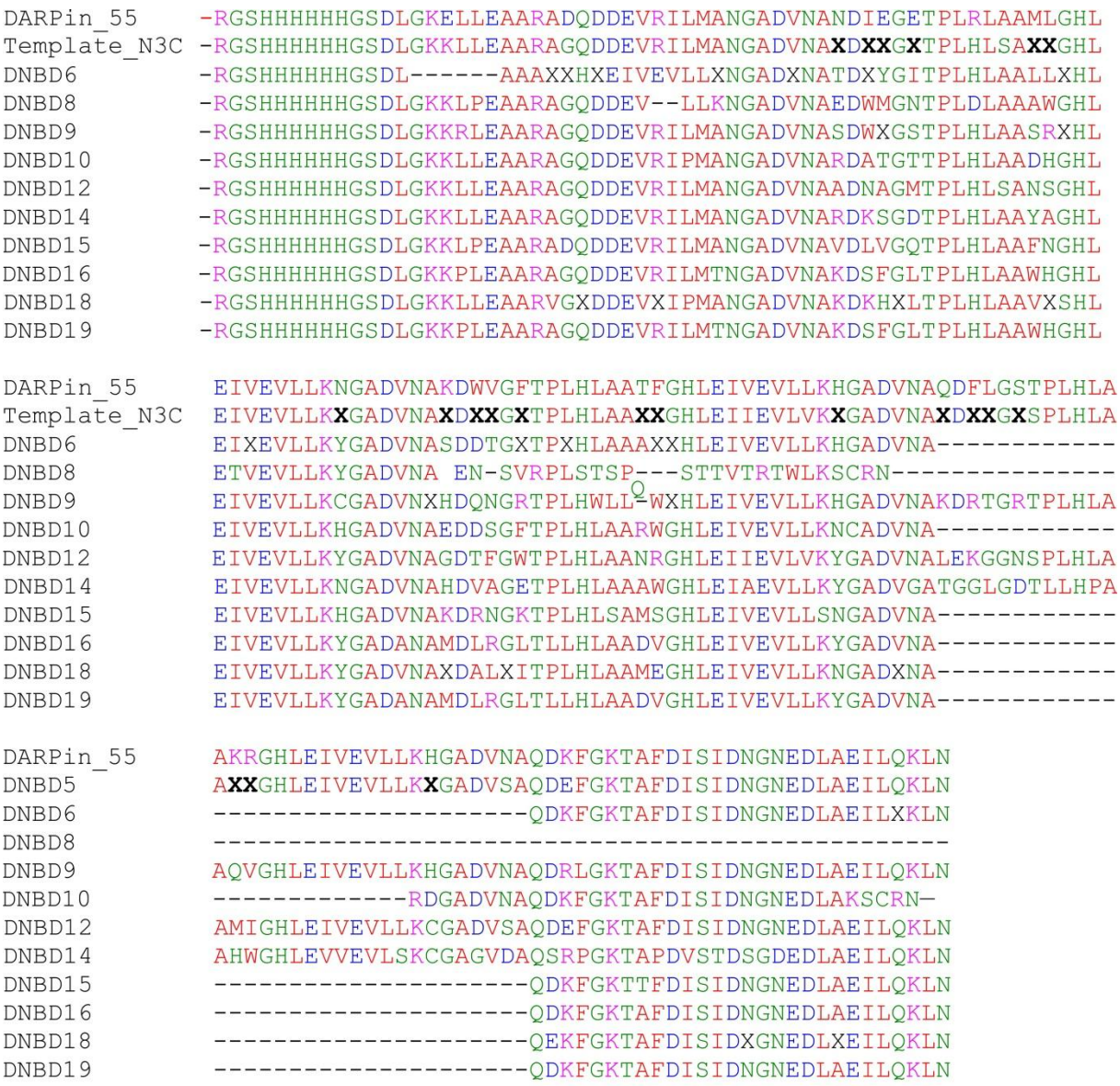

Figure_D4: Multiple sequence alignment of NBD specific DARPins. DARPin_55 is a MsbA specific DARPin and template_N3C shows randomized positions of N3C DARPins denoted by **X**. The DNBD_6, 10, 15, 16, 18, 19 are N2C DARPins and DNBD_8 lacks the C-terminal cap. The alignment was created with ClustalW2.

the isolated NBD but not in full length MsbA (Figure_D6). Neither DNBD_14 nor DARPin_55 binds to the maltose binding protein, which indicates that the selected DARPins, DNBD_14 and DARPin_55 are specific for their respective target protein.

D.2.3 ATPase activity of the purified NBD of MsbA

The ATPase activity of purified full length MsbA and isolated NBD of MsbA were measured by detecting the release of P_i from ATP in a colorimetric malachite green assay as described in Chapter B. To measure the background ATPase activities, the ATPase deficient mutant

E506Q[11] of MsbA was used as a control. Full length MsbA was used as a positive control for ATPase activity. The ATPase activities of the NBD and NBD_E506Q were measured at varying concentration increasing from 1.8 µM to 15 µM. The isolated NBD does not hydrolyze ATP as indicated by virtually identical ATPase activities of NBD and NBD_E506Q (Figure_D7A). DNBD_14 did not modulate the ATPase activity of full length MsbA, which corroborates the ELISA finding that DNBD_14 does not bind to full length MsbA (Figure_D7B).

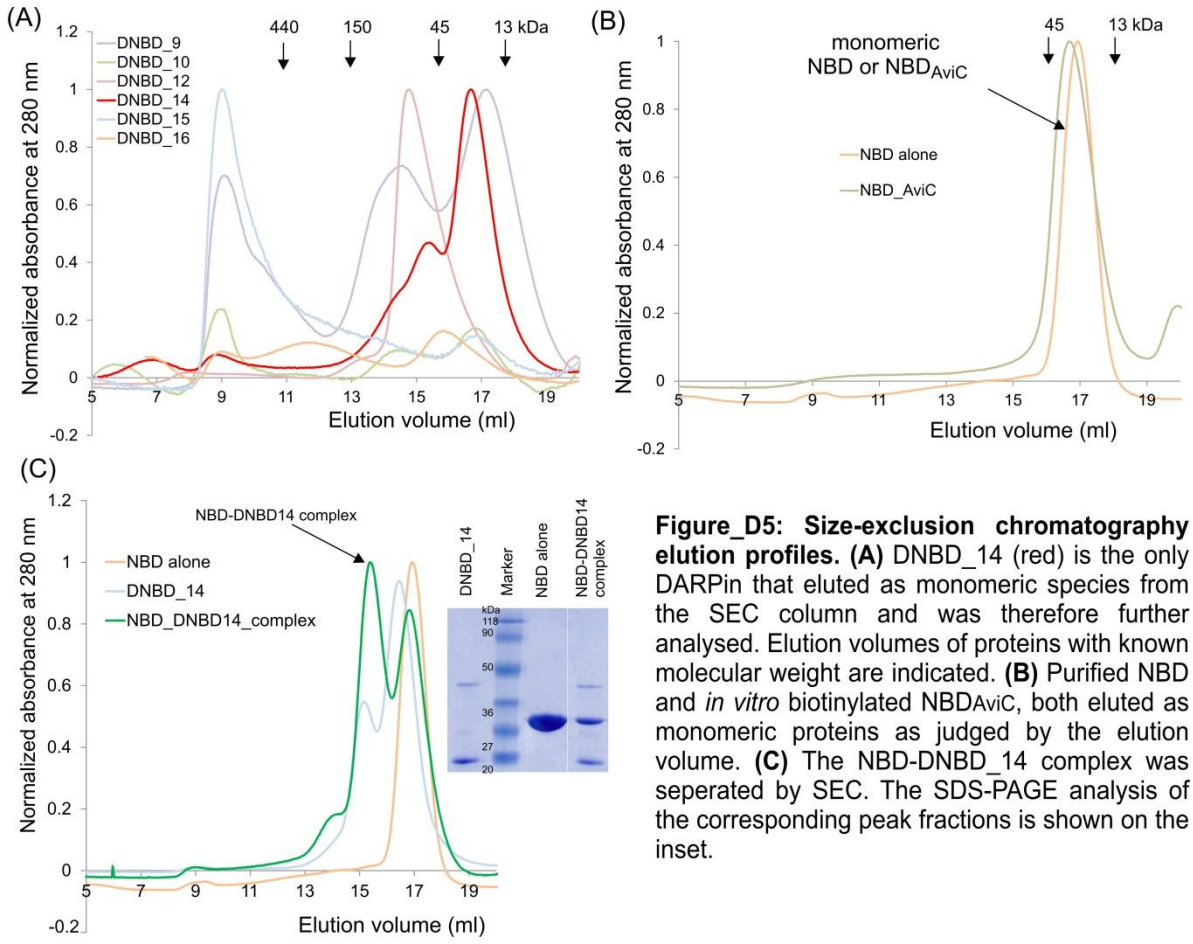

Figure_D5: Size-exclusion chromatography elution profiles. (A) DNBD_14 (red) is the only DARPin that eluted as monomeric species from the SEC column and was therefore further analysed. Elution volumes of proteins with known molecular weight are indicated. **(B)** Purified NBD and *in vitro* biotinylated NBDAviC, both eluted as monomeric proteins as judged by the elution volume. **(C)** The NBD-DNBD_14 complex was seperated by SEC. The SDS-PAGE analysis of the corresponding peak fractions is shown on the inset.

D.2.4 Crystallization experiments with the NBD of MsbA alone and in complex with DARPin DNBD_14

NBD of MsbA and DNBD_14 were purified by IMAC separately. IMAC purified DNBD_14 was further purified by SEC and fractions containing monomeric DNBD_14 were mixed with purified NBD of MsbA. The NBD-DNBD_14 complex was separated from the excess DARPin DNBD_14 by SEC (Figure_D5C). The NBD and the NBD-DNBD_14 complex were concentrated to 15 mg/ml to perform crystallization experiments. Various screens from the NCCR structural Biology platform were used, testing a wide range of PEG, buffers, salt

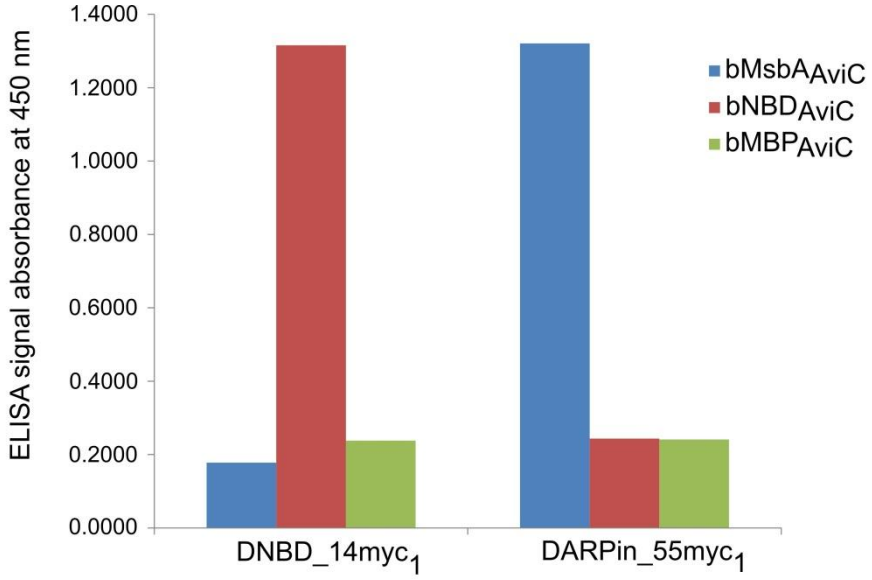

Figure_D6: Specificity of selected DARPins. DNBD_14 and DARPin_55 bind to isolated NBD and full length MsbA, respectively. Biotinylated maltose binding protein (MBP) was used as a negative control.

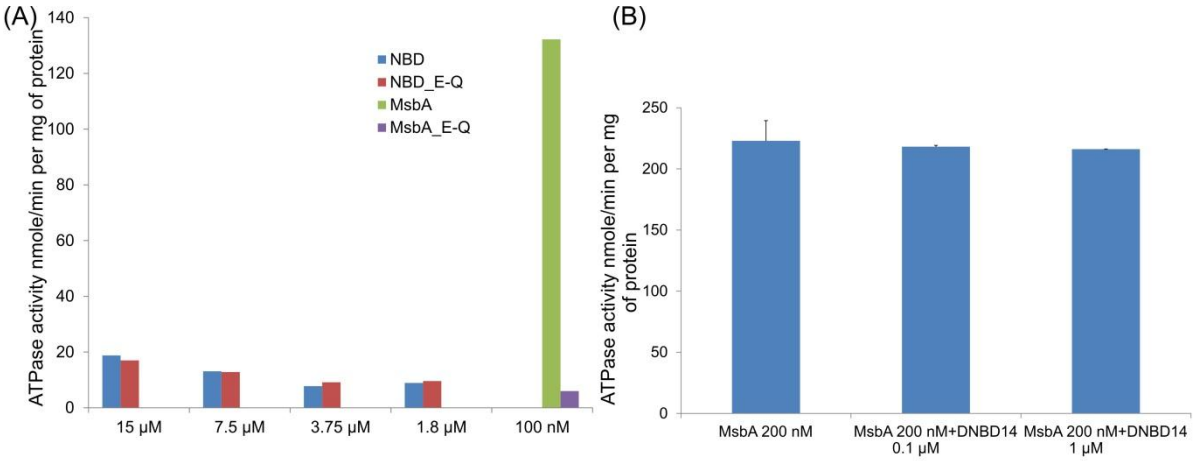

Figure_D7 (A) ATPase activity of the NBD of MsbA: IMAC-purified NBD does not show basal ATPase activity. NBD_E506Q and MsbA were used as negative and positive controls, respectively. **(B) Modulation of ATPase activity of MsbA by DNBD_14:**The NBD-specific DARPin does not affect the basal ATPase activity of full length transporter MsbA.

concentrations etc. None of the crystallization experiments with the NBD alone and with the NBD-DNBD_14 complex indicated signs for crystal formation.

D.3 Discussion

The selection of specific and monomeric binders of any scaffold (Fab, nanobody, DARPin etc) for membrane proteins is a challenging task. We have observed that using full-length ABC transporters as target proteins for *in vitro* selection of DARPins either yielded binders, which were binding to the transmembrane domain (MsbA-Chapter B, LmrCD-Chapter E) or yielded

binders that aggregate. DARPins bound to the TMD cannot be used for crystallization because they cannot reach beyond the detergent micelle layer and therefore do not increase the hydrophilic area needed to increase the chances for the formation of specific intermolecular interactions that help in the formation of a well ordered crystal lattice. In the present study we tried to avoid these problems by selecting DARPins against the cytosolic NBD of MsbA.

The isolated NBD of MsbA was purified in a monomeric and ATPase inactive form. Selected DARPin binders were selected against the NBD of MsbA and tested for their target specificity by ELISA. About 10 NBD specific DARPins were found after screening 1500 clones. A monomeric/dimeric NBD-specific DARPin was found and named DNBD_14. The DNBD_14 did not modulate the ATPase activity of full length MsbA. The DNBD_14's epitope was analyzed by ELISA. DNBD_14 binds to the isolated NBD but does not bind to full length MsbA. The inability of DNBD_14 to bind to full length MsbA suggests that the epitope on the NBD is masked by interactions with the TMD in the full length protein. This made it impossible to use DNBD_14 as a chaperone for co-crystallization with full length MsbA.

Moreover, the NBD-DNBD_14 complex did also not crystallize. To reach the goal to obtain MsbA-binder complex crystals, the following experiments can be envisaged: (i) besides DARPins, binders of other scaffolds such as Fab, scFv and nanobody can be selected against the NBD of MsbA, (ii) the enriched libraries of any scaffold selected against the NBD could be screened for binding full length MsbA, which would provide binders that bind to the cytosolic part of the full length protein, and (iii) the modulation of ATPase activity of full length protein in complex with DARPins could be analyzed in 96 well-plates, which would be useful to delineate functionally interesting clones.

D.4 Experimental procedure

D.4.1 Cloning, expression and purification of the NBD of MsbA

The nucleotide binding domain coding gene sequence was amplified from *E.coli msbA* gene using forward primer NBD_MsbA_PstI and reverse primer reverse_MsbA_ XbaI. The PCR amplified product flanked by PstI and XbaI restriction sites was ligated into the *E. coli* expression vector pBAD24[12] yielding the expression vector pBADNBD$_{His10}$ (expressed protein termed NBD$_{His10}$). For the Avi tagged NBD construct, the NBD coding sequence was cloned into the *E. coli* expression vector pBAD_$_{AviC}$ yielding the expression vector pBADNBD$_{AviC}$

(expressed protein termed NBD_{AviC}). The NBD over-expression was performed in *E.coli* BL-21(DE3) cells, grown in 2YT media. The protein expression was induced at OD_{600} of 0.7 – 0.8 with 0.02% L-arabinose (Sigma) for 12-14 hours at 25°C. Harvested cell pellets were resuspended in 20 mM Tris/HCl (pH 7.4) buffer containing 150 mM NaCl, 25 µg/ml DNaseI and protease inhibitor cocktail (Sigma). Cells were lysed using an EmulsiFlex-C3 (Avestin) cell disrupter. Unbroken cells and cell debris were removed by centrifugation at 20000 rpm (SS34 rotor) for 30 min at 4°C and the cleared lysate was loaded onto a Ni^{2+}-NTA gravity flow column containing 1.5 ml resin (Qiagen). The resin was washed with 55 mM imidazole pH 7.5, 20 mM Tris/HCl (pH 7.4), 150 mM NaCl and the NBD was eluted from the column using 250 mM imidazole pH 7.5 (7 ml) in the same buffer.

The Avi-tagged NBD was expressed and purified as described above. *In vitro* enzymatic biotinylation was done as described in Chapter C.4.3 and the biotinylated NBD was termed $bNBD_{AviC}$. Every NBD preparation used in this work was separated from aggregated material by gel filtration in 20 mM Tris/HCl (pH 7.5), 150 mM NaCl using a Superdex 200 10/300 (GE Healthcare) column. Fractions of the main peak corresponding to monomeric NBD were pooled. Purified and biotinylated $bNBD_{AviC}$ was supplemented with 10% glycerol, snap-frozen in liquid nitrogen and stored at -80°C.

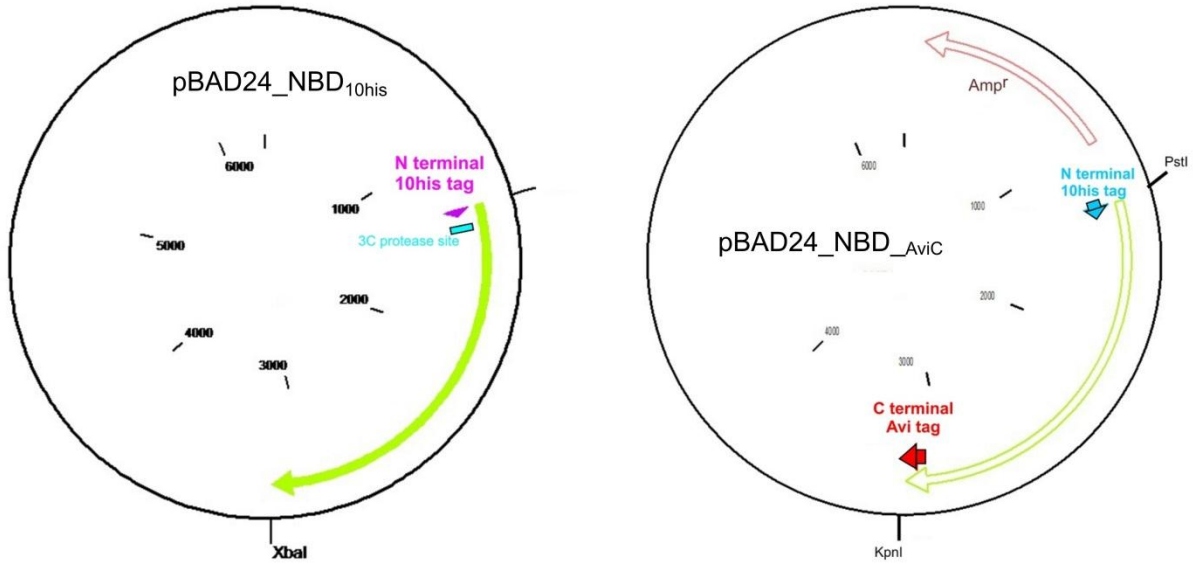

Figure_D8. Plasmid map of NBD. (A) NBD construct used in crystallization studies with cleavable 10his tag at N-terminus. **(B)** C-terminal Avi-tag NBD construct used in ribosome display and ELISA screening.

D.4.2 Selection, screening and purification of DARPins

The selection of DARPins against the NBD was performed by Dr. Thilo Schroeder. The DARPins pool after the 4th selection round was amplified with the primers EWT5 and MTS46. The PCR amplified product was digested using BamHI/HindIII and ligated into the pQE30-based (Qiagen) vector containing an N-terminal RGS-6his tag. For epitope mapping, selected DARPins (DNBD_14 and DARPin_55) were amplified with the primers EWT5 and WTC4. The PCR amplified product was digested using BamHI/HindIII and ligated into the pQE30-myc$_1$ vector (constructed by Sibylle Engeler) containing an N-terminal RGS-6his tag and a C-terminal myc$_1$ tag. All plasmids used in the study were sequenced at Microsynth. DARPin expression and purification are described in Chapter C.4.2.2.

D.4.3 Preparation of the NBD of MsbA and the NBD-DNBD_14 complex for crystallization and ATPase assay

NBD was purified by IMAC and concentrated by using the 20 kDa cutoff filter (Amicon) and further purified by SEC. IMAC purified DNBD_14 was gel-filtrated and fractions containing monomeric protein were mixed with the IMAC purified NBD at a 3:1 ratio. The NBD-DNBD_14 complex was separated from the excess DNBD_14 by SEC (Figure_D4C). The NBD alone and the NBD-DNBD_14 complex were concentrated to 14- 16 mg/ml and 15-18 mg/ml concentration, respectively by using a 20 kDa cutoff filter (Amicon) for crystallization experiments.

To measure the basal ATPase activity of NBD, an ATPase inactive mutant NBD_E506Q[11] was purified in a similar way as the NBD (described above). The NBD_E506Q was used as a background control in ATPase assays. NBD and NBD_E-Q were used at different concentrations from 15 µM to 1.8 µM (serially diluted). MsbA was used as a positive control. The effect of DNBD_14 on the basal ATPase activity of MsbA (200 nM) was measured at different concentrations of DNBD_14 (0.1 and 1.0 µM) (Figure_D7). The ATPase assay was performed as described in Chapter B.

D.5 References

1. Blight, M.A. & Holland, I.B. Structure and function of haemolysin B, P-glycoprotein and other members of a novel family of membrane translocators. *Mol Microbiol* **4**, 873-80 (1990).
2. Locher, K.P. Review. Structure and mechanism of ATP-binding cassette transporters. *Philos Trans R Soc Lond B Biol Sci* **364**, 239-45 (2009).
3. Higgins, C.F. Multiple molecular mechanisms for multidrug resistance transporters. *Nature* **446**, 749-57 (2007).
4. Hung, L.W. et al. Crystal structure of the ATP-binding subunit of an ABC transporter. *Nature* **396**, 703-7 (1998).
5. Haffke, M., Menzel, A., Carius, Y., Jahn, D. & Heinz, D.W. Structures of the nucleotide-binding domain of the human ABCB6 transporter and its complexes with nucleotides. *Acta Crystallogr D Biol Crystallogr* **66**, 979-87 (2010).
6. Davidson, A.L. & Chen, J. ATP-binding cassette transporters in bacteria. *Annu Rev Biochem* **73**, 241-68 (2004).
7. Geourjon, C. et al. A common mechanism for ATP hydrolysis in ABC transporter and helicase superfamilies. *Trends Biochem Sci* **26**, 539-44 (2001).
8. Seeger, M.A. & van Veen, H.W. Molecular basis of multidrug transport by ABC transporters. *Biochim Biophys Acta* **1794**, 725-37 (2009).
9. Higgins, C.F. ABC transporters: from microorganisms to man. *Annu Rev Cell Biol* **8**, 67-113 (1992).
10. Binz, H.K. et al. High-affinity binders selected from designed ankyrin repeat protein libraries. *Nature Biotechnology* **22**, 575-582 (2004).
11. Schultz, K.M., Merten, J.A. & Klug, C.S. Characterization of the E506Q and H537A Dysfunctional Mutants in the *E. coli* ABC Transporter MsbA. *Biochemistry* **50**, 3599-3608 (2011).
12. Guzman, L.M., Belin, D., Carson, M.J. & Beckwith, J. Tight regulation, modulation, and high-level expression by vectors containing the arabinose PBAD promoter. *J Bacteriol* **177**, 4121-30 (1995).

CHAPTER E

Tuning the drug efflux activity of an ABC transporter *in vivo* by *in vitro* selected DARPin binders

Markus A. Seeger[1,2*], Anshumali Mittal[2], Saroj Velamakanni[1], Michael Hohl[2], Stefan Schauer[3], Ihsene Salaa[1], Markus G. Grütter[2] and Hendrik W. van Veen[1*]

[1]Department of Pharmacology, University of Cambridge, UK

[2]Department of Biochemistry, University of Zurich, Switzerland

[3]Functional Genomics Center Zurich, University of Zurich, Switzerland

OPEN ACCESS Freely available online

PLoS one

Tuning the Drug Efflux Activity of an ABC Transporter *in vivo* by *in vitro* Selected DARPin Binders

Markus A. Seeger[1,2]*, Anshumali Mittal[2], Saroj Velamakanni[1], Michael Hohl[2], Stefan Schauer[3], Ihsene Salaa[1], Markus G. Grütter[2], Hendrik W. van Veen[1]*

1 Department of Pharmacology, University of Cambridge, Cambridge, United Kingdom, **2** Department of Biochemistry, University of Zurich, Zurich, Switzerland, **3** Functional Genomics Center Zurich, University of Zurich, Zurich, Switzerland

Abstract

ABC transporters use the energy from binding and hydrolysis of ATP to import or extrude substrates across the membrane. Using ribosome display, we raised designed ankyrin repeat proteins (DARPins) against detergent solubilized LmrCD, a heterodimeric multidrug ABC exporter from *Lactococcus lactis*. Several target-specific DARPin binders were identified that bind to at least three distinct, partially overlapping epitopes on LmrD in detergent solution as well as in native membranes. Remarkably, functional screening of the LmrCD-specific DARPin pools in *L. lactis* revealed three homologous DARPins which, when generated in LmrCD-expressing cells, strongly activated LmrCD-mediated drug transport. As LmrCD expression in the cell membrane was unaltered upon the co-expression of activator DARPins, the activation is suggested to occur at the level of LmrCD activity. Consistent with this, purified activator DARPins were found to stimulate the ATPase activity of LmrCD *in vitro* when reconstituted in proteoliposomes. This study suggests that membrane transporters are tunable *in vivo* by *in vitro* selected binding proteins. Our approach could be of biopharmaceutical importance and might facilitate studies on molecular mechanisms of ABC transporters.

Citation: Seeger MA, Mittal A, Velamakanni S, Hohl M, Schauer S, et al. (2012) Tuning the Drug Efflux Activity of an ABC Transporter *in vivo* by *in vitro* Selected DARPin Binders. PLoS ONE 7(6): e37845. doi:10.1371/journal.pone.0037845

Editor: Dan Zilberstein, Technion-Israel Institute of Technology, Israel

Received January 20, 2012; **Accepted** April 30, 2012; **Published** June 4, 2012

Funding: Funding provided by the Swiss National Science Foundation Prospective Researcher (to MAS), European Molecular Biology Organization Long Term fellowship (to MAS), Novartis Foundation (to MAS), Swiss National Science Foundation, Ambizione Fellowship (to MAS), Research Credit (Forschungskredit) of the University of Zurich (to MAS), British Society for Antimicrobial Chemotherapy (to HWvV), and Biotechnology and Biological Sciences Research Council (to HWvV). The funders had no role in study design, data collection and analysis, decision to publish, or preparation of the manuscript.

Competing Interests: The authors have declared that no competing interests exist.

* E-mail: m.seeger@bioc.uzh.ch (MAS); hwv20@cam.ac.uk (HWvV)

Introduction

In the past decade, unprecedented progress has been made in the elucidation of ten complete ABC transporter structures solved by X-ray crystallography, which guide current functional studies on these transport proteins [1–5]. However, the mechanisms of transport of both, ABC importers and exporters are still controversial [6]. One reason for the uncertainties is due to the fact that crystal structures represent snapshots of the proteins in specific conformations. In order to describe the transport cycle in detail, several structures of the same transporter captured in different conformational states need to be solved. This often requires the trapping of the transport protein in a specific conformational state which, for crystallized primary-active transporters, was achieved by using non-hydrolyzable nucleotide analogs such as AMP-PNP [7,8] or various nucleotide trapping agents such as vanadate, aluminium fluoride and beryllium fluoride [9,10], or by generating mutant proteins that are unable to hydrolyze ATP [11]. However, as these different techniques interrupt the catalytic cycle of ATP hydrolysis at similar stages, the repertoire of conformations that can be stabilized is limited.

To overcome this limitation, we used designed ankyrin repeat proteins (DARPins) which represent a novel binding scaffold [12]. DARPins typically consist of two or three internal ankyrin repeat units encoding the randomized surface flanked by an N-terminal and a C-terminal capping repeat [13,14]. DARPins are devoid of disulfide bonds, easy to produce in *E. coli* and extraordinarily robust [15]. High-affinity binders have been raised against a growing number protein targets [16,17]. Amongst these is an AcrB specific DARPin that was co-crystallized with AcrB to obtain the highest resolution structure at 2.5 Å of this membrane protein to date [18,19].

Traditionally, monoclonal antibodies (mAbs) specific for integral membrane proteins have been generated using the hybridoma technology [20]. This procedure relies on the natural generation of binders against the targeted protein in mice [21–26]. However, the process of binder selection after the injection of the protein sample into the animal is beyond experimental control. *In vitro* selections using either phage display or ribosome display in contrast allow binder selection under defined conditions [27,28]. Nevertheless, the small number of less than ten published studies on the complete *in vitro* selection of binders (Fab fragments and DARPins) against detergent-purified membrane proteins embodies the difficulties in using membrane proteins for this purpose [18,29–36].

ABC transporters play a pivotal role in the active transport of molecules in organisms of all kingdoms of life. The mammalian multidrug transporter ABCB1 (also termed P-glycoprotein or MDR1) has probably attracted most attention of all ABC transporters, since it can play an important role in the extrusion of noxious substances out of the cell, and has been linked to drug

resistance in tumor cells [37,38]. Prokaryotic homologues of ABCB1 such as LmrA from *Lactococcus lactis* and MsbA from *Escherichia coli*, and analogues such as LmrCD from *L. lactis* were studied in detail and are involved in the transport of drugs, lipids and small ions [39–45]. ABC transporters use the energy of ATP binding and hydrolysis catalyzed by the nucleotide binding domains (NBDs) to translocate substrates through the membrane domain (MDs). For this purpose, the NBDs need to dimerize in a sandwich-like fashion forming two composite catalytic sites [46]. The amino acids involved in ATP binding and hydrolysis are encoded by a number of highly conserved sequence motifs including Walker A, Walker B, ABC Signature and H-loop (for review, see [2]).

In LmrCD, one of the two composite catalytic sites at the NBDs deviates from the consensus sequence and is postulated to mediate ATP binding, but not ATP hydrolysis [47]. The deviation from the canonical sequence concerns the catalytically important Walker B glutamate and H-loop histidine that are changed to aspartate and glutamine, respectively. The same substitutions are found in the non-canonical sites of the antigen peptide transporter TAP1/2 and the yeast multidrug transporter Pdr5 [48,49]. Here, we demonstrate the successful *in vitro* selection of binders against detergent-solubilized LmrCD using ribosome display. Moreover, we use the lactococcal cells for a novel *in vivo* functional screen applicable for multidrug transporters, and we characterize the functional consequences of DARPin binding to LmrCD.

Results

Selection of DARPins Against Detergent Solubilized LmrCD

We cloned the *lmrCD* genes with a His10-tag N-terminally to LmrC, and were able to purify functionally active LmrCD to homogeneity from lactococcal membrane vesicles. The proteins could be isolated as heterodimeric species from size exclusion chromatography (SEC) columns (Figure S1A and B). Interestingly, the heterodimeric complex of LmrCD was stable when the purified protein was analyzed by nano-electrospray mass spectrometry [50]. In order to immobilize LmrCD during the DARPin selection procedure, an Avi-tag was introduced C-terminally to LmrD, which allowed for site-specific enzymatic biotinylation of a lysine residue comprised within the Avi-tag sequence (biotinylated LmrCD is denoted $bLmrCD_{AviC}$) [51]. The DARPin selection was performed using the ribosome display method with DARPins including three internal randomized repeats (N3C DARPins) (Figure 1A) [12,18,28]. A total of 4 sequential selection rounds were performed in which catalytically active $bLmrCD_{AviC}$ and orthovanadate-trapped $bLmrCD_{AviC}$ were used as two independent protein formulations. In the presence of 1 mM ATP, LmrCD could be trapped by orthovanadate with a concentration giving half-maximal inhibition of ATP hydrolysis (IC_{50}) of 120 μM which is in agreement with a recent study on the heterodimeric ABC transporter BmrCD [52] (data not shown). The orthovanadate concentration (1 mM) used during the DARPin selections comfortably exceeded this IC_{50}. It should be noted that around 0.6 mM of ATP originating from the *in vitro* translation buffer and around 40 mM magnesium acetate were present during the incubation of the DARPins with the target protein. This means that in case of the non-trapped $bLmrCD_{AviC}$ formulation, the DARPins were selected against transporters slowly hydrolyzing ATP and presumably adopting various conformational states.

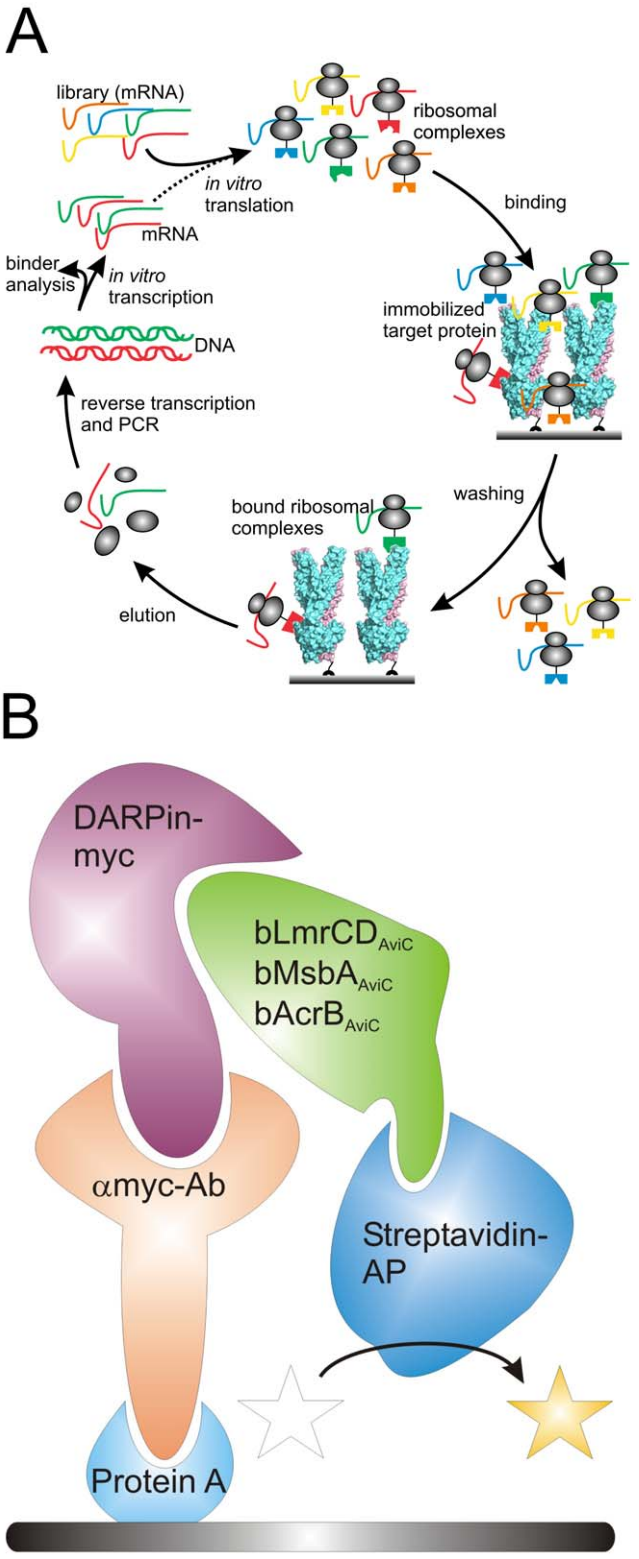

Figure 1. Ribosome display and ELISA set-up. (**A**) Sketch delineating one DARPin selection round using ribosome display (adopted from [31]). The DARPin library in form of mRNA is *in vitro* translated and stable ribosomal complexes linking the phenotype (folded DARPins) with the genotype (translated mRNA) are generated. The ribosomal complexes are allowed to bind to immobilized $bLmrCD_{AviC}$. After a washing step of variable length (depending on selection stringency), bound ribosomal complexes are destabilized and

mRNA encoding for potential target-specific DARPins is liberated. The eluted mRNA is amplified by reverse transcription and PCR to double stranded DNA, which is *in vitro* transcribed into mRNA for another round of selection or used for binder analysis. (**B**) Schematic drawing of the ELISA set up. Protein A is coated onto the ELISA well and is decorated with an anti-myc antibody that immobilizes the DARPins via the C-terminal Myc5-tag. Upon binding of purified, biotinylated target protein (e.g. LmrCD, AcrB or MsbA in our study) to DARPin, the target protein is detected using a streptavidin-alkaline phosphatase the activity of which was detected colourimetrically at OD_{405} using p-nitrophenyl phosphate as a substrate.
doi:10.1371/journal.pone.0037845.g001

Identification of LmrCD-specific DARPin Binders by ELISA

We analyzed 190 clones from the DARPin pools, enriched over four selection rounds against untreated or vanadate-trapped $bLmrCD_{AviC}$, by an established ELISA protocol (95 DARPins for each protein formulation) (Figure 1B, Figure 2) [31]. From the initial ELISA (not shown) we chose the clones giving rise to the 30 most intense ELISA signals against $bLmrCD_{AviC}$ (15.8% of examined clones) for a second comparative ELISA (Figure 3A). Besides LmrCD, the ABC transporter MsbA and the secondary-active multidrug transporter AcrB were used in the assay (prepared as proteins biotinylated at the C-terminal Avi-tag). From the 30 ELISA-positive DARPins, 8 were exclusively binding to $bLmrCD_{AviC}$ but not to $bMsbA_{AviC}$ or $bAcrB_{AviC}$ (4.2% of all examined clones), whereas the other 22 DARPins were promiscuously binding to all membrane proteins used in the specificity ELISA (Figure 3A). The quality of the control proteins $bMsbA_{AviC}$ and $bAcrB_{AviC}$ was confirmed by using target-specific DARPins in the ELISA assay (AcrB-specific DARPin 110819 is described [18]; the selection of the MsbA-specific DARPin_55 will be published elsewhere). The genes encoding the eight LmrCD-specific DARPins were sub-cloned, expressed without the C-terminal Myc5-tag and analyzed by size exclusion chromatography. Four of these DARPins displayed a substantial degree of aggregation (soluble aggregates) and were therefore excluded. The other four LmrCD-specific DARPins (α-LmrCD#1-4) ran as monomeric or dimeric species on SEC taking the elution profile of the monomeric control DARPin E3_5 as a reference (Table 1, Figure S1C). Three out of these four DARPins exhibited tight binding to purified LmrCD, and eluted in complex with their target from the size exclusion column. Thus, the initially chosen 190 DARPin clones could be narrowed down to 3 specific high-affinity binders, corresponding to a hit rate of 1.6%. A fifth high-affinity DARPin (α-LmrCD#5) was found in another ELISA screen identical to the one above (not shown).

Identification of Activators of LmrCD by Functional Screening in L. Lactis

LmrCD-mediated daunomycin resistance in *L. lactis* [53] was used for screening of DARPins that affect LmrCD activity. Individual DARPins of the pool obtained after four selection rounds (Figure 2; note: these are not the DARPin binders identified by ELISA from the previous section) were expressed at high levels in the cytoplasm of *L. lactis* using the nisin-inducible lactococcal vector pNZ8048 (estimated to 2–5% of total soluble protein, not shown) [54]. We first attempted to find DARPins whose expression lead to a decrease of LmrCD-dependent daunomycin resistance (inhibitors). Around 20 apparent inhibitors were found by screening 400 DARPin clones expressed in *L. lactis*. A closer inspection of these initial hits however, revealed that they were false positives; lactococcal cells expressing these DARPins grew considerably slower than cells expressing the control DARPin E3_5*. When these DARPin inhibitors were expressed in the *L. lactis* strain lacking the chromosomal *lmrCD* genes (*L. lactis* NZ9000 Δ*lmrA* Δ*lmrCD* [55]), the apparent inhibition was also observed. Hence, the increased drug susceptibility of *L. lactis* expressing these DARPins was independent of LmrCD. Surprisingly, we also found DARPins the expression of which increased daunomycin resistance in *L. lactis*, suggesting enhancement of LmrCD activity. Three strong activators (DARPin_Act1-3) were found in a screen including 1128 clones (Figure 2). In cell growth experiments, the daunomycin resistance of *L. lactis* NZ9000 expressing the activator DARPins was compared to the control DARPin E3_5* in the wildtype and the Δ*lmrCD* background (Figure 4A and B). In wildtype cells, the IC_{50} for daunomycin was increased by a factor of 3.3, 2.6 and 1.7 upon the production of DARPin_Act1, DARPin_Act2, and DARPin_Act3, respectively. Importantly, the expression of the activator DARPins in the *L. lactis* NZ9000 Δ*lmrA* Δ*lmrCD* background did not affect the daunomycin resistance of the cells, indicating an LmrCD-specific functional stimulation. The knock-out of *lmrCD* in *L. lactis* results in an 8.3-fold decrease of the IC_{50} for daunomycin (Figure 4A and B). Therefore, the DARPin-induced stimulation of LmrCD-mediated drug transport by a factor up to 3.2 is substantial. The DARPins α-LmrCD#1-5 that were identified in the ELISA screen to bind to LmrCD (see previous section) were also assayed regarding the potential modulation of the LmrCD-mediated drug resistance in *L. lactis*. Although DARPins α-LmrCD#1-5, the DARPin activators and DARPin E3_5* were overproduced equally well in *L. lactis*, expression of DARPins α-LmrCD#1-5 did not alter the drug resistance of lactococcal cells towards daunomycin (not shown).

Further Characterization of the LmrCD-activating DARPins

The chromosomal knock-out of the *lmrCD* gene on *L. lactis* has been shown to result in an increased susceptibility of the lactococcal cells towards Hoechst 33342 (3.6 fold difference between wiltype *L. lactis* and the Δ*lmrCD* mutant) [53]. We therefore tested whether the DARPin_Act1 to Act3 are also capable of increasing the LmrCD-mediated transport of Hoechst 33342. However, in contrast to the observations on daunomycin resistance in *L. lactis* (Figure 4) the expression of the DARPin activators did not increase the resistance towards Hoechst 33342 (not shown).

The observed LmrCD-associated daunomycin resistance in *L. lactis* could be due to enhanced drug efflux by LmrCD. However, as the entry of fluorescent daunomycin from the aqueous buffer into cells followed by its intercalation in DNA results in a minor quenching of total fluorescence, detection of daunomycin transport by fluorescence spectroscopy is hampered by a poor signal-to-noise ratio in the fluorescence data. In an alternative assay, we studied the LmrCD-mediated transport of non-fluorescent, hydrophobic 2′,7′-bis-(2-carboxyethyl)-5(6)-carboxyfluorescein acetoxymethyl ester (BCECF-AM), which is extruded from the plasma membrane by bacterial and mammalian multidrug ABC transporters before it can be hydrolyzed in the cytoplasm into fluorescent BCECF by non-specific esterases [56–58]. In this assay, a slower increase in the fluorescence signal is associated with enhanced extrusion of BCECF-AM from the cell. As BCECF is a pH-sensitive fluorophore, valinomycin and nigericin were added to the cells prior to the transport measurement to dissipate the electrochemical proton gradient across the plasma membrane, so that the intracellular pH was made equal to the constant pH of the extracellular buffer. In agreement with the observations for daunomycin, increased BCECF-AM efflux was observed upon expression of DARPi-

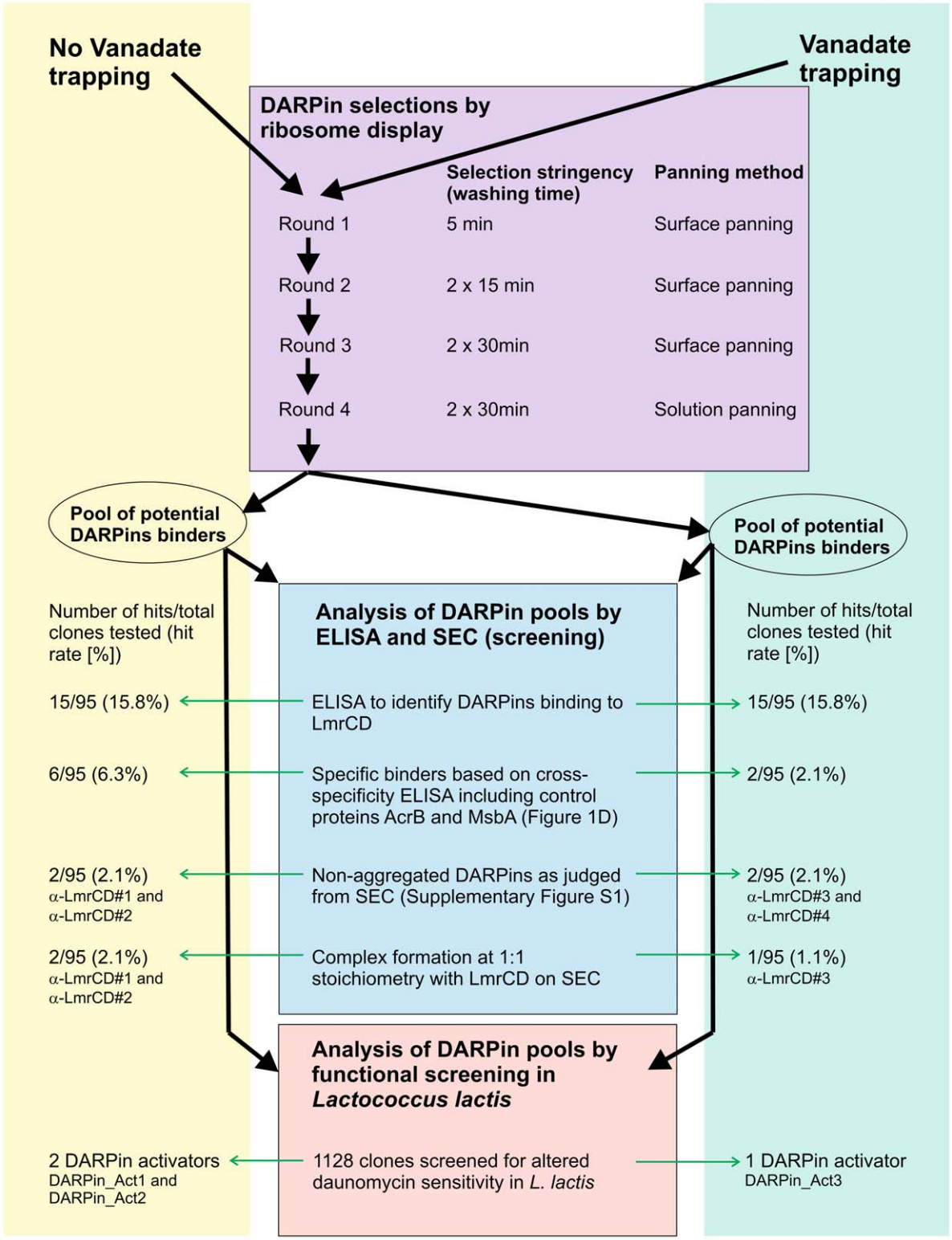

Figure 2. Workflow of DARPin selection and screening. DARPins were selected by ribosome display against LmrCD with and without vanadate trapping (purple rectangle). After four sequential selection rounds of increasing stringency, the pools of potential binders were analyzed either by ELISA and SEC (blue rectangle) or in a functional screen in *L. lactis* (red rectangle).
doi:10.1371/journal.pone.0037845.g002

n_Act2 in wildtype *L. lactis*, whereas DARPin_Act2 expression in the *lmrCD* knockout-strain did not affect transport (Figure 4C).

Sequencing revealed that DARPin_Act1 lacked the N-terminal cap repeat and therefore exhibited severe aggregation (but not precipitation) in purified form as demonstrated in SEC experi-

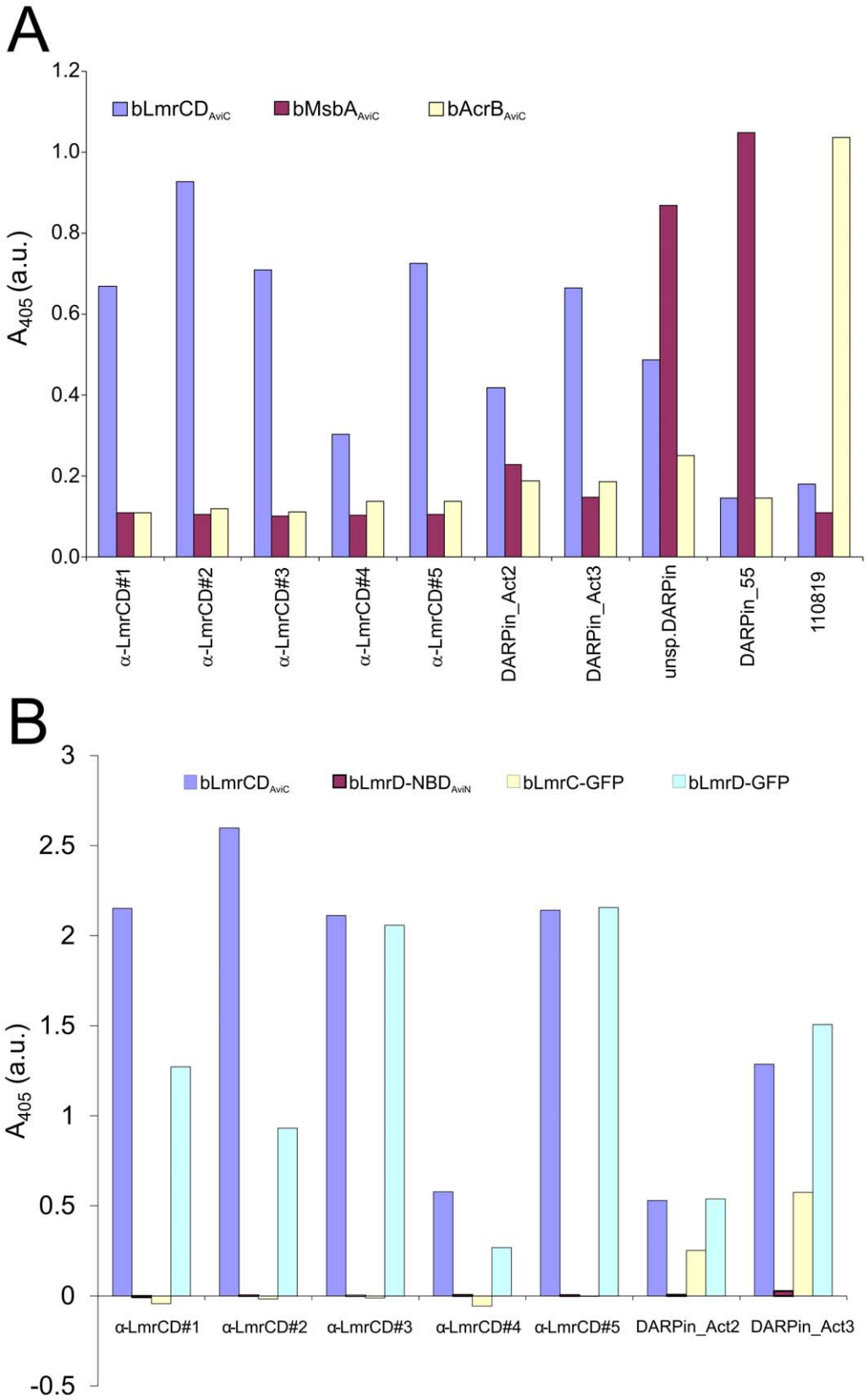

Figure 3. Identification and characterization of DARPin binders by ELISA (**A**) Specificity ELISA using bLmrCD$_{AviC}$, bMsbA$_{AviC}$ and bAcrB$_{AviC}$ as target proteins. Seven DARPins (α-LmrCD#1-5, DARPin_Act2 and DARPin_Act3) were found to be highly specific for bLmrCD$_{AviC}$. Many initial DARPin binder-hits promiscuously bound to bLmrCD$_{AviC}$, bMsbA$_{AviC}$ and bAcrB$_{AviC}$ as exemplified with the ''unsp. DARPin'' and were therefore not useful for further analysis. DARPins specific for bMsbA$_{AviC}$ (DARPin_55) and bAcrB$_{AviC}$ (110819) were used as a positive control. (**B**) ELISA analyzing

binding of the LmrCD-specific DARPins shown in (A) to LmrC (bLmrC-GFP), LmrD (bLmrD-GFP) and the nucleotide binding domain of LmrD (bLmrD-NBD_{AviN}). Binding to LmrCD ($bLmrCD_{AviC}$) was confirmed as positive control.
doi:10.1371/journal.pone.0037845.g003

ments (Table 1, Figure S1D). This impeded further biochemical and biophysical characterization of DARPin_Act1. Although DARPin_Act2 was of the expected N3C format, it was prone to form soluble aggregates (hexamers), presumably due to a high number of hydrophobic residues found in its randomized positions. DARPin_Act3 predominantly existed as a monomer and the aggregated species could successfully be removed by SEC.

Expression of LmrCD-activating DARPins does not Increase the LmrCD Production Level

The observed gain of cellular drug resistance and enhanced rates of substrate efflux in DARPin producing cells could be explained if DARPin expression would upregulate the expression level of LmrCD. In order to compare the amounts of expressed LmrCD protein in the plasma membrane from DARPin-producing and control cells, we introduced a V5-tag downstream to the *lmrD* copy on the chromosome by homologous recombination. Cells producing the V5-tagged version of LmrD ($LmrD_{V5}$) were as resistant to daunomycin as the wildtype cells. A specific band for $LmrD_{V5}$ could be detected by Western blotting with an anti-V5 antibody (Figure 5A). *L. lactis* NZ9000 *lmrD*$_{V5}$ expressing the activator DARPins and the control DARPin E3_5* were grown in the absence of drug and in the presence of the daunomycin concentration (see Materials and Methods). The amount of $LmrD_{V5}$ was then analyzed by Western blotting whereas the total protein was quantified using SYPRO ruby staining. The $LmrD_{V5}$ production level was consistently increased by a factor of around 1.5 upon the exposure to daunomycin irrespective of the DARPin expressed (Figure 5B). However, the activator DARPins did not lead to a significant increase in $LmrD_{V5}$ production compared to the control cells, indicating that the DARPin activators directly stimulate the drug efflux activity of existing transporters.

LmrCD-specific DARPins Bind to LmrD in a 1:1 Stoichiometry Covering at least Three Partially Overlapping Epitopes

To gain further insights into the binding epitopes of the LmrCD-specific DARPins, LmrC and LmrD were expressed separately including GFP fused to the C-termini. The proteins were purified by Ni^{2+}-NTA chromatography, followed by chemical biotinylation and size exclusion chromatography (Figure S1E). Further, the isolated NBDs of LmrC and LmrD were purified from *E. coli*. Whereas the expression of the NBD of LmrC gave rise to soluble aggregates exclusively (which were not used for further analysis), purification of the NBD of LmrD yielded (besides soluble aggregates) monomeric protein that was enzymatically biotinylated ($bLmrD\text{-}NBD_{AviN}$) (Figure S1F). Binding of these isolated parts of LmrCD to α-LmrCD#1-5 and the activator DARPins was then tested in an ELISA (Figure 3B). All DARPins were found to bind to the LmrD chain, but none of them recognized the NBD of LmrD or the LmrC chain suggesting that the epitope(s) are likely to be located at the membrane domain of LmrD. Alternatively, the isolated NBD of LmrD might adopt a conformation different to the one found in the full-length transporter which might not be recognized by the DARPins or the binding epitope covers a shared surface located on the MD and the NBD of LmrD.

The binding epitopes were further analyzed in a competition ELISA, in which $bLmrCD_{AviC}$ was pre-incubated with a tenfold excess of each DARPin devoid of the Myc-tag and probed for binding to every $DARPin_{myc5}$ immobilized via the Myc-tag (Figure 6A). Based on the results of this competition ELISA, the LmrCD-specific DARPins are proposed to bind to at least three partially overlapping epitopes (Figure 6B). The first epitope (epitope 1 of binders α-LmrCD#2 and α-LmrCD#4) and the second epitope (epitope 2 of binders α-LmrCD#3 and α-LmrCD#5) do not overlap (i.e. no competition for binding between these two pairs of DARPins to LmrCD was observed). In

Table 1. Biophysical properties of LmrCD-specific DARPins.

DARPin	Oligomeric state [a]	Binding stoichiometry (DARPin: LmrCD) [b]	K_D (nM) [c]	k_a ($\times 10^5$ $M^{-1}s^{-1}$) [c]	k_d ($\times 10^{-2}$ s^{-1}) [c]	$K_{D,\,eq.}$ (nM) [d]
Binders						
α-LmrCD#1	Monomer	1.11: 1	10.0	7.40	0.738	10.7
α-LmrCD#2	Dimer/Trimer	0.96: 1	3.9	5.29	0.205	9.2
α-LmrCD#3	Monomer	0.73: 1	53.4	12.3	6.59	53.5
α-LmrCD#4	Monomer	No complex	167	2.00	3.34	173
α-LmrCD#5	Monomer	0.75: 1	43.0	5.10	2.19	45.2
Activators						
DARPin_Act1	Soluble aggregates	n.d. [e]	n.d.	n.d.	n.d.	n.d
DARPin_Act2	Hexamer	n.d. [e]	46.7	0.17	0.079	66.8
DARPin_Act3	Monomer	1.16: 1	50.5	4.36	2.20	54.9

[a]Derived from elution volume of main peak on Superdex 200 10/300 GL column (Figure S1).
[b]Determined by protein chip analysis (Figure 7B).
[c]Values obtained by SRP analysis using a 1:1 binding model (Figure 7C).
[d]Value obtained by SPR analysis using binding equilibrium data (Figure 7D).
[e]Separation of the DARPin-LmrCD complex from DARPin aggregates was not possible on SEC (Figure S1).
doi:10.1371/journal.pone.0037845.t001

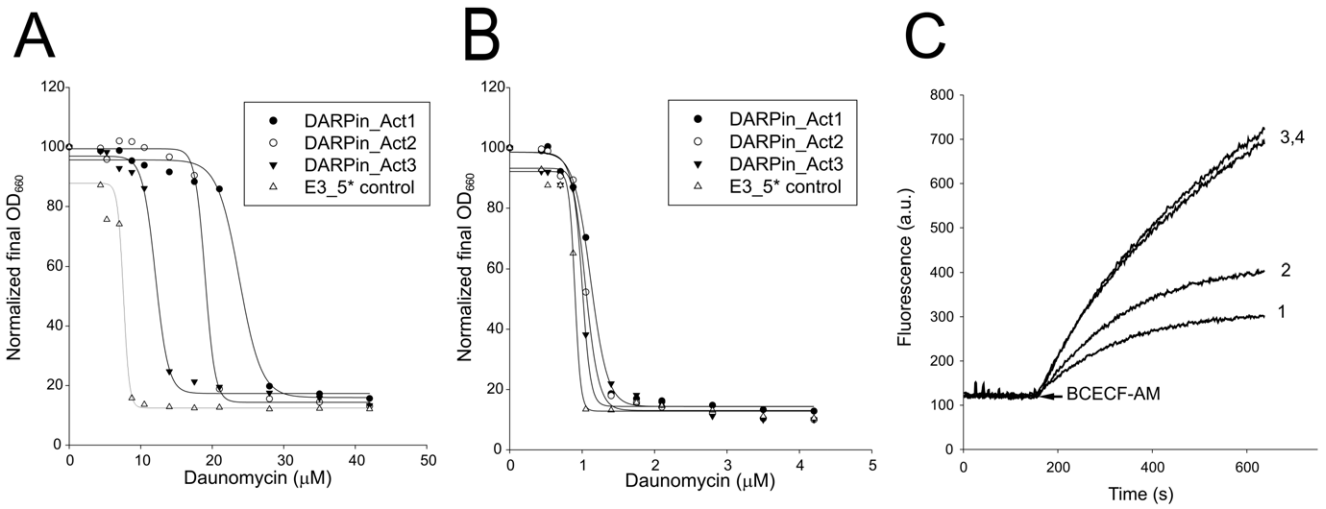

Figure 4. Identification of LmrCD-activating DARPins. (**A**) Overexpression of DARPin_Act1 (●), DARPin_Act2 (○), DARPin_Act3 (▼) in wildtype *L. lactis* increases the resistance towards daunomycin compared to cells expressing control DARPin E3_5* (not interacting with LmrCD) (Δ). (**B**) No differences were observed when experiments in (A) were performed with cells lacking the chromosomal copy of *lmrCD*. (**C**) BCECF-AM transport measurements in pre-energized wildtype *L. lactis* cells demonstrate activation of LmrCD-mediated extrusion upon expression of DARPin_Act2 (trace 1) but not of control DARPin E3_5* (trace 2). No activation of LmrCD activity was observed upon expression of DARPin_Act2 (trace 3) or control DARPin E3_5* (trace 4) in *L. lactis* Δ*lmrCD* cells. Shown are representative data from at least three independent measurements (n≥3).
doi:10.1371/journal.pone.0037845.g004

contrast, binding of α-LmrCD#1 and the DARPin activators (DARPin_Act2 and DARPin_Act3) to LmrCD is competed by DARPins recognizing epitopes 1 and 2 as well as by themselves. Hence the binding epitopes of α-LmrCD#1 and the DARPin activators are suggested to partially overlap with the first two epitopes. Nevertheless, conformational communication between two well-separated sites resulting in apparent competition of binding cannot be excluded. The presence of two distinct epitopes, one for α-LmrCD#1 (epitope 3) and the other for activator DARPins (epitope 4), is supported by the large differences in sequence between α-LmrCD#1 and the activator DARPins (Figure 6B, Figure S2). Trapping of LmrCD with vanadate did not help to generate DARPins different from the ones selected in the absence of trapping agent as DARPin α-LmrCD#2 (non-vanadate DARPin) shares the epitope with α-LmrCD#4 (vanadate DARPin), and α-LmrCD#5 (non-vanadate DARPin) shares the epitope with α-LmrCD#3 (vanadate DARPin). Clearly, "vanadate" DARPins do not bind to a shared epitope that is distinct from the epitope of the "non-vanadate" binders.

The stoichiometry of binding between the DARPins and LmrCD after SEC was determined by protein chip technology (Agilent Technologies) allowing accurate quantification of protein amounts (Figure 7A and B, Table 1). DARPin_Act3 as well as α-LmrCD#1, α-LmrCD#2, α-LmrCD#3 and α-LmrCD#5 form 1:1 complexes with LmrCD (Table 1). DARPin_Act1 and DARPin_Act2 formed soluble aggregates impeding their separation from LmrCD on SEC whereas the affinity of α-LmrCD#4 appeared to be too low to allow co-elution with LmrCD from the gel filtration column. Therefore, the stoichiometry of binding could not be determined for these DARPins.

Determination of the Dissociation Constants by Surface Plasmon Resonance (SPR)

The affinities of the isolated DARPins to LmrCD were determined by SPR measurements using a Biacore instrument. Detergent purified $bLmrCD_{AviC}$ was immobilized on a streptavidin-coated chip and binding of the DARPins was assessed (Figure 7C and D, Table 1). When using a two-state reaction model (see Materials and Methods), the observed data fitted very close to the predicted data. However, to assess whether DARPin binding to LmrCD is correctly described by a two-state reaction model, 400 nM of α-LmrCD#3 was injected for 100 s, 200 s and 400 s, and DARPin dissociation phases were compared (Figure S3). The dissociation curves obtained, superimposed almost perfectly, suggesting that DARPin dissociation was independent of the association time. These findings indicate that the use of the two-state reaction model is inappropriate. Therefore, all data were fitted using a simple 1:1 binding model (see Materials and Methods), which allowed for the calculation of the dissociation constants (K_D) from the association and dissociation rate constants k_a and k_d (Table 1). To determine equilibrium binding constants ($K_{D,eq.}$, see Materials and Methods, Figure 7D and Table 1), injection times were chosen that allowed DARPin binding to reach equilibrium (Figure 7C). With the exception of α-LmrCD#2 and DARPin_Act2, the K_D and $K_{D,eq.}$ were found to be almost identical. Since $K_{D,eq.}$ is unaffected by known SPR artifacts such as mass transport and analyte rebinding [59], we refer to the $K_{D,eq.}$ to describe the affinities of the DARPins for LmrCD in this study. The $K_{D,eq.}$ values of the majority of LmrCD-specific DARPins were between 9 nM and 67 nM with the exception of the $K_{D,eq.}$ of 173 nM for α-LmrCD#4. Confirming the SPR measurements, α-LmrCD#4 binding to LmrCD was too weak for co-elution of the protein complex during SEC (Table 1); the ELISA signal was considerably lower than for the other binders (Figure 3A).

DARPin Binding to Membrane-embedded LmrCD

The binding of DARPins to inside-out membrane vesicles (ISOVs) containing either overproduced $AcrB_{AviC}$ or $LmrCD_{AviC}$ was further characterized (Figure 8). Based on an analysis using a protease-cleavable LmrCD-GFP construct (see Materials and Methods), ISOV preparations were found to contain up to 10% of the membrane vesicles in the right-side-out orientation (right-side-out membrane vesicles, RSOVs). Total binding was determined as the amount of DARPin bound to ISOVs containing the

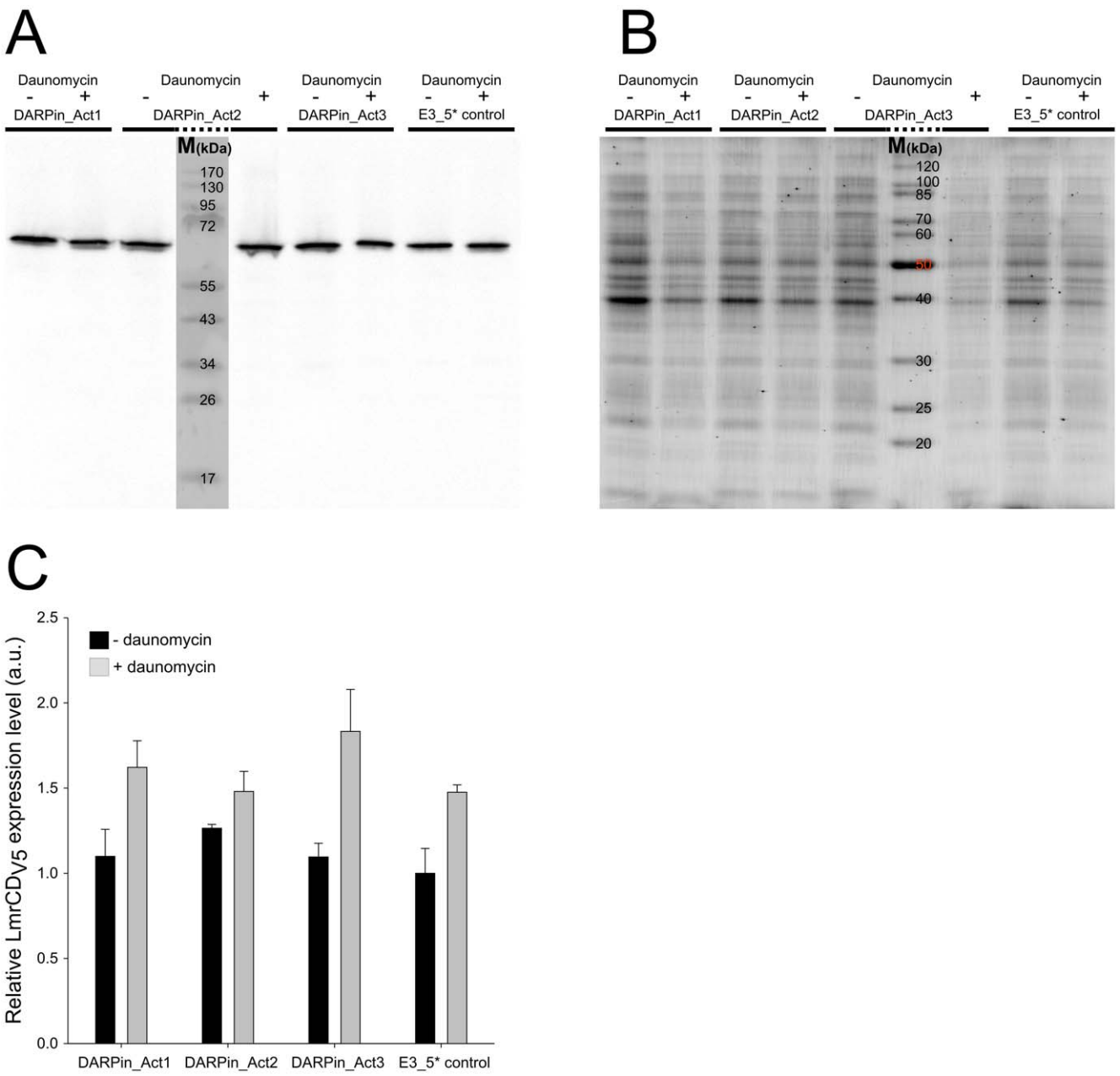

Figure 5. DARPin expression does not significantly alter expression of LmrCD proteins. (**A**, **B**) A V5-tag was introduced in frame at the 5′-end of genomic *lmrD* in *L. lactis* (denoted *L. lactis NZ9000 lmrD*$_{V5}$). Plasmid-encoded DARPin activators or the control DARPin E3_5* were expressed in *L. lactis NZ9000 lmrD*$_{V5}$ in the presence and absence of daunomycin (14 μM for DARPin_Act3 and E3_5* and 28 μM for DARPin_Act1 and DARPin_Act2, respectively). The expression levels of genomic LmrD$_{V5}$ were then quantified by comparing the Western blot signal obtained using an anti-V5 antibody (A) with total protein detected by SYPRO ruby staining (B). (**C**) The relative amounts of LmrD$_{V5}$ expression were quantified by densitometry. Each bar represents the average of three independent data points (n = 3) of which one data point is shown in (A) and (B).
doi:10.1371/journal.pone.0037845.g005

overexpressed target protein. Background binding refers to binding of the respective DARPin to ISOVs containing an overexpressed membrane protein that is not recognized by the binder. For the AcrB-specific DARPin 110819, the membrane vesicles used for the determination of background binding thus contained overexpressed LmrCD and *vice versa*. Specific binding was then calculated by subtracting background binding from total binding. Binding of all six DARPins tested was target-specific, meaning that total binding was stronger than background binding. The AcrB-specific DARPin 110819, whose structure has been solved in complex with AcrB by X-ray crystallography, was used as control. As expected, DARPin 110819 binds relatively poorly to ISOVs despite its high reported binding affinity of 28 nM because the binding epitope on AcrB is located at the periplasmic loops and is therefore predominantly hidden in the vesicle lumen [18]. The binding signal for DARPin 110819 therefore originates from the estimated 10% RSOVs present in the ISOV preparation. Despite the fact that AcrB is expressed better than LmrCD (not shown), binding of α-LmrCD#2 and DARPin_Act3 to LmrCD-containing ISOVs resulted in signals that were around three times

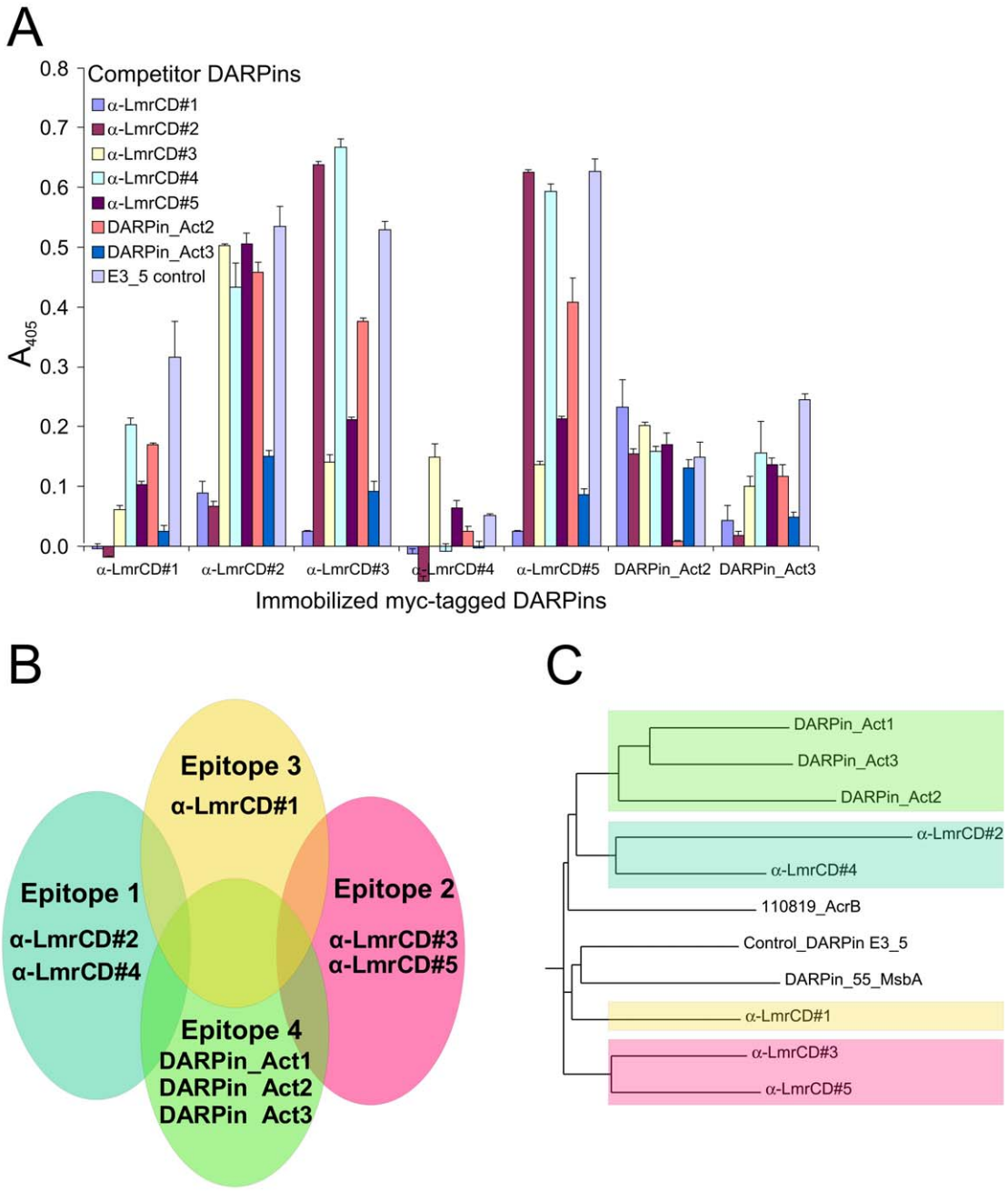

Figure 6. Epitope mapping of LmrCD-specific DARPins by ELISA. (**A**) Analysis of the LmrCD-specific DARPins by a competition ELISA. Binding of $bLmrCD_{AviC}$ to immobilized Myc-tagged DARPins was competed with an excess of DARPins devoid of Myc-tag. (**B**) Schematic drawing of the four proposed binding epitopes on LmrCD recognized by the LmrCD-selective DARPins based on the results of the competition ELISA shown in (A). The number of the epitopes follows the numbering in the main text. (**C**) The phylogenetic tree of the LmrCD-specific DARPins corresponds well with the proposed binding epitopes. The branches of the phylogenetic tree are highlighted with the color code used to label the four suggested binding epitopes in (B).
doi:10.1371/journal.pone.0037845.g006

bigger than the ones of DARPin 110819 binding to AcrB-containing ISOVs (Figure 8A). Since the binding affinities of α-LmrCD#2 (9 nM) and DARPin_Act3 (55 nM) are in the same order of magnitude as of DARPin 110819 (28 nM), these LmrCD-specific DARPins appear to recognize epitopes at the cytoplasmic portion of LmrD, which are accessible in ISOVs. Specific binding of α-LmrCD#1 on the other hand is half as high as for DARPin 110819 whereas it is roughly the same for α-LmrCD#3. DARPin binding to these epitopes is therefore either restricted in membrane-embedded LmrCD or the epitope is only accessible from the physiological outside of the membrane. We also attempted to perform these DARPin binding experiments using RSOVs generated from *E. coli* using the EDTA-lysozyme method [60]. Studies on the accessibility of a C-terminal GFP fusion partner on LmrD to protease cleavage from the external surface of membrane vesicles indicated that, despite careful preparations, a substantial portion (up to 50%) of LmrCD-GFP containing membrane vesicles were in the inside-out orientation, and that

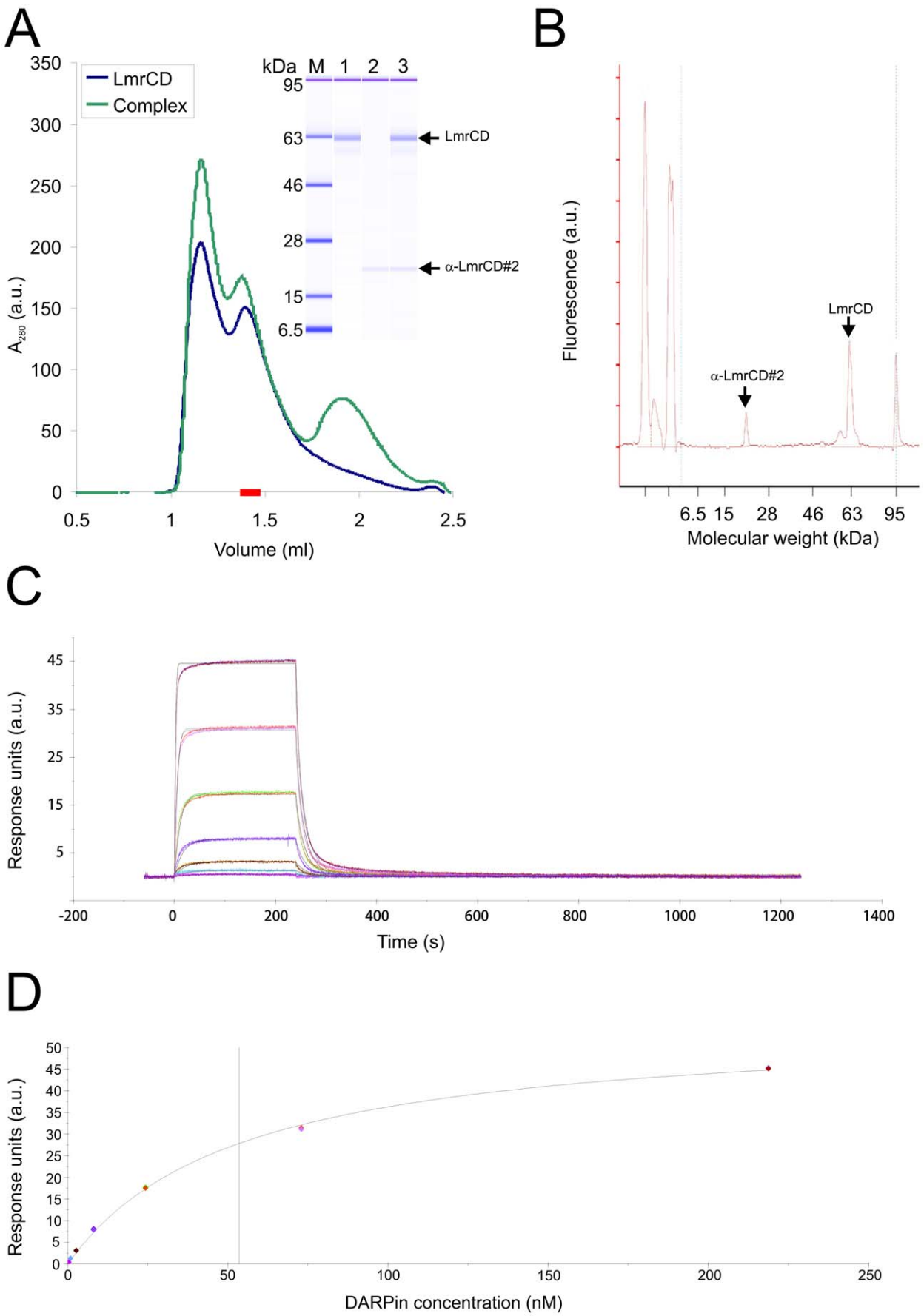
A
LmrCD
Complex
kDa M 1 2 3
95
63
46
28
15
6.5
LmrCD
α-LmrCD#2
A_{280} (a.u.)
Volume (ml)
B
Fluorescence (a.u.)
LmrCD
α-LmrCD#2
Molecular weight (kDa)
C
Response units (a.u.)
Time (s)
D
Response units (a.u.)
DARPin concentration (nM)

Figure 7. Biophysical characterization of the DARPin-LmrCD complexes. (**A**, **B**) Stoichiometry analysis as exemplified by the LmrCD/α-LmrCD#2 complex. (A) LmrCD and the LmrCD/α-LmrCD#2 complex were separated by SEC (Superdex 200 PC3.2/30, GE Healthcare) with a void volume $V_0 = 0.85$ ml and a total volume $V_t = 2.4$ ml. A fraction corresponding to heterodimeric LmrCD in complex with α-LmrCD#2 complex (red bar) was subjected to protein chip analysis (lane 3, inset). LmrCD and the DARPin α-LmrCD#2 were also analyzed (lanes 1 and 2, inset). The peak at a retention volume of 1.2 ml corresponds to aggregated LmrCD. (B) The peak area of the protein chip chromatogram corresponding to LmrCD and α-LmrCD#2 of lane 3 in (A) were calibrated with dilution series of LmrCD and DARPin of known protein concentrations (not shown) and were used to determine the stoichiometry of the LmrCD-DARPin complexes (Table 1). (**C**) Affinities of the DARPins to LmrCD were determined by surface plasmon resonance as shown for α-LmrCD#3. The colored lines correspond to the measured traces at different DARPin concentrations, the fitted curves (1:1 binding model) are shown as black lines. (**D**) The steady state DARPin binding signals achieved at the end of the association phase shown in (C) were plotted against the DARPin concentration and fitted using an equilibrium binding equation equivalent to the Michaelis-Menten equation. In this analysis, equilibrium dissociation constants ($K_{D,\ eq.}$) were generated.
doi:10.1371/journal.pone.0037845.g007

therefore, this type of membrane vesicles could not be used to study the accessibility of the binding epitopes (data not shown). Background binding to ISOVs varied between the different DARPins and correlated with the aggregation behavior on SEC (Figure S1). Low background binding was observed for the DARPins α-LmrCD#1, α-LmrCD#3 and the AcrB-DARPin 110819, whereas α-LmrCD#2, DARPin_Act2 and DARPin_Act3 interacted with membrane vesicles lacking the target protein (Figure 8A).

Specific binding of DARPin_Act2 to LmrCD in ISOVs was low in the initial binding experiment, most likely due to its slow on-rate of binding (Figure 8A, Table 1). Therefore, binding of DARPin_Act2 and α-LmrCD#3 to membrane-embedded LmrCD in ISOVs was determined at a prolonged incubation time (200 min instead of 40 min) and at increasing DARPin concentrations (0.35 μM as in the initial experiment, 1 μM and 2 μM) (Figure 8B). Although background binding of DARPin_Act2 remains high, specific binding was substantially increased, in particular at a DARPin concentration of 2 μM. For the DARPin α-LmrCD#3 on the other hand, background binding was very low and maximal specific binding was achieved already at a concentration of 1 μM. Taken together, these binding assays suggest that specific protein-protein interactions between the activator DARPins and membrane-embedded LmrCD are likely to provide the basis for the activation of LmrCD-mediated drug transport, although indirect mechanisms due to binding of the DARPin activators to the membrane cannot be excluded. Binding of DARPin_Act2 and DARPin_Act3 to LmrCD-containing ISOVs indicates that the DARPin activators can bind to their epitope on LmrD when expressed in the cytoplasm of *L. lactis*. If we assume a protein concentration of 200 mg/ml in the cytoplasm of *L. lactis* [61] and estimate the DARPin expression level to amount for 2% of total protein (not shown), the DARPin concentration inside the cell is about 4 mg/ml or 200 μM. The DARPin concentration in the cell exceeds its binding affinities by more than three orders of magnitude and therefore the binding epitopes are saturated with bound DARPins.

DARPin Activators Stimulate the Basal ATPase Activity of LmrCD Reconstituted in Proteoliposomes

To further elucidate the mechanism by which the DARPin activators stimulate the function of LmrCD, detergent-purified LmrCD was reconstituted into proteoliposomes made of polar *E. coli* lipids and egg-phosphatidylcholine mixed at a ratio of 3:1 [55]. Reconstituted LmrCD exhibits basal ATPase activities that are three times lower than the activity of purified LmrCD in its micellar form (not shown). Addition of increasing concentrations of daunomycin to reconstituted LmrCD (5–200 μM) increased its ATPase activity in a dose-dependent manner, reaching two-fold stimulation at 200 μM daunomycin (Figure 9A). The ATPase activity of reconstituted LmrCD in the presence of the DARPin activators and the control DARPin E3_5 was then compared to samples to which no DARPins were added (Figure 9B). The addition of DARPin E3_5 did not change the ATPase activity of LmrCD at any concentration of daunomycin. On the other hand, ATP hydrolysis of LmrCD was significantly stimulated upon addition of the three DARPin activators up to 1.6 fold in case of DARPin_Act2. These observations in proteoliposomes were found to be statistically significant in three independent reconstitution experiments, one of which is shown in Figure 9B. The DARPin activators are therefore capable of increasing the ATPase activity of LmrCD to a similar extent as 50 μM of daunomycin for which a 1.8 fold increase is seen (Figure 9A and B). The increase of LmrCD's ATPase activity by the DARPin activators and daunomycin was found to be additive, suggesting that the molecular mechanism underlying these stimulatory effects are distinct. Basal and DARPin_Act2-stimulated ATPase activity of reconstituted LmrCD was further elucidated over a range of ATP concentrations (Figure 9C). The data was fitted using the Hill equation, and the apparent K_m for ATP and V_{max} of the ATPase reaction as well as the Hill coefficient were determined. The errors represent standard errors of the parameters derived from nonlinear regression analysis. In presence of DARPin_Act2, the apparent affinity of LmrCD for ATP was not significantly altered ($K_{m,app}$ of 0.85±0.06 mM and 0.73±0.09 mM for DARPin_Act2 and E3_5, respectively). V_{max} on the other hand was doubled in the presence of DARPin_Act2 (V_{max} of 500±22 nmol/min/mg of protein versus 247±19 nmol/min/mg of protein). The Hill coefficient was found to be unaltered in presence of DARPin_Act2 (2.0±0.3 and 2.0±0.5 for DARPin_Act2 and E3_5, respectively). The sigmoidal nature of the fitted curve suggests positive cooperativity between the non-canonical and the consensus composite catalytic site of LmrCD, a finding reminiscent of the maltose transporter and the isolated NBDs of HlyB [62,63].

Discussion

The *in vitro* selection of binders against integral membrane proteins using ribosomal display is very fast (2–3 weeks of lab work under ideal circumstances) and the biochemical conditions can be controlled. Nevertheless, only few successful examples of *in vitro* selected binders specific for membrane protein have been reported, most likely due to the many unknowns that exist regarding enrichment of specific binders against these hydrophobic proteins [18,29–36]. In this work we have made important progress in the screening procedure of DARPins raised against membrane proteins. We found that successful *in vitro* selection depends on two critical factors. Firstly, the quality of the target protein preparation is crucially important for success. LmrCD has proven to be a suitable target since it could be purified to near homogeneity, was catalytically active and could be isolated as heterodimeric species by SEC (Figure S1A and B). Secondly, during DARPin identification it is important to introduce a cross-specificity ELISA using a set of different membrane proteins.

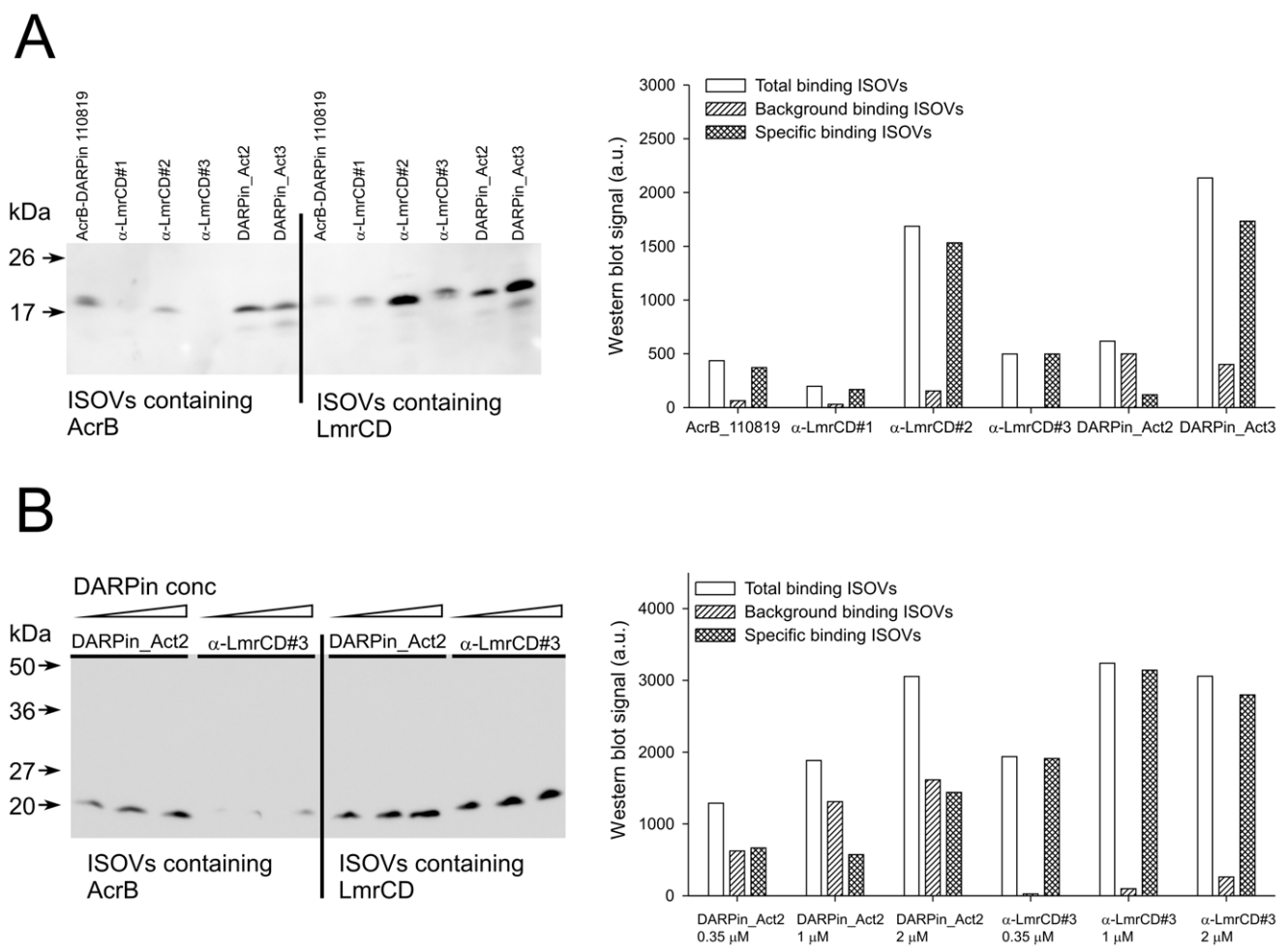

Figure 8. DARPin binding to membrane-embedded LmrCD. (**A**) Six DARPins (each at a 350 nM concentration) specific for AcrB or LmrCD were probed for binding to ISOVs containing either overproduced $AcrB_{AviC}$ or $LmrCD_{AviC}$. Bound DARPins were detected on Western blot (left panel). The signals of the DARPin-specific bands were quantified by densitometry (right panel). Total binding denotes the quantified amount of DARPin bound to membrane vesicles containing overexpressed target protein. Background binding refers to binding to membrane vesicles containing overexpressed $LmrCD_{AviC}$ in case of the AcrB DARPin 110819, or overexpressed $AcrB_{AviC}$ when LmrCD-specific DARPins were used. Specific binding was calculated by subtracting background binding from total binding. (**B**) Binding of DARPin_Act2 and α-LmrCD#3 to ISOVs containing either overproduced $AcrB_{AviC}$ or $LmrCD_{AviC}$ was further assessed using increasing concentrations of DARPin (0.35 μM, 1 μM and 2 μM) and analyzed by Western blot (left panel). The data was quantified as in (A) (right panel). The data represent typical results observed in n = 3 experiments.
doi:10.1371/journal.pone.0037845.g008

Using optimally prepared LmrCD, we obtained a relatively large number of DARPins (around 70%) that showed strong cross-reactivity with MsbA and AcrB. Further analysis showed that many of these unspecific DARPins formed soluble aggregates. Both observations might relate to the hydrophobicity of the target proteins, which can drive selection of hydrophobic binding surfaces in DARPins that tend to aggregate in an aqueous environment. Indeed, DARPin aggregation was not observed at all when DARPins were selected against a soluble test protein (MBP) using the same selection procedure (data not shown). On the other hand, the highly specific DARPins were much less aggregation-prone and about half of them were monomeric as judged from comparing the SEC profiles of the DARPins under study with the monomeric control DARPin E3_5 (Figure S1C). Because the cross-specificity ELISA was performed with DARPin-containing crude cell extracts, there was no need to purify the DARPins for the initial specificity analysis, which greatly accelerated the identification of binders. This screening regime would also be applicable to more difficult membrane protein targets with a further decreased binder hit rate.

A handful of the LmrCD-specific DARPin binders were subsequently characterized by surface plasmon resonance and size exclusion chromatography. With the exception of the DARPin α-LmrCD#4, the $K_{D,eq.}$ values for binding were found to range between 9 and 67 nM. The binding stoichiometry of these high-affinity binders with heterodimeric LmrCD is 1:1. The LmrCD-specific DARPins are suggested to recognize at least three overlapping epitopes on the LmrD chain. The surface of LmrD might therefore harbor one or several hot spot epitopes that are preferably recognized by the DARPins. Recently, a hot spot epitope that is recognized by nine highly diverse DARPins has been reported for AcrB [19]. The fact that a handful of high quality DARPins specific for LmrCD could be readily identified, indicates that the randomized DARPin scaffold is sufficiently diverse to recognize a multitude of binding sites on the membrane protein target. Given the high binding affinities achieved and the various epitopes recognized on LmrCD, these DARPins can be

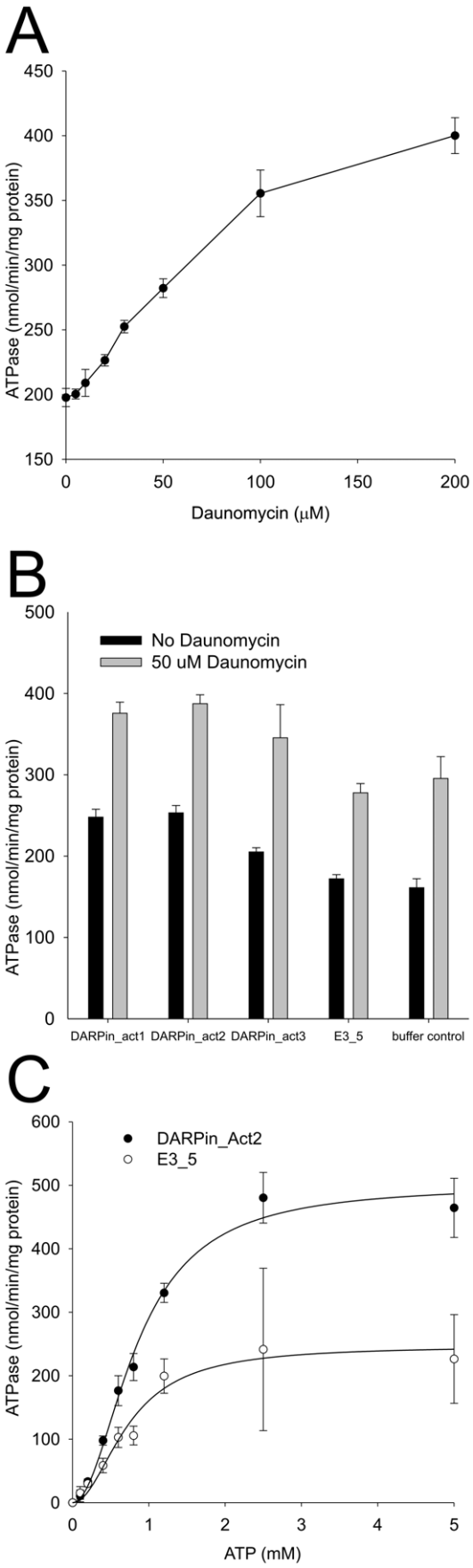

Figure 9. ATPase activity of reconstituted LmrCD is stimulated by DARPin activators and daunomycin. Each symbol or bar represents the average of three data points. (**A**) The ATPase activity of reconstituted LmrCD is stimulated in the presence of daunomycin in a dose-dependent manner. (**B**) Reconstituted LmrCD (protein:lipid ratio of 1:50, proteoliposomes diluted to obtain an LmrCD concentration of 70 nM) was incubated with DARPin activators and control DARPin E3_5* (2.5 μM) and the ATPase activity was determined in the absence and presence of 50 μM daunomycin (triplicates). As a control, buffer instead of DARPins were added to LmrCD. According to t-test analysis, the measured ATPase activity differences between DARPin_Act1 to Act3 and the buffer control are statistically significant ($p<0.01$ in the absence and $p<0.05$ in the presence of daunomycin, respectively). (**C**) The ATPase activities of LmrCD in the presence of DARPin_Act2 and E3_5 were determined over a range of ATP concentrations. The data points were fitted to the Hill equation.
doi:10.1371/journal.pone.0037845.g009

used for chaperone-assisted membrane protein crystallography [64].

Binding experiments using LmrCD-containing ISOVs suggest that the DARPins α-LmrCD#2 and DARPin_Act3 bind to epitopes located at the cytoplasmic side of LmrCD. DARPin activators expressed in the *L. lactis* cells are therefore expected to readily reach their binding epitope *in vivo*. Since these DARPins recognize full-length LmrD, but not the isolated NBD of LmrD, it is likely that they bind to the cytoplasmic loops of the membrane domain of LmrD. The other LmrCD-specific DARPins tested (α-LmrCD#1 and α-LmrCD#3) were found to bind to membrane-embedded LmrCD as well. However, the relatively weak binding signals suggest that access to the binding epitopes is either partially restricted by the lipid bilayer or that the binding epitope is only accessible from the physiological outside of the cell, which is hidden in the vesicle lumen of ISOVs. In the latter case, the binding signal would originate from the approximate 10% of RSOVs found in ISOV preparations.

The drug resistance phenotype in *L. lactis* associated with the genomic expression of LmrCD was used to screen our pre-selected DARPins for those that influence the functional properties of this multidrug transporter. We observed the production of DARPins in the cytoplasm of *L. lactis* with a relatively low toxicity compared to expression in *E. coli*. Three homologous DARPins (DARPin_Act1, Act_2, and Act3) were obtained, which enhance the LmrCD-associated resistance to daunomycin and activate efflux of BCECF-AM, but which, surprisingly, do not alter the resistance to Hoechst 33342. This finding is reminiscent to a study on ABCB1, in which small molecules were found to increase its transport activity for some drugs whereas the transport of other drugs was not affected or even decreased [65].

We considered the possibility of an increased LmrCD production level in *L. lactis* in the presence of DARPin activators that might act as folding chaperones. To test this hypothesis, a V5-tag was introduced in frame with *lmrD* on the chromosome of *L. lactis*, an approach that, to the best of our knowledge, was carried out for the first time in this bacterium. With this tool it was demonstrated that the expression of the activator DARPins in *L. lactis* does not lead to changes in LmrCD production levels in the presence as well as in the absence of daunomycin. As a proof of concept, LmrCD expression was increased 1.5-fold in the presence of daunomycin, which agrees well with RT-PCR experiments detecting a transient two-fold increase of mRNA transcription from *lmrCD* upon drug stimulation [66]. From this experiment we concluded that the increased daunomycin resistance as well as the enhanced BCECF-AM efflux originates from a direct stimulation of the activity of LmrCD transporters as a consequence of DARPin binding.

To gain more insight into the potential mechanism underlying the activation of drug transport, the influence of the DARPin activators on the ATPase activity of reconstituted LmrCD was studied. The DARPin activators were found to stimulate the ATPase activity of reconstituted LmrCD to a similar extent as daunomycin applied at a concentration of 50 μM. Activation of the basal ATPase activity of LmrCD upon DARPin expression is a plausible explanation for the observed daunomycin resistance increase in *L. lactis*. However, it cannot explain why the resistance of lactococcal cells to Hoechst 33342 was not affected by the expression of the DARPin activators. The exact mechanism behind the modulation of LmrCD-mediated drug transport by the DARPin activators is possibly much more complex. Recent studies on Pdr5, a heterodimeric multidrug transporter of *Saccharomyces cerevisiae* revealed a single mutation at one NBD which abolished drug resistance against rhodamine-like compounds whereas transport of other drugs was unaffected [67]. Likewise, a screen identified small molecules dramatically altering the drug transport profile of ABCB1 based on a molecular mechanism that remains elusive [65]. These findings cannot yet be comprehensively explained by current models of ABC transporter mechanism and illustrate the limitation of our knowledge.

Beyond the activation of the basal ATPase by the DARPin activators, we speculate that DARPin binding to LmrCD might stabilize a conformational transition state at a rate-limiting step during daunomycin and BCECF-AM transport. DARPin binding could, for example, increase the overall rate of transport by stabilizing the inward-facing state resulting in increased fractional occupation during substrate binding, or enhance the dissociation of the substrate from outward-facing LmrCD. But also the resetting of LmrCD from the outward-facing to the inward-facing state after ATP hydrolysis and drug release might be accelerated by the DARPin activators. Finally, in addition to these possible effects of DARPin binding on the maximal rate of efflux, DARPin binding might directly influence the drug binding affinity of LmrCD by imposing structural changes in drug binding surfaces. The effect of DARPins on the mechanism of transport in *in vitro* models (e.g. proteoliposomes) will be studied in future work.

In conclusion, we obtained three DARPins that activate multidrug export by LmrCD in intact cells and stimulate the ATPase activity of the transporter reconstituted into proteoliposomes. Our work demonstrates the potential of *in vitro* selected artificial binding molecules to manipulate membrane transport processes *in vivo*. Unlike chemical modulators, binding proteins have the potential to stabilize any conformational (transition) state of a membrane transporter, and offer the possibility to functionally and structurally study membrane proteins in unprecedented ways. When targeting membrane transporters associated with human disease, DARPins could therefore be of great biopharmaceutical importance.

Materials and Methods

Molecular Cloning and Expression of lmrCD and Other Transporters

The primers and genetic constructs are listed in Table S1 and Table S2. The *lmrCD* genes as well as the genes of *msbA* and *acrB* were cloned with a coding region for an Avi-tag sequence at their 3′-end, which allows the site-specific biotinylation of the target proteins for the purpose of protein immobilization during ribosome display and ELISA. A DNA fragment encoding the Avi-tag sequence flanked by the restriction sites NheI and BamHI was formed by annealing the two oligonucleotides avitag_for and avitag_rev, and was ligated into the *E. coli* cloning vector pGEM using the NcoI and XbaI restriction sites, yielding pGEM_Avi. The *lmrCD* genes were amplified from the chromosome of *Lactococcus lactis* subsp. *cremoris* MG1363 using the primers lmrCD_DecaHisN_AviC_for for introduction of an N-terminal His10-tag in LmrC and lmrCD_AviC_rev to add a C-terminal Avi-tag to LmrD. The PCR product was cut with NcoI and XbaI and cloned into the pGEM_Avi digested with NcoI and NheI yielding pGEMLmrCD$_{AviC}$. Two independent clones were sequenced and were found to carry a nucleotide substitution compared to the published sequence of *Lactococcus lactis* subsp. *cremoris* MG1363 [68] at the triplet position of C179 in LmrC, which is an arginine in our clone (TGC → CGC). In addition, a construct lacking the C-terminal Avi-tag was cloned by amplifying *lmrCD* from pGEMLmrCD$_{AviC}$ using the forward primer lmrCD_NdeI_Presc_that introduces a linker and a prescission protease cleavage site at the 5′-end, and the reverse primer lmrCD_rev. The PCR product was digested using NdeI/XbaI and ligated into pGEMLmrCD$_{AviC}$ cut with the same enzymes, resulting in plasmid pGEMLmrCD. The tagged *lmrCD* genes were then sub-cloned via NcoI/XbaI either into the lactococcal pNZ8048 vector [54] or the *Escherichia coli* expression vector pBAD24 [69] yielding the expression vectors pNZLmrCD$_{AviC}$, pNZLmrCD, pBADLmrCD$_{AviC}$ and pBADLmrCD, respectively. The *msbA* gene was cloned into pGEM_Avi via the restriction sites NcoI/NheI amplifying the *msbA* gene with the primers msbA_-DecaHisN_for and msbA_AviC_rev from the clone pNZMsbA [44] yielding pGEMMsbA$_{AviC}$. The gene of *acrB* from *E. coli* devoid of NcoI sites (Murakami and van Veen, unpublished) was amplified with the primers acrB_HisC_AviC_for and acrB_His-C_AviC_rev and cloned via NcoI/NheI into pGEM_AviC yielding pGEMAcrB$_{AviC}$. The tagged *msbA* and *acrB* genes were sub-cloned into pBAD24 using the restriction sites NcoI and XbaI resulting in pBADMsbA$_{AviC}$ and pBADAcrB$_{AviC}$. All sequences were confirmed by DNA sequencing. The genes coding for *lmrC*, *lmrD* and *lmrCD* were also cloned in frame with a C-terminal GFP (that is cleavable by 3C protease) into pBAD24 applying the recently developed FX-cloning method [70]. Similarly, coding regions of the NBDs of LmrC and LmrD (which includes residues G336 to D579 and G424 to E664 of LmrC and LmrD, respectively) were cloned into a FX-vector adding a His10-tag, a 3C protease cleavage site and an Avi-tag to the 5′-end of the cloned genes (Geertsma and Dutzler, unpublished). The Walker B glutamate of the consensus ATPase site of LmrCD was mutated to glutamine using a quick-change standard protocol (LmrD_E587Q). LmrCD protein containing a C-terminal Avi-tag (LmrCD$_{AviC}$) was produced in and purified from *L. lactis* NZ9000 Δ*lmrA* Δ*lmrCD* [55] following published protocols [45,71]. The enzymatic site-specific biotinylation of the Avi-tag was carried out *in vitro* using purified BirA yielding biotinylated LmrCD$_{AviC}$ (bLmrCD$_{AviC}$) [51], which was then used for DARPin selection and ELISA. MsbA$_{AviC}$ and AcrB$_{AviC}$ were expressed in *E. coli* harboring the corresponding pBAD24 expression vectors and were purified and biotinylated accordingly.

DARPin Selection

The N3C DARPin library was chosen to select binders against biotinylated LmrCD$_{AviC}$ (bLmrCD$_{AviC}$) using the ribosome display method [12,28,72]. In all selection rounds, 0.03% DDM was used as detergent instead of the commonly used Tween-20 in the standard ribosome display buffer WBT-BSA, containing 50 mM Tris-acetate pH 7.5, 150 mM NaCl, 50 mM MgOAc, and 0.5% BSA. For the DARPin selection against vanadate-trapped bLmrCD$_{AviC}$, the protein was incubated with 1 mM ATP and 1 mM Na_3VO_4 (freshly boiled as 100 mM stock, pH 9–10)

prior to (1 h on ice) and during the incubation with the ribosomal complexes. For the first three rounds, the selection was carried out using the surface panning method by immobilizing $bLmrCD_{AviC}$ via neutravidin on a solid support as described in the protocol of Zahnd et al. [72]. The washing times before mRNA elution, were set to 5, 2×15 and 2×30 min in the first, the second and the third selection round, respectively. The fourth selection round was carried out with the solution panning method [31]. 60 nM of $bLmrCD_{AviC}$ was added to the stabilized DARPin *in vitro* translation mixture (260 µl) and panned for 90 min. Streptavidin-coated magnetic beads (20 µl suspension Dynabeads MyOne Streptavidin T1, Invitrogen) were used to capture the biotinylated $bLmrCD_{AviC}$ with bound ribosomal complexes during 15 min. The beads were rinsed twice with 300 µl WBT-BSA containing 0.03% β-DDM (WBT-BSA-DDM), placed into a fresh tube, and washed for 30 min. After another tube change and another 30 min of washing, the mRNA was eluted and purified according to the standard protocol [72].

Crude Cell Extracts and ELISA

The pools of DARPins from the 4th selection round were expressed from the vector $pQE30_{myc5}$ [31] in *E. coli* XL-1 Blue yielding DARPins carrying an N-terminal RGS-His6 tag (with the protein sequence MRGSHHHHHH) and a C-terminal Myc5-tag (with five times the sequence MEQKLISEEDLNE). DARPin-containing crude cell extracts were used to identify LmrCD-specific binders by ELISA as described [31]. The DNA sequences of all identified DARPins have been deposited in GenBank under the accession numbers JQ425604-JQ425611.

SEC of Isolated DARPins and the LmrCD-DARPin Complexes

The Myc5-tag fusion with the DARPins leads to the formation of higher oligomeric species (not shown), and the DARPins were therefore sub-cloned into the pQE30 vector (Qiagen) devoid of a Myc-tag for further analysis and purified via Ni^{2+}-NTA chromatography and SEC (Superdex 200 10/300 GL, GE Healthcare) according to standard procedures [14]. For the quantification of the stoichiometric compositions of the LmrCD-DARPin complexes, Ni^{2+}-NTA purified LmrCD (10 µM) was mixed with a twofold excess of freshly gel-filtrated DARPin and incubated for 30 min. The protein mixture was separated by SEC (Superdex 200 PC3.2/30, GE Healthcare), after which fractions were analyzed by on-chip protein analysis according to the manufacturer's protocol (Protein 80 Kit, Agilent Technologies).

Surface Plasmon Resonance

The affinities of selected DARPins towards detergent purified $bLmrCD_{AviC}$ were determined by surface plasmon resonance on a Biacore T100 machine (GE Healthcare). Because initial SRP measurements in a buffer containing 0.03% DDM were difficult to interpret, the dissociation constants were determined in the presence of Tween-20 instead. To test the stability of LmrCD in Tween-20, DDM was replaced with highly pure Tween-20 (Anapoe-20, 0.05%, Anatrace) in the washing and elution step during LmrCD purification by Ni^{2+}-NTA chromatography. LmrCD purified using Tween-20 exhibited an ATPase activity of 297±24 nmol/min/mg of protein and its SEC elution profile was indistinguishable from the one obtained with DDM (not shown). For the SRP measurement, the detergent was changed from DDM to Tween-20 after the immobilization of $bLmrCD_{AviC}$ on the Biacore chip, which lead to highly accurate and undisturbed measurements. The target protein was purified freshly as described above and 600 response units (RU) were immobilized in flow cell 2 of a streptavidin-coated SA chip (GE Healthcare), whereas flow cell 1 was used for referencing. Affinities were determined in 20 mM Tris/HCl pH 7.5, 150 mM NaCl containing 0.05% (v/v) Tween-20 at 10°C and a flow rate of 20 µl/min. The DARPin concentration was determined by OD_{280} using a NanoDrop1000 Photospectrometer and calculated based on theoretical extinction coefficients (www.expasy.ch/tools/protparam.html). For each DARPin, a 3-fold dilution series of six different concentrations were used for the kinetic measurements (concentration ranges: 0.1 nM–72.9 nM for α-LmrCD#1, α-LmrCD#2; 0.3 nM –218.7 nM for α-LmrCD#3, α-LmrCD#5 and DARPin_Act3; 1 nM –729 nM for α-LmrCD#4; 3 nM - 2187 nM for DARPin_Act2). Every DARPin concentration was injected twice starting with the lowest concentration, increasing to the maximal concentration and then decreasing back to the lowest concentration. The association and dissociation phases were set as follows (the first number denotes association time/the second number denotes dissociation time): α-LmrCD#1, α-LmrCD#2 and DARPin_Act2 (700 s/2400 s); α-LmrCD#3 (240 s/1000 s); α-LmrCD#4, α-LmrCD#5 and DARPin_Act3 (400 s/1200 s). The data were best fitted using a two-state reaction model. This model assumes that the DARPin (A) and LmrCD (B) form an initial complex (AB) with an association rate constant k_{a1} (in M^{-1} s^{-1}) and a dissociation rate constant k_{d1} (in s^{-1}). This initial complex (AB) is then converted into an alternative complex (AB*) with the association rate constant k_{a2} (in s^{-1}) and a dissociation rate constant k_{d2} (in s^{-1}). In this model, the dissociation constant K_D (M) is calculated using the following equation:

$$K_D = \frac{k_{d1}}{k_{a2}} \cdot \frac{k_{d2}}{(k_{d2} + k_{a2})}$$

However, a control experiment in which a saturating concentration of a DARPin was injected for varying times revealed, that the two-state reaction model is inappropriate (see Results and Figure S3). Therefore, the data were fitted using a simple 1:1 binding model and the dissociation constant K_D was calculated using the following equation in which k_a is the association rate constant and k_d the dissociation rate constant:

$$K_D = \frac{k_d}{k_a}$$

In addition, the steady-state response units at the end of each injection (i.e. when association and dissociation are in equilibrium) were plotted against the injected DARPin concentration (Figure 7D). The equilibrium constant $K_{D,eq.}$ was determined by non-linear regression using an equilibrium binding equation equivalent to the Michaelis-Menten equation in which R denotes the SPR response at equilibrium, R_{max} denotes the maximal SPR response and [DARPin] is the DARPin concentration:

$$R = \frac{R_{max}[\text{DARPin}]}{K_{D,eq.} + [\text{DARPin}]}$$

Functional Screening in *L. lactis*

The control DARPin E3_5 [14] was cloned into the lactococcal vector pNZ8048 from which it was expressed in *L. lactis*. During the course of the study, DNA sequencing of the pNZ8048 clone of the control DARPin E3_5 revealed the replacement of the second repeat with the duplicated sequence of the third repeat in a recombination event. This variant of E3_5 (E3_5*) was monomeric (not shown) and was used as control DARPin in the functional experiments in *L. lactis*. For the functional screening of the DARPins in *L. lactis*, the DARPin pools of the 4th selection round were expressed from pNZ8048 in the presence of nisin A (10 ng/ml) and daunomycin (10 μM or 18 μM to screen for inhibitors or activators, respectively). The plasmids encoding for potential inhibitory or activating DARPins were isolated, sequenced and retransformed into wildtype *L. lactis* NZ9000 and *L. lactis* NZ9000 Δ*lmrA* Δ*lmrCD*. Resistance towards daunomycin and Hoechst 33342 was determined by growing the cells at various drug concentrations. A pre-culture devoid of nisin (150 μl) was inoculated 1:100 with an overnight culture, after which cells were grown for 210 min. The preculture was then diluted 1:100 into medium containing 10 ng/ml nisin after which daunomycin was added to various concentrations, and growth of cells was allowed for 15 to 18 h. Final OD_{660} were measured and normalized by setting the final OD_{660} reached in the absence of drug to 100. Normalized values were plotted versus the daunomycin concentration. The curves were fitted with a 4-parameter sigmoidal equation in which y stands for the normalized final OD_{660}, y_0 describes the background OD_{660}, x stands for the daunomycin concentration, x_0 is the inflection point of the curve, and a and b are fitting parameters (SigmaPlot 10, default settings).

$$y = y_0 + \frac{a}{1 + e^{-(\frac{x - x_0}{b})}}$$

IC_{50} for daunomycin was defined as the daunomycin concentration at which the OD_{660} after growth for 15–18 h is half as high as in the absence of the drug.

Transport Assay with BCECF-AM

L. lactis NZ9000 and *L. lactis* NZ9000 Δ*lmrA* Δ*lmrCD* harboring the expression plasmids for DARPin_Act2 and the unselected DARPin E3_5* were grown to an OD_{660} of 0.6 and induced for 2 h with 5 ng/ml nisin A. Cells were harvested and washed twice with ice-cold fluorescence buffer (50 mM potassium phosphate pH 7.0, 5 mM $MgSO_4$). For the fluorescence measurements, the OD_{660} was adjusted to 0.5 and the cells were pre-energized by the addition of 0.5% glucose whilst stirring. Nigericin and valinomycin (1 μM each) were added prior to the addition of the fluorescent substrate. Non-fluorescent BCECF-AM was added at a final concentration of 0.2 μM. Subsequently, the formation of the fluorescent BCECF was monitored at excitation and emission wavelengths of 502 nm and 525 nm, respectively using slit widths of 2.5 nm and 4 nm, respectively.

Quantification of LmrCD Production Levels in *L. lactis* by the Introduction of a V5-tag

The sequence of the V5 tag (with the protein sequence GKPIPNPLLGLDST) was introduced in frame with the genomic *lmrD* gene at its 3′-end in *L. lactis* using the Campbell-type recombination method [73]. The DNA sequence of the V5 tag containing the appropriate sticky overhangs was generated by annealing the oligonucleotides V5-tag_for and V5-tag_rev and cloned as double-stranded DNA fragment into pGEM_Avi cut with BamHI/NheI yielding pGEM_V5 and thereby replacing the Avi-tag sequence. An 860 bp stretch of chromosomal DNA downstream to the *lmrD* gene was amplified with the primers lmrD_V5_for1 and lmrD_V5_rev1 and introduced into pGEM_V5 using the restriction sites BamHI/XbaI resulting in pGEMLmrCD_{V5}*. The last 1583 bp of *lmrD* were amplified with the primers lmrD_V5_for2 and lmrD_AviC_rev, cut with NcoI/XbaI and cloned in frame with the V5 tag sequence into pGEMLmrCD_{V5}* cut with NcoI/NheI yielding pGEMLmrD_{V5}. The DNA fragment on pGEMLmrD_{V5} containing the V5 tag sequence flanked by a part of *lmrD* and a stretch of DNA downstream of the *lmrD* gene on the *L. lactis* chromosome was sub-cloned into pORI280 via NcoI/XbaI and transformed into *E. coli* EC1000 (repA$^+$) resulting in the plasmid pORI280LmrD_{V5} [73,74]. Wildtype *L. lactis* NZ9000 was transformed with pORI280LmrD_{V5} as described [55] yielding three blue colonies after 3 days of incubation at RT. PCR analysis of the chromosomal DNA revealed that two of these clones were the result of the Campbell-type integration of pORI280LmrD_{V5}. The second recombination step was performed by growing a positive clone for a total of 50 cell divisions in the absence of erythromycin and the subsequent screening for white colonies on M17 agar plates. Two white colonies were found (out of around 4000 colonies screened) and confirmed to encode the *lmrD* gene fused with the V5 tag sequence by Western blotting. This new strain was named *L. lactis* NZ9000 *lmrD_{V5}*. The plasmids encoding the activator DARPins and the control DARPin E3_5* were transformed into *L. lactis* NZ9000 *lmrD_{V5}*. A 1:100 inoculated preculture of transformed cells was grown for 210 min in M17, 0.5% maltose, 5 μg/ml chloramphenicol and 50 μl thereof were used to inoculate 5 ml of the same medium containing 10 ng/ml nisin with or without daunomycin addition (14 μM for DARPin_Act3 and E3_5* and 28 μM for DARPin_Act1 and DARPin_Act2, respectively). Each sample was prepared in triplicates. The cultures were grown for 15 h and harvested by centrifugation. Cells were resuspended in 350 μl of 50 mM Na-HEPES (pH 7), 1 mM $MgSO_4$, 10% (wt/v) glycerol, 1 mM PMSF, 25 μg/ml DNaseI and trace amounts of lysozyme. After the addition of glass beads (300 mg, 0.1-mm diameter), samples were disrupted in a FastPrep device (MP Fastprep-24, MB Biomedicals) twice for 30 s at force 6.5. Cell membranes were harvested by centrifugation (55000 g) resuspended by SDS-PAGE loading dye and the proteins were separated on a 10% tricine gel [75]. Each sample was analyzed on two SDS-PAGE gels, one dedicated to Western blotting and the other to the analysis of the protein amounts with SYPRO ruby staining (a total of 6 gels due to the triplicates). For the Western blotting analysis, the gels were blotted onto a nitrocellulose membrane (wet blotting) and blocked in TBST (TBS containing 0.1% Tween-20) supplied with 5% milk powder overnight. The anti-V5 antibody (Sigma, clone V5-10, 1:3000 diluted in TBST) was panned for 160 min and the membrane was washed three times for 10 min with TBST. After incubation with a secondary anti-mouse HRP antibody (Jackson ImmunoResearch Laboratories, 1:2500 in TBST) and another three washing steps, the Western blot signal was detected with a LAS-3000 imaging system (Fujifilm) using ECL reagent (PIERCE). The second SDS-PAGE gel corresponding to the samples analyzed by Western blot was stained with SYPRO ruby staining (Invitrogen) and the fluorescent signal was read with the LAS-3000 imaging system. The Western blots and the ruby-stained gels were quantified using the Aida software (Raytest). The data were normalized by setting the LmrD_{V5} level determined in cells expressing the control DARPin in the absence of drugs to 1. The standard deviations of the triplicates were calculated.

DARPin Binding to Membrane Inserted Target Protein in ISOVs

For the production of membrane vesicles, $LmrCD_{AviC}$ and $AcrB_{AviC}$ were overproduced in *E. coli* C43 (DE3). Inside-out membrane vesicles (ISOVs) were obtained after cell disruption at 20000 psi (Constant Systems). ISOVs containing overexpressed LmrCD-GFP were prepared to determine the membrane vesicle orientation by cleaving off the GFP at the external side using 3C protease, followed by SDS-PAGE and quantification of the cleavage reaction using in-gel fluorescence of remaining LmrCD-GFP and cleaved GFP. Based on these experiments, ISOV preparations contained 10% or less membrane vesicles of the opposite (right-side-out) orientation. The membrane vesicles were diluted at a protein concentration of 0.2 mg/ml in 1 ml of TBS, pH 7.4. In a first set of experiments (Figure 8A) DARPins (350 nM) were allowed to bind for 40 min to the ISOVs. In a second set of experiments (Figure 8B), the DARPin_Act2 and α-LmrCD#3 used at concentrations of 0.35 μM, 1 μM and 2 μM were allowed to bind for 200 min. The membranes were harvested by centrifugation for 20 min at 55000 g. The pellets were resuspended with 800 μl of TBS to wash off unbound DARPins, spun again, after which the pellets were resuspended with SDS-PAGE loading dye (40 μl). Total membrane proteins in membrane vesicles, and bound DARPins, were separated by SDS-PAGE using tricine gels [75] and blotted onto nitrocellulose membranes. The protein mixture was separated by SDS-PAGE [75] and the bound DARPins were quantified by Western blotting using RGS-His antibody (Qiagen) and detection by ECL (PIERCE).

Reconstitution of LmrCD and ATPase Activity Assay

Ni^{2+}-NTA-purified LmrCD expressed in *L. lactis* was reconstituted at a protein:lipid ratio of 1:50 (w/w) into acetone-washed and ether-extracted total *E. coli* lipids mixed with egg phosphatidylcholine (Avanti) in a ratio 3:1 (w/w) in 50 mM K-HEPES pH 7.0 following published protocols [41,76]. Where indicated, SEC-purified DARPins (2.5 μM) were added to the proteoliposomes and incubated in 50 mM K-HEPES pH 7 for 12 h. Daunomycin (where indicated) and $MgSO_4$ (10 mM) were added shortly prior to the assay start. The ATPase assay was performed in 96-well PCR plates on the heating block of a PCR machine. 40 μl of reconstituted LmrCD (70 nM, including DARPins and daunomycin where appropriate) was added to 10 μl of 5-fold stock of highly pure ATP solution (SigmaUltra, 1 mM final concentration if not stated otherwise, dissolved in ddH_2O adjusted to pH 7 using KOH) whilst the temperature was set to 4°C. The ATP hydrolysis reaction was initiated by changing the temperature to 30°C for 20 min and stopped by denaturing the samples at 80°C for 30 s. LmrCD mutated at the Walker B glutamate of the consensus composite ATPase site (LmrD_E587Q) was reconstituted and used for background subtractions. This mutation was shown previously and confirmed by us to be incapable of hydrolyzing ATP [47]. The amount of generated Pi was quantified colorimetrically using the malachite green/molybdate method [55]. The datapoints of the ATPase activities measured at increasing ATP concentrations (Figure 9C) were fitted with the 3 parameter Hill equation (Sigmaplot 10, default settings), in which y denotes the ATPase activity, x stands for the concentration of ATP, a corresponds to V_{max}, b denotes the Hill coefficient, and c corresponds to $K_{m,app}$.

$$y = \frac{ax^b}{c^b + x^b}$$

Data Analysis

Statistical analyses were performed with the Student's t-test with a 95% confidence interval for the sample mean. If not stated otherwise, error bars represent the standard deviation (SD).

Supporting Information

Figure S1 Preparation of biotinylated target proteins for the DARPin selections and ELISAs, and characterization of selected DARPins by SEC. (A) SDS-PAGE analysis of purified $LmrCD_{AviC}$. The protein bands corresponding to overproduced $LmrCD_{AviC}$ are apparent in the total detergent-solubilized membrane fraction (lane 1). Pure protein is eluted from the Ni^{2+}-NTA column (lane 2). (B) Ni^{2+}-NTA purified $LmrCD_{AviC}$ shown in (A) was *in vitro* biotinylated and separated by SEC to remove aggregated protein and excess biotin. Fractions of the peak at 12.50 ml corresponding to heterodimeric $bLmrCD_{AviC}$ were used for the DARPin selections and ELISA (red bar). The strong peak at the void volume of the column (9 ml) besides aggregated LmrCD also contained genomic DNA that escaped from DNaseI treatment (as evidenced by the strong A_{254} signal relative to the A_{280} signal). (C, D), Gel filtration profiles of studied DARPins on Superdex 200 column. The maxima of the main peaks were as follows: (C) α-LmrCD#1:16.84 ml; α-LmrCD#2:15.11 ml; α-LmrCD#3:16.37 ml; LmrCD#4:16.80 ml; α-LmrCD#5:17.01 ml; E3_5:16.89 ml (D) DARPin_Act1:10.32 ml; DARPin_Act2:13.25 ml; DARPin_Act3:16.38 ml. (E, F), SEC profiles of LmrC-GFP and LmrD-GFP (E) as well as of $LmrD\text{-}NBD_{AviN}$ (F). The fractions indicated by the red bar were used for the ELISA shown in Figure 3B.
(TIF)

Figure S2 Sequence alignment of the LmrCD-specific DARPins identified in this study. The sequence of the consensus designed DARPin framework is given in the top line, where "x" stands for all amino acids except proline, glycine and cysteine and "y" stands for histidine, glutamine or tyrosine.
(TIF)

Figure S3 SPR control experiment disfavors a two-state reaction model of DARPin binding to LmrCD. The fits of the SPR sensograms were found to match better using a two-state reaction model instead of a 1:1 binding model (see Materials and Methods). To test whether the two-state reaction model was appropriate for fitting, a saturating concentration of α-LmrCD#3 (400 nM) was injected onto a SPR SA-chip containing 600 RU of immobilized $bLmrCD_{AviC}$ for 100 s, 200 s and 400 s (each injection was performed twice). The traces were superimposed at the starting point of the dissociation curve. DARPin dissociation is virtually identical irrespective of the duration of association time, indicating that the two-state reaction model is not appropriate. Therefore, all SPR data were fitted using a 1:1 binding model (Figure 7C and Table 1).
(TIF)

Table S1 Primers used in this study.
(DOC)

Table S2 Genetic constructs used in this study.
(DOC)

Acknowledgments

We thank Gaby Sennhauser for the introduction into the ribosome display method and Barbara Flückiger and Sibylle Engeler for technical assistance. Daniel Gutmann, Henrietta Venter and all the other former and current members of the Van Veen laboratory are acknowledged for stimulating discussions.

Author Contributions

Conceived and designed the experiments: MAS MGG HWvV. Performed the experiments: MAS AM. Analyzed the data: MAS SS HWvV. Contributed reagents/materials/analysis tools: AM SV MH SS IS. Wrote the paper: MAS HWvV.

References

1. Gutmann DA, Ward A, Urbatsch IL, Chang G, van Veen HW (2010) Understanding polyspecificity of multidrug ABC transporters: closing in on the gaps in ABCB1. Trends Biochem Sci 35: 36–42.
2. Seeger MA, van Veen HW (2009) Molecular basis of multidrug transport by ABC transporters. Biochim Biophys Acta 1794: 725–737.
3. Locher KP (2009) Review. Structure and mechanism of ATP-binding cassette transporters. Philos Trans R Soc Lond B Biol Sci 364: 239–245.
4. Rees DC, Johnson E, Lewinson O (2009) ABC transporters: the power to change. Nat Rev Mol Cell Biol 10: 218–227.
5. Gottesman MM, Ambudkar SV, Xia D (2009) Structure of a multidrug transporter. Nat Biotechnol 27: 546–547.
6. Jones PM, O'Mara ML, George AM (2009) ABC transporters: a riddle wrapped in a mystery inside an enigma. Trends Biochem Sci 34: 520–531.
7. Dawson RJ, Locher KP (2007) Structure of the multidrug ABC transporter Sav1866 from *Staphylococcus aureus* in complex with AMP-PNP. FEBS Lett 581: 935–938.
8. Dawson RJ, Locher KP (2006) Structure of a bacterial multidrug ABC transporter. Nature 443: 180–185.
9. Toyoshima C (2008) Structural aspects of ion pumping by Ca^{2+}-ATPase of sarcoplasmic reticulum. Arch Biochem Biophys 476: 3–11.
10. Oldham ML, Chen J (2011) Snapshots of the maltose transporter during ATP hydrolysis. Proc Natl Acad Sci U S A 108: 15152–15156.
11. Oldham ML, Khare D, Quiocho FA, Davidson AL, Chen J (2007) Crystal structure of a catalytic intermediate of the maltose transporter. Nature 450: 515–521.
12. Binz HK, Amstutz P, Kohl A, Stumpp MT, Briand C, et al. (2004) High-affinity binders selected from designed ankyrin repeat protein libraries. Nat Biotechnol 22: 575–582.
13. Forrer P, Stumpp MT, Binz HK, Plückthun A (2003) A novel strategy to design binding molecules harnessing the modular nature of repeat proteins. FEBS Lett 539: 2–6.
14. Binz HK, Stumpp MT, Forrer P, Amstutz P, Plückthun A (2003) Designing repeat proteins: well-expressed, soluble and stable proteins from combinatorial libraries of consensus ankyrin repeat proteins. J Mol Biol 332: 489–503.
15. Merz T, Wetzel SK, Firbank S, Plückthun A, Grütter MG, et al. (2008) Stabilizing ionic interactions in a full-consensus ankyrin repeat protein. J Mol Biol 376: 232–240.
16. Boersma YL, Chao G, Steiner D, Wittrup KD, Plückthun A (2011) Bispecific designed ankyrin repeat proteins (DARPins) targeting the epidermal growth factor receptor inhibit A431 cell proliferation and receptor recycling. J Biol Chem 286: 41273–41285.
17. Stefan N, Martin-Killias P, Wyss-Stoeckle S, Honegger A, Zangemeister-Wittke U, et al. (2011) DARPins Recognizing the Tumor-Associated Antigen EpCAM Selected by Phage and Ribosome Display and Engineered for Multivalency. J Mol Biol 413: 826–843.
18. Sennhauser G, Amstutz P, Briand C, Storchenegger O, Grütter MG (2006) Drug Export Pathway of Multidrug Exporter AcrB Revealed by DARPin Inhibitors. PLoS Biol 5: e7.
19. Monroe N, Sennhauser G, Seeger MA, Briand C, Grütter MG (2011) Designed ankyrin repeat protein binders for the crystallization of AcrB: plasticity of the dominant interface. J Struct Biol 174: 269–281.
20. Kohler G, Milstein C (1975) Continuous cultures of fused cells secreting antibody of predefined specificity. Nature 256: 495–497.
21. Ball WJ, Jr. (1986) Uncoupling of ATP binding to Na^+,K^+-ATPase from its stimulation of ouabain binding: studies of the inhibition of Na^+,K^+-ATPase by a monoclonal antibody. Biochemistry 25: 7155–7162.
22. Mechetner EB, Roninson IB (1992) Efficient inhibition of P-glycoprotein-mediated multidrug resistance with a monoclonal antibody. Proc Natl Acad Sci U S A 89: 5824–5828.
23. Hamada H, Tsuruo T (1986) Functional role for the 170- to 180-kDa glycoprotein specific to drug-resistant tumor cells as revealed by monoclonal antibodies. Proc Natl Acad Sci U S A 83: 7785–7789.
24. Debiec H, Ronco PM (1993) Identification and epitope analysis of the renal Na^+/Pi cotransport protein using monoclonal antibodies. J Biol Chem 268: 13356–13363.
25. Padan E, Venturi M, Michel H, Hunte C (1998) Production and characterization of monoclonal antibodies directed against native epitopes of NhaA, the Na^+/H^+ antiporter of *Escherichia coli*. FEBS Lett 441: 53–58.
26. Hunte C, Michel H (2002) Crystallisation of membrane proteins mediated by antibody fragments. Curr Opin Struct Biol 12: 503–508.
27. Clackson T, Hoogenboom HR, Griffiths AD, Winter G (1991) Making antibody fragments using phage display libraries. Nature 352: 624–628.
28. Hanes J, Plückthun A (1997) *In vitro* selection and evolution of functional proteins by using ribosome display. Proc Natl Acad Sci U S A 94: 4937–4942.
29. Rubinstein JL, Holt LJ, Walker JE, Tomlinson IM (2003) Use of phage display and high-density screening for the isolation of an antibody against the 51-kDa subunit of complex I. Anal Biochem 314: 294–300.
30. Rothlisberger D, Pos KM, Plückthun A (2004) An antibody library for stabilizing and crystallizing membrane proteins - selecting binders to the citrate carrier CitS. FEBS Lett 564: 340–348.
31. Huber T, Steiner D, Rothlisberger D, Plückthun A (2007) *In vitro* selection and characterization of DARPins and Fab fragments for the co-crystallization of membrane proteins: The Na^+-citrate symporter CitS as an example. J Struct Biol.
32. Esteban O, Bernal RA, Donohoe M, Videler H, Sharon M, et al. (2008) Stoichiometry and localization of the stator subunits E and G in *Thermus thermophilus* H^+-ATPase/synthase. J Biol Chem 283: 2595–2603.
33. Uysal S, Vasquez V, Tereshko V, Esaki K, Fellouse FA, et al. (2009) Crystal structure of full-length KcsA in its closed conformation. Proc Natl Acad Sci U S A 106: 6644–6649.
34. Milovnik P, Ferrari D, Sarkar CA, Plückthun A (2009) Selection and characterization of DARPins specific for the neurotensin receptor 1. Protein Eng Des Sel 22: 357–366.
35. Hotzel I, Chiang V, Diao J, Pantua H, Maun HR, et al. (2011) Efficient production of antibodies against a mammalian integral membrane protein by phage display. Protein Eng Des Sel 24: 679–689.
36. Kim J, Stroud RM, Craik CS (2011) Rapid identification of recombinant Fabs that bind to membrane proteins. Methods.
37. Szakacs G, Paterson JK, Ludwig JA, Booth-Genthe C, Gottesman MM (2006) Targeting multidrug resistance in cancer. Nat Rev Drug Discov 5: 219–234.
38. Pajic M, Iyer JK, Kersbergen A, van der Burg E, Nygren AO, et al. (2009) Moderate increase in Mdr1a/1b expression causes *in vivo* resistance to doxorubicin in a mouse model for hereditary breast cancer. Cancer Res 69: 6396–6404.
39. Doerrler WT, Reedy MC, Raetz CR (2001) An *Escherichia coli* mutant defective in lipid export. J Biol Chem 276: 11461–11464.
40. Lubelski J, Mazurkiewicz P, van Merkerk R, Konings WN, Driessen AJ (2004) ydaG and ydbA of *Lactococcus lactis* encode a heterodimeric ATP-binding cassette-type multidrug transporter. J Biol Chem 279: 34449–34455.
41. Reuter G, Janvilisri T, Venter H, Shahi S, Balakrishnan L, et al. (2003) The ATP binding cassette multidrug transporter LmrA and lipid transporter MsbA have overlapping substrate specificities. J Biol Chem 278: 35193–35198.
42. Velamakanni S, Lau CH, Gutmann DA, Venter H, Barrera NP, et al. (2009) A multidrug ABC transporter with a taste for salt. PLoS One 4: e6137.
43. Venter H, Shilling RA, Velamakanni S, Balakrishnan L, Van Veen HW (2003) An ABC transporter with a secondary-active multidrug translocator domain. Nature 426: 866–870.
44. Woebking B, Reuter G, Shilling RA, Velamakanni S, Shahi S, et al. (2005) Drug-lipid A interactions on the *Escherichia coli* ABC transporter MsbA. J Bacteriol 187: 6363–6369.
45. Woebking B, Velamakanni S, Federici L, Seeger MA, Murakami S, et al. (2008) Functional role of transmembrane helix 6 in drug binding and transport by the ABC transporter MsbA. Biochemistry 47: 10904–10914.
46. Hopfner KP, Karcher A, Shin DS, Craig L, Arthur LM, et al. (2000) Structural biology of Rad50 ATPase: ATP-driven conformational control in DNA double-strand break repair and the ABC-ATPase superfamily. Cell 101: 789–800.
47. Lubelski J, van Merkerk R, Konings WN, Driessen AJ (2006) Nucleotide-binding sites of the heterodimeric LmrCD ABC-multidrug transporter of *Lactococcus lactis* are asymmetric. Biochemistry 45: 648–656.
48. Leppert G, McDevitt R, Falco SC, Van Dyk TK, Ficke MB, et al. (1990) Cloning by gene amplification of two loci conferring multiple drug resistance in *Saccharomyces*. Genetics 125: 13–20.
49. Powis SJ, Townsend AR, Deverson EV, Bastin J, Butcher GW, et al. (1991) Restoration of antigen presentation to the mutant cell line RMA-S by an MHC-linked transporter. Nature 354: 528–531.
50. Barrera NP, Isaacson SC, Zhou M, Bavro VN, Welch A, et al. (2009) Mass spectrometry of membrane transporters reveals subunit stoichiometry and interactions. Nat Methods 6: 585–587.
51. Cull MG, Schatz PJ (2000) Biotinylation of proteins *in vivo* and *in vitro* using small peptide tags. Methods Enzymol 326: 430–440.
52. Galian C, Manon F, Dezi M, Torres C, Ebel C, et al. (2011) Optimized purification of a heterodimeric ABC transporter in a highly stable form amenable to 2-D crystallization. PLoS One 6: e19677.

53. Lubelski J, de Jong A, van Merkerk R, Agustiandari H, Kuipers OP, et al. (2006) LmrCD is a major multidrug resistance transporter in *Lactococcus lactis*. Mol Microbiol 61: 771–781.
54. de Ruyter PG, Kuipers OP, de Vos WM (1996) Controlled gene expression systems for *Lactococcus lactis* with the food-grade inducer nisin. Appl Environ Microbiol 62: 3662–3667.
55. Venter H, Velamakanni S, Balakrishnan L, van Veen HW (2008) On the energy-dependence of Hoechst 33342 transport by the ABC transporter LmrA. Biochem Pharmacol 75: 866–874.
56. Bolhuis H, van Veen HW, Molenaar D, Poolman B, Driessen AJ, et al. (1996) Multidrug resistance in *Lactococcus lactis*: evidence for ATP-dependent drug extrusion from the inner leaflet of the cytoplasmic membrane. EMBO J 15: 4239–4245.
57. Hollo Z, Homolya L, Davis CW, Sarkadi B (1994) Calcein accumulation as a fluorometric functional assay of the multidrug transporter. Biochim Biophys Acta 1191: 384–388.
58. Homolya L, Hollo Z, Germann UA, Pastan I, Gottesman MM, et al. (1993) Fluorescent cellular indicators are extruded by the multidrug resistance protein. J Biol Chem 268: 21493–21496.
59. Schuck P, Zhao H (2010) The role of mass transport limitation and surface heterogeneity in the biophysical characterization of macromolecular binding processes by SPR biosensing. Methods in molecular biology 627: 15–54.
60. Kaback HR (1971) Bacterial Membranes. Methods Enzymol 22: 99–120.
61. Zimmerman SB, Trach SO (1991) Estimation of macromolecule concentrations and excluded volume effects for the cytoplasm of *Escherichia coli*. J Mol Biol 222: 599–620.
62. Davidson AL, Laghaeian SS, Mannering DE (1996) The maltose transport system of *Escherichia coli* displays positive cooperativity in ATP hydrolysis. J Biol Chem 271: 4858–4863.
63. Zaitseva J, Jenewein S, Wiedenmann A, Benabdelhak H, Holland IB, et al. (2005) Functional characterization and ATP-induced dimerization of the isolated ABC-domain of the haemolysin B transporter. Biochemistry 44: 9680–9690.
64. Sennhauser G, Grütter MG (2008) Chaperone-assisted crystallography with DARPins. Structure 16: 1443–1453.
65. Kondratov RV, Komarov PG, Becker Y, Ewenson A, Gudkov AV (2001) Small molecules that dramatically alter multidrug resistance phenotype by modulating the substrate specificity of P-glycoprotein. Proc Natl Acad Sci U S A 98: 14078–14083.
66. Agustiandari H, Lubelski J, van den Berg van Saparoea HB, Kuipers OP, Driessen AJ (2008) LmrR is a transcriptional repressor of expression of the multidrug ABC transporter LmrCD in *Lactococcus lactis*. J Bacteriol 190: 759–763.
67. Ernst R, Kueppers P, Klein CM, Schwarzmueller T, Kuchler K, et al. (2008) A mutation of the H-loop selectively affects rhodamine transport by the yeast multidrug ABC transporter Pdr5. Proc Natl Acad Sci U S A 105: 5069–5074.
68. Wegmann U, O'Connell-Motherway M, Zomer A, Buist G, Shearman C, et al. (2007) Complete genome sequence of the prototype lactic acid bacterium *Lactococcus lactis* subsp. *cremoris* MG1363. J Bacteriol 189: 3256–3270.
69. Guzman LM, Belin D, Carson MJ, Beckwith J (1995) Tight regulation, modulation, and high-level expression by vectors containing the arabinose P_{BAD} promoter. J Bacteriol 177: 4121–4130.
70. Geertsma ER, Dutzler R (2011) A versatile and efficient high-throughput cloning tool for structural biology. Biochemistry 50: 3272–3278.
71. Balakrishnan L, Venter H, Shilling RA, van Veen HW (2004) Reversible transport by the ATP-binding cassette multidrug export pump LmrA: ATP synthesis at the expense of downhill ethidium uptake. J Biol Chem 279: 11273–11280.
72. Zahnd C, Amstutz P, Plückthun A (2007) Ribosome display: selecting and evolving proteins *in vitro* that specifically bind to a target. Nat Methods 4: 269–279.
73. Leenhouts KJ, Kok J, Venema G (1991) Replacement recombination in *Lactococcus lactis*. J Bacteriol 173: 4794–4798.
74. Venter H, Shahi S, Balakrishnan L, Velamakanni S, Bapna A, et al. (2005) Similarities between ATP-dependent and ion-coupled multidrug transporters. Biochem Soc Trans 33: 1008–1011.
75. Schagger H, von Jagow G (1987) Tricine-sodium dodecyl sulfate-polyacrylamide gel electrophoresis for the separation of proteins in the range from 1 to 100 kDa. Anal Biochem 166: 368–379.
76. Rigaud JL, Pitard B, Levy D (1995) Reconstitution of membrane proteins into liposomes: application to energy-transducing membrane proteins. Biochim Biophys Acta 1231: 223–246.

APPENDIX

A1. CHAPTER F

Expression, purification and DARPin selection against the bacterial ABC exporters LmrA & YDDA

F.1 Introduction

Multidrug resistance (MDR) is observed in medical treatment, where cells become resistant to the structurally distinct and relatively lipophilic drugs. MDR is frequently a manifestation of overexpression of active transporters which vectorially pump a variety of drug molecules across the lipid membrane. P-glycoprotein is one of the best studied ABC transporters and is associated with increased efflux of drugs in cancer cells[1,2]. P-glycoprotein and its bacterial homologs MsbA (from Gram-negative *E.coli*) and LmrA (from Gram-positive *Lactococcus lactis*)[3] were shown to be polyspecific drug pumps[4]. There is a plethora of biochemical information available for ABC exporters but detailed structural information is limited, despite the reported crystal structures of Sav1866 (PDB ID 2HYD), 3 closely homologues of MsbA (PDB ID 3B60, 3B5W and 3B5X), P-glycoprotein (PDB ID 3G5U), and TM287/288 (PDB ID 3QF4). In order to describe a detailed transport mechanism, a transport protein needs to be crystallized in multiple conformations. No single homolog of any ABC exporter has yet been crystallized in multiple conformations which would describe the distinct states of the transport cycle. This demonstrates the difficulty to crystallize membrane transporters in different conformations.

In addition, factors such as poor over-expression, conformational heterogeneity and the amphipathic nature hamper membrane protein crystallography. In the past, crystallization chaperones have been used to overcome the conformational heterogeneity and to extend the hydrophilic surface area[5-7]. This can facilitate the crystallization of proteins difficult to crystallize. Crystallization chaperones such as DARPin have also been successfully used to crystallize proteins in novel conformations. This has been demonstrated for the multidrug transporter AcrB, which was co-crystallized with a DARPin in an asymmetric conformation (PDB ID 2J8S)[8].

In this chapter the use of DARPins for the co-crystallization of ABC transporter as an alternative to antibody fragments was explored. LmrA, the first bacterial ABC multidrug transporter from *Lactococcus lactis*[9] was chosen as candidate to select DARPins against and to use these DARPins as chaperones to crystallize LmrA. LmrA is a homodimer ABC exporter[9]. One monomer consists of 590 amino-acids forming a hydrophobic domain with 6 transmembrane helices and a hydrophilic ATP-binding cassette domain. Since, LmrA is a prokaryotic homolog of MDR proteins such as P-glycoprotein, structure determination of these proteins facilitated by a specific DARPin would be a significant contribution towards understanding the function of clinically relevant transporters.

The second homodimeric ABC transporter chosen was YDDA consisting of two polypeptide chains of 64985 Da molecular weight each. The *yddA* gene is identified as a putative gene for an ABC transporter in the *E.coli* genome[10,11]. It is classified as a putative homodimeric exporter (http://www.uniprot.org/uniprot/P31826) of unknown function.

F.2 Results

F.2.1 Biochemical characterization of LmrA (ATPase activity)

Detergent solubilized ($C_{12}E_8$) LmrA was purified by IMAC. The homogeneity and the purity of the purified protein were analyzed by size-exclusion chromatography (SEC) and SDS-PAGE. LmrA eluted as homogeneous dimer in SEC (Figure_F1). The ATPase activity of detergent purified LmrA was performed using the method described in experimental procedure (F.4.2). Detergent purified LmrA is functional, as it exhibited basal ATPase activity (Figure_F1C).

F.2.2 Characterization of DARPins specific for LmrA

Selection and screening of DARPins against LmrA was performed by Dr. Markus Seeger. The N2C DARPin library was used for DARPins selection by ribosome display. LmrA and LmrA-specific binders were expressed and purified by IMAC. Purified LmrA and selected DARPins were mixed at a ratio of 1:3 and were incubated for 15 minutes at 4°C. The LmrA-DARPin complexes were separated from the excess DARPin by SEC. The fractions containing the LmrA-DARPin complex were analyzed by SDS-PAGE (Figure_F2B). All DARPins were found to form a complex with LmrA. The SDS-PAGE analysis suggested that DARPins H2, F3 and G6 seem to be forming a sub-stoichiometric complex with LmrA, because the bands of the DARPins appeared relatively weak on coomassie-stained gel (Figure_F2B). A quantitative

analysis to analyze the stoichiometry for different LmrA-DARPin complexes was not performed.

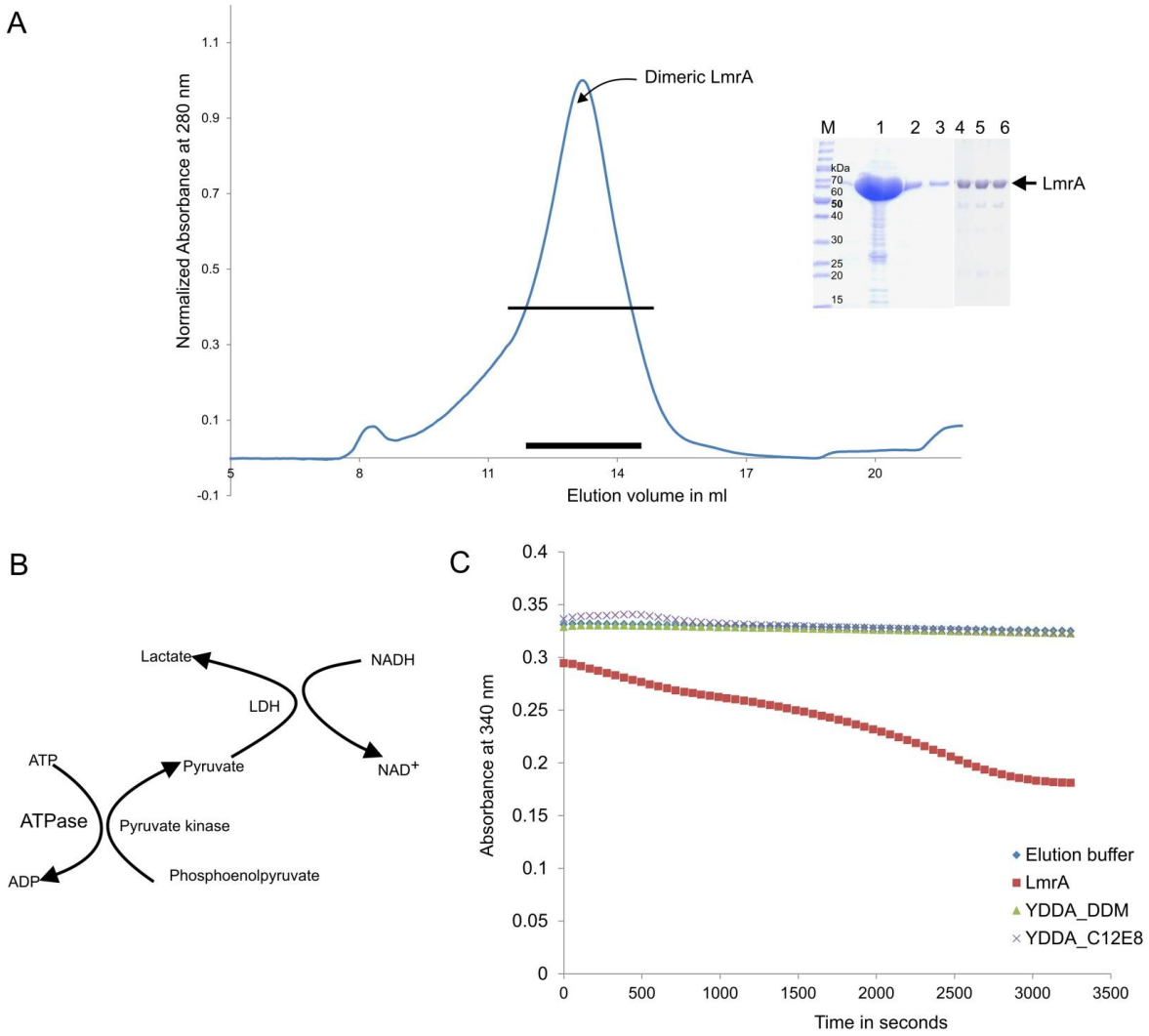

Figure_F1: (A) Size-exclusion chromatography and SDS-PAGE analysis of LmrA. IMAC purified LmrA fractions (lane 1 to 3) were concentrated and analyzed by SEC. The fractions corresponding to the peak region were analyzed by SDS-PAGE (Lane 4-6). **(B,C) ATPase activity assay.** Detergent purified LmrA showed basal ATPase activity (red line), while YDDA did not show basal ATPase activity in either detergent (β–DDM and $C_{12}E_8$). The amount of phosphate released from ATP hydrolysis can be measured by following the decrease in NADH concentration in the coupled enzymatic assay illustrated in Figure B.

F.2.3 Crystallization of LmrA alone and the LmrA-DARPin complexes

IMAC purified LmrA was purified by SEC and LmrA-DARPin complex was formed as described above. LmrA and the LmrA-DARPin complex were concentrated to 10-18 mg/ml and used for crystallization in 1:1, 1:2 and 1:3 ratios of protein and mother liquor respectively. Mackinnon screens (GS020-GS025) from the NCCR structural Biology platform were used to set up crystallization plates. We used different nucleotides (ATP and ADP) and their non-

hydrolyzing analogs (AMP-PNP, ADP-VO_4^{-3}) as ligand, which might have increased the homogeneity of the purified protein. Crystallization efforts for LmrA alone and in complex with DARPins did not yield any suitable condition for crystal growth.

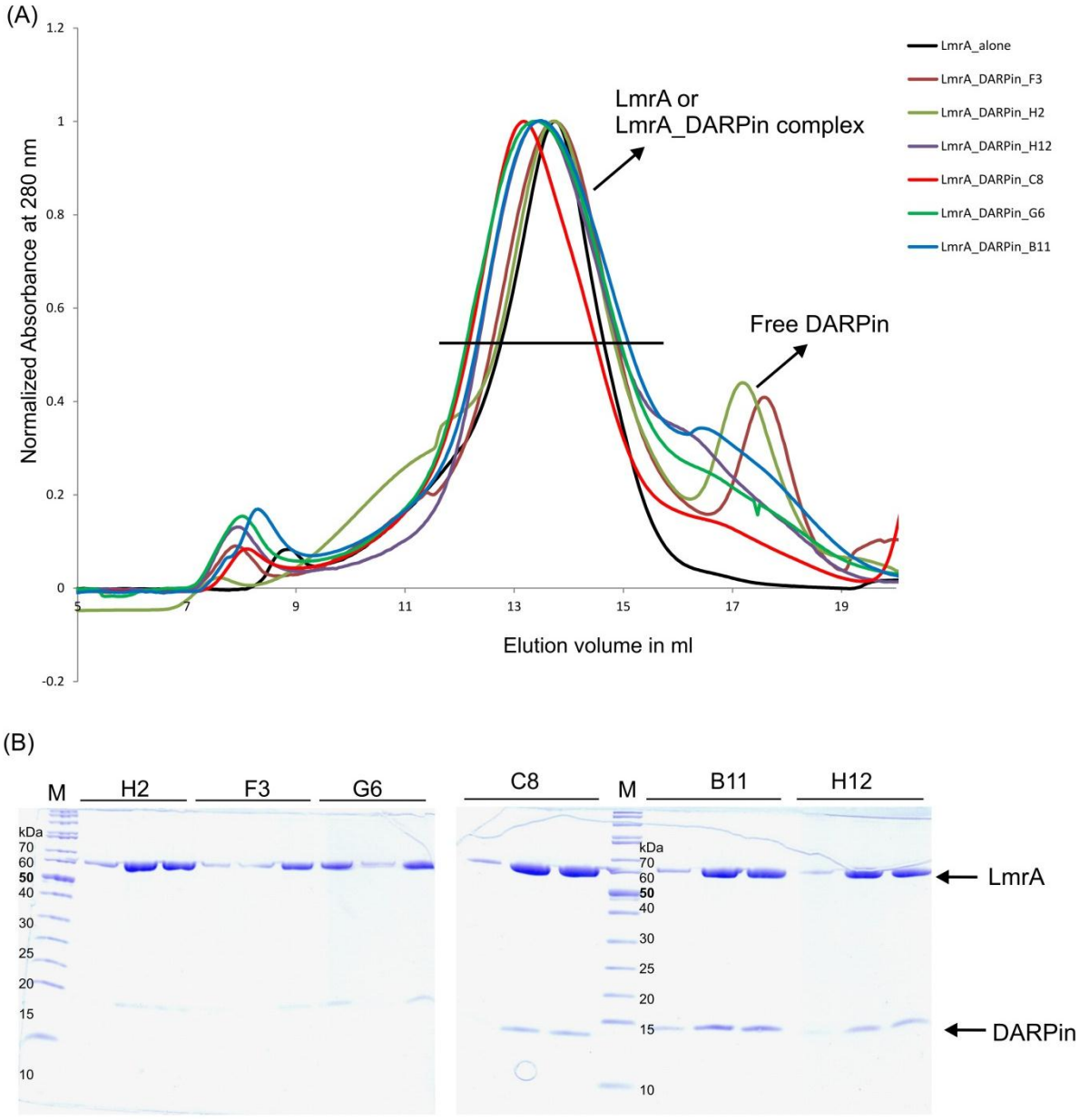

Figure_F2: (A) Size-exclusion chromatography and SDS-PAGE analysis of LmrA-DARPin complexes. The LmrA-DARPin complexes were seperated from the excess of DARPin by SEC. **(B)** SDS-PAGE analysis of corresponding peak fractions of LmrA-DARPin complexes eluted by SEC.

F.2.4 Biochemical characterization of YDDA (ATPase assay)

Detergent (β-DDM) solubilized YDDA was purified by IMAC. The homogeneity and purity of purified protein was analyzed by SEC and SDS-PAGE, respectively. YDDA eluted as homodimeric and homogenous protein in SEC. Detergent purified YDDA showed no basal ATPase activity (Figure_F1C).

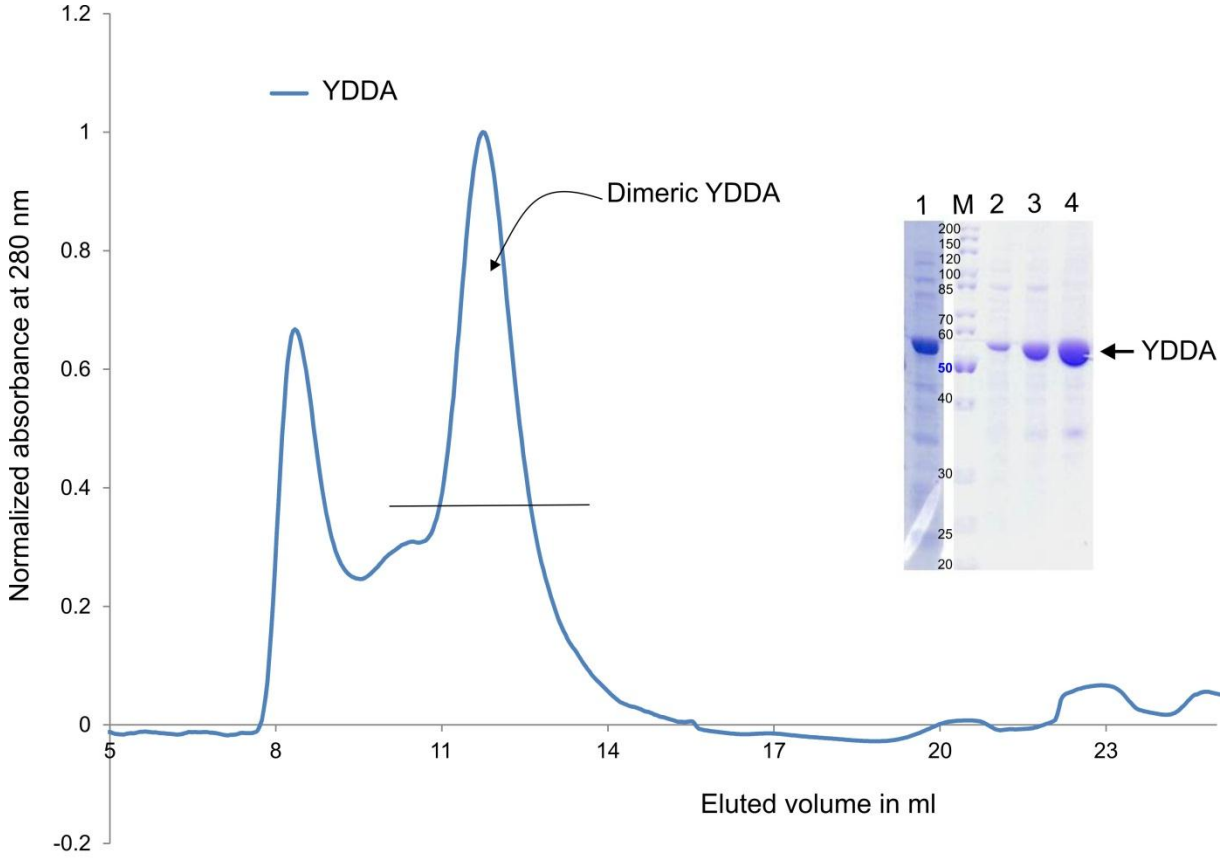

Figure_F3 Size-exclusion chromatography and SDS-PAGE analysis of YDDA. IMAC purified YDDA fractions (lane 1) were concentrated and analyzed by size-exclusion chromatography for homogeneity. Dimeric YDDA fractions were analyzed by SDS-PAGE for purity (lane 2-4).

F.2.5 Screening of YDDA specific DARPins

DARPin selection against YDDA was performed by Christian Spoerri using a N3C DARPin library. The enriched pool of DARPins after the third round of RD was subcloned into the expression vector pQE30. About 200 DARPin clones were analyzed for binding to bYDDA$_{AviC}$ by crude extract ELISA. Maltose binding protein was used as a negative control in crude extract ELISA. 9 specific binders for YDDA were found (Figure_F4).

F.2.6 Analysis of the YDDA-DARPin complex formation

Sequencing of the 9 YDDA-specific DARPins revealed that they were unique and therefore were used for further experiments (Figure_F5). 6 binders were overexpressed and purified by Ni^{+2}-NTA chromatography. IMAC purified DARPin and YDDA were mixed at a 3:1 ratio, and incubated for 15 minutes at 4°C. The YDDA-DARPin complex was separated from the excess DARPin by SEC. SDS-PAGE analysis indicated complex formation for all selected DARPins with YDDA (Figure_F6).

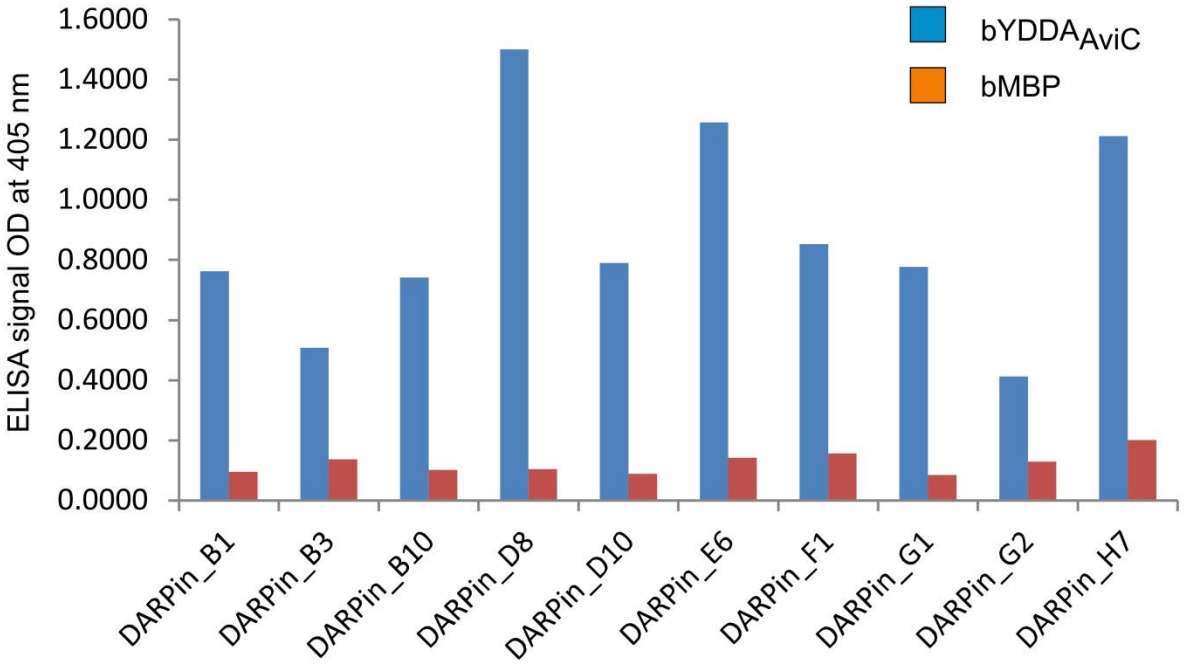

Figure_F4: Screening of YDDA specific DARPins by ELISA. Biotinylated MBP (bMBP) was used as a control.

```
N3C_template    MRGSHHHHHHGSDLGKKLLEAARAGQDDEVRILMANGADVNAXDXXGXTPLHLAAXXGHL
DARPin_B3       MRGSHHHHHHGSDLGKKLLEAARAGQDDEVRILMANGADVNARDNDGDTPLHLAAWHGHL
DARPin_B10      MRGSHHHHHHGSDLGKKLLEAARAGQGDEVRILMANGVDVNATDMNGTTPLHLAAWNGHL
DARPin_D8       MRGSHHHHHHGSDLGKKLLEAARAGQDDEVHILMANGADVNAQDRIGVTPLHLAAYNGHL
DARPin_D10      MRGSHHHHHHGSDLGKKLLEAARAGQDDEVRILMANGADVNASDYHGTTPLHLAAWEGHL
DARPin_E6       MRGSHHHHHHGSDLGKKLLEAARAGEDDEVRILMTNGADVNAYDXEGVTPLHLAAWDGHL
DARPin_G1       MRGSHHHHHHGSDLGKKLLEAARVGQDDEVRILMANGADVNAMDTQGITPLHLTAWYGHL
DARPin_G2       MRGSHHHHHHGSDLGKKLLEVARAGQDDEVRILMANGADVNARDRFGSTPLHLAAWDGHL

N3C_template    EIVEVLLKXGADVNAXDXXGXTPLHLAAXXGHLEIVEVLLKXGADVNAXDXXGXTPLHLA
DARPin_B3       EIVEVLLKNGADVNAEDATGLTPLHLAAYKGHLEIVEVLLKYGADVNATDDHGSTPLHLA
DARPin_B10      EIVEVLLKYGADVNADDWTGLTPLHLAAYLGHLEIVEVLLKYGADVNAKDDKGSTPLHLA
DARPin_D8       EIVEVLLKNGADVNAFDDYGITPLHLAAFV-HLEIVEVLLKHGADVNANDKNGTTPLHLT
DARPin_D10      EIVEVLLKHGADVNADDDHXLTPLHLAAYYGHLEIVEVLLKYGADVNAYDDHGSTPLHLA
DARPin_E6       EIVEVLLKXGADVNADDWTGLTPLHLAAYLGHLEIVEVLLKNGADVNADDVHGSTPLHLA
DARPin_G1       EIVEVLLKHGADVNAADKNGFTPLHLAANRGHLEIVEVLLKYGADVNAFDSLGSTPLHLA
DARPin_G2       EIVEVLLKYGADVNAEDKSGITPLHLAAYRGHLEIVEVLLKHGADVNASDLNGSTPLHLA

N3C_template    AXXGHLEIVEVLLKXGADVNAQDKFGKTAFDISIDNGNEDLAEILQKLN
DARPin_B3       ARIGHLEIVEVLLKNSADVSAQDKFGKTAFDISIDNGNEDLAEILQKLN
DARPin_B10      AIRGHLEIVEVLLKYGADVNAQDKFGKTAFDISIDNGNEDLAEILQKLN
DARPin_D8       AKDGHLEIVEVLLKYGADVNAQDKFGKTAFDISIDNGNEDLAEILQKLN
DARPin_D10      AKDGHLEIVKVLLKYGADVNAQDKFGKTAFDISIDNGNEDLAEILQKLN
DARPin_E6       AYRGHLEIVEVLLKNGADVNAQDKFGKTAFDISIDNGNEDLAEILQKLN
DARPin_G1       AIEGHPEIVEVLLKHGADVNAQDKFGKTAFDISIDNGNEDLAEILQKLN
DARPin_G2       ARTGHLEIVEVLLKYGADVNAQDKFGKTAFDISIDNGNEDLAEILQKLN
```

Figure_F5: Multiple sequence alignment of YDDA specific DARPins. N3C_template shows randomized positions of a N3C DARPin by **X**. The multiple alignment shows the diversity among the selected YDDA specific DARPins. The multiple alignment was created with ClustalW2. The names of the clones are given on the left side of the respective sequence.

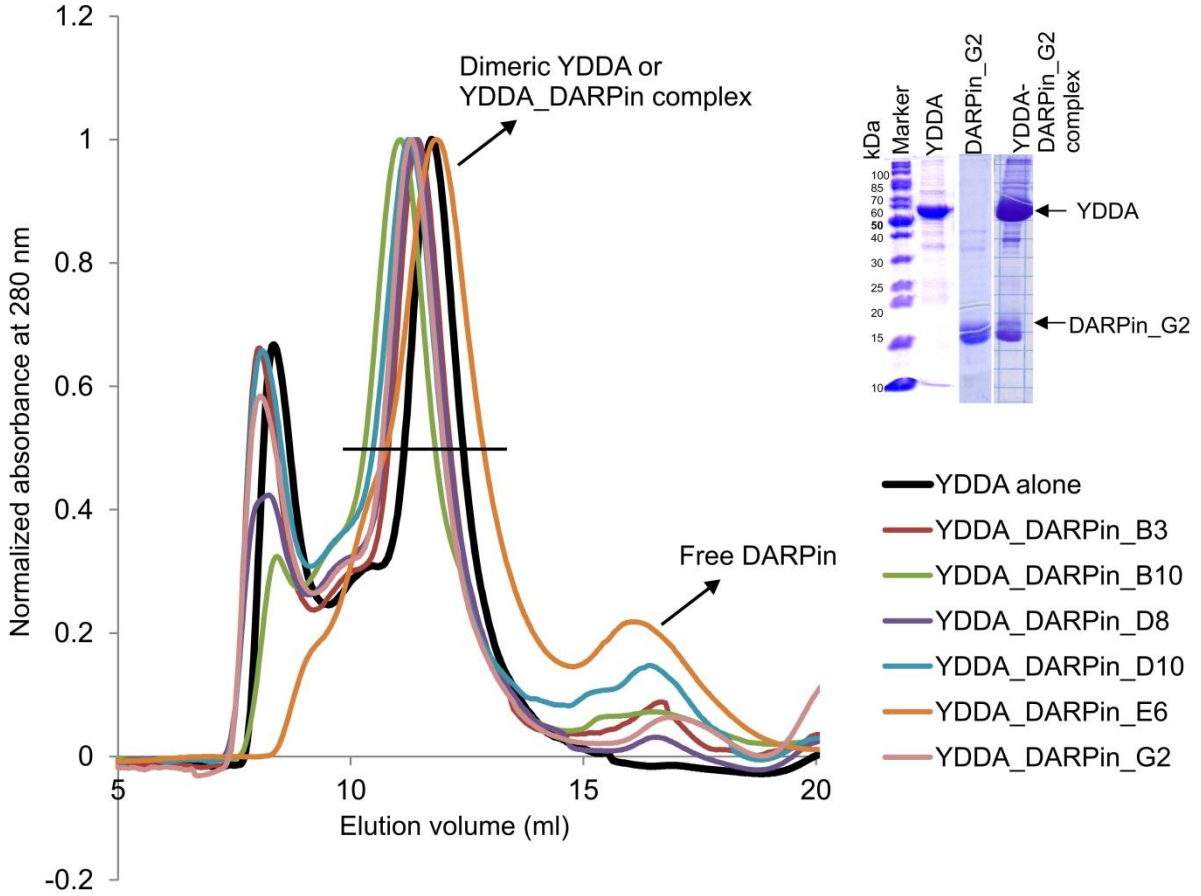

Figure_F6: Size-exclusion chromatography analysis of YDDA-DARPin complex formation. IMAC purified DARPin and YDDA were mixed at a 3:1 ratio. The YDDA-DARPin complex was separated from the excess free DARPins by SEC. The SDS-PAGE analysis of the corresponding peak fractions is shown on the inset. For clarity, SDS-PAGE analysis of the YDDA-DARPin_G2 complex is shown on the inset.

Further, IMAC purified DARPins were analyzed by SEC for homogeneity. All preparations contained higher oligomeric forms of DARPin besides the monomeric form. In order to rule out the possibility that DARPins co-elute with YDDA due to the occurrence of higher oligomeric states, YDDA and DARPins were gel-filtrated individually before complex formation. To this end, equal volume (500 µl) of homogenous fractions of DARPin (monomeric) and YDDA (Dimeric) were mixed. An additional concentration step was omitted to avoid the formation of DARPin oligomers. The mixture (1 ml) was separated by SEC and the fractions corresponding to the YDDA-DARPin complex were analyzed by SDS-PAGE (Figure_F7). In contrast to the initial analysis, it was later found that monomeric DARPins purified by SEC do not elute in complex with YDDA. This suggested that: i) soluble aggregates of DARPins interact unspecifically with YDDA and therefore elute as a pseudo-complex, and/or ii) soluble aggregates of DARPin co-elute with YDDA in SEC.

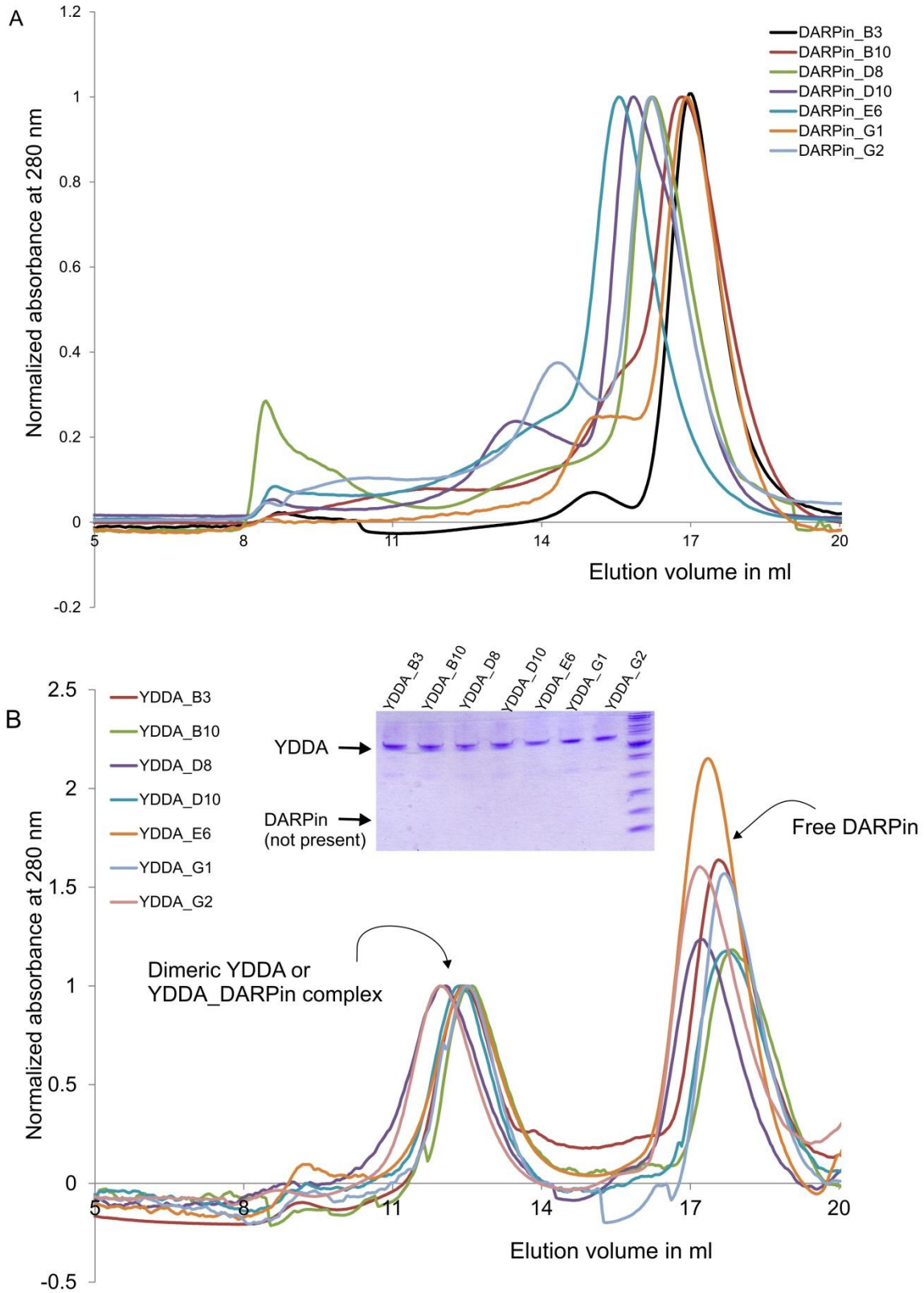

Figure_F7: SEC analysis of DARPins and YDDA-DARPin complex formation (A) IMAC purified DARPins were concentrated, analyzed by SEC and fractions containing monomeric DARPins were collected for complex formation with YDDA. **(B)** Equal volume (500 µl each) of monomeric DARPin and YDDA were mixed and incubated. The YDDA-DARPin complex was seperated from the excess DARPin by SEC. SDS-PAGE analysis of the corresponding fractions shows that none of the selected DARPins co-eluted with YDDA in SEC.

It has to be noted here that these experiments were performed prior to the work on MsbA described in the Chapter B and C. based on our experience with YDDA, an additional step of gel-filtration of IMAC purified DARPin was routinely included to remove soluble aggregates of DARPin, prior to complex formation with the target protein.

F.3 Discussion

This chapter describes the first attempts of DARPin assisted crystallography of membrane proteins in this thesis. The lessons learned here are discussed below and helped to improve the selection and screening procedures of binders against MsbA and LmrCD (Chapters B, C and E).

Two ABC transporter proteins namely LmrA and YDDA were successfully expressed and purified. LmrA is the first multidrug transporter protein found in Gram positive bacteria, while YDDA is from Gram-negative bacteria and its function is unknown. LmrA and YDDA could be purified as dimeric and homogenous proteins in detergents $C_{12}E_8$ and β-DDM, respectively. Detergent purified LmrA exhibited basal ATPase activity, while YDDA did not show basal ATPase activity. Addition of a substrate might be required to stimulate the ATPase activity of YDDA. Subsequently, we selected specific DARPin binders against the two detergent solubilized ABC transporters LmrA and YDDA. LmrA-specific DARPins were used for co-crystallization experiments (Figure_F2A). Despite serious efforts, all crystallization attempts were unsuccessful. No suitable condition was found from where LmrA alone or the LmrA-DARPin complex would crystallize.

N2C DARPin binders were initially used to co-crystallize LmrA. Therefore, N3C rather than N2C DARPins for binder selections against YDDA were chosen because it was reasoned that their bigger size could better facilitate crystal contacts[6,8]. Complex formation between purified YDDA and DARPin was analyzed by gel-filtration. In an initial set of experiments, ELISA-positive binders were used directly after IMAC for complex formation with YDDA. In these experiments, it was found that all DARPin eluted in complex with YDDA as analyzed by size-exclusion chromatography. However, a careful examination of the oligomeric state of DARPin binders raised the concern, that most of them were forming soluble aggregates (Figure_F7A), and thus the elution fractions of these oligomers coincide with the elution of YDDA. To test this hypothesis, we mixed YDDA with freshly gel- filtrated monomeric DARPin and avoided any further concentration of the YDDA-DARPin mixture.

SDS-PAGE analysis of the complex eluted by SEC showed that the DARPins did not elute in complex with YDDA (Figure_F7B). This analysis suggested that the higher oligomers of DARPin were responsible for the presumed protein-complex obtained earlier. Only a stoichiometry analysis of the target protein-DARPin complex can reveal either a sub-stoichiometric complex (suggesting low affinity between the target protein and the binder) or a higher-stoichiometry (implying that the binder might be forming soluble aggregates). For YDDA, a number of rather weak binders have been obtained that give an ELISA signal but do not co-elute in complex with YDDA in SEC. The reason for the accumulation of unspecific DARPin could be due to: (i) surface panning in ribosome display, where a target protein is immobilized on a solid surface. Besides certain advantages of surface panning (requires smaller amounts of target protein), it has several disadvantages: a part of the protein surface is always masked during immobilization and unspecific DARPin binding to the microtiter plate surface has also been observed[12]. An alternative method is to use solution panning, where a biotinylated target protein is first mixed with binder library in solution and protein complexes are captured using streptavidin coated magnetic beads. Solution panning was successfully used for DARPin selection against MsbA, described in Chapter C.2.2, and (ii) ELISA format used in screening of YDDA specific binders. The ELISA format used involves target protein immobilization on a solid surface via Neutravidin-biotin interaction, upon which the three dimensional structures might be compromised during the 8-10 hours long ELISA experiment which involves washing steps and room temperature incubation. An ELISA format where a target protein is added to ELISA experiment at a very late stage is therefore better suited for delicate membrane proteins. Huber et al. have reported an ELISA protocol for successful binder screening for CitS[12], in which the DARPin is immobilized first via myc-tag and biotinylated target protein is added towards the end of the protocol. For the screening of MsbA-specific DARPins, we have used the ELISA set up based on myc-tagged DARPins.

F.4 Experimental procedure

F.4.1 Cloning, expression and purification

F.4.1.1 LmrA

Lactococcus lactis cells transformed with pNZ8048_lmrA[13] were a kind gift of Hendrik van Veen at Cambridge University, Cambridge. *Lactococcus lactis* carrying pNZ8048_lmrA were

grown in M17 media (OXOID CM 0817) at 30°C to an OD_{600} of 0.8. Protein expression was induced with Nisin (40 pg/ml final concentration) for 3–4 h at 30 °C. Harvested cell pellet was resuspended in 20 mM Tris-Cl (pH 7.4), 150 mM NaCl, 25 µg/ml DNaseI and protease inhibitor cocktail (Sigma) and cells were incubated with lysozyme (2mg/ml) for 30 minutes at 30°C. Cells were lysed using EmulsiFlex-C3 (Avestin) cell disrupter. Unbroken cells and cell debris were removed by centrifugation at 8000 rpm (HiCen XL, A8.20 rotor) for 10 min at 4°C and membrane vesicles were then harvested by centrifugation at 45,000 rpm (Ti70, Sorvall ultracentrifuge) for 60 min at 4°C. LmrA was solubilized using 1% $C_{12}E_8$ and 0.1% β-DDM in 1X-TBS from membrane vesicles at 4°C for 90 minutes. The insolubilized membrane fraction was removed by centrifugation at 45,000 rpm for 60 min at 4°C and the cleared lysate was loaded onto a Ni^{2+}-NTA gravity flow column containing 1.5 ml resin (Qiagen). The resin was washed with 30 mM imidazole pH 7.5, 1X-TBS and 0.03 % $C_{12}E_8$ (50 ml), and the protein was eluted in the 1X-TBS, 250 mM imidazole pH 7.5, 10% glycerol and 0.03 % $C_{12}E_8$ (7 ml). All gel-filtration experiments were performed using a Superose 6, 10/300, column (GE Healthcare).

F.4.1.2 YDDA

The *yddA* gene with and without C-terminal Avi tag was cloned in the *E.coli* expression vector pET28-CH by Dr. Daniel Frey in our laboratory[14]. Plasmids harboring the *ydda* gene were transformed into *E.coli* BL-21(DE3) cells and cells were grown in 2YT media at 37°C. Protein production was induced at OD_{600} of 0.7 – 0.8 with 0.2 mM IPTG for 12-14 hours at 18°C. Harvested cell pellets were resuspended in 20 mM Tris/HCl (pH 7.4), 150 mM NaCl, 25 µg/ml DNaseI and protease inhibitor cocktail (Sigma) and cells were lysed using EmulsiFlexC3 (Avestin) cell disrupter. Unbroken cells and cell debris were removed by centrifugation at 8000 rpm (SS34 rotor) for 10 min at 4°C and membrane vesicles were then harvested by centrifugation at 45,000 rpm (Ti70 rotor) for 60 min at 4°C. YDDA was solubilized from membrane vesicles using 1% β-DDM in 50 mM Tris/HCl (pH 7.4), 150 mM NaCl (TBS) at 4°C for 90 minutes. The insolubilized membrane fraction was removed by centrifugation at 45,000 rpm (Ti70 rotor) for 60 min at 4°C and cleared lysate was loaded onto a protino Ni-IDA resin (Macherey-Nagel) gravity flow column containing 1.5 ml resin. The resin was washed with 2.5 mM imidazole pH 7.5, TBS and 0.03 % β-DDM (50 ml) and YDDA was eluted from the column using 150 mM imidazole pH 7.5 (7 ml) in the same buffer. The protein was concentrated in a 100 kDa cutoff concentrator and aggregated material was separated by SEC in 20 mM Tris/HCl (pH 7.5), 150 mM NaCl and 0.03% β-DDM. $YDDA_{AviC}$ was expressed

and purified similarly as described above and purified YDDA was supplemented with 10% glycerol and was snap-frozen in liquid nitrogen and stored at -80°C. All gel-filtration experiments were performed using a Superdex 200, 10/300, column (GE Healthcare column).

F.4.1.3 Designed Ankyrin Repeat Proteins (DARPins)

RD selection using the N2C DARPin library and screening by ELISA against LmrA was done by Dr. Markus Seeger, while the N3C DARPin library was used for selection against YDDA by Christian Spörri.

For YDDA, the DARPins pool from the 3rd selection round was amplified with the primers EWT5 and MTS46. The PCR amplified product was digested using BamHI/HindIII restriction enzyme and ligated into pQE30 (Qiagen) containing an N-terminal RGS-6his tag. Expression and purification of DARPins are described in Chapter C (C.4.2.2).

F.4.2 ATPase assay

The coupled enzyme ATPase assay is based on the conversion of phophoenolpyruvate (PEP) to pyruvate by pyruvate kinase coupled to the conversion of pyruvate to lactate by lactate dehydrogenase (LDH). The latter step requires NADH which is oxidized to NAD^+. NADH, but not NAD^+, absorbs strongly at 340 nm, enabling to calculate the NADH concentration by monitoring the absorbance at 340 nm. The assay was done in buffer 20 mM Tris-Cl (pH 7.4), 150 mM NaCl and 0.03% of β-DDM or 0.05% of $C_{12}E_8$. The final concentration of the reagents used in the assay were NADH (0.3 mM), PEP (4 mM), pyruvate kinase (55 µg/ml), LDH (12 µg/ml), $MgCl_2$ (3.3 mM) and ATP (3.3 mM).

F.7 References

1. Higgins, C.F. ABC transporters: from microorganisms to man. *Annu Rev Cell Biol* **8**, 67-113 (1992).
2. Higgins, C.F. Multiple molecular mechanisms for multidrug resistance transporters. *Nature* **446**, 749-57 (2007).
3. van Veen, H.W. et al. A bacterial antibiotic-resistance gene that complements the human multidrug-resistance P-glycoprotein gene. *Nature* **391**, 291-5 (1998).
4. Reuter, G. et al. The ATP binding cassette multidrug transporter LmrA and lipid transporter MsbA have overlapping substrate specificities. *J Biol Chem* **278**, 35193-8 (2003).
5. Griffin, L. & Lawson, A. Antibody fragments as tools in crystallography. *Clinical & Experimental Immunology* **165**, 285-291 (2011).
6. Sennhauser, G. & Grutter, M.G. Chaperone-assisted crystallography with DARPins. *Structure* **16**, 1443-53 (2008).
7. Ostermeier, C., Iwata, S., Ludwig, B. & Michel, H. Fv fragment-mediated crystallization of the membrane protein bacterial cytochrome c oxidase. *Nat Struct Biol* **2**, 842-6 (1995).
8. Sennhauser, G., Amstutz, P., Briand, C., Storchenegger, O. & Grütter, M.G. Drug Export Pathway of Multidrug Exporter AcrB Revealed by DARPin Inhibitors. *PLoS Biology* **5**, e7 (2007).
9. van Veen, H.W., Margolles, A., Muller, M., Higgins, C.F. & Konings, W.N. The homodimeric ATP-binding cassette transporter LmrA mediates multidrug transport by an alternating two-site (two-cylinder engine) mechanism. *EMBO J* **19**, 2503-14 (2000).
10. Kobayashi, N., Nishino, K. & Yamaguchi, A. Novel macrolide-specific ABC-type efflux transporter in *Escherichia coli*. *J Bacteriol* **183**, 5639-44 (2001).
11. Paulsen, I.T., Sliwinski, M.K. & Saier, M.H., Jr. Microbial genome analyses: global comparisons of transport capabilities based on phylogenies, bioenergetics and substrate specificities. *J Mol Biol* **277**, 573-92 (1998).
12. Huber, T., Steiner, D., Rothlisberger, D. & Pluckthun, A. *In vitro* selection and characterization of DARPins and Fab fragments for the co-crystallization of membrane proteins: The $Na^{(+)}$-citrate symporter CitS as an example. *J Struct Biol* **159**, 206-21 (2007).
13. Margolles, A., Putman, M., van Veen, H.W. & Konings, W.N. The purified and functionally reconstituted multidrug transporter LmrA of *Lactococcus lactis* mediates the transbilayer movement of specific fluorescent phospholipids. *Biochemistry* **38**, 16298-306 (1999).
14. Frey, D. Biochemical and Structural Studies of Dimethylarginine Dimethylaminohydrolase-1, the ABC transporter Superfamily and the Sodium Citrate Transporter CitS. *PhD Thesis submitted to UZH* (2007).

A.2 Abbreviations

3D	three-dimensional
aa	amino acid
ABC	ATP-binidng cassette
AcrB	Acriflavine resistance protein B
AMP-PNP	Adenylyl-imidodiphosphate
ADP/ATP	Adenosine diphosphate/ Adenosine triphosphate
AP	Alkaline phosphatase
$bMsbA_{AviC}$	Biotinylated-$MsbA_{AviC}$
BCECF-AM	2', 7'-bis-(2-carboxyethyl)-5(6)-carboxyfluorescein acetoxymethyl ester
BirA	Biotin ligase enzyme
BSA	Bovine serum albumin
$C_{12}E_8$	Dodecyl octaethylene glycerol ether
CitS	Citrate transporter
DARPin	Designed ankyrin repeat protein
DDM	n-dodecyl-β-D-maltoside
DNA	Deoxyribonucleic acid
DNBD	DARPin for the nucleotide binding domains
DTT	Dithiothreitol
EC	Enzyme commission
E.coli	*Escherichia coli*
EDTA	Ethylenediaminetetraacetic acid
ELISA	Enzyme-linked immunosorbent assay
EPR/ESR	Electron paramagnetic resonance/Electron spin resonance
GPCR	G-protein coupled receptor
HEPES	4-(2-hydroxyethyl)-1-piperazineethanesulfonic acid

IgG	Immunoglobulin G
IC50	Half maximal inhibitory concentration
IMAC	immobilized metal-ion affinity chromatography
ISOVs	Inside-out membrane vesicles
KD	Equilibrium dissociation constant
IPTG	Isopropyl β-D-1-thiogalactopyranoside
LPS	Lipopolysaccharide
M5M	1,5-pentanediyl bismethanethiosulfonate
M11M	3,6,9-trioxaundecane-1,11-diyl bismethanethiosulfonate
MBP	Maltose binding protein
MDR	Multidrug resistance
mRNA	Messenger ribonucleic acid
MTS	Methanethiosulfonate
NAD^+	Nicotinamide adenine dinucleotide
NBD	Nucleotide binding domain
OD	Optical density
PCR	Polymerase chain reaction
P-gp	P-glycoprotein
PDB	Protein data bank
RD	Ribosome display
RSOVs	Right-side-out membrane vesicles
RT	Room temperature
SDS-PAGE	Sodium dodecylsulfate polyacrylamide gel electrophoresis
SPR	Surface plasmon resonance
TBS_{150}	20 mM Tris/HCl (pH 7.4), 150 mM NaCl
TMD	Transmembrane domain

UDM	n-undecyl-β-d-maltopyranoside

A.3 Oligonucleotides

● ***Oligonucleotide for the construction of expression vectors for MsbA_E.coli constructs***

Name of the primer	***Sequence of the primer***
E-Q_For	5'-CTG ATT CTG GAC CAA GCT ACC TCG GC-3'
E-Q_REV	5'-GCC GAG GTA GCT TGG TCC AGA ATC AG-3'
MsbA_D-G_ for	5’-CCT CGG CTC TGG GAA CCG AAT CC-3’
MsbA_D-G_ Rev	5‘-GGA TTC GGT TCC CAG AGC CGA GG-3’
MsbA_PstI_For	5’-AAA ACT GCA GAT GCA TAA CGA CAA AGA TCT CTC TAC-3’
forward_MsbA	5'-ATA TCC ATG GGC CAT CAC CAT CAC CAT CAT CAT CAT CAT CAC AGC-3'
Reverse_MsbA	5' ATA TTC TAG ATT ATT ATT GGC CAA ACT GC-3'

● ***Oligonucleotide for the construction of expression vectors for NBD of MsbA_E.coli constructs***

NBD_MsbA_KpnI	5’-AAA GGT ACC TTG GCC AAA CTG CAT TTT GTG AAG-3’
NBD_MsbA_PstI	5’-AAA CTG CAG ATG CGT GCG ACT GGC GAC GTG GA-3’
NBD_MsbA_XbaI	5’-AAA TCT AGA TTA TTA TTG GCC AAA CTG CAT TTT GTG AAG-3’
NBD 537H_A_F	5’-CTC TGG TGA TTG CCG CCC GCT TGT CTA CCA T-3’
NBD 537H_A_R	5’-ATG GTA GAC AAG CGG GCG GCA ATC ACC AGA G-3’

● ***Oligonucleotide for the construction of expression vectors for TMD of MsbA_E.coli constructs***

MsbAEC_TM_S_KpnI	5’-AAA AGG TAC CCT CCT GCT CAC TGT CCA GAA TG-3’
MsbAEC_TM_L_KpnI	5’-AAA AGG TAC CAT TGC GGA ATT CCA CGT CGC CAG-3’

● ***Oligonucleotide for the construction of expression vectors for MsbA_E.coli constructs used in cross-linking and EPR study***

MsbA25A-C_F	5’-GTG GCC AAC CAT TTG CCC TTT CAA AGC GG-3’
MsbA25A-C_R	5’-CCG CTT TGA AAG GGC AAA TGG TTG GCC AC-3’
MsbA65_F2	5’-GCT CCG TGC TGT GCT GGA TGC CGC T-3’
MsbA65_R2	5’-AGC GGC ATC CAG CAC AGC ACG GAG C-3’
MsbA_71_F	5’-CCG CTG GTG TGC ATC GGG CTG ATG-3’
MsbA_71_R	5’-CAT CAG CCC GAT GCA CAC CAG CGG-3’
MsbA_C88-S_F	5’-GTC TCC AGC TAC AGC ATC TCC TGG GTA-3’
MsbA_C88-S_R	5’-TAC CCA GGA GAT GCT GTA GCT GGA GAC-3’
MsbA R103_C_F2	5’-ACC ATG CGT CGC TGC CTG TTT GGT CAC-3’
MsbA R103_C_R2	5’-GTG ACC AAA CAG GCA GCG ACG CAT GGT-3’

MsbA_173_F 5’-G ATC ATT TTG ATT TGC CTG GCA CCG ATT -3’
MsbA_173_R 5’- C AAT CGG TGC CAG GCA AAT GAT C-3’

MsbA191N-C_F 5’-CGA AGC GTT TTC GCT GCA TCA GTA AAA ACA TG-3’
MsbA191N-C_R 5’-CAT GTT TTT ACT GAT GCA GCG AAA ACG CTT CG-3’

MsbA_261_F 5’-ATC GCC TCT TTG TGC CTG GCG TTT GTT-3’
MsbA_261_R 5’-AAC AAA CGC CAG GCA CAA AGA GGC GAT-3’

MsbA206S-C_F 5’-CAG GTG ACC ACC TGC GCA GAA CAA ATG-3’
MsbA206S-C_R 5’-CAT TTG TTC TGC GCA GGT GGT CAC CTG-3’

MsbA246S-C_F 5’-GGA TGA AAA TGG TTT GCG CCT CTT CCA TCT C-3’
MsbA246S-C_R 5’-GAG ATG GAA GAG GCG CAA ACC ATT TTC ATC C-3’

MSBA_ C315-S_F 5’-GGT ATG GCG GCT AGC CAG ACG CTG TTT-3’
MSBA_ C315-S_R 5’-AAA CAG CGT CTG GCT AGC CGC CAT ACC-3’

MsbA_482_F 5’- GCG TGC TGC TCT GCG GCG GTC AGC G-3’
MsbA_482_R 5’- CGC TGA CCG CCG CAG AGC AGC ACG C-3’

MsbA_A518C_F 5’-C GAA TCC GAA CGT TGC ATT CAG GCG GCA C-3’
MsbA_A518C_R 5’-G TGC CGC CTG AAT GCA ACG TTC GGA TTC G-3’

MsbA L539_C_f2 5’-GAT TGC CCA CCG CTG CTC TAC CAT TGA AA-3’
MsbA L539_C_R2 5’-TTT CAA TGG TAG AGC AGC GGT GGG CAA TC-3’

● ***Oligonucleotide for the construction of expression vectors for MsbA_ST or MsbA_VC constructs***
MsbA_ST_PstI_F 5’-AAA ACT GCA GAT GCA TAA CGA TAA AGA TCT CTC TAC G-3’
MsbA_ST_KpnI_R 5’-AAA AGG TAC CTT ATC ATT GGC CAA ATT GCA TCT TAT GTA G-3’

MsbA_ST_XbaI_R 5’-AAA ATC TAG ATT ATC ATT GGC CAA ATT GCA TCT TAT GTA G-3’
MsbA_VC_R_XbaI 5’-AAA TCT AGA TTA TCA TTC ACC AAA CTG GAT GCG ATG-3’

MsbA_VC_F_PstI 5’-AAA CTG CAG ATG TCA TTG CAC TCT GAC GAA TCT A-3’
MsbA_VC_R_KpnI 5’-AAA GGT ACC TTC ACC AAA CTG GAT GCG ATG-3’

● ***Oligonucleotide for the construction of expression vectors for DARPin_55 used in cross-linking and EPR study***
DARPin55_C12_F 5’-CCA TCA CGG ATG CGA CCT GGG TAA GG-3’
DARPin55_C12_R 5’-CCT TAC CCA GGT CGC ATC CGT GAT GG-3’

DARPin55_C29_F 5’-GAT CAG GAC GAC TGC GTT CGT ATC CTG-3’
DARPin55_C29_R 5’-CAG GAT ACG AAC GCA GTC GTC CTG ATC-3’

DARPin55_C151_F 5’- GTA AGA CCG CTT TCT GCA TCT CCA TCG ACA ACG G-3’
DARPin55_C151_R 5’- CCG TTG TCG ATG GAG ATG CAG AAA GCG GTC TTA C-3’

DARPin55 C160_F 5‘-CGG TAA CGA GTG CTG GCT GAA ATC-3’
DARPin55 C160_R 5’-GAT TTC AGC CAG GCA CTC GTT ACC G-3‘

A.4 Plasmids

A.4.1 *E.coli* expression vector

Plasmid name	Comment/relevant details	Reference
1). MsbA_lyzlnk_EC	10his-tag followed by 3C protease site at N-terminus, *E.coli* MsbA gene, Amp^r, Arabinose induction	This thesis
2). MsbA_lyzlnk_EC_(E-Q)	10his-tag followed by 3C protease site at N-terminus, *E.coli* MsbA(E506Q) mutant gene, Amp^r, Arabinose induction	This thesis
3). MsbA_lyzlnk_ST	10his-tag at N-terminus, *S.typhimurium* MsbA gene, Amp^r, Arabinose induction	This thesis
4). MsbA_lyzlnk_VC	10his-tag at N-terminus, *V.cholerae* MsbA gene, Amp^r, Arabinose	This thesis
5). MsbA_AviC	10his-tag at N-terminus and Avi-tag at C-terminus, *E.coli* MsbA gene, Amp^r, Arabinose induction	This thesis
6). MsbA_VC_AviC	10his-tag at N-terminus and Avi-tag at C-terminus, *V.cholerae* MsbA gene, Amp^r, Arabinose induction	This thesis
7). MsbA_ST_AviC	10his-tag at N-terminus and Avi-tag at C-terminus, *S.typhimurium* MsbA gene, Amp^r, Arabinose induction	This thesis
8). MsbA cys less	10his-tag followed by 3C protease site at N-terminus, *E.coli* MsbA cysteine less gene, Amp^r, Arabinose induction	This thesis
9). MsbA_lyzlnk_25	10his-tag followed by 3C protease site at N-terminus, *E.coli* single cysteine MsbA gene, Amp^r, Arabinose induction	This thesis
10). MsbA_lyzlnk_65, MsbA_lyzlnk_78, MsbA_lyzlnk_88, MsbA_lyzlnk_103, MsbA_lyzlnk_173, MsbA_lyzlnk_191, MsbA_lyzlnk_206, MsbA_lyzlnk_246, MsbA_lyzlnnk_315, MsbA_lyzlnk_482, MsbA_lyzlnk_518, MsbA_lyzlnk_539, (the mutated residue number is denoted in each construct).	10his-tag followed by 3C protease site at N-terminus, *E.coli* single cysteine MsbA mutants, Amp^r, Arabinose induction	This thesis
11). NBD_lyzlnk_EC	10his-tag followed by 3C protease site at N-terminus, NBD of *E.coli* MsbA, Amp^r, Arabinose induction	This thesis
12). NBD_lyzlnk_Ec_E-Q	10his-tag followed by 3C protease site at N-terminus, NBD (E506Q) of *E.coli* MsbA, Amp^r, Arabinose induction	This thesis
13). NBD_EC_AviC	10his-tag at N-terminus and Avi-tag at C-terminus, NBD of *E.coli* MsbA, Amp^r, Arabinose induction	This thesis
14). TM_EC_AviC	10his-tag at N-terminus and Avi-tag at C-terminus, TMD of *E.coli* MsbA, Amp^r, Arabinose induction	This thesis
15). pQE_MTS55	6his-tag at N-terminus, MsbA specific DARPin named as DARPin_55, Amp^r, IPTG induction	This thesis
16). pQE_MTS55_N Cys, pQE_MTS55_C Cys, pQE_MTS55_12 Cys, pQE_MTS55_29 Cys, pQE_MTS55_151 Cys, pQE_MTS55_160 Cys	6his-tag at N-terminus, single cysteine mutants of MsbA specific DARPin_55, Amp^r, IPTG induction	This thesis
17). pQE_DARPin55 $_{myc5}$	6his-tag at N-terminus, 5X(myc tag) at C-terminus, DARPin_55, Amp^r, IPTG induction	This thesis
18). pQE_DNBD14	6his-tag at N-terminus, *E.coli* MsbA_NBD specific DARPin, Amp^r, IPTG induction	This thesis
19). pET28-CH_ydda	6his-tag at C-terminus, *E.coli* YDDA, Kan^r, IPTG induction	Daniel Frey

A.4.2 *L. lactis* expression vector

20). pNZ8048lmrA	6his-tag at N-terminus, L.lactis expression, Cm^r, Nisin induction	Markus Seeger

Amp^r- Ampicillin resistance
Cm^r- Chloramphenicol resistance

A.5 Curriculum Vitae

Personal information

Name	Anshumali Mittal
Date of birth	March 11, 1982
Place of birth	Udham Singh Nagar, Uttaranchal, India
Nationality	Indian

Education

05/2007 to present	**University of Zürich, Zürich, Switzerland** PhD program in Molecular Life sciences
08/2005 to 04/2007	**Indian Institute of Science, Bangalore, India** Junior Research Fellow Supervisor: Prof. Raghavan Varadarajan
07/2002 to 06/2004	**Jawaharlal Nehru University, New Delhi, India** Degree: M.Sc. Life Sciences Thesis Supervisor: Prof. B. C. Tripathy
07/1999 to 05/2002	**Aligarh Muslim University, Aligarh, India** Degree: B.Sc. (HONS)

Publications

1). Asymmetry in the homodimeric ABC transporter MsbA recognized by a DARPin.

Anshumali Mittal, Simon Böhm, Markus G Grütter, Enrica Bordignon* and Markus A Seeger*

(J. Biol. Chem, June 8, 2012, Volume 287, Number 24, 20395-20406)

2). Tuning the drug efflux activity of an ABC transporter in vivo by in vitro selected DARPin binders.

Markus A. Seeger, **Anshumali Mittal**, Saroj Velamakanni, Michael Hohl, Ihsene Salaa, Markus G. Grütter and Hendrik W. van Veen

(PLoS ONE, June 2012, Volume 7, Issue 6, e37845)

Conferences

1). 9th International NCCR Symposium on New Trends in Structural Biology
(September 1 - 2, 2011 | University of Zurich, Switzerland)
Poster presentation

2). Gordon Research conference (mechanism of membrane transport)
(June 19-24, *2011* | University of New England in Biddeford, USA)
Poster presentation

3). 8th International NCCR Symposium on New Trends in Structural Biology
(September 2 - 3, 2010 | University of Zurich, Switzerland)
Poster presentation

4). 7th International NCCR Symposium on New Trends in Structural Biology
(September 7 - 8, 2009 | University of Zurich, Switzerland)
Poster presentation